



**University of  
Reading**

Department of Archaeology

School of Archaeology, Geography, and Environmental

Science

**Holocene Climate Change and Variability  
in the Eastern Fertile Crescent: A  
Speleothem Study**

Matt Bosomworth

A Thesis Submitted for the Degree of

Doctor of Philosophy

March 2021

## Abstract

The Eastern Fertile Crescent (EFC), an area encompassing parts of Iraq, Syria, Turkey and Iran, was an important centre for numerous major societal transformations during the Holocene (11,650 yr BP – Present). Climate change is often cited as an important mechanism that influenced these developments. However, there is an absence of palaeoclimate data in the region with the temporal resolution and chronological precision needed to help support theories regarding human-environmental interactions. Moreover, there are significant discrepancies in the way existing environmental records from Southwest Asia are currently interpreted.

Here I address these outstanding problems by producing the first high-resolution palaeoclimate record from the EFC to cover most of the Holocene (*c.* 10,560 yr BP – Present) by geochemically examining a stalagmite (SHC-03) from Iraqi Kurdistan. Stalagmite trace element (Mg/Ca & Sr/Ca) and  $^{87}\text{Sr}/^{86}\text{Sr}$  data reveal long-term changes in moisture availability, while  $\delta^{18}\text{O}$ ,  $\delta^{13}\text{C}$  and Mg/Ca data provide collective evidence for shorter-term climate variability. The stalagmite record indicates climatic conditions between *c.* 10,560 – 7,000 yr BP were relatively dry, while conditions between *c.* 7,000 yr BP – Present were wetter and more stable, consistent with existing pollen studies from the EFC. These long-term hydrological changes were indirectly associated with the evolution of the Indian Ocean Monsoon over the course of the Holocene. Superimposed on these trends, were quasi-cyclical *c.* 1500 yr oscillations between wetter and drier conditions, as well as more abrupt multi-decadal events. The new multi-proxy record reveals that long-term changes in the  $\delta^{18}\text{O}$  composition of the stalagmite were strongly influenced by  $\delta^{18}\text{O}$  changes of the source of moisture, rather than rainfall amount, limiting its effectiveness as a palaeoclimate proxy in the EFC.

The stalagmite record allowed the testing of existing hypotheses concerning human-environmental relationships. In this thesis I focussed on one archaeological case study - the early urbanisation of Northern Mesopotamia during the 6<sup>th</sup> and 5<sup>th</sup> Millennium BP. Comparisons between the new palaeoclimate and existing archaeological datasets suggests moisture availability may have been an important influence on the ability to sustain and develop larger, urban settlements during this period.

## **Declaration of Original Authorship**

I confirm that this is my own work and that the use of all material from other sources has been properly and fully acknowledged.

Signed:

MATTHEW JOHN BOSOMWORTH

## Acknowledgements

I would like to thank my supervisors, Prof. Dominik Fleitmann (Basel), Prof. Roger Matthews (Reading) and Prof. Alistair Pike (Southampton) for their friendly support, guidance, and advice throughout the project.

I am also grateful to Dr. Diary A.M. Al-Manmi (Sulaymaniyah), his students, and Dr. Mark Altaweel (UCL) for their contributions and previous work at Shalaih Cave which has led to this project. I would also like to express my gratitude to Kamal Rasheed Raheem and the Sulaymaniyah Antiquities Directorate for their help accessing and exporting samples. I am also grateful to Azad Sangawi (Sulaymaniyah) for his help collecting samples and his hospitality throughout my time in Kurdistan.

There are many people I need to thank for their help for the fundamental analytical aspects of this project. This includes Anne Dudley for support using the ICP-OES at the University of Reading. The staff at BGS, particularly Prof. Melanie Leng, Dr. Diana Sahy and Hilary Sloane, for training, providing access to facilities, and processing the isotope and dating samples. Finally, I need to thank Dr. Matt Cooper (NOC) for his training in, and processing of the, strontium isotope measurements

I would like to express my gratitude to Dr Wendy Matthews (Reading) (and Roger again) for giving me the opportunity to participate in excavations in Iraqi Kurdistan as an undergraduate student, which launched my interest in the archaeology, history, and environment of the region. I would also like to thank Dr. Pascal Flohr, for her work and discussions concerning the palaeoenvironment of the region.

This work would not have been possible without the financial support of the AHRC SWW DTP studentship and a grant from the NERC Isotope Geoscience Facilities Steering Committee.

Finally, I would like to thank my parents for their support throughout. Unfortunately, my father passed away during this project, but I know he'd be wanting to know what was taking so long! Special thanks need to be given to my wife Rachel for dealing with the financial burden that being a perpetual student entails.

## Contents

Abstract.....	i
Declaration of Original Authorship .....	ii
Contents .....	iv
Table of Figures .....	viii
1 Introduction, Rationale and Aims .....	1
1.1 Research Rationale.....	1
1.2 Aims.....	9
1.3 Structure.....	9
1.4 Terminology and Conventions.....	10
2 Topography, Present Day Climate, and Vegetation of the EFC .....	13
2.1 Topography.....	13
2.2 Present Climate .....	15
2.3 Present Day Vegetation of the EFC .....	22
2.4 Summary .....	23
3 Palaeoclimate of the EFC and Southwest Asia.....	25
3.1 Causes of Past Climate Change .....	25
3.2 Sources of Palaeoclimate Information .....	27
3.3 The Climate of Southwest Asia from 20,000 yr BP to Present: Current Understanding .....	35
3.4 Summary .....	50
4 Caves, Speleothem Geochemistry and Palaeoclimate Proxies .....	51
4.1 Karst, Caves and Speleothems .....	51
4.2 Speleothems as Palaeoclimate Archives .....	58

4.3	Dating Speleothems - U-Th Dating .....	59
4.4	Palaeoclimate Proxies .....	61
4.5	Stable Isotopes .....	62
4.6	Trace Elements.....	78
4.7	Strontium Isotopes .....	83
4.8	$^{234}\text{U}/^{238}\text{U}$ Activity ratios .....	85
5	Interpreting $\delta^{18}\text{O}$ records from Southwest Asia .....	87
5.1	How speleothem $\delta^{18}\text{O}$ variability is interpreted .....	87
5.2	The Isotopic Composition of the Eastern Mediterranean Sea.....	91
5.3	Summary .....	97
6	Site Selection, Geology and Shalaih Cave.....	98
6.1	Shalaih Cave .....	98
6.2	Climate.....	102
6.3	Suitability of Shalaih Cave to Capture Regional Climate Change .....	102
6.4	History of Research.....	103
6.5	Monitoring Data Results .....	104
6.6	Human and Animal Impact.....	111
6.7	Previous Investigations .....	112
7	Material and Methods .....	114
7.1	Sample Selection.....	114
7.2	Analytical Methods.....	119
8	Results and Proxy Interpretation.....	125
8.1	Uranium Series Dating.....	125

8.2	Stable Isotope ( $\delta^{18}\text{O}$ & $\delta^{13}\text{C}$ ) Analysis.....	129
8.3	Trace Element Analysis .....	151
8.4	Strontium Isotope ( $^{87}\text{Sr}/^{86}\text{Sr}$ ) Analysis .....	160
8.5	Uranium Isotopes .....	162
8.6	Fluid Inclusion Analysis .....	165
9	Palaeoclimate Interpretation and Implications of the SHC-03 Record .....	168
9.1	Long-Term Trends .....	168
9.2	Short-term climate variability .....	178
9.3	Summary .....	185
10	Human-Environmental Relationships: Theoretical Considerations & Archaeo-Demographic Proxies .....	187
10.1	Studying Human-Environmental relationships .....	187
10.2	Archaeo-Demographic Proxies .....	190
10.3	Summary .....	199
11	Complex Societies and Urbanisation in Northern Mesopotamia .....	201
11.1	Geographic Scope and Environmental Context .....	203
11.2	Archaeological Background.....	204
11.3	The Role of the Environment on Urbanisation: Current Understanding .....	214
11.4	SHC-03: Correlations with Settlement Trajectories in Northern Mesopotamia .....	216
12	Conclusions and Future Recommendations .....	226
12.1	Conclusions.....	226
12.2	Limitations and Future Recommendations .....	228
13	Bibliography .....	232

14	Appendix.....	279
14.1	Appendix A – European and Southwest Asian Speleothem ( $\delta^{18}\text{O}$ ) Records .....	280
14.2	Appendix B – Record Correlations .....	281
14.3	Appendix C - Detrending Normalising and Producing MAI scores .....	282
14.4	Appendix D – Correcting for Interlaboratory Variation .....	286
14.5	Appendix E - Organic Carbon Analysis.....	287

## Table of Figures

Figure 1: The location of the EFC (red line) within the wider Fertile Crescent (black line). .....	8
Figure 2: Tectonic subdivision of the NW segment of the Zagros Fold–Thrust Belt. ....	14
Figure 3: Köppen climate classifications for areas of Southwest Asia. ....	16
Figure 4: The position of major synoptic systems .....	17
Figure 5: Schematic representation of the influence of the NCP on circulation patterns in the Mediterranean. ....	21
Figure 6: The location of existing Holocene or near Holocene long palaeoclimate records collected from Southwest Asia.....	34
Figure 7: Main isotopic records from lake sediment and speleothem records from Southwest Asia ...	42
Figure 8: Oak pollen and $\delta^{18}\text{O}$ data from lake sediments from in or near the EFC .....	49
Figure 9: The worldwide distribution of carbonate and evaporite rocks, demonstrating the global distribution of karstic environments. ....	52
Figure 10: Conceptual diagram illustrating the geochemical processes involved in speleothem formation. Figure produced in InkScape.....	55
Figure 11: Decay chain series of $^{238}\text{U}$ . ....	61
Figure 12: Schematic figure illustrating the many different processes which exist in the water cycle that can influence the $\delta^{18}\text{O}$ value of rain and cave waters, and subsequently, speleothem calcite. From Lachniet (2009, p. 413).....	70
Figure 13: The Eastern Mediterranean Meteoric Water Line, the Global Meteoric Water Line, and the Bazian Meteoric Water Line. ....	72
Figure 14: Different mechanisms above and in the karst system which can influence the $\delta^{13}\text{C}$ composition of speleothem carbonate.....	77
Figure 15: The effect prior calcite precipitation has on Mg/Ca and Sr/Ca values. milar effect on Sr/Ca and Ba/Ca ratios, as well as $\delta^{13}\text{C}$ values. ....	80
Figure 16: Monitoring data from Soreq Cave in Israel .....	88

Figure 17: Comparison between $\delta^{18}\text{O}$ profiles of an eastern Mediterranean marine sediment core and the Soreq Cave speleothem record.....	89
Figure 18: $\delta^{18}\text{O}$ profiles of EMSS marine sediment cores, alongside Levantine and Iranian speleothem records, as well as a speleothem record from Qunf Cave, Oman. ....	95
Figure 19: Annual temperature and salinity surface composition of the Mediterranean. ....	96
Figure 20: Location of Shalaih Cave. ....	100
Figure 21: Image of the sinkhole within which the entrance to Shalaih cave is located .....	101
Figure 22: Schematic plan of Shalaih Cave with annotations. ....	101
Figure 23: Correlation of precipitation variability between Shalaih Cave and other areas of Southwest Asia .....	103
Figure 24: Drip rates from a location within Shalaih Cave compared to precipitation data recorded above the cave. ....	105
Figure 25: Temperature data recorded inside and outside Shalaih Cave. ....	106
Figure 26: Humidity data recorded inside and outside Shalaih Cave. ....	106
Figure 27: Rain and drip water $\delta\text{D}$ and $\delta^{18}\text{O}$ values from Shalaih Cave compared to local, regional and global water lines.. ....	108
Figure 28: Relationship between the isotopic composition and the amount of rainfall above Shalaih Cave .....	110
Figure 29: The isotopic composition of cave drip-water with Shalaih Cave alongside precipitation amount above the cave.....	111
Figure 30: Images of the two previously investigated stalagmites from Shalaih Cave .....	113
Figure 31: The stalagmite SHC-03 collected for this PhD study.....	115
Figure 32: Scanned Images of stalagmite SHC-03. ....	117
Figure 33: Zoomed in high resolution image of Slab 7. ....	117
Figure 34: Scanned image of SHC-04 .....	118
Figure 35: Age model produced in COPRA for stalagmite SHC-03. ....	128

Figure 36: $\delta^{18}\text{O}$ and $\delta^{13}\text{C}$ measurements from the SHC-03 stalagmite.....	131
Figure 37: Scatter of the $\delta^{18}\text{O}$ and $\delta^{13}\text{C}$ data which .....	132
Figure 38: Modelled vs actual $\delta_{18}\text{O}$ value plot for pre-existing speleothem studies from Europe and Southwest Asia and the new SHC-03 record.....	135
Figure 39: Comparison between the recently produced Kuna Ba composite $\delta_{18}\text{O}$ record and the SHC-03 $\delta_{18}\text{O}$ record.....	137
Figure 40: Key Holocene long speleothem and marine $\delta_{18}\text{O}$ from Southwest Asia.....	139
Figure 41: Standardised $\delta^{18}\text{O}$ Records from Southwest Asia and the Eastern Mediterranean Sea.....	142
Figure 42: A comparison between long-term trends of SHC-03 and PS0009PC.....	142
Figure 43: Schematic figure explaining the relationship between $\delta^{18}\text{O}$ records from Southwest Asia, the EMSS and Oman.....	143
Figure 44: Trace element (Mg/Ca, Sr/Ca, Ba/Ca) data from the SHC-03 stalagmite.....	152
Figure 45: Mg/Ca profile superimposed on the stable isotope profiles .....	154
Figure 46: $\ln(\text{Mg}/\text{Ca})$ vs $\ln(\text{Sr}/\text{Ca})$ plot to test the influence of PCP on SHC-03 trace element data.	157
Figure 47: The $^{87}\text{Sr}/^{86}\text{Sr}$ and $^{234}\text{U}/^{238}\text{U}_0$ data from SHC-03.....	164
Figure 48: $\delta^{18}\text{O}$ vs $\delta\text{D}$ versus plot of fluid inclusions samples from SHC-03.....	166
Figure 49: Key geochemical proxies from stalagmite SHC-03, annotated with their associated interpretations.....	169
Figure 50: Comparisons between trace element and $^{234}\text{U}/^{238}\text{U}_0$ proxies from the Katalekhhor Cave and Shalaih Cave records.....	171
Figure 51: Comparison between the SHC-03 Mg/Ca data with selected pollen data.....	175
Figure 52: Schematic illustration of how different proxies change in response to changes in the amount of spring rainfall to explain the current interpretation of these proxies.....	176
Figure 53: The combined mean anomaly records.....	180
Figure 54: Schematic position of major synoptic systems and location of key records discussed in this chapter.....	183

Figure 55: Comparison between the SHC-03 MAI and Fi data with other records and regional climate indices covering the last 6,000 years. ....	184
Figure 56: Location of key Late Chalcolithic and Early Bronze Age sites in northern Mesopotamia	206
Figure 57: Schematic illustration of the scale and distribution of urban settlements in Southern and Northern Mesopotamia, 5000-2000 BC.....	214
Figure 58: Map showing the location of Shalaih Cave relative to sites in the Khabur Basin and North Jazira. ....	218
Figure 59: Graph showing the new palaeoclimate data (Mg/Ca, MAI and FI) from Shalaih cave and Mg/Ca data from Lake Van. ....	219
Figure 60: Comparison between the SHC-03 MAI record with settlement trajectories in the North Jazira region of Northern Mesopotamia, SPD population reconstruction from Northern Mesopotamia and isotopic data from archaeobotanical remains from Northern Mesopotamia.....	223
Figure 61: Figures showing the process of detrending and normalising the SHC-03 proxy data.....	285
Figure 62: Averaging of values to produce a mean anomaly index.....	285
Figure 63: Plot showing the Sr correction needed for the data produced at the two different laboratories. ....	286

# 1 Introduction, Rationale and Aims

## 1.1 Research Rationale

Over the last 150 years average global temperatures have increased by about 1°C (IPCC, 2013; NOAA, 2020), predominantly as a consequence of anthropogenic greenhouse gas emissions. By the end of the 21<sup>st</sup> century, global temperatures are predicted to exceed 2°C above pre-industrial levels if no mitigation measures are implemented (Collins et al., 2013). The impact of rising temperatures has already resulted in profound changes in the natural environment including an increase in the occurrence of droughts, floods, wildfires, other types of extreme weather, sea level rise, and biodiversity loss, with the likelihood of these events increasing as temperatures continue to rise (IPCC, 2014). Moreover, these climate related events are further exacerbated by more direct human impacts on natural systems such as deforestation, habitat destruction and increasing resource consumption (IPCC, 2019). Climate change has led to, and will continue to result in, devastating outcomes for vulnerable populations around the world, particularly in low to middle income countries. These outcomes include reduced food security, social instability, migration, poverty and increased mortality (IPCC, 2014, p. 13). Consequently, understanding how the climate and environment will change in the future, the impact and associated risks these changes will pose to present and future human societies, and what adaptive and mitigative responses are required to limit the negative impacts of these changes on human and natural systems has become a major concern for scientists, politicians, and the wider public (e.g. IPCC, 2014).

One way in which this concern can be approached, and partially addressed, is by taking a deep-time perspective to analyse the nature of past climate and environmental change, the responses of historical and pre-historical human societies to such changes, as well as the impact of past human-activities on the natural environment, which might provide important lessons that could help mitigate against the environmental challenges facing societies today and in the future (Van De Noort, 2011). As a result, the investigation of human-environmental interactions has become a major research theme within archaeological, palaeoenvironmental and other related studies (Kintigh et al., 2014a; Carleton and Collard, 2020) and it has been described as one of the five major topics which cover the ‘*Grand Challenges for Archaeology*’ (Kintigh et al., 2014a). The investigation of past human-environmental

interactions can help address important archaeological questions, as outlined by Kintigh *et al.*, (2014b, p. 880), including:

1. *“Why do foragers engage in plant and animal management, and under what circumstances does management of a plant or animal lead to its domestication?”*
2. *Why do agricultural economies emerge, spread, and intensify, and what are the relationships among productive capacity, population, and innovation?*
3. *What factors drive or constrain population growth in prehistory and history?*
4. *How do humans respond to abrupt environmental change?*
5. *How do humans perceive and react to changes in climate and the natural environment over short- and long-terms?”*

In this thesis, I attempt to address these research themes and questions, drawing on new palaeoclimate data which will be produced in this project in conjunction with existing archaeological datasets.

Southwest Asia, particularly the Fertile Crescent (Figure 1), offers an ideal geographical setting to explore human-environmental interactions for many reasons. Firstly, the region has a long and rich history of human occupation throughout the Holocene (*c.* 11,650 yr BP – Present). It is widely accepted to have been a global centre for the emergence of a number of major societal developments during this period, including the emergence of agricultural societies and animal husbandry (Zeder, 2011; Bar-Yosef, 2017), urban settlements (Lawrence and Wilkinson, 2015; Algaze, 2018), city-states (Algaze, 1993, 2005) and empires (McMahon, 2012) alongside the many social, technological and economic changes associated with these fundamental transformations. Secondly, there are important features of the climate of Southwest Asia which make it attractive to study from a paleoenvironmental standpoint. Like much of the wider Mediterranean region, Southwest Asia lies in a transition zone between major climate regimes, including North Atlantic, monsoonal and Siberian systems (Luterbacher and Xoplaki, 2003; Lionello *et al.*, 2006; Ulbrich *et al.*, 2012; Rohling *et al.*, 2013). For this reason, relatively subtle shifts in atmospheric patterns can lead to substantial changes in the region’s climate (Giorgi and Lionello, 2008) which, consequently, should make past climatic changes more readily observable in palaeoclimate datasets than in other more climatically homogenous regions, therefore making the

articulation of human-environmental relationships more direct. Finally, from a contemporary standpoint, Southwest Asia has been identified as a climate change ‘hotspot’ (Giorgi, 2006) which is becoming increasingly susceptible to water shortages due to a combination of drought and poor water management (e.g. over irrigation, water storage) (Chmela, 2011; Nabih, 2018) and is the world’s most water scarce region (Joffé, 2016; Hofste et al., 2019). Water shortages and drought have been argued to be a significant contributory factor for recent social instability in the region, particularly in Syria (Gleick, 2014) and Iraq (The BBC, 2018; Hasan, 2020). Studying the climate of the recent and distant past can put modern water pressures into a meaningful historical context (e.g. Flohr et al., 2017), help understand the forcing mechanisms behind changes in water availability, and finally, help test climate model accuracy through data-model comparisons in order to improve model accuracy for future climatic changes, of which there are still many uncertainties (Black et al., 2010; Barlow et al., 2016; Tabari and Willems, 2018).

In order to investigate the nature of past climate and environmental change and its relationship with human societies, high-resolution and precisely-dated environmental and cultural chronologies are required to allow for accurate and reliable comparisons between the two on a human timescale (Contreras, 2016). However, a major constraint for the investigation of past human-environmental interactions has been the ability to access or collect suitable palaeoclimate or palaeoenvironmental data which can achieve the proxy resolution and/or dating precision needed to reliably link environmental and archaeological data. Fortunately, technological and analytical advances in palaeoclimate, palaeoenvironmental, and archaeological, sciences over the last few decades have started to overcome this limitation, providing improved chronologies and proxy data. These improvements have included the high-resolution geochemical analysis of lake sediments (e.g. Jones et al., 2006; Sharifi et al., 2015), the application of AMS <sup>14</sup>C dating (Bronk Ramsey et al., 2004) and application of Bayesian statistics to improve the chronological precision of both archaeological and palaeoenvironmental samples and accuracy of age models (Ramsey, 2009; Manning et al., 2014) and, importantly for the work of this thesis, the use of speleothems as palaeoclimate records.

Speleothems are secondary carbonate deposits found within caves, such as stalagmite or stalactites. They form due to the degassing of cave drip waters which are over-saturated in calcium carbonate ( $\text{CaCO}_3$ ). Consequently, speleothem carbonate locks-in important chemical information of the drip water at the time of formation which, when analysed, can be used to gain an insight into past environmental parameters, such as temperature or rainfall amount, which makes them a potentially important source of climatic information. There are many advantages of using speleothems to produce palaeoclimate records which allow them to provide the analytical information needed to address human-environmental questions:

- They are a multi-proxy palaeoclimate archive containing a variety of measurable parameters that can provide palaeoclimate information; which include stable isotopes ( $\delta^{18}\text{O}$  and  $\delta^{13}\text{C}$ ) (Fairchild et al. 2006), trace elements (Fairchild and Treble, 2009), growth rates and other more novel climate proxies (e.g. strontium isotopes, pollen, fluid inclusions, clumped isotopes).
- Their (generally) closed system, carbonate structure provides the ideal material for uranium series (U-Th) dating. The U-Th dating method provides highly precise dates which permits the creation of accurate and reliable age models to enable better chronological constraints for the timing of climatic events. Moreover, the development of U-Th dating methodology to allow for very small amounts of carbonate to be dated (e.g. Hoffmann et al., 2007) has been one of the instrumental reasons for the significant rise of speleothem studies over the last few decades (Fairchild and Baker, 2012).
- They are commonly found around the world wherever carbonate karstic environments are present, which makes them critical for the investigation of local, regional and inter-regional conditions and particularly valuable for the investigation of conditions in semi-arid regions, such as Southwest Asia, where other types of palaeoclimate archives are relatively rare.

Over the last few decades, the western wing of the Fertile Crescent, particularly the Levant and parts of southern Anatolia, has witnessed a relatively high number of Holocene palaeoclimate investigations. These studies have included the analysis of speleothems from Soreq (Bar-Matthews et al., 1997, 1999, 2003; Bar-Matthews and Ayalon, 2011) and Jeita Caves (Verheyden et al., 2008; Cheng et al., 2015) as

well as the geochemical analysis of lake sediments (Kolodny et al., 2005; Jones et al., 2006; Develle et al., 2010; Dean et al., 2015, 2018). These environmental studies, alongside a long, vibrant, and rich history of archaeological research in the region (Akkermans and Schwartz, 2003; Steiner and Killebrew, 2014), have allowed for more comparisons between palaeoclimate and archaeological datasets in the region to be made (e.g., Roberts et al., 2011, 2017; Clarke et al., 2016; Flohr et al., 2016; Lawrence et al., 2016; Palmisano et al., 2021).

However, the Eastern Fertile Crescent (EFC) (Figure 1) (see Section 1.4.1 for definition) is a region which has been under-investigated in terms of palaeoclimate and archaeological research. There is a scarcity of palaeoclimate records in the region covering the entire, or even parts of the, Holocene. Much of our present knowledge is based on the multi-proxy analysis of a handful of lake sediment records from the Iranian and Turkish Zagros; Lakes Zeribar (van Zeist and Bottema, 1977; Stevens et al., 2001), Mirabad (van Zeist and Bottema, 1977; Stevens et al., 2006) and Lake Van (Wick et al., 2003). These studies, while providing a good record of long-term environmental changes in the Holocene, are poorly resolved (<c.200 years per data point) and have significantly large age uncertainties. There also exists an important discrepancy in the way different environmental proxies have been interpreted in these records, particularly an inconsistency in the interpretation of pollen and geochemical data from these lakes (Stevens et al., 2001, 2006; Roberts, 2002; Jones, 2013; Asouti and Kabukcu, 2014). The absence of high-resolution, precisely dated records in the region covering the Holocene, alongside the discrepancy in the interpretation of existing records, leaves a large spatial and temporal gap in the understanding of Holocene climate change and variability in the EFC that makes it difficult to evaluate how conditions may have differed here to other parts of Southwest Asia, known to be an environmentally and climatically heterogeneous region.

From an archaeological perspective, social instability and political tensions resulted in relatively little archaeological work in the EFC during much of the latter half of the 20<sup>th</sup> century (Ur, 2017). However, over the last c.20 years the EFC, particularly in Iraqi Kurdistan, has witnessed a '*renaissance*' in archaeological fieldwork (Kopanias and Macginnis, 2016; Ur, 2017). The findings of these new archaeological studies along with revaluations of older excavations (Zeder, 2008) are revealing that the

region, like the Western Fertile Crescent, was an important centre for many important societal developments during the Holocene including the emergence of sedentary Neolithic societies during the early Holocene (Matthews and Nashli, 2013; Riehl et al., 2013; Willcox, 2013; Matthews et al., 2020a) and more complex, urban settlements during the middle Holocene (Ur, 2010). Many of these societal developments have been connected in some way to climate and environmental change (Wright, 1993; Bar-Yosef, 2017; Roberts et al., 2017). However, without the necessary palaeoclimate data it is difficult to test whether these hypotheses about human-environmental relationships are supported in the EFC. Therefore, these new archaeological studies have provided fresh impetus to improve our understanding of Holocene environmental change and variability in the region in order to investigate human-environmental interactions, as well as addressing important palaeoenvironmental questions.

To address this absence of palaeoclimate/palaeoenvironmental data from the EFC, two pilot studies have been recently conducted on speleothems from Iraqi Kurdistan (Flohr et al., 2017; Amin Al-Manmi et al., 2019) by teams associated with this PhD project. They were able to demonstrate that variations in speleothem calcite  $\delta^{18}\text{O}$  and  $\delta^{13}\text{C}$  values were likely to be sensitive and accurate recorders of effective moisture above the caves and therefore show that speleothems from the region had the potential to address outstanding palaeoenvironmental issues. However, these records have so far only been able to characterise 1,000 – 2,000 year-long periods of the Holocene. These studies have also recently been supported by other speleothem investigations carried out by other studies in the Iraqi and Iranian Zagros (Sinha et al., 2019; Andrews et al., 2020). However, there are still no high-resolution palaeoclimate records from the EFC which cover the entire Holocene.

Therefore, following the success of these previous projects, this PhD thesis seeks to build upon their work and improve the spatial and temporal availability of palaeoclimate data in the EFC, address the present palaeoclimate research imbalance between the EFC and other parts of Southwest Asia, and address outstanding questions regarding Holocene climate change in the region. I will achieve this aim by producing the first high resolution (< decadal) palaeoclimate record from the EFC to cover the Holocene through the analysis of a speleothem collected from Shalaih Cave, Iraqi Kurdistan (Figure 1). This analysis will be achieved by conducting a multi-proxy geochemical study, including the production

of precise uranium-series dates, highly resolved  $\delta^{18}\text{O}$ ,  $\delta^{13}\text{C}$  and trace element profiles alongside more novel approaches such as strontium isotope analysis. The production of this new record will allow for a more nuanced integration with archaeological data from the EFC and provide an opportunity to examine and test existing hypotheses about human-environmental relationships in this archaeologically important region.

In order to examine human responses to past climate/environmental change in the EFC, I have selected an archaeological case study to concentrate on in the final part of the thesis. This case study will look at the development of large urban settlements in the middle Holocene (c.6,350 – 4,200 yr BP) and it has been selected for three main reasons.:

1. It represents an important period of cultural transformation during the Holocene that had global significance and consequences, but originated, partly, in the EFC. However, there is currently an absence of suitable climate or environmental data from the region covering this period. Therefore, this study aims to provide the environmental context in which this important cultural change first occurred.
2. While there is a general lack of suitable climate data from the EFC, there are many studies which have linked changes in the climate and environment to these changes in settlement patterns during this period. For instance, climate instability has been cited several times as a cause for the decline of, or changes to, Mesopotamian societies during the middle Holocene (Staubwasser and Weiss, 2006; Charles et al., 2010). These studies provide hypotheses which can, and will, be tested with the new palaeoclimate data produced in this thesis.
3. Finally, these middle Holocene communities represent relatively simple, largely self-sufficient societies who were heavily dependent on rainfed, agricultural production and their local environment for their subsistence, as well as their economic and demographic growth, in a highly water stressed region. These environmental conditions may make the articulation of causal links between climate and cultural change (if present) more straightforward than later, more economically complex societies.

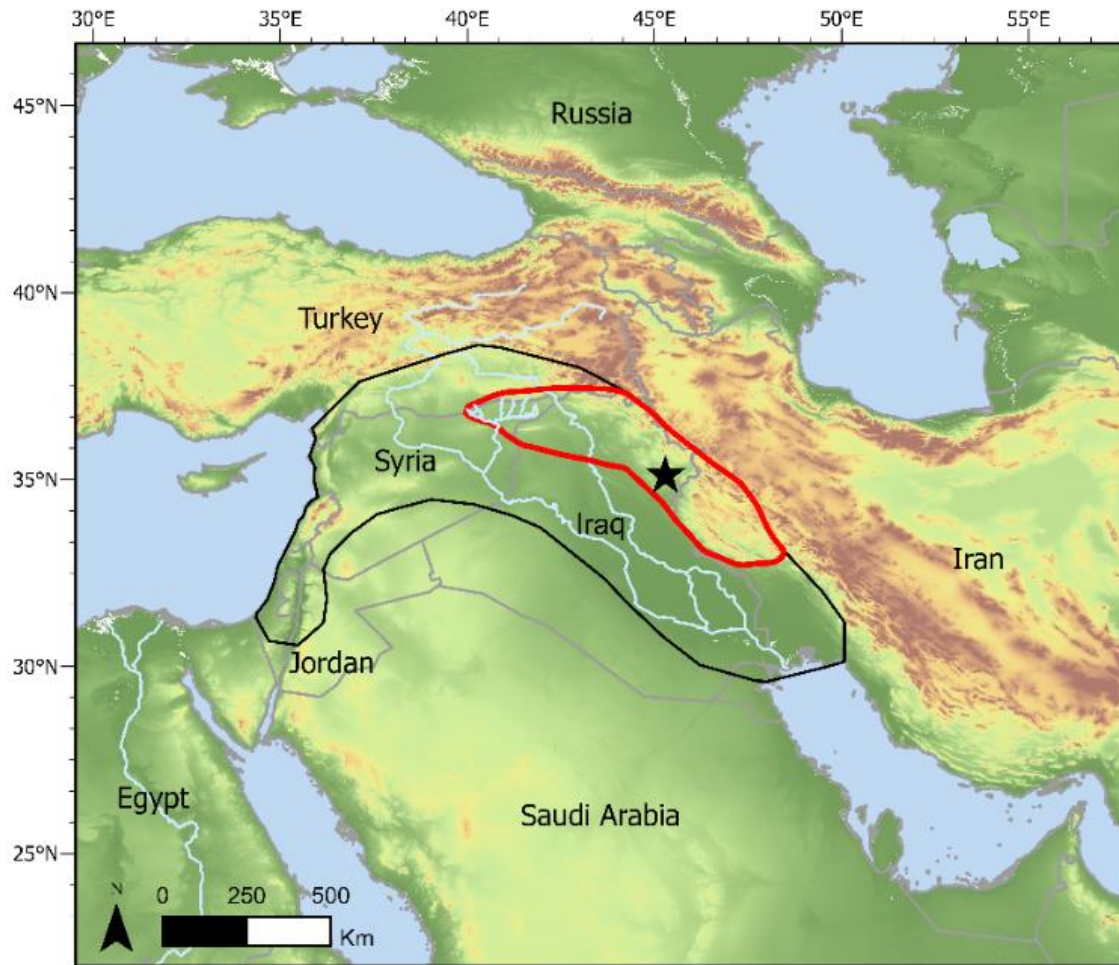


Figure 1: The location of the EFC (red line) within the wider Fertile Crescent (black line). The EFC is the geographical focus of this thesis. While somewhat a subjective term, this is a region which shares broadly similar environmental and climatic features. Its southwestern limit is defined by the 300mm rain isolate, the limit for rainfed agriculture. The southern edge stops at the beginning of the Khuzestan plain in Iran and Southern Mesopotamia in Iraq, where the alluvial floodplains here represent a very different environment to the hilly steppes of the EFC. The north-eastern and northern edge are marked by the higher elevations of the Zagros and Taurus mountains, where more mountainous and continental climates are found. Black star shows the location of Shalaih Cave where speleothem samples have been collected for analysis in this study.

## 1.2 **Aims**

To summarise, the principal aims of this PhD thesis are:

1. To test the suitability of a speleothem from Shalaih Cave (SHC-03) for palaeoclimate reconstruction through a multi-proxy geochemical approach.
2. To investigate how the climate and environment of the EFC changed during the Holocene, and how this palaeoclimate record compares to existing palaeoclimate archives of the region and beyond.
3. To identify the possible forcing mechanisms behind observed climate change during this period.
4. To test existing hypotheses regarding the responses of human societies to climate and environmental change and variability in the EFC, considering the new palaeoclimate record generated using the Shalaih Cave speleothem.

## 1.3 **Structure**

The structure of this thesis comprises two major sections. The first section (Chapters 2 – 9) will focus on past palaeoclimate and environmental work in the EFC and Southwest Asia, before concentrating on the new palaeoclimate research on a stalagmite sample from Shalaih Cave. The second section (Chapters 10 - 12) articulates and investigates the relevant archaeological evidence in the light of the new palaeoclimate evidence established and analysed in the first section of the thesis.

Chapter 2 critically outlines the present-day climate and environmental parameters for the study region to establish the environmental context for the main focus of the thesis. Chapter 3 reviews existing research into Holocene palaeoclimate change and variability and evaluates current issues in palaeoclimate and palaeoenvironmental research in the EFC and Southwest Asia which this project aims to address. Chapters 4 & 5 critically discuss speleothem geochemistry and examines how speleothems can be used to reconstruct past climate variability while exploring the challenges involved in these types of investigations, focusing on the analyses used in this project. Chapter 6 introduces the study site for the speleothem investigation and reviews previous work conducted at the site. Chapter 7

explains the materials used and the main analytical approaches employed in this project. Chapter 8 outlines the results of the data analysis and discusses the underlying controls on the proxy data retrieved from the SHC-03 stalagmite in order to understand to what extent the data may be used as proxies for climatic change and variability. Chapter 9 reviews the palaeoclimate of the EFC based on the data produced from the SHC-03 record and how they compare to existing data from Southwest Asia and what implications these findings have. Chapter 10 reviews the general theoretical background for, as well as the concepts and challenges associated with, human-environmental investigations in order to provide the context for the approaches taken in the latter part of this thesis. Chapter 11 examines societal responses to climate change and variability in Northern Mesopotamia during the middle Holocene (c.6,350 – 4,200 yr BP) integrating the new climate data produced in this thesis. Chapter 12 will summarise the main findings of this thesis and make recommendations for future work based on these conclusions.

## **1.4 Terminology and Conventions**

### **1.4.1 Geographical Terminology**

The Eastern Fertile Crescent (EFC) has been selected as the geographical focus for this project. For the purposes of this study, the EFC is an area within the Fertile Crescent which broadly encompasses parts of present-day north-eastern Syria, south-eastern Turkey, Iraqi Kurdistan and parts of western Iran (Figure 1). While this definition is rather arbitrary, it provides a useful geographical framework to work with in this thesis, as areas within this region share broadly similar climate, environmental and topographical characteristics (See Chapter 2).

When discussing features for, or data from, the wider region beyond the EFC and Fertile Crescent, this project uses the broad term ‘Southwest Asia’ as a useful reference when discussing conditions or data from the wider region not necessarily found within the Fertile Crescent. This term includes areas of central and eastern Turkey and northern Iran (Figure 1). The term is synonymous with often similarly used broad geographical terms like ‘The Middle East’ or the ‘The Near East’, but here the single term is used to avoid any confusion. Importantly, and for the purposes of this study, ‘Southwest Asia’ does

not include the Arabian Peninsula, which would normally come under this umbrella term, as it is influenced by different climate dynamics.

The geographical focus of Chapter 11 will be on ‘Northern Mesopotamia’ in the western side of the EFC. The definition of this region, and Mesopotamia more widely, will be discussed further in that chapter.

#### 1.4.2 Chronological Conventions

When reviewing palaeoclimate, environmental and archaeological data and comparing one to another it is important to have tight chronological control wherever possible. One problem that faces an investigation of this type is that different disciplines use different chronological conventions. Archaeologists often favour the use of AD/BC or CE/BCE conventions, whereas palaeoclimatologists and environmentalists often refer to dates in BP (Before Present) or ka (Thousands of Years Ago). For the purposes of consistency and to avoid confusion, this thesis will refer to dates in calendar years BP (yr BP), where P = 1950 CE, unless otherwise specified. Moreover, dates from radiocarbon chronologies, if used, are calibrated, unless specified. When using archaeological data which has originally been presented in an CE/BCE (AD/BC) format in its publication, this project has converted these dates simply by adding 1950 to BCE dates (e.g. 1500 BCE = 1500 + 1950 = 3,450 Years BP) and subtracting CE dates from 1950 (e.g. 1800 CE = (1950 – 1800 = 150 yr BP).

#### 1.4.3 Environmental Terminology

Finally, key climate and environmental terms which have similar, but distinct, definitions should also be defined to avoid any confusion. For the purposes of this thesis, the term ‘Environment’ predominantly refers to the natural environment which can be defined as the *‘natural, physical surroundings in which human life takes place’* (Lauesen, 2013), which includes vegetation, geology, soils, water and the climate. ‘Climate’, a component of the environment, is defined as a *‘the average weather, or more rigorously, as the statistical description in terms of the mean and variability of relevant quantities over a period of time ranging from months to thousands or millions of years’* (IPCC 2007: 78). ‘Climate variability’ is defined as *‘variations in the mean state and other statistics (such as standard deviations, the occurrence of extremes, etc.) of the climate on all spatial and temporal scales*

*beyond that of individual weather events' (IPCC 2007: 79). Whereas 'Climate Change' is described as a 'change in the state of the climate that can be identified (e.g. by using statistical tests) by changes in the mean and/or variability of its properties, and that persists for an extended period, typically decades or longer' (IPCC 2007: 78).*

## 2 Topography, Present Day Climate, and Vegetation of the EFC

Southwest Asia has a highly heterogeneous climate and can be divided into several environmental zones (Figure 3). This heterogeneity is caused by the complex interactions between major climate systems, the distribution of land and water masses and the existence of diverse topography. As a result, when investigating the palaeoclimate of a specific area within the region, it is important to consider sub-regional specific features which will influence the environment. This section will explore the present-day topography, major climate dynamics and vegetation of the EFC. Understanding these present-day environmental features is essential for this project as it seeks to reach an accurate insight into how they might have changed in the past.

### 2.1 Topography

The landscape of the EFC is dominated by the Zagros mountain range and associated folded zones. The Zagros mountains run NW-SE and extend for over 2,500 km from southern Turkey to the Persian Gulf in south-east Iran (Figure 3). The mountain range was formed as the result of the collision between the Arabian and Eurasian tectonic plates. While debated, the main period of uplift is thought to have occurred during the middle to late Miocene (c.12.4 – 7 million years ago), although collision continues today (Khadiivi, 2010). On the Iraqi side of the mountains, the Zagros fold thrust belt has resulted in the existence of four distinct geomorphological zones creating distinct environmental landscapes (Figure 2). These zones are listed here with their approximate elevation range (above sea level): 1) The thrust zones (imbricated zone) where the highest elevations are reached (> 2,500 m), 2) The high folded zone (mountain foothills; 600 m – 2,500 m), 3) the low folded zone (the foothills; 200 m – 600 m) and 4) the Mesopotamian foreland basin (Mesopotamian plain; < c.200 m) (Le Garzic et al., 2019; Zebari et al., 2019).

The mountain range has a critical influence on local and regional climate. In Iraqi Kurdistan, orographic uplift caused by the heightened elevation of the mountainous areas results in considerably more rainfall than the rest of Iraq. In some parts of Iraqi Kurdistan rainfall can reach over 1,000 mm of per year, either as rain or snow (Stevanović et al., 2009). The mountain range also acts as an orographic barrier,

limiting the amount of moisture reaching Iran on the leeward side of the mountain range, particularly during spring, receiving up to 50% less moisture than the windward (Iraqi) side (Brookes, 1982; Stevens et al., 2006). The Zagros mountains are also understood to modify large-scale atmospheric circulation patterns across the Mediterranean (Simpson et al., 2015). The Zagros, along with the Taurus Mountains, feed the two major rivers of southwest Asia, the Tigris and Euphrates. The sources of both rivers are found in the Turkish Taurus in the north and they flow through Syria and Iraq down to the Persian Gulf in the south, the Tigris receiving additional water from major tributaries, such as the Greater Zab, Lesser Zab and Diyala rivers, which originate in the Iraqi Zagros zone (Figure 2). These rivers provide the major source of water for populations living in the hyper-arid environments of Syria and southern Iraq which have allowed these areas to be habitable by large urban populations, including Baghdad and Basra.

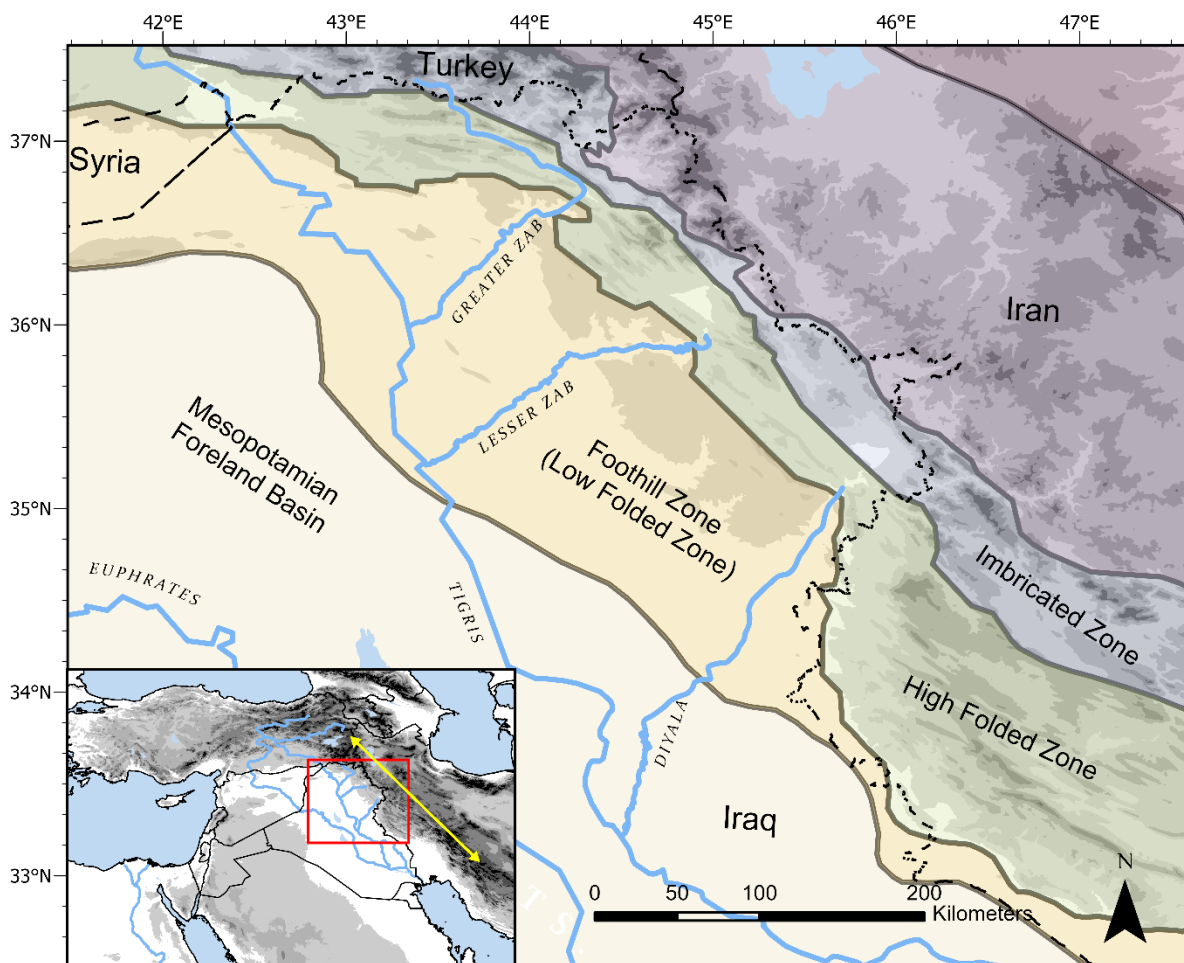


Figure 2: Tectonic subdivision of the NW segment of the Zagros Fold–Thrust Belt. Figure modified after Zebari et al., (2019) and references within. Yellow double headed arrow in the inset image marks the extent of the Zagros mountain chain.

## 2.2 Present Climate

The climate of the EFC can generally be described as a hot-summer Mediterranean type (Csa) according to the Köppen climate classification system (Figure 3), characterised by hot, dry summers and wet, mild winters (Kottek et al., 2006). However, towards lower elevations and latitude, the climate becomes a hot, semi-arid steppe climate type (Bsh). While, towards higher elevations the climate enters a hot, dry summer continental climate type (Dsa).

The EFC, like much of wider Southwest Asia and the Mediterranean, is located at the transition zone of tropical circulation and mid-latitude synoptic systems which predominantly control the climate of the region (Giorgi and Lionello, 2008; Ulbrich et al., 2012). The balance between winter and summer conditions, and the relative strength of these two major synoptic systems, is the key to water availability in most of Southwest Asia. The approximate position of these systems in summer and winter are illustrated in Figure 4. The winter climate of the EFC is dominated by moist, mid-latitude westerlies storm-tracks from the Mediterranean and North Atlantic (Ulbrich et al., 2012), with the majority of precipitation originating from storms generated in the Mediterranean (Kaufman et al., 1998; Enzel et al., 2003; Mustafa et al., 2015). During late spring, increased northern hemisphere heating leads to the northward migration of sub-tropical anticyclone (high-pressure) belt associated with the Inter-tropical Convergence Zone (ITCZ) and Indian Summer Monsoon (ISM) system to the south (Djamali et al., 2010). This leads to the northward displacement of the westerlies and causes intense subsidence over the EFC and low-level northerly winds over the region, leading to hot, arid conditions as a result of the ‘*monsoon-desert mechanism*’ as described by Rodwell and Hoskins (1996, 2001). The anticyclone belt retreats in autumn and the moist westerlies dominate the region again leading to the initiation of rainfall once again. As a consequence of these large-scale atmospheric dynamics, the majority of precipitation falls between November and March (98% falls between October and May (Flohr et al., 2017)). Due to the fine balance between these synoptic systems, even relatively small changes of the circulation patterns (e.g. strength of mid-latitude westerlies) can result in significant fluctuations in the timing, amount and trajectory of cyclonic storms which form and travel over the eastern Mediterranean, which makes the entire region particularly susceptible to climate variability (Ulbrich et al., 2012). In the

following section, more detail about the systems described above will be provided, as well other less dominant, but still important, systems that influence the region which need to be considered.

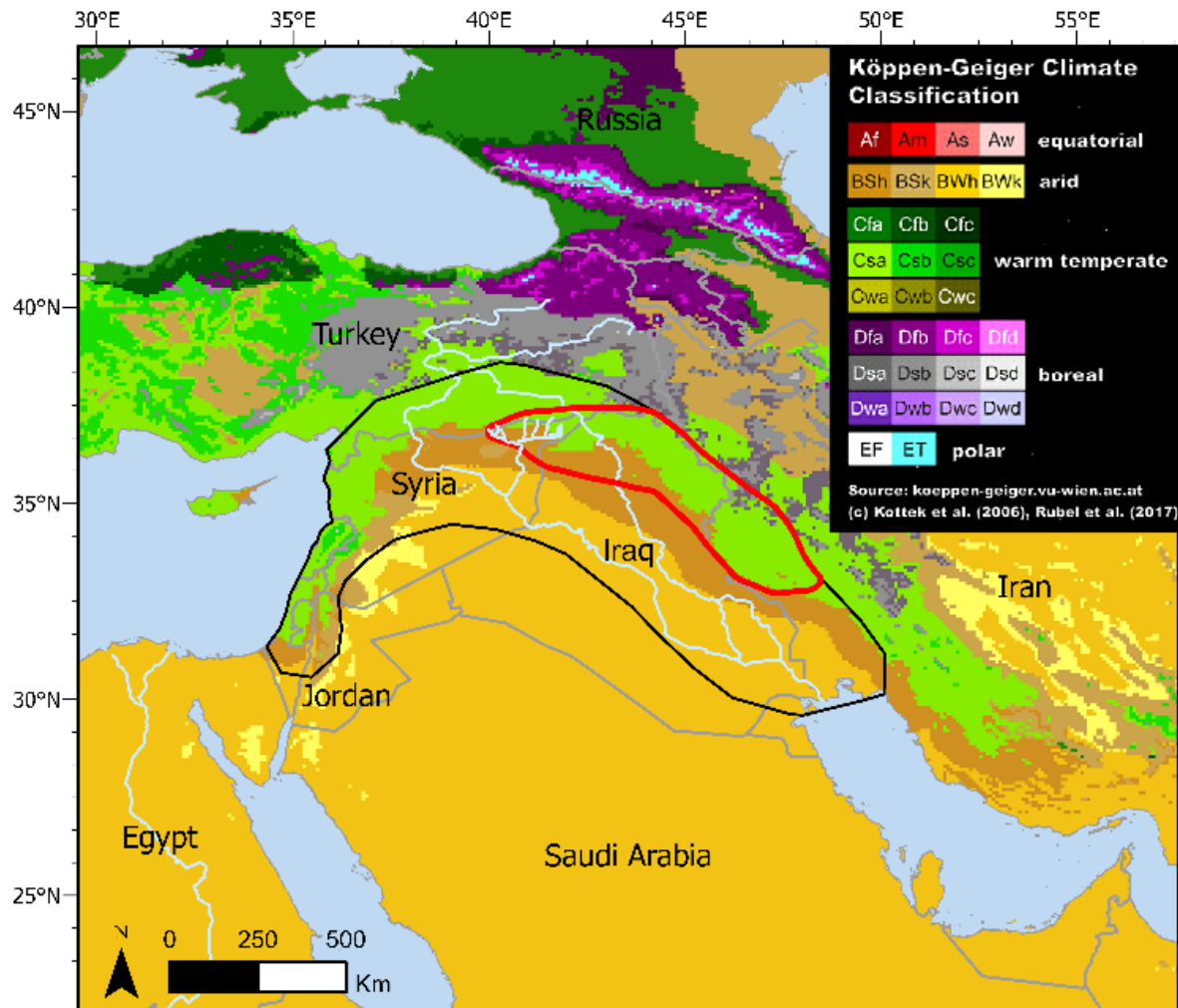


Figure 3: Köppen climate classifications for areas of Southwest Asia. The EFC (red line) primarily comes under the hot-summer Mediterranean (Csa) criteria along with much of the wider Fertile Crescent (black line), but changes in the higher and lower elevations of the region. This figure also illustrates the large amount of climate heterogeneity in Southwest Asia with many climate zones within a relatively small area. Climate classification data obtained from Kottek et al., (2006).

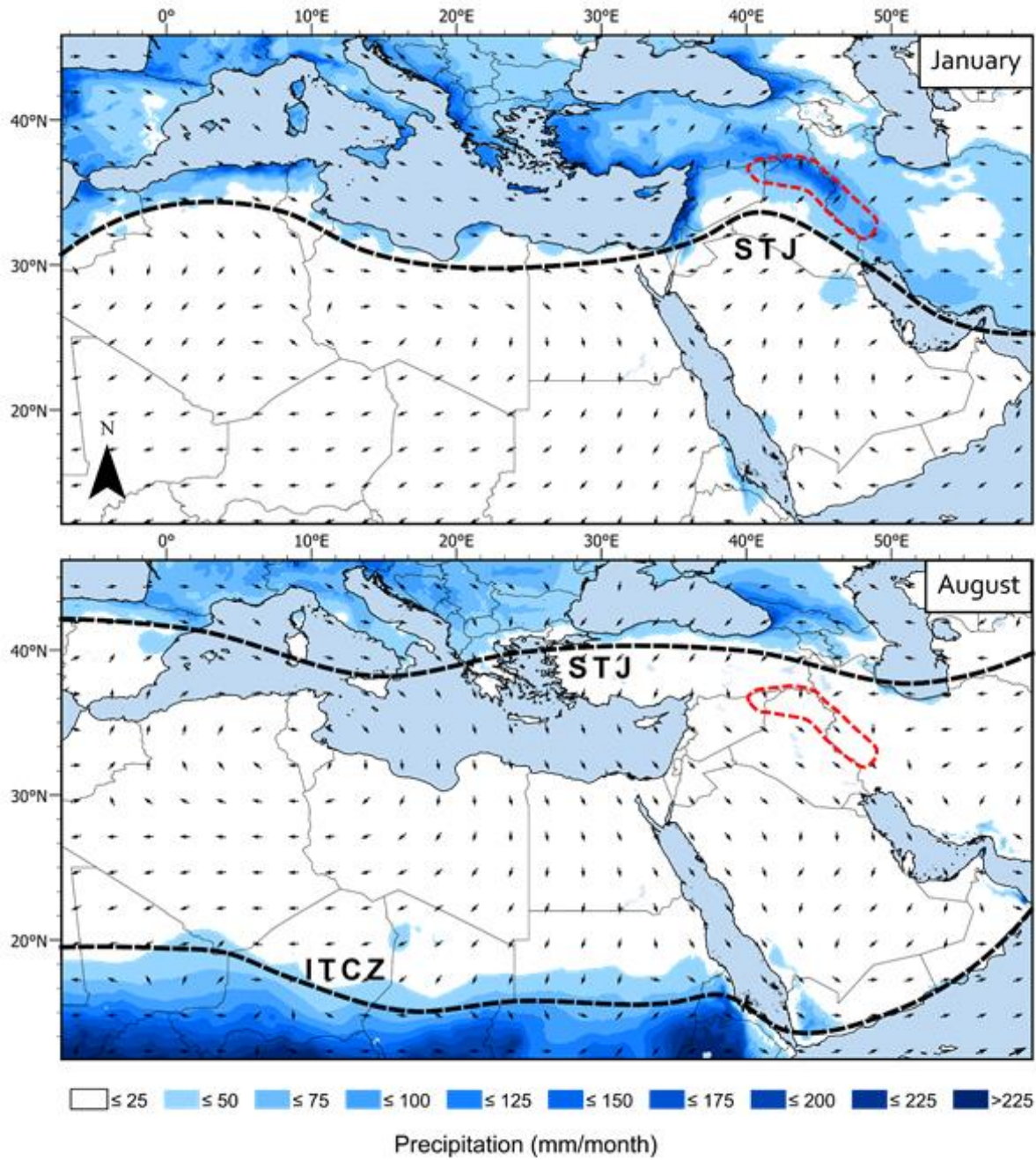


Figure 4: The position of major synoptic systems in winter (top) and summer (bottom) and their influence on precipitation in the EFC (red dashed line), Southwest Asia and the wider Mediterranean region. In winter, the sub-tropical jet (STJ) lies south of the Fertile Crescent which allows moist westerlies to carry precipitation into the region. In the summer, increased northern hemisphere solar insolation results in the northward migration of the inter-tropical convergence zone which shifts the position of the STJ further north, blocking westerlies from penetrating the region resulting in hot, arid conditions dominating the EFC and Southwest Asia. Black arrows indicate wind direction at 850 hpa (<http://iridl.ldeo.columbia.edu>). Precipitation data (CRU TS 4.03 with  $0.5 \times 0.5^\circ$  spatial resolution) collected from the University of East Anglia Climatic Research Unit (Jones and Harris, 2008) via the KMNI climate explorer (<http://climexp.knmi.nl>) (Van Oldenborgh et al., 2009).

### 2.2.1 The Influence of the Mediterranean Sea

A special feature of the climate of Southwest Asia is the influence of the Mediterranean Sea. Given the region's latitude and continental setting, Southwest Asia should have a much more arid and less mild climate than it does (Burstyn et al., 2019). However, the presence of the Mediterranean as a large body of water provides an important source of moisture. Furthermore, the Mediterranean's enclosed nature and longitudinal temperature gradient (Figure 19) provides the ideal conditions for cyclogenesis (Lionello et al., 2006; Burstyn, 2013). Depressions that form in the Mediterranean are responsible for the majority of rainfall that falls in Southwest Asia, particularly extratropical cyclones which pass, intensify or develop over Cyprus, known as Cyprus Lows (Saaroni et al., 2010). However, contributions of moisture from the Arabian Sea, Persian Gulf, Red Sea, and Indian ocean also influence the region (Evans and Smith, 2006).

### 2.2.2 Tropical Systems

The Indian Summer Monsoon (ISM) is part of the larger African-Asian monsoon and refers to a season of strong winds and heavy rainfall that affects the east coast of Africa, the very southern tip of the Arabian Peninsula and the Indian sub-continent. During summer (June–September), increased northern hemisphere solar insolation, causes landmasses to warm and leads to the formation of low pressure systems causing humid, relatively cool, moist sea air to flow in from the area of higher pressure over the Indian Ocean (Fleitmann et al., 2007; Rohling et al., 2013). The monsoonal rain belt is associated with the ITCZ, a narrow latitudinal zone of wind convergence and precipitation (Fleitmann et al., 2007). The EFC is not directly influenced by the ISM and thus no rainfall is associated with it, and there is no evidence that it has at all during the Holocene (Tzedakis, 2007). However, it has a remote influence on the climate through the monsoon-desert mechanism (Rodwell and Hoskins, 2001). The ascending branch of the Hadley circulation cell leads to atmospheric descent over mid-latitudes at approximately 30° north of the position of the ITCZ which results in very arid conditions during the summer months. The strengthening of the Monsoon can cause the expansion of the Hadley Cell which leads to the northward shift of the ITCZ's most northernly limit in summer, which consequently also results in the poleward movement of the sub-tropical high pressure belt (Djamali et al., 2010; Hu et al., 2018). As a

result, strengthened monsoon systems can cause a longer and more intense period of aridity in the sub-tropical regions such as the EFC during summer (Djamali et al., 2010).

### 2.2.3 North Atlantic Climate Dynamics

The intensity, location and direction of westerly storm tracks that pass through the Mediterranean region are themselves to a large extent controlled by conditions in the North Atlantic (Brayshaw et al., 2010), particularly the North Atlantic Oscillation (NAO). The NAO is the dominant atmospheric mode in the North Atlantic sector and refers to the north-south dipole and relative difference of atmospheric pressure at sea level between the Icelandic Low and the Azores High pressure systems situated above the North Atlantic (Hurrell and Deser, 2009).

A positive NAO (NAO (+)) phase describes a situation where the relative pressure difference between the two nodes is increased, i.e. Icelandic system becomes lower and the Azores system becomes higher. The NAO (+) mode forces winter storm tracks to follow a more northerly route which results in wetter, milder conditions in northern Europe and drier conditions in southern Europe. A negative phase (NAO (-)) refers to a situation where the relative pressure difference decreases (i.e. Icelandic system becomes higher and the Azores system becomes lower). The NAO (-) mode forces storm tracks to take a more southerly route leading to wetter conditions in southern Europe, while northern Europe comes under the influence of cold, dry conditions. Due to the impact on westerly storm tracks, the NAO has a significant influence on European and Mediterranean climates and is often cited as a major cause for past variability in both precipitation and temperature across Europe (e.g. Luterbacher et al., 2004; Xoplaki et al., 2004).

As much of the precipitation that falls in Southwest Asia derives from westerly storm tracks, it might be expected that the region would be influenced by NAO variability much like the southern Europe. However, the influence and impact of the NAO on southwest Asia is still a matter of debate. Some studies have observed a weak correlation between NAO and precipitation in Southwest Asia in which a positive (negative) phase leads to reduced (enhanced) winter precipitation, like the rest of the Mediterranean region (Cullen et al., 2002; López-Moreno et al., 2011). On the other hand, there have been some investigations which have indicated Southwest Asia responds in an opposite manner to the

western Mediterranean, referred to as the Mediterranean Oscillation (Roberts et al., 2012). Modelling studies have also suggested that high rainfall events are much more likely to occur under a NAO positive phase, but suggested that a negative NAO phase has little influence on precipitation variation (Black, 2012); more specifically, Black et al., (2012) suggest that high pressure centred over Southern Europe during NAO positive conditions diverts storm tracks south through Southwest Asia, leading to increased precipitation.

Additionally, while the relationship between the NAO and present-day climate in Southwest Asia can be tracked through observable instrumental data, it is possible that the relationship between NAO variability and conditions in Southwest Asia differed over longer timescales and this might have important implications modelling future relationships between the NAO and conditions in Southwest Asia (Black, 2012). High resolution palaeoclimate data can be used to investigate this teleconnection and assess the predictability of the NAO on palaeoclimate conditions, as they have done for Western Europe (Trouet et al., 2009).

#### 2.2.4 Siberian Anticyclone

The Siberian anticyclone (SA) is a continental polar air mass which originates over Russia, north east of the EFC (Saaroni et al., 1996). While its influence on the EFC is generally less dominant than Atlantic and Tropical systems, it can cause the outbreak of cold, dry, but relatively stable weather conditions to occur. The SA is at its strongest during the winter months. It has been suggested that the SA was a major cause for increased aridity during periods of rapid climate change during the Holocene (Rohling et al., 2019). The importance of the Siberian Anticyclone on regional climate in the Southwest Asia increases further east into the continent (e.g. Iran) (Kehl, 2009; Sharifi et al., 2015).

#### 2.2.5 North Sea-Caspian Pattern (NCP)

The NCP refers to an upper level atmospheric teleconnection identified between two poles located in the North Sea and Caspian Sea at the 500 hPa geopotential level (Kutiel et al., 2002). Like the NAO, the NCP is measured by an index which represents the normalised pressure differences between the two poles, either as a positive or negative phase. A negative index refers to a phase in which there exists higher pressure over the Caspian Sea and lower pressure over the North Sea, while the opposite is the

case for a positive phase (Kutiel and Benaroch, 2002). A negative phase (NCP (-) leads to anticlockwise circulation around the North Sea pole of the NCP and increased clockwise circulation around the Caspian Sea pole of the NCP, leading to southerly/south westerly circulation (Figure 5). Conversely, a positive phase leads to clockwise circulation around the North Sea pole of the NCP and anticlockwise circulation around the Caspian Sea pole of the NCP, leading to northerly circulation. The link between the NCP index and precipitation varies depending on specific location and moisture sources and its influence on European climate is less dominant than the NAO (Black, 2012). However, there is evidence that precipitation variability in Southwest Asia is strongly modulated by the NCP, and the inter-annual difference in precipitation between the different phases can be as much as 50 %. More specifically, a positive phase results in north easterly circulation between the two poles, which leads to westerly flow toward Southwest Asia which draws in moisture from the Black Sea and Mediterranean resulting in increased precipitation over the region, while a negative phase leads to south-westerly circulation, drawing in continental air from the east and therefore no moisture (Kutiel et al., 2002).

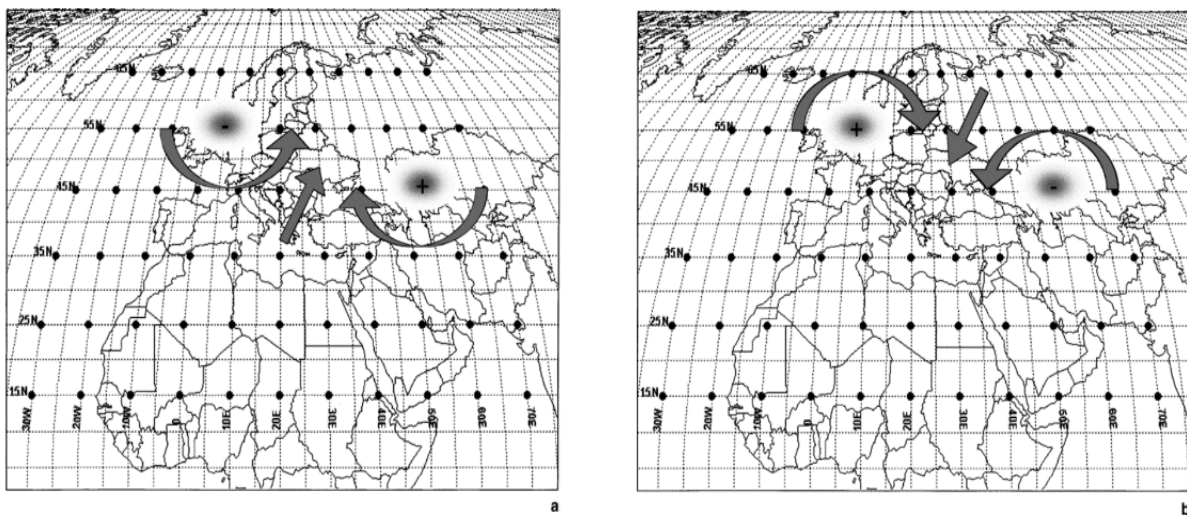


Figure 5: Schematic representation of the influence of the NCP on circulation patterns in the Mediterranean. Left (a) represents a NCP positive phase, while on the right (b) represent a NCP negative phase. From Kutiel and Benaroch (2002).

### **2.3 Present Day Vegetation of the EFC**

The distribution and type of natural vegetation in any given region is both a control on, and influenced by, environmental change and therefore the study of vegetation is a crucial part of any type of palaeoclimate or palaeoenvironmental investigation. Understanding the present-day distribution of vegetation types helps to identify the relationship between vegetation and climate/environmental parameters (e.g., moisture, temperature, seasonality), which provides a modern ecological analogue to compare palaeoenvironmental vegetation reconstructions (e.g. pollen studies) to in order to aid the interpretation of the data, and similarly potentially aids the interpretation of vegetation proxies of speleothems, such as carbon isotopes. From an archaeological perspective, they also provide an insight into the different potential food and strategic resources available to past human populations, including the likely natural distribution of progenitors of crop domesticates.

All of the EFC ecologically falls under the Irano-Turanian phytogeographical zone (Djamali et al., 2012). Much of our understanding of the distribution of vegetation of the region is the result of pioneering work carried out by the Israeli botanist, Michel Zohary; published in his book the '*Geobotanical foundations of the Middle East*' (Zohary, 1973), as well important botanical investigations more specially focused on Iraq carried out by Evan Guest and Ali Al-Rawi (Guest and Al-Rawi, 1966). The natural distribution of vegetation within the EFC broadly follows the geomorphological zones and associated altitudes as described earlier in this chapter (Section 2.1) (Figure 2) which causes distinct precipitation boundaries in a region where moisture is the major limiting factor for plant growth (Boisvenue and Running, 2006), with the exception of the low temperatures encountered at the higher elevations of the Zagros Mountains. There are four major biogeographical zones which can be found in the EFC, which are briefly summarised here.

- 1) At low altitudes (<700m) where annual precipitation generally falls below 500mm per annum, much of the region is covered in steppe grassland (referred to as *Mesopotamian lowland savannas* by Zohary, 1973). This can be further divided into two sub-zones. Where rainfall is below 300 mm a<sup>-1</sup>, this can be considered a dry-steppe, composed of sparse grassland and steppe shrub species such as wormwood (*Artemisia herba-alba*) and yarrow (*Achillea conferta*)

(Charles et al., 2010). Where rainfall is between 300 – 500 mm a<sup>-1</sup>, this can be considered a moist steppe environment, this is also composed of steppe-shrub species, but is also home to steppe woodland, such as pistachio (e.g. *Pistacia atlantica*), other xerophytic small trees or shrubs and less drought tolerant grass species (Charles et al., 2010).

- 2) At elevations of between c.700m and 2000m, where precipitation is >500 mm a<sup>-1</sup>, much of the natural vegetation is composed of the ‘Kurdo-Zagrosian steppe-forest’ regime, mainly composed of *deciduous oak woodland*’ (*xerophilous deciduous Quercus brantii Lindl*) at lower altitudes and Pistachio scrubland (*Pistacia- Amygdalus* (almond) (Zohary, 1973).
- 3) At altitudes of above c.2,000m which marks the approximate location of the upper timber line low temperatures inhibit the growth of steppe-forest vegetation, and therefore sub-alpine plants dominate the vegetation assemblage (Zohary, 1973).
- 4) In other specific areas that are in close proximity to or can access plentiful and perennial supplies of freshwater, (i.e. river or lake sides), steppe-grasslands in more arid zones give way to riverine forest environments. This is made up of ash (*Fraxinus*), willow (*Salix*, e.g. *acmophylla*) and poplar (*Populus*, e.g. *euphratica*) (Charles et al., 2010).

While, these vegetation analogues are based on annual rainfall amount and temperature, it is important to note that many species, including oak, are susceptible to changes in the seasonal distribution of rainfall, such as the amount of rainfall in spring, which is potentially more important than absolute annual rainfall amount (Zohary, 1973; El-Moslimany, 1986). Furthermore, some researchers suggest that caution should be taken when using modern analogues as they may not be truly ‘*pristine*’ environments and may themselves be largely the result of anthropogenic impact, rather than “natural climax vegetation” (Asouti and Kabukcu, 2014).

## 2.4 Summary

This chapter has provided a brief review of the modern-day climate and environment of the EFC. The climate of the region is primarily controlled by the interaction and seasonal behaviour of North Atlantic and tropical atmospheric systems. The position and strength of these systems throughout the year causes a distinct seasonal disparity in the distribution of rainfall and results in the semi-arid conditions of the

region. Subtle changes in the behaviour of these systems and associated climate indices, such as the NAO, makes the region highly susceptible to precipitation variability. The combination of precipitation and altitudinal gradients has resulted in distinct ecological zones to exist in the EFC. In the next chapter I will explore how these systems and conditions are currently understood to have changed in the past and the methods employed examine these changes.

### **3 Palaeoclimate of the EFC and Southwest Asia**

In this chapter I will review the current understanding of Holocene climate change and variability in the EFC, as well as wider Southwest Asia, to provide the historical research context for the work carried out in this project. To do this, I will look at records from the Levant, Turkey, and Iran. However as discussed in the previous chapter, Southwest Asia has a highly heterogeneous climate and therefore it is possible that conditions represented by these records do not truly reflect those of the EFC. As I will show in this chapter, it is necessary to look at these records due to the absence of detailed Holocene-long palaeoclimate records from the EFC (Figure 6) and filling this spatial gap is a major aim of this thesis. By examining these records, it will also highlight current gaps and inconsistencies in research, as well as spatial variability in conditions, which this project will also hope to address.

Before I review this previous work, I will provide a summary of some fundamental principles associated with palaeoclimate research that need to be considered in this project, as well as an outline of methods used to investigate past climate and environmental change.

#### **3.1 Causes of Past Climate Change**

A key aim for any palaeoclimate or palaeoenvironmental investigation is to understand the primary driver(s) for observed local, regional, or global changes in climate and/or the environment. Therefore, it is necessary to understand the processes which ultimately govern the Earth's climate, which will be briefly summarised here. Causes for climate variability (so-called Forcings) can be divided between those which are external, occurring outside the earth system (e.g., orbital change, solar output) and internal mechanisms, which exist within the earth system (e.g., global ice sheet cover, greenhouse gas emissions, vegetation) ultimately responding to external processes through complex feedback mechanisms. Causes for glacial and interglacial cycles and multi-millennial scale variability are predominantly related to cyclical changes in the Earth's orbital parameters, which influence the amount and distribution of solar energy reaching the Earth. Three orbital cycles with varying lengths, known as Milankovitch cycles, have been identified (Berger, 1988; Roberts, 2014):

- Orbital eccentricity (*c.*100,000-year cycle) - Refers to the extent to which the Earth's orbit around the sun deviates to and from a complete circle and is the only one of the three cycles which causes the earth to receive different absolute amounts of solar radiation.
- Axial tilt (*c.*41,000-year cycle) - Also known to as obliquity, refers to the variability of the earth's angle in respect to its orbital plane, which varies between 22.1° and 24.5° over the cycle.
- Precession (*c.*21,000-year cycle) - Refers to the changes in the orientation of the earth axial tilt. Both axial tilt and precession alter the seasonal distribution of solar energy between the southern and northern hemisphere.

These cycles are superimposed on, and combine with, one another which make patterns in past climatic changes complex (Berger, 1992). On the Holocene timescale that this project is concerned with, the precession cycle has had the most significant influence on changes in the Earth's climate. More specifically, as the length of the Holocene is essentially half of the precession cycle, at the beginning of the Holocene the cycle lay at the other end of the sequence than it does today (i.e. the perihelion occurred in July rather than January, as it is today) and therefore northern hemisphere summers now occur when Earth is farthest from the sun, whereas at *c.*10,000 yr BP the northern hemisphere summers occurred when Earth was closest to the sun and would have been receiving *c.*8% more solar radiation than it does currently (Roberts, 2014).

On shorter timescales during the Holocene (annual to multi-centennial periods), perhaps the most significant causes of climate change is variability in solar output (solar irradiance) superimposed on long-term changes in insolation (Steinilber et al., 2012), but volcanic aerosols and other greenhouse gas emissions have also had an important influence (Mayewski et al., 2004). Another cause for significant short term climate events, particularly during the early Holocene, have been delayed mechanisms related to deglaciation, for instance abrupt global cold and dry events at *c.*9,200 and *c.*8,200 yr BP (Chapter 3.3.2.2) are linked to the expulsion of large amounts glacial meltwater from ice dammed lakes disrupting thermohaline circulation in the North Atlantic (Rohling and Pälike, 2005; Fleitmann et al., 2008).

While these orbitally induced climatic changes are reasonably well understood (e.g., Steinhilber et al., 2009, 2012), it is the impact these changes have on regional atmospheric dynamics that determine regional and local climatic conditions. This is particularly important in areas like Southwest Asia which are located in transitional zones between multiple systems (e.g. North Atlantic or Monsoonal systems), as discussed in the previous chapter. Most long-term changes in hydrological conditions in Southwest Asia can be attributed to variations in these regional climate dynamics (Jones et al., 2019), either because they have been strengthened, weakened and/or shifted position. However, there is still much debate about how these systems interacted and responded to forcing mechanisms during the Holocene (e.g., Djamali et al., 2010; Sharifi et al., 2015).

## **3.2 Sources of Palaeoclimate Information**

### **3.2.1 Palaeoclimate Archives**

To investigate past climate and associated environmental change and variability, it is necessary to examine suitable materials that record past fluctuations in conditions; materials which do this are known as palaeoclimate archives. Common palaeoclimate archives are ice cores, tree rings, lake sediments and speleothems. These archives contain chemical or physical characteristic(s) which, while do not act as a direct recorder of past environmental change (such as a thermometer, rain gauge or barometer), are thought to be influenced by such changes and can act as a substitute when trying to reconstruct past climates or environments (e.g., temperature, available moisture, ecology) (Fairchild & Baker 2012). These characteristics are known as proxies and can be analysed and measured through a variety of chemical or visual methods by investigators. However, the interpretation of these proxies is often not straightforward and is one of the major challenges when examining a palaeoclimate archive.

### **3.2.2 Palaeoclimate Modelling**

An alternative approach to investigate past climate change is the application of computer-based palaeoclimate simulations. Palaeoclimate models assess how the climate may have varied based on the understanding of how local, regional and global climate dynamics change in response to known, or estimated, variations in forcing mechanisms such as solar radiation, greenhouse gas concentrations and ice-sheet cover (Brayshaw et al., 2011a). The use of palaeoclimate models, in combination with proxy

studies, have a number of benefits. Firstly, they can provide an insight into climate variation in areas which are poorly covered by palaeoclimate proxy reconstructions. Secondly, the ability to simultaneously examine change on a local, regional and global level, as well as experiment with different inputs, can provide a clearer understanding of the different atmospheric processes which may have caused past climate variation. Finally, they can be used to help address conflicting palaeo-proxy interpretations. A number of palaeo-modelling studies investigating Holocene climate in the Eastern Mediterranean were performed as part of the *Water, Life and Civilisation Project* at the University of Reading using the Hadley Centre HadSM3 global climate model (Black et al., 2010; Brayshaw et al., 2011a; Mithen and Black, 2011). Therefore, these studies can also be used, in combination with proxy data, to help provide an insight in past climate variations during the Holocene in the Fertile Crescent.

### 3.2.3 Existing Palaeoclimate and Palaeoenvironmental Data from Southwest Asia

Finding suitable palaeoclimate archives is a notable problem in continental, semi-arid regions like Southwest Asia. Here, the main types of archive currently available which cover the entire or most of the Holocene are lake sediments and speleothems. Within this, some geographical areas are much better spatially covered than others (Finné et al., 2011) (Figure 6). Those relatively well covered include the Levant (particularly Israel) and Turkey, while Iraq is void of any high-resolution records that cover the majority of the Holocene; in fact it is only very recently that any high resolution, precisely dated records from the country have been produced at all (Flohr et al., 2017; Amin Al-Manmi et al., 2019; Sinha et al., 2019). This disparity in spatial coverage is partly the result of the availability of archives (e.g. lakes are found in wetter areas), but it is also largely down to a general research bias toward some regions, often because socio-political problems throughout much of the 20<sup>th</sup> and early 21<sup>st</sup> century have hampered academic research of all kinds in countries like Iraq and Iran.

Key Holocene, or near-Holocene, long palaeoclimate records from Southwest Asia which exist are summarised in Table 1 and visualised geographically in Figure 6. Here, the main paleoclimatic information that can be retrieved from the different types of archive available in Southwest Asia will be summarised and then the existing records will be reviewed.

### 3.2.4 Lake Sediment Records

The analysis of sediment cores taken from lakes is by far the most intensively studied type of archive in Southwest Asia with a number of lake sediment records distributed throughout the region. Historically, pollen analysis (*palynology*) has been the most widely applied method to investigate past environmental conditions within lake sediments (e.g. van Zeist and Wright, 1963; Zeist and Bottema, 1977). The analysis of pollen grains allows for the reconstruction of past vegetation around the lake. The type and abundance of vegetation is, prior to strong human influences, related to climate and environmental conditions, particularly rainfall and temperature. Therefore, based on modern day understanding of environmental thresholds (e.g. Chapter 2.3) for different plant taxa, pollen analysis can be used to produce palaeorainfall estimates (Roberts 2000). However, anthropogenic activities can also have a significant or dominant impact on vegetation, and this can mask or modify any climatic signal (Roberts et al., 2004), although this can be itself useful for archaeological purposes when looking at land use change (e.g. England et al., 2008). Low pollen preservation rates in many areas of Southwest Asia can limit the spatial and temporal coverage of palynological studies.

Hydrologically closed lakes from semi-arid regions like Southwest Asia, where evaporation exceeds precipitation, will often contain saline water and have variable water levels. Both salinity and water level are dependent on the balance between evaporation (output) and precipitation (input) commonly referred to in terms of the precipitation/evaporation ratio (P:E). There are a number of geochemical and geomorphological indicators that can be used to reconstruct past fluctuations in this water balance (Roberts et al., 2012). Notably, this includes the analysis of oxygen isotopes ( $\delta^{18}\text{O}$ ) of bulk carbonates found within lake sediments, which has arguably replaced pollen as the main proxy to reconstruct past changes in hydrological conditions. The analysis of authigenic carbonates is probably the most frequently studied parameter in lake sediments for isotope analysis, but the analysis of biogenic (skeletal carbonates such as shells) is also common practice (Leng and Marshall, 2004). The  $\delta^{18}\text{O}$  of lake water responds to water balance similarly to salinity and lake level (higher  $\delta^{18}\text{O}$  during periods of increased evaporation, lower  $\delta^{18}\text{O}$  during periods of increased precipitation/freshwater flux) and therefore can be used as a proxy for water balance (P:E) (Leng and Marshall, 2004). However, the specific causal

controls will differ between sites, mainly reliant on how closed or open the lake system is. There are also other controls on lake  $\delta^{18}\text{O}$  values that need to be considered, this includes seasonality (Stevens et al., 2001, 2006; Dean et al., 2018) and changes in the isotopic composition of the moisture source (Develle et al., 2010), which is investigated in greater detail in Chapter 5. A major benefit of this proxy is the ability to examine  $\delta^{18}\text{O}$  values in multiple types of archive (lake, marine, speleothem), and therefore it provides a ‘*common currency*’ to compare palaeoclimate reconstructions of different material types (Roberts et al., 2017, p. 4).

An additional and increasingly more common proxy that has been investigated in lake sediments is the relative abundance of trace metals in sediments. For instance, Lemke and Sturm (1997) use Mg/Ca ratios from Lake Van as a proxy for hydrological conditions. More recently, the use of high-resolution XRF core-scanners has seen the production of high resolution, trace element geochemical analysis of lake sediment cores (Sharifi et al., 2015; Ön et al., 2017). This has been particularly useful to develop dust records, a proxy for local or regional aridity. Furthermore, the use of core scanners to produce high resolution records overcomes one of the main limitations of lake sediment records (temporal resolution). Other types of proxies from lake sediment cores include geological (e.g. grain size), diatom, plant macrofossil and charcoal analysis (Wasylikowa et al., 2006; Roberts, 2014).

Methods used to date lake sediments include radiocarbon ( $^{14}\text{C}$ ) dating of organic material or U-Th dating of lake carbonates. However, the lack of suitable dateable material in lake sediments (e.g., charcoal for  $^{14}\text{C}$  or closed system carbonates for U-Th dating) often makes the construction of robust age models difficult and even when organic material is present, other problems such as the reservoir or hard water effects may limit the accuracy and reliability of dates. Additionally, it is difficult to construct high-resolution (annual or near-annual) records (although as stated the use of core scanners is changing this) using lake sediments making the identification of short-term, sudden palaeoclimate variability hard to identify. However, where annual varves exist and can be counted, they can greatly improve the accuracy of lake sediment age models and temporal resolution (Wick et al., 2003; Jones et al., 2006). This approach has in rare cases, allowed for the comparison between lake sediments and instrumental records, greatly helping the ability to interpret proxy information correctly (Jones et al., 2006).

#### 3.2.4.1 Existing Lake Sediment Records from the EFC and Southwest Asia

Research into lake sediments in the EFC extends relatively far back in time (e.g. van Zeist and Wright, 1963). Pioneering work was carried out by the American geologist H.E Wright in association with the Iraq-Jarmo Archaeological Project, headed by Robert and Linda Braidwood in the 1950s and 1960s. Wright, along with Dutch palynologist Willem Van Zeist, carried out palaeoenvironmental research on a number of lake sediments to help provide the environmental context for the emergence of agriculture in the region, which at the time was thought to have coincided with the end of the LGM (Wright 1962; 68). The most successful of these studies was the analysis on sediment cores from Lake Zeribar in the Iranian Zagros (Figure 6), the first detailed palaeoenvironmental record covering the Pleistocene-Holocene transition in the region (van Zeist and Wright, 1963; van Zeist and Bottema, 1991). Other lakes that were intensively investigated in the Iranian Zagros by the same or related teams include Lake Urmia (Bottema, 1986; Djamali et al., 2008) and Lake Mirabad (Figure 6) (van Zeist and Bottema 1977). Since the 1970s research in the Zagros region of Iran has been limited, therefore much of our current palaeoenvironmental understanding is still dependent on these early investigations. However, developments in analytical techniques have allowed the re-examination of the same cores with new methods, such as the utilisation of stable isotope analysis of lake carbonates; firstly, at Lake Zeribar (Stevens et al. 2001) and then Lake Mirabad (Stevens et al. 2006), as well as plant macrofossil and diatom analysis (Wasylikowa, 2005a; Wasylikowa et al., 2006). These Iranian lake records ultimately provide the closest existing studies to the study region of this thesis and therefore provide important records to compare any data produced in this project to.

Other important lake sediment records from Southwest Asia include a record from Neor Lake in northern Iran (Figure 6) (Sharifi et al., 2015), which is an unusually highly resolved and well dated multi-proxy lake sediment record. However, this record found on the coast of the Caspian-sea, is more heavily influenced by the Siberian anticyclone system than the rest of the study region and therefore could well be responding to changes in the behaviour of climate systems that are less dominant in the rest of Southwest Asia. Central and southern Turkey host a number of lake bodies that have been intensively studied for palaeoenvironmental purposes. Perhaps the most intensively studied is Lake Van

in the south-east of the country (Lemcke and Sturm, 1997; Wick et al., 2003) (Figure 6) and located fairly close to the EFC. Other paleoenvironmental studies have examined lake sediments from lakes Eski Acigöl (Roberts et al., 2001) and Lake Nar (Jones et al., 2006; Dean et al., 2015) in central Turkey. Perhaps the most comprehensive palaeoclimate work has been carried out in the Levant. Lake Sediment records that cover the late Pleistocene and Holocene in the Levant include the Ghab Valley in Syria (e.g. Niklewski and Van Zeist, 1970; van Zeist and Woldring, 1980; Yasuda et al., 2000), the Hula Basin in northern Israel (e.g. Horowitz, 1974; van Zeist et al., 2009), the Birkat Ram crater lake also in northern Israel (e.g. Schwab et al., 2004) and the Dead Sea (Migowski et al., 2006; Litt et al., 2012) and more recently, geochemical analysis on a lake sediment collected from Yammoûneh Lake, Lebanon (Develle et al., 2010).

### 3.2.5 Speleothems

The use of speleothems as a palaeoclimate archive in Southwest Asia extends relatively far back into the 1990s with the pioneering work of Miriam Bar-Matthews and her team in Israel (Bar-Matthews et al., 1996). Speleothems have two main advantages over most lake sediment records<sup>1</sup> in that they can be precisely dated via U-series dating methods and are routinely sampled for proxy data at a very high temporal resolution (potentially sub-annual). Commonly investigated proxies from speleothems include oxygen and carbon isotopes and trace elements. A more detailed description of speleothem geochemistry and the interpretation of their proxies is covered in Chapters 4 and 5.

The ability to produce very well dated, high resolution records make speleothem records very suitable candidates to examine the timing of rapid climate change events, human-environmental relationships and palaeoclimate teleconnections. While speleothems are now commonly used to examine regional Holocene climate variability in Southwest Asia, this has predominantly been done using the only two speleothem records that cover the entire Holocene in the region, Soreq Cave in Israel (Bar-Matthews et al., 1997) and Jeita Cave in Lebanon (Figure 6) (Verheyden et al., 2008; Cheng et al., 2015). Although

---

<sup>1</sup> Although, the investigation of lake sediments have themselves advantages over speleothems, particularly when examining past ecological changes.

very recently a new speleothem from Katakhor Cave in Iran has been produced which provides the first, near-Holocene long speleothem record from just east of the EFC (Figure 6) (Andrews et al. 2020). However, like lake sediments the interpretation of proxies from speleothems is not always straightforward, and many mechanisms must be taken into consideration (again outlined in further detail in Chapters 4 and 5).

Name	Type	Lat (E)	Lon (N)	Key Proxies	Selected References
Eski Acigöl	Lake	34.54	38.55	Pollen, $\delta^{18}\text{O}$	(Roberts et al., 2001; Jones and Roberts, 2008)
Nar	Lake	34.46	38.34	Pollen, $\delta^{18}\text{O}$	(Jones et al., 2006; Dean et al., 2015, 2018)
Ghab	Lake	36.25	35.65	Pollen	(Yasuda et al., 2000)
Yammouneh	Lake	36.00	34.06	Pollen, $\delta^{18}\text{O}$	(Develle et al., 2010)
Dead Sea	Lake	35.39	31.47	Pollen, Lithology	(Migowski et al., 2006; Litt et al., 2012)
Van	Lake	43.00	38.50	Pollen, $\delta^{18}\text{O}$ , Mg/Ca	(Lemcke and Sturm, 1997; Wick et al., 2003)
Urmia	Lake	45.47	37.58	Pollen, $\delta^{18}\text{O}$	(Bottema, 1986)
Neor	Lake	48.56	37.96	XRF, $\delta^{13}\text{C}$ , $\delta\text{D}$	(Sharifi et al., 2015)
Zeribar	Lake	46.11	35.13	Pollen, $\delta^{18}\text{O}$	(van Zeist and Bottema, 1977; Stevens et al., 2001; Wasylkova et al., 2006)
Mirabad	Lake	47.72	33.08	Pollen, $\delta^{18}\text{O}$ , Sr/Ca	(van Zeist and Bottema, 1977; Stevens et al., 2006)
Jeita	Speleothem	35.65	33.95	$\delta^{18}\text{O}$ , $\delta^{13}\text{C}$ , Sr/Ca	(Verheyden et al., 2008; Cheng et al., 2015)
Soreq	Speleothem	35.02	31.76	$\delta^{18}\text{O}$ , $\delta^{13}\text{C}$ , Sr/Ca	(Bar-Matthews et al., 1997, 2003; Bar-Matthews and Ayalon, 2011)
Katakhor	Speleothem	49.51	35.85	$\delta^{18}\text{O}$ , $\delta^{13}\text{C}$	(Andrews et al., 2020)

Table 1: Information of key Holocene or near-Holocene long palaeoclimate records discussed in this chapter with key proxies used in their examination alongside their key references.

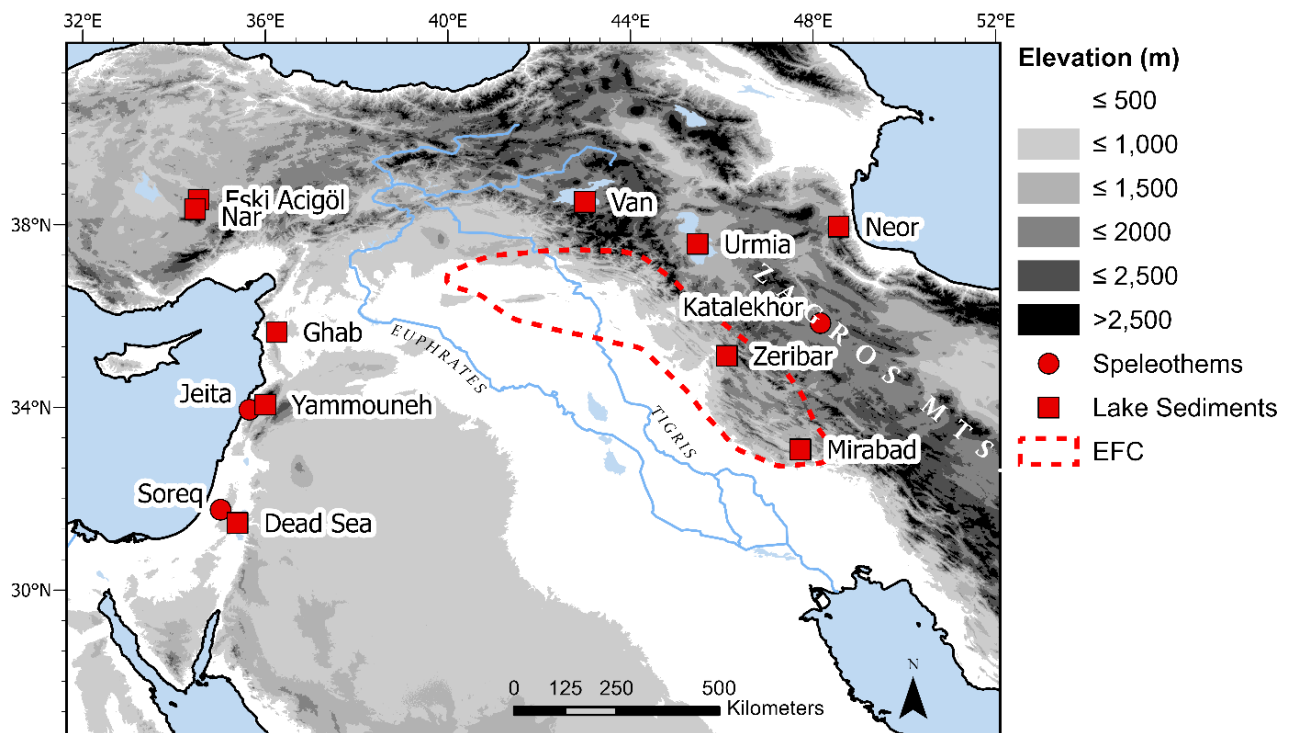


Figure 6: The location of existing Holocene or near Holocene long palaeoclimate records collected from Southwest Asia that are discussed in this chapter. Red dotted line is the study area of this project, showing that only two lake sediment records are currently present in the region.

### **3.3 The Climate of Southwest Asia from 20,000 yr BP to Present: Current Understanding**

Using the records identified in the previous section, I will now summarise the current understanding of palaeoclimate change and variability in Southwest Asia, beginning with a quick summary of conditions during the late Pleistocene and then a more in-depth examination of Holocene conditions. Reviewing the existing palaeoclimate data is not a straightforward task as each proxy and record comes with its own limitations; they can often provide different and even conflicting signals which means that each investigation's interpretation of conditions differs slightly or very significantly, which may be the result of real heterogeneous conditions or the result of the inherent challenges in interpreting the proxy signals accurately.

#### **3.3.1 Late Pleistocene Palaeoclimate**

While not the focus of this thesis, to correctly provide the right context for Holocene palaeoclimate change, the following discussion provides a general overview of palaeoclimate conditions during the last deglaciation period (*c.* 20,000 – 11,650 yr BP).

The last glacial period (also known as the LGM) reached its peak between *c.* 25,000 – 18,000 years ago. Conditions at this time throughout Southwest Asia were thought to be both much colder and more arid than present. In the isotopic data, this is characterised by their most positive  $\delta^{18}\text{O}$  values in all records from the region. Deglaciation after this, as the world's major ice sheets retreated and thinned, was characterised by a generally ameliorating climate, leading to warmer and wetter conditions in Southwest Asia, which includes a particular warm and wet period known as the Bølling-Allerød interstadial (*c.* 14,550 and 12,850 yr BP) (Rasmussen et al., 2014). This amelioration in climate was, however, interrupted by the Younger Dryas, a late glacial climatic reversal, which according to Greenland ice core chronologies occurred between 12,850 – 11,650 BP (Rasmussen et al., 2014).

For a more specific examination of conditions in the EFC, the only record that covers this period is the Zeribar lake sediment record from Iran. During the LGM,  $\delta^{18}\text{O}$  values from lake carbonates at Lake Zeribar are at their most positive (*c.* -1‰ VPDB). Pollen assemblages from Lake Zeribar and Lake Urmia are dominated by *Artemisia* and Chenopodiaceae and there is an absence of arboreal tree pollen

(e.g., *Quercus*, *Pistacia*). This represents a steppe/semi-desert type environment representative of arid and cold conditions (Freitag, 1977), and is also corroborated by plant macrofossil (Wasylikowa, 2005b; Wasylikowa et al., 2006) and diatom assemblages from the core (Snyder et al., 2001). Records from across the Southwest Asia indicate that these ecological conditions were pretty much ubiquitous across the wider region during the LGM, with the exception of small areas of refugia in the lower Levant (Asouti and Austin, 2005; Asouti et al., 2015). Following the LGM, the Zeribar  $\delta^{18}\text{O}$  record displays a steady shift toward more negative  $\delta^{18}\text{O}$  values indicating increasing moisture availability during the late glacial period. Wetter conditions are also indicated by the presence, albeit small, of pistachio in the pollen assemblage and a decrease in *Artemisia*. This wetter phase broadly coincides with the Bølling–Allerød oscillation (c.14,550 and 12,850 yr BP). However, the pollen assemblage is still dominated by steppe vegetation and arboreal pollen is present, suggesting a rather dry and cold climate persisted. This persistence of steppe conditions is in contrast to the situation in the Levant where steady afforestation seems to be occurring during the late glacial period (Asouti & Kabukcu 2014). The Younger Dryas is identifiable in the Zeribar isotope record as a shift to more positive  $\delta^{18}\text{O}$  values (Figure 7), an increase in diatom-inferred conductivity (Snyder et al., 2001) and plant macrofossil evidence that indicates increased salinity and lower lake levels (Wasylikowa 2005). The timing of the Younger Dryas in the Lake Zeribar record (c.14,000 and 12,000 yr BP) and Lake Van record (c.11,620 and 10,460 yr BP) occur slightly earlier and later, respectively, than the now recognised timing of the global climate event (c.12,850 – 11,650), this is likely due to poor chronologies of the two lake records (e.g. the Lake Van record has missing varves) rather than the climatic events occurring at different times.

### 3.3.2 Holocene Climate Change and Variability

The Holocene is the present current interglacial period and is defined by North Greenland Ice Core Project's NGRIP2 ice core to have begun c.11,650 Yr BP, following the termination of the Younger Dryas (Walker et al., 2009; Rasmussen et al., 2014). The Holocene can be characterised by warmer and more stable climatic conditions, globally, relative to the preceding glacial phase of the late Pleistocene. However, there is clear evidence of both long-term change and short-term variability in Holocene climate (e.g. Wanner et al., 2015). From an archaeological perspective, the Holocene also encompasses

the time-period in which, for the only time in the *c.*300,000 years of human history, populations shifted from nomadic, hunter-gatherer modes of living to the large-scale, agriculturally supported, and industrial, urban lifestyles many humans inhabit today, a process which has occurred within a relatively short period of *c.*10,000 years. For this reason, understanding the nature of Holocene climate change and variability is crucial in order to provide the environmental context in which these cultural developments occurred. This section will summarise the nature of Holocene climate change and variability in Southwest Asia examining both long-term change and short-term fluctuations. The section will also examine the evidence of vegetation change in the Holocene, particularly during the early and middle Holocene (where there is less human interference), using pollen and plant macrofossil data collected from lake sediments in the EFC.

#### 3.3.2.1 Long Term, Millennial Scale Trends

The beginning of the Holocene is characterised by a period of climate amelioration (i.e., shift to wetter conditions) following the end of the Younger Dryas (*c.*11,650 yr BP), indicated by a change from higher to lower  $\delta^{18}\text{O}$  values in isotope records (Figure 7). The speed and nature of this climate improvement varies between records. For instance, at the central Turkish lakes, Nar and Eski Acigöl,  $\delta^{18}\text{O}$  values shift rapidly and reach their most negative values of the entire Holocene within a matter of centuries and suggest the climate recovered rapidly after the end of the Younger Dryas (Roberts et al., 2001, 2016; Dean et al., 2015). On the other hand,  $\delta^{18}\text{O}$  values from Levantine speleothems and lake sediments from the EFC display a slower rate of recovery between *c.*11,650 – 10,000 yr BP (Bar-Matthews et al., 1997; Cheng et al., 2015).

After this recovery, all  $\delta^{18}\text{O}$  records from Southwest Asia are characterised by relatively low values between *c.*10,000 and *c.*7,000 yr BP. For this reason, several studies have suggested that this period of the Holocene represents a time of optimal climatic conditions, referred to variously as the ‘*Holocene climate optimum*’ (Rohling and De Rijk, 1999), ‘*Holocene wet phase*’ (Robinson et al., 2006, p. 1522) and the ‘*Levantine moist period*’ (Weninger et al., 2009, p. 21). This wet period coincides with a period of maximum summer solar insolation in the northern hemisphere, which is thought to have resulted in more intense and southerly positioned westerlies penetrating the region, alongside increased

cyclogenesis in the Eastern Mediterranean, ultimately leading to higher amounts of rainfall (Dean et al., 2015). Increased solar insolation also resulted in the northward migration of the mean latitudinal position of the ITCZ during the summer months, resulting in increased Indian Ocean and African Monsoon precipitation in the Arabian peninsula and northern Africa (Fleitmann et al., 2007; Weldeab et al., 2007; Hennekam et al., 2014). As a consequence, wetter conditions in northern Africa resulted in the ‘*Greening of the Sahara*’ (Tierney et al., 2017) as well as increased freshwater runoff into the Mediterranean (e.g. via the Nile), contributing to sapropel formation in the eastern Mediterranean between 10,100 and 6,400 yr BP (Rohling et al., 2013; Hennekam et al., 2014).

Other evidence for moist conditions in Southwest Asia during this time, in addition to  $\delta^{18}\text{O}$  datasets, are provided by the Soreq Cave  $\delta^{13}\text{C}$  record which shows a large amplitude positive shift of  $\sim 8\%$  (Figure 7), which is explained in terms of periods of heavy rains (deluge events) which limited soil water interaction (Bar-Matthews et al., 1997, 2003). Cheng et al., (2015) use  $\delta^{13}\text{C}$  and Sr/Ca from the Jeita Cave speleothem record as their main proxies for moisture availability and these indicate that the early to middle Holocene was a period of relatively high moisture availability, although reaching a peak around 7,000 – 6,000 yr BP, indicating optimum conditions slightly later than most of the  $\delta^{18}\text{O}$  profiles. Hydrogen isotopic composition ( $\delta\text{D}$ ) of Alkanoic acids from Lake Neor in Northern Iran also show a broadly similar trend to  $\delta^{18}\text{O}$  records from the Southwest Asia, with the most negative  $\delta\text{D}$  values identified c.9,000 yr BP. The interpretation of low  $\delta^{18}\text{O}$  values from the Katakhor speleothem from Iran during this time period is also supported by changes in speleothem growth rate and uranium isotope data (Andrews et al., 2020).

However, there have been some studies, particularly from the EFC, which have suggested that this period may not have been as wet as these isotopic studies suggest. Mg/Ca data from Lake Van, a proxy for effective moisture, do not display their most optimum values (low Mg/Ca) until after 7,000 yr BP, and therefore the period beforehand may have been relative dry (Wick et al., 2003). Moreover, while similar trends in the  $\delta^{18}\text{O}$  timeseries are identified at lakes Zeribar and Mirabad in the Iranian Zagros with the records from the rest of Southwest Asia (Figure 7), the  $\delta^{18}\text{O}$  variability in these lake records were initially interpreted to represent changes in seasonality rather than changes in the amount of

rainfall (Stevens et al., 2001, 2006). Specifically, Stevens et al., (2001; 2006) suggest lower  $\delta^{18}\text{O}$  values reflect an increase in the relative amount of precipitation falling in the winter months compared to spring rainfall, as winter rainfall has lower  $\delta^{18}\text{O}$  values than spring precipitation. Consequently, based on this interpretation, low  $\delta^{18}\text{O}$  values between c.10,000 – 7,000 yr BP represent increased seasonality rather than a change in rainfall amount.

Discrepancies in the interpretation of  $\delta^{18}\text{O}$  records from the region does not solely apply to records from the EFC. For example, the  $\delta^{18}\text{O}$  profile of Jeita Cave is broadly similar to that of the Soreq cave record, but is interpreted in terms of changes in the isotopic composition of the source of moisture rather than moisture availability (Cheng et al., 2015). Develle et al. (2010) argues similarly to Cheng et al (2015) that the so-called source effect has a large influence on  $\delta^{18}\text{O}$  values for Lake Yammouneh in Lebanon but suggests this was amplified by increased precipitation during the early Holocene. The correct interpretation of the trend observed in  $\delta^{18}\text{O}$  records during the early to middle Holocene is still a matter of ongoing debate (Jones and Roberts, 2008; Develle et al., 2010; Rohling et al., 2015; Dean et al., 2018), which is explored further in Chapter 5 of this thesis.

After c.7,000 yr BP, it is widely accepted that the climate of Southwest Asia enters a period of transition from wetter to drier conditions characterised by a shift from lower to higher  $\delta^{18}\text{O}$  values in palaeoclimate records from the region, although the exact timing and nature of this shift varies between records. This shift to drier conditions is sometimes referred to as the '*Middle Holocene Environmental Transition*' (Roberts et al., 2011) and coincides with a shift toward increasing aridity across northern hemisphere sub-tropics and cooler conditions at higher latitudes related to decreasing solar insolation (Clarke et al., 2016). Alongside the  $\delta^{18}\text{O}$  profiles, other proxy-data from palaeoclimate records provide evidence of a shift to drier conditions. In the Jeita Cave speleothem record, the middle Holocene transition is marked by two abrupt jumps in the  $\delta^{13}\text{C}$  and Sr/Ca at c.5,900 and c.5,300 yr BP (Cheng et al., 2015). Evidence of drier conditions is provided by increased dust deposition from 6300 to 5000 yr BP in the Neor Lake record in Iran and a shift to more positive  $\delta\text{D}$  values (Sharifi et al., 2015). On a wider regional scale, decreasing summer solar insolation resulted in the migration of the ITCZ southward and a decrease in monsoon precipitation (Fleitmann et al., 2007) and, associated with a

weakening of the African monsoon, the end of the African humid period and Green Sahara phase c.5,500 years ago (Tierney et al., 2017).

However, once again some records from the EFC provide some disagreement to this consensus. While lake sediment isotope records see a shift from lower to higher  $\delta^{18}\text{O}$  values like other records from Southwest Asia, this has been interpreted by some studies to represent a relative increase in the amount of spring rainfall rather than a decrease in annual rainfall amount (Stevens et al., 2001, 2006), and for this reason conditions may have actually been relatively wet with optimum conditions reached between peak between c.5,800 and 4,300 yr BP. This interpretation appears to be supported by low Sr/Ca values at Lake Mirabad during this time as well (Stevens et al., 2006). However, the low  $\delta^{18}\text{O}$  values seen in the middle Holocene and Lake Zeribar and Mirabad could conversely represent drier conditions if the  $\delta^{18}\text{O}$  is interpreted to represent P:E balance (Jones and Roberts, 2008). Similarly, Mg/Ca values from Lake Van exhibit their lowest values between 6,000 and 4,000 which was interpreted to represent a period of optimum conditions (Wick et al., 2003). If these interpretations are correct for these records, a transition to drier conditions occurs much later around 4,000 yr BP. Again, this discrepancy does not necessarily solely apply to the EFC. For instance, there are some records from the Levant which suggest more favourable conditions during the middle Holocene. Lake level reconstructions from the Dead Sea suggests generally high lake levels between 6,300 yr BP and 3,500 yr BP which suggests increase precipitation into the lake and therefore wetter conditions in the Levant (Migowski et al., 2006; Litt et al., 2012).

After the transitional phase of the early Holocene,  $\delta^{18}\text{O}$  values stabilise for much of the rest of the Holocene which suggests conditions in Southwest Asia remain relatively dry resembling those of the present day. However, superimposed on this are periods of centennial scale variability between wetter and drier conditions.

The late Holocene is generally better covered spatially and temporally in terms of palaeoclimate data in Southwest Asia, with a number of annual or near annually resolved records now existing in the region covering some (Jones et al., 2006; Cook et al., 2016; Flohr et al., 2017) or all (Sinha et al., 2019) of this period. Within the last two thousand year a number of records have identified a long-term drying trend.

A high resolution record from Lake Nar indicates increasingly arid conditions during the last 1,700 years (Jones et al., 2006). A shift to more positive  $\delta^{18}\text{O}$  values in stalagmites from Soreq Cave. The long-term aridification trend is also supported by a continuous increase in dust content in Lake Neor sediments from Iran. A stalagmite from Gejkar Cave Iraq identified a similar long-term aridification trend which began c.1050 yr BP (Flohr et al., 2017). However, in the Jeita cave record, both the  $\delta^{18}\text{O}$  and  $\delta^{13}\text{C}$  are both relatively low and suggest wetter conditions persisted during this period (Cheng et al., 2015).

### 3.3.2.2 Short-term, Decadal to Centennial Climate Variability

While climatic conditions of the Holocene have been relatively stable compared to the preceding Pleistocene, the emergence of high-resolution datasets over the last couple of decades are beginning to clearly show the existence of rapid and abrupt climate variability (decadal to centennial scale periods of change). Notably, several investigations have proposed the existence of quasi-cyclical global climate variability which caused cooling in high latitudes and aridity in tropical and sub-tropical regions (like Southwest Asia) alongside major atmospheric changes. These reoccurring periods of climatic anomalies have become known as rapid climate change (RCC) events (Mayewski et al., 2004). Mayewski et al (2004) identified six intervals of abrupt global climate change: 9,000-8,000, 6000–5000, 4200–3800, 3500–2500, 1200–1000, ~600-150 yr BP (Figure 7).

There are thought to have been multiple causes for the observed global RCC events, which include changes in solar variability as well increases in volcanic aerosols or greenhouse gas emissions (Mayewski et al., 2004). Some of the events have also be closely associated with periods of increased ice rafting in the North Atlantic, known as ‘Bond Events’, potentially Holocene equivalents of the glacial Dansgaard–Oeschger cycles (Bond et al., 1997). Nine of these Bond events have been identified (Bond events 0 – 8) (Bond et al., 2001).

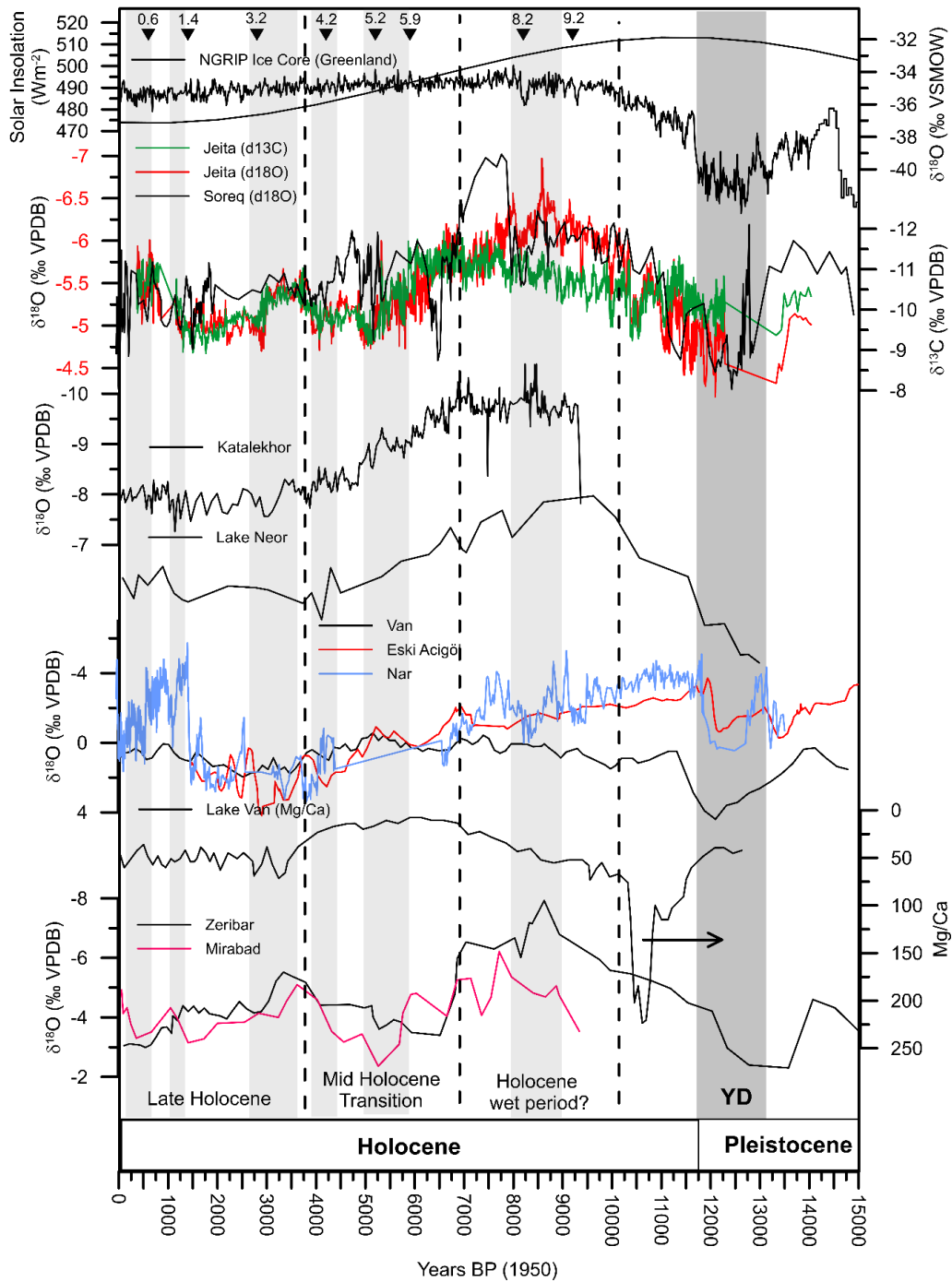


Figure 7: Main isotopic records from lake sediment and speleothem records (See Table 1 for references) from Southwest Asia alongside the NGRIP Ice core (Walker et al., 2009) and solar insolation record (Berger and Loutre, 1991). The majority of the Southwest Asian records have lower values between 10,000 and 6,000 yr BP, which has been used to suggest the existence of a Holocene wet period. Faded grey bars indicate periods of rapid climate change as identified by Mayewski et al., (2004). Black inverted triangles indicate timing of abrupt climate events which have been identified in a number of records from Southwest Asia. Also shown is the Mg/Ca record from Lake Van, which indicates a slightly later optimum period than the

isotope data. Black arrow marks where the Younger Dryas is visible in the Lake Van record in comparison to the actual timing of the event, demonstrating the large age errors associated with this record.

Identifying the duration, exact nature, and existence of the abrupt RCC events in Southwest Asia is a key aim for palaeoclimate and palaeoenvironmental studies in the region. There have been many investigations from the region which have identified the existence of cold, dry abrupt climatic shifts associated with these events at 8.2 (Bar-Matthews et al., 2003), 5.2 (Bar-Matthews and Ayalon, 2011; Clarke et al., 2016), 4.2 (Cullen et al., 2000; Staubwasser and Weiss, 2006; Kaniewski et al., 2018), 3.2 (Weninger et al., 2009), 0.6 ka BP, which have been linked with global RCCs and Bond events (Figure 7). There have also been some dry events, such as the 10.2 (Weninger et al., 2009) and 9.2 ka (Fleitmann et al., 2008; Dean et al., 2015) events, identified in records from the region which do not necessarily correspond to global RCCs. All of these cold, dry events have usually expressed themselves as, and identified by, a positive isotopic shift in  $\delta^{18}\text{O}$  records from the region.

However, while the existence of short-term variability within the Holocene is not disputable, the presence of these global and regionally synchronous, cyclical variations in, and the impact they had on, Southwest Asia is still a matter of ongoing debate and some have suggested that evidence of globally synchronous and periodic climate change events is weak (Wanner et al., 2008). One major problem is the often-large inconsistencies between different records regarding the identification and timing of dry events in records from the Southwest Asia. For example, the 4.2 ka dry event is arguably one of the most studied climatic events of the Holocene. It has been identified by a sharp peak in dolomite dust in a marine core from the coast of Oman (Cullen et al., 2000), isotopic shifts in lake sediments cores from Turkey (Eastwood et al., 2007; Dean et al., 2015) and most recently in increased dolomite dust deposition in a speleothem from Iran (Carolin et al., 2019). However, the event does not seem to present in high resolution speleothem records from the Levant (Bar-Matthews et al., 2003; Cheng et al., 2015) and similarly, Finne et al. (2011) in their review of palaeoclimate reconstruction from the Mediterranean, suggests that only two records from the whole Mediterranean show evidence of the event. The identification of these types of events is particularly challenging in areas like the EFC where there is a notable absence of high-resolution datasets which can be used to capture them.

The detection of abrupt events and understanding the nature and magnitude of them in Southwest Asia is particularly important from an archaeological perspective. Many of these events have been linked, sometimes controversially, to sudden changes in the archaeological record (Weninger et al., 2009). For instance, the 8.2 ka event has been linked to the collapse and abandonment of Neolithic sites (Staubwasser and Weiss, 2006; Weninger et al., 2006) and large-scale migration (Weninger et al., 2006). The 5.2 ka event has been linked to the decline of early Bronze Age societies in Mesopotamia, specifically of the Uruk culture phenomenon (Staubwasser and Weiss, 2006; Charles et al., 2010) and the 4.2 ka event has been linked to the collapse of the Akkadian Empire in Mesopotamia (Staubwasser and Weiss, 2006), as well as other Bronze Age societies across the eastern Mediterranean. However, some recent systematic studies have questioned the impact of some of these abrupt events on human societies (e.g. Wossink, 2009; Flohr et al., 2016; Lawrence et al., 2016; Palmisano et al., 2021).

The ability to sample speleothem proxies at a high resolution and precisely date them makes them a very suitable and advantageous archive to investigate the existence and magnitude of such climate change events (Fairchild and Baker 2012). The recent production of a few high resolution speleothem records from the EFC from Gejkar Cave (Flohr et al., 2017) and Kuna Ba Cave (Sinha et al., 2019) have started to provide a better understanding of short-term Holocene climate variability in the region. In the latter study, the presence of an abrupt dry event centred around c.2650 and 2500 yr B.P, whereas both studies show little evidence of an abrupt dry event centred around 600 yr BP and the last 100 years. While these two records have provided a better insight into the nature of short-term variability during the latter Holocene, there are still no high-resolution records from the EFC that extend continuously further back than 4,000 yr BP, which this current project hopes to address.

### 3.3.3 Evidence of Vegetation Change during the Holocene

Palynological studies of lake sediments in the EFC predominantly focus on the existence and relative abundance of three main plant types:

- Steppic herbs (*Artemisia* and *Chenopodiaceae*) which represent relatively dry conditions
- Grasses (*Poaceae*) (including cereal-types) representative of intermediate conditions

- Broad-leaf trees representing wetter conditions, of which oak (*Quercus*) and Pistachio (*Pistachia*) often receives the most focus (Roberts et al., 2017)

Using modern day understanding of their associated distribution within their annual rainfall analogues (e.g. Chapter 2.3), palynological studies can be used to estimate past moisture availability. Chenopodiaceae and *Artemisia* are often dominant in areas with less than 100mm of annual rainfall, grasses are more common in areas with between *c.*100 – 300mm, Pistachio (*Pistacia*) in areas with between *c.*300–500mm and deciduous oak (*Quercus*) in areas with more than *c.*500mm of precipitation (Rossignol-Strick, 1995).

The three main pollen sequences which cover the Holocene from or near the EFC are Lakes Zeribar, Urmia and Van, all three show generally similar patterns in vegetation changes during the Holocene. At the start of the Holocene there is an overall decrease in herb steppe vegetation and a sharp increase in grass pollen indicating a shift to wetter conditions following the Pleistocene. However, they show a very slow increase in arboreal pollen with oak concentrations in EFC lake record negligible until the middle Holocene, peak values are reached *c.*6,000 yr BP (Figure 8) and suggests that for much of the early Holocene the EFC was dominated by an open savannah type grassland landscape. Early studies of these pollen sequences suggested a relatively dry early Holocene (van Zeist and Bottema, 1977; Roberts and Wright, 1993), with precipitation not exceeding the threshold needed to support the expansion of broad-leaf tree forests. However, this understanding contradicts some of the evidence of more recent geochemical data for the lakes as discussed in the previous section indicating a wetter early Holocene period, which poses somewhat of a conundrum (See section 3.3.4 - 'The Early Holocene Precipitation Paradox'). This picture of vegetation change in the EFC is in contrast to that identified in the Levant and central Anatolia during the same period. Pollen sequences from sites such as Lake Ghab (Yasuda et al., 2000), Lake Huleh (Baruch and Bottema, 1999), Aammiq wetlands (Hajar et al., 2008) and Eski Acigöl (Roberts et al., 2001) indicate a quicker increase in arboreal tree species during the early Holocene in response to wetter and warmer conditions, which is in general agreement with the findings of isotopic data from lakes and speleothems in the region.

### 3.3.4 The Early Holocene Precipitation Paradox

The apparent discrepancy between oak pollen concentrations and  $\delta^{18}\text{O}$  values (Figure 8) from lake sediment records during the early Holocene represents one of the largest unsolved problem in paleoenvironmental studies in the EFC and has been discussed thoroughly a number of times in academic literature (e.g., Roberts, 2002; Jones and Roberts, 2008; Jones, 2013; Asouti and Kabukcu, 2014; Jones et al., 2019). As discussed in the previous section, early pollen studies of lake sediments from the EFC argued that low arboreal pollen quantities during the early Holocene were evidence of relatively dry conditions (van Zeist and Bottema, 1977; Roberts and Wright, 1993). However, more recent stable isotope data from paleolimnological studies exhibit lower  $\delta^{18}\text{O}$  values during the early Holocene, suggesting wetter conditions than present (Roberts *et al.* 2008), in agreement with conditions in the Levant and Anatolia.

The contradiction has been termed the '*early Holocene precipitation paradox*' (e.g., Stevens et al., 2006, p. 498; Jones, 2013). Archaeologically, this overlaps with the emergence and development of Neolithic farmers and pastoralists, these themselves are developments that have been linked to climate variability (See Chapter 11). Thus, answering this question is not only important from a palaeoenvironmental perspective, but also crucial if the correct environmental context is to be provided for these important archaeological developments. There have been many attempts to offer explanations for the contradiction. Perhaps most commonly, many studies have sought to identify other, non-climate related, mechanisms to explain the delay in the expansion of oak woodland. Roberts (2002) suggests that anthropogenic activity, both as a deliberate act of environmental management and accidental processes, would have impeded the expansion of oak woodland in the region. These activities may have included burning, woodland clearances and, indirectly, grazing by managed animal species (e.g. *Caprines*). This is to some extent supported by increases of charcoal, particularly of awn fragments from grasses in lake sequences (Wasylikowa et al., 2006).

Moreover alternative anthropogenic explanations exist. Asouti & Kabukcu (2014) suggest that 'oak park woodland' in the Central Zagros, rather than representing a type of natural climax vegetation type, is actually itself an anthropogenic vegetation type. They argue that early agriculturists in the region

caused the displacement of grasslands by grazing, cultivation and settlement expansion, similar to Roberts (2002). However, unlike Roberts (2002), they suggest that rather than impeding the expansion of arboreal species, these agriculturists actively selected for, maintained and managed the existence of oak woodland which was an important source of fuel and fodder (Asouti and Kabukcu, 2014). Over time, this would have led to the eventual displacement of grass and herb species in favour of oak and other arboreal species. Therefore, changing vegetation regimes during the early and middle Holocene represent the influence of human activity and agency, rather than, and masking, the impact climate variability would have had on the natural ecological landscape.

Other investigations have suggested that the ecological properties of the tree species themselves may have been responsible for the delay. Prior to the Holocene, pollen investigations suggest arboreal species in the region were rare or non-existent. As a result, due to their relatively slow rates of dispersal and the initial lack of suitable edaphic conditions (van Zeist and Bottema, 1991), it took a relatively long-time for arboreal species to spread from their glacial refugia (Roberts 2002). This would have caused a migratory lag between climate becoming suitable for their growth and the actual timing of their expansion into the region.

However, there have been studies which still maintain the lag in oak pollen is a response to climate variability and have therefore sought to explain alternative reasons for  $\delta^{18}\text{O}$  variation other than changes in effective moisture. For instance, as mentioned previously in this chapter, Stevens *et al.* (2001, 2006) interpreted changes in  $\delta^{18}\text{O}$  values as a shift in seasonality; arguing that lower  $\delta^{18}\text{O}$  values indicate a higher proportion of winter rainfall relative to spring rainfall. This interpretation is supported by other investigations which have suggested that an intensified monsoon system during the early Holocene would have shifted the sub-tropical high pressure belt further north and strengthened high pressure systems during spring, displacing moist mid-latitude westerlies and preventing them from reaching the region (Djamali *et al.*, 2010). Djamali *et al.* (2010) argue that spring rains only began to penetrate the region when the monsoon began to weaken during the middle Holocene, providing suitable conditions for the spread of oak woodland. Macrofossil data from Lake Zeribar also provide evidence wetter conditions during the middle Holocene rather than before (Wasylikowa *et al.*, 2006).

Moreover, similar patterns of a delay and subsequent expansion of arboreal pollen have also been identified in other parts of the Mediterranean, including Sicily (Sadori and Narcisi, 2001; Tinner et al., 2009) (Figure 8), Malta (Gambin et al., 2016) and Spain (Pantaléon-Cano et al., 2003). Therefore, the notion that anthropogenic activity would have led to identical responses in the environment in these different locations at the same time would be a remarkable coincidence, and the archaeological evidence to support large anthropogenic influences during the early Holocene in these regions is weak, with these ecological shifts occurring before or just around the arrival of Neolithic agricultural groups (Tinner et al., 2009) and therefore makes it difficult to assign anthropogenic explanations to these changes (Tzedakis, 2007). From a climate perspective however, these other areas are located at similar latitudes to the EFC and therefore are under the influence of similar climate regimes as each other and as a result adds support to the idea that a change in climate dynamics, related to enhanced summer insolation, was the cause of the delay as proposed by Djamali et al. (2010) and Tzedakis (2007).

Ultimately, a consensus is yet to be reached on the correct explanation for the paradox. Further palaeoclimate investigations, perhaps utilising alternative archives (such as speleothems) may be needed to answer it. It is possible that a combination of a number of, or all, the explanations provided have some basis in truth.

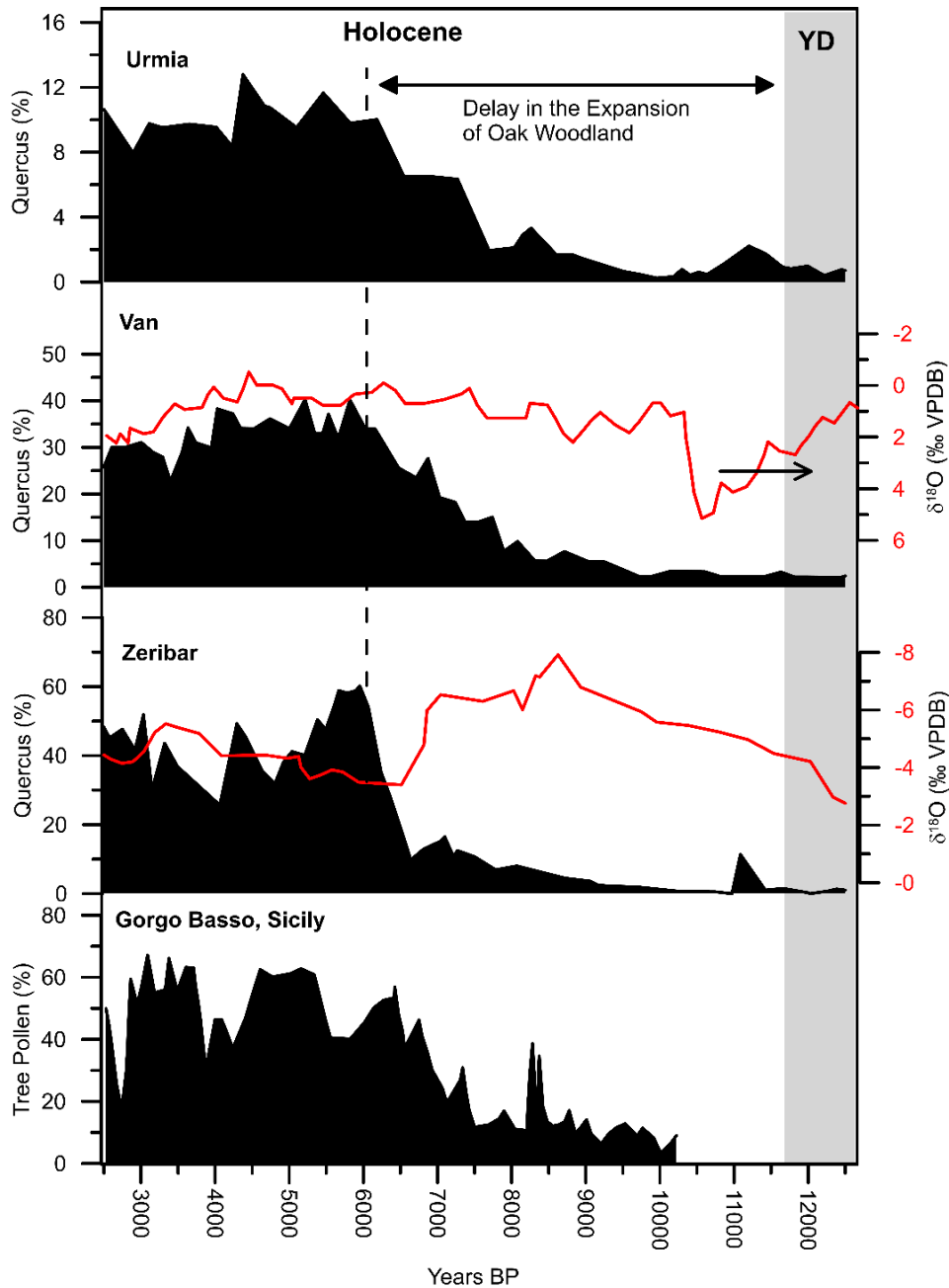


Figure 8: Oak pollen and  $\delta^{18}\text{O}$  data from lake sediments from in or near the EFC, as well as a pollen sequence from Sicily which displays a similar profile through the Holocene. Oak pollen percentages are low for much of the early to middle Holocene which were initially interpreted to be the result of climate aridity. However,  $\delta^{18}\text{O}$  values from some of these lake sediments, and other archives in Southwest Asia, are generally low during the early Holocene, indicative of wetter conditions during the same period. This apparent discrepancy between the two proxies is referred to as the *early Holocene precipitation paradox*. The apparent delay in oak and other tree species into the region has been instead attributed to anthropogenic activities. The pollen sequence from Sicily (Tinner et al., 2009) provides evidence that the delays in the Holocene expansion of woodland were encountered in other areas of the Mediterranean at a similar latitude to the EFC, potentially indicating that the delay was instead related to the behaviour of wider regional climate dynamics rather than local anthropogenic processes (Tzedakis, 2007).

### 3.4 Summary

This chapter has identified the key Holocene, or near-Holocene, long records that currently exist in Southwest Asia. Using these records, the chapter reviewed the current evidence for, and the nature of, Holocene climate change and variability. Furthermore, by summarising the current general understanding of climatic conditions during the Holocene, it has also shown that there are important questions or discrepancies that are still outstanding and need to be addressed:

- There are still large spatial and temporal gaps in the coverage of palaeoclimate studies in Southwest Asia. Importantly for the aims of this study, there are currently no high-resolution, well-dated Holocene long records from the EFC, and no Holocene long records of any type from Iraq. The absence of suitable palaeoclimate data from the EFC makes it difficult to determine how similar, or different, conditions may have been compared to other parts of Southwest Asia, such as the Levant. Moreover, the lack of high-resolution records makes it impossible to identify the existence and magnitude of abrupt climate change events during the Holocene and their resulting impact on local environment and human responses to such changes in the EFC.
- While  $\delta^{18}\text{O}$  is the most widely employed proxy for palaeoclimate investigations in the region, there are still considerable uncertainties in how  $\delta^{18}\text{O}$  values are interpreted in palaeoclimate records from Southwest Asia, particularly from the EFC and this problem is explored further in Chapter 5. Related to this point, is the apparent discrepancy in the way pollen and  $\delta^{18}\text{O}$  values are interpreted in lake sediment records from Iran and south-east Turkey, known as the ‘*early Holocene precipitation paradox*’, which has resulted in conflicting interpretations of climatic conditions during the early to middle Holocene.

## 4 Caves, Speleothem Geochemistry and Palaeoclimate Proxies

### 4.1 Karst, Caves and Speleothems

#### 4.1.1 Karst Systems

Carbonate speleothems and dissolutional cave systems are predominantly found in karst environments. Karst is a type of geological setting that can be characterised by high porosity, fracturing and subterranean drainage. These systems are principally found in geology with high solubility such as limestone and dolomite, while rock structure and lithology are also important in karst system development (Ford and Williams, 2007). The karst system can be divided into two principal zones, the vadose (unsaturated) and the phreatic (saturated) zones (Gillieson, 2009). The vadose zone includes the soil, epikarst and transmission zones. The epikarst, literally '*skin of the karst*', refers to the top thin zone at the top of the karst system immediately below the soil zone. Water, from precipitation or ground water, percolates through cracks, fissures and seepage through the vadose zones into the phreatic zone (Williams, 2008). Karst environments are found worldwide and comprise approximately 10% of the world ice-free continental areas (Ford and Williams, 2007) (Figure 9).

Karst geology in Southwest Asia is abundant (Figure 9) and therefore the geological potential for speleothems and, consequently, speleothem based palaeoclimate investigations is high. However, there have been relatively few speleothem studies in the region. Therefore, there remains a large scope to survey and identify potential caves with speleothems suitable for palaeoclimate investigations to fill in the existing temporal and spatial gaps which exist in the region.

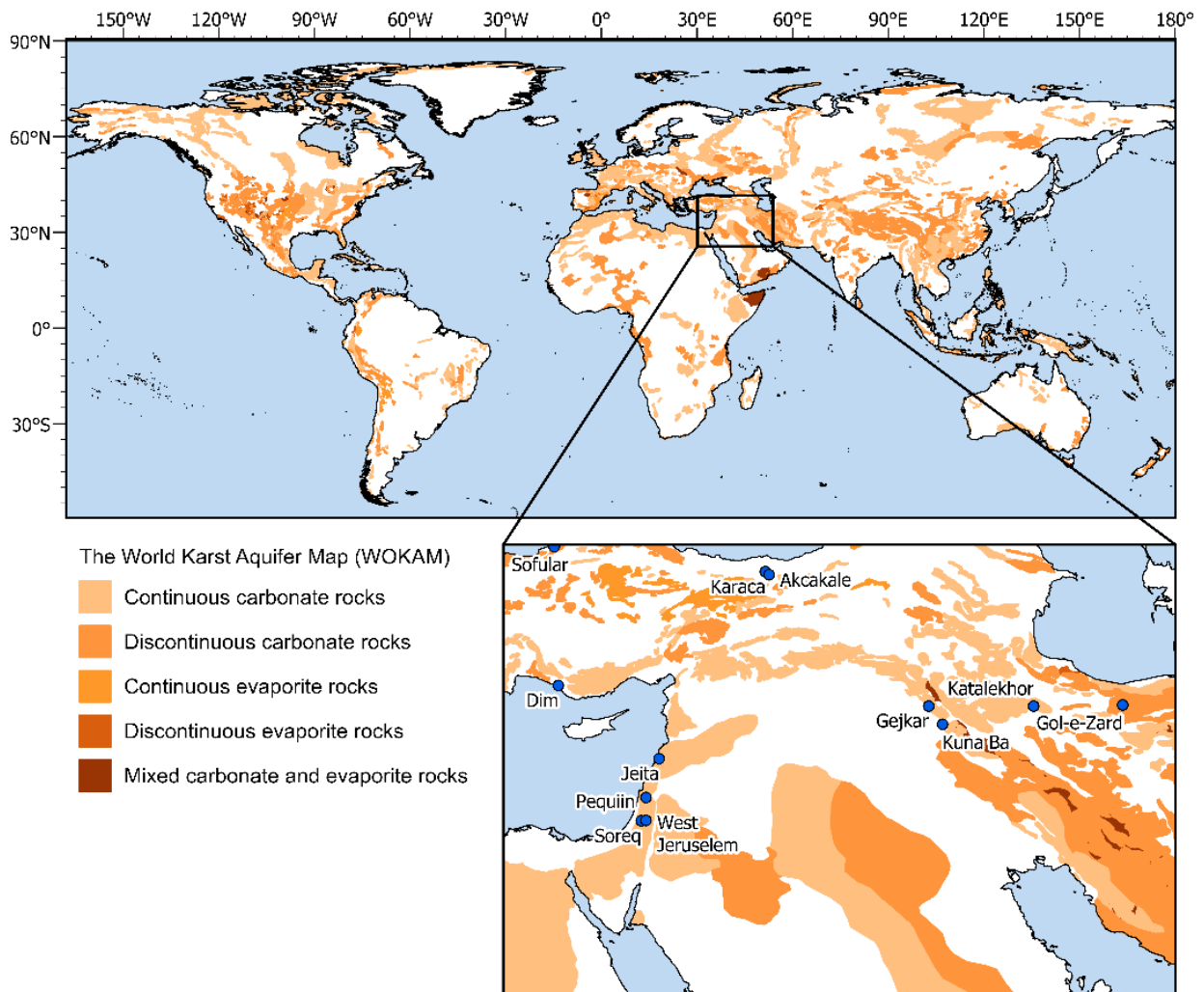


Figure 9: The worldwide distribution of carbonate and evaporite rocks, demonstrating the global distribution of karstic environments..Inset: Zoomed in on Southwest Asia and, for some context, the location of caves where key existing speleothem investigations have already taken place are illustrated with blue dots. Map generated using karst data obtained from the World Karst Aquifer Mapping project (WOKAM) (Chen et al., 2017).

#### 4.1.2 Speleothems

The term speleothem (from the Greek: *Spelaion*, Cave; *thema*, deposit) refers to any secondary cave mineral deposit or formation (Moore, 1952). However, the term is most widely used, and is used here, to refer to secondary calcium carbonate ( $\text{CaCO}_3$ ) deposits. While many others exist, key types of speleothems include:

**Stalagmites:** These rise from the cave floor in a column like structure formed through drip water from the cave ceiling. They generally have a simple growth structure that make them the favoured formation of choice for palaeoclimate investigations (Fairchild et al., 2006). The shape and diameter of stalagmites will depend on water flow rate, water saturation and water drop height.

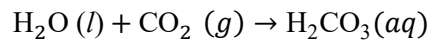
**Stalactites:** Formed on and hang from the cave ceiling. There are two main types of stalactite; delicate cylindrical soda-straw stalactite and massive, conical stalactites. While their growth structure may be more complicated than stalagmites, they have been used successfully for palaeoclimate reconstruction (Bar-Matthews et al., 2003) and are sometimes favoured for conservation reasons because they are commonly found broken on the cave floors (Fairchild et al., 2006).

**Flowstones:** This a general term for laminated, sheet-like deposits of carbonate, formed where water flows down the walls or along the floors of a cave. Flowstones are laterally extensive which make them useful to produce replicate core samples, but they often have complex and non-uniform growth behaviour and potentially contain high levels of impurities, which makes them more challenging to study from a palaeoclimate perspective. Where found overlying cave art, they can provide a unique tool to date prehistoric paintings (e.g. Pike et al., 2012).

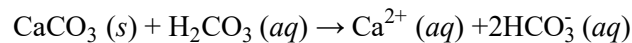
#### 4.1.3 Speleothem Formation

For speleothems to form, cave drip waters must move from a dissolution to a precipitation regime. The processes can be separated into three regions of the karst aquifer: (1) the soil and epikarst zones, (2) the bedrock, and (3) the cave environment and is schematically illustrated in Figure 10, all occurring in the vadose (unsaturated) zone of the karst system.

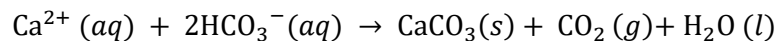
- 1) In the first of these regions, rainwater percolates through the soil and upper bedrock. Within the soil and epikarst, high partial pressure of CO<sub>2</sub> (pCO<sub>2</sub>) is present, as a result of biological respiration, and decomposition of organic materials (Fairchild and Baker, 2012). As the infiltrating water mixes with soil CO<sub>2</sub>, the CO<sub>2</sub> dissolves into solution and forms carbonic acid (H<sub>2</sub>CO<sub>3</sub>), summarised in the following equation:



- 2) During the next stage the now acidic infiltrating water percolates further down the karst system and reaches the limestone bedrock. Here, the high partial pressure of CO<sub>2</sub> allows it to dissolve the bedrock carbonate and become supersaturated in Ca, summarised in the following equation:



- 3) In the final stage, the solution continues down the karst system, until it meets a gas phase (the cave), where the pCO<sub>2</sub> of the atmosphere is much lower than the solution. This results in disequilibrium between the two phases and causes a chemical reaction that leads to the degassing of CO<sub>2</sub> and the precipitation of CaCO<sub>3</sub> out of the solution. It is out of this CaCO<sub>3</sub> that speleothem formations are composed of. This reaction is summarised in the following equation.



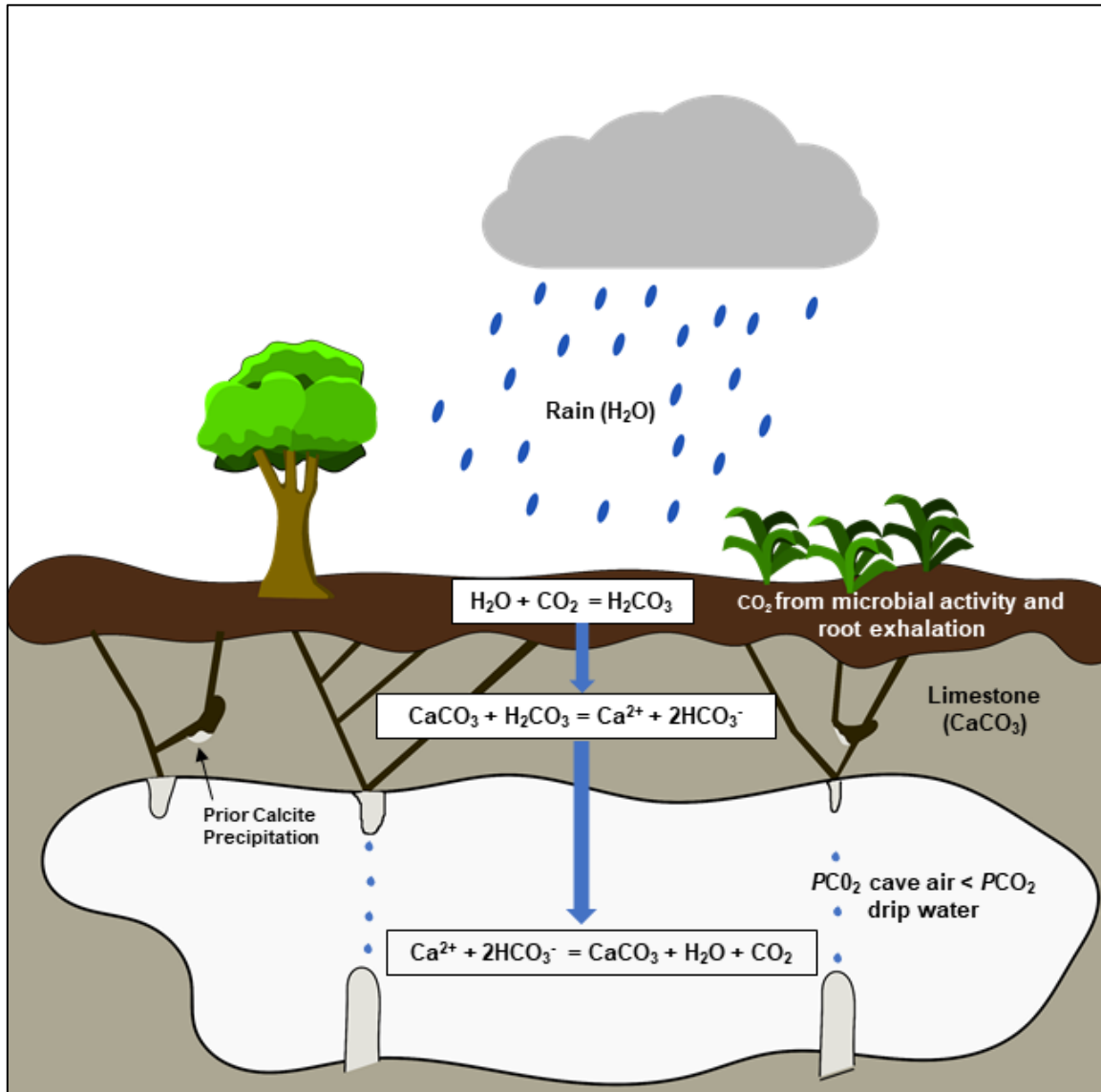


Figure 10: Conceptual diagram illustrating the geochemical processes involved in speleothem formation. Figure produced in InkScape.

#### 4.1.4 Prior Calcite Precipitation

One fundamental property of a cave system is that infiltrating waters will pass from a dissolution regime to a precipitation regime (Fairchild et al., 2006) primarily because they encounter a gas phase with lower  $p\text{CO}_2$  than that with which they have previously equilibrated. It is common to find cases where the drip waters feeding a speleothem have already undergone some change as a result of calcite precipitation up flow in the karst system (Figure 10). This is known as prior calcite precipitation (PCP) (Fairchild and Treble, 2009). This can have an important influence on the geochemical composition of the stalagmite, examined later in this chapter.

#### 4.1.5 Speleothem Minerology

Speleothems used for palaeoclimate reconstruction are usually composed of one of two  $\text{CaCO}_3$  polymorphs, calcite or aragonite. Calcite is the most common and stable polymorph of  $\text{CaCO}_3$ . In calcite, each  $\text{Ca}^{2+}$  ion is surrounded by six  $\text{CO}_3^{2-}$  anions in a rhombohedral structure. Aragonite is a less common high-pressure polymorph of  $\text{CaCO}_3$  and forms when the growth of calcite is inhibited. In aragonite, the  $\text{Ca}^{2+}$  ions are surrounded by nine  $\text{CO}_3^{2-}$  anions organised in a orthorhombic crystal structure (Ford and Williams, 2007).

Two important mechanisms that lead to the formation of aragonite over calcite are related to the inclusion of two trace divalent cations found in cave drip water,  $\text{Mg}^{2+}$  and  $\text{Sr}^{2+}$ .  $\text{Mg}^{2+}$  ions have been shown to poison the growth centres on calcite crystal thus inhibiting calcite growth (Davis et al., 2000).  $\text{SrCO}_3$  has the same crystal structure as aragonite and therefore early precipitation of  $\text{SrCO}_3$  provides a nucleus on which aragonite can grow. Therefore, increased concentrations of either of these elements could inhibit the growth of calcite and promote the growth of aragonite.

Aragonite often develops distinctive morphologies, which includes a fibrous, acicular (needle-like) appearance, which can make it quite easy to identify (Frisia et al., 2002). Where the two minerals exist in the same speleothem it may represent separate episodes of growth under different conditions (Railsback et al., 1994), or partial secondary alteration of aragonite to calcite.

#### 4.1.6 Diagenesis & Recrystallisation

The diagenetic alteration, or neo-morphism, of speleothem carbonate is a common problem to consider when investigating them for palaeoclimate purposes. Neo-morphism is the process of in-situ transformation of a mineral into a polymorph (Bajo et al., 2016). For speleothem carbonate, this can include the recrystallisation of aragonite to calcite, or, calcite to calcite. The identification of recrystallisation can often be observed through a change in the texture of the carbonate fabric. Although, more detailed analysis of the chemical composition of the speleothem can also be used to identify the existence of recrystallisation, especially when diagenesis is not readily visible to the naked eye (Bajo et al., 2016). Recrystallisation can lead to the resetting of the chemical properties or leaching of different elements within the speleothem carbonate, this can lead to inaccurate ages and modification of proxy information, making time series data unreliable (Fairchild et al., 2006). Therefore, avoiding areas which have undergone recrystallisation when sampling is important.

#### 4.1.7 Hiatuses

A hiatus is a temporary interruption in the growth of a speleothem. There are a number of climate related and non-climate related mechanisms that exist which might cause a speleothem to exhibit a hiatus in growth (Breitenbach et al., 2012). In arid and semi-arid regions an obvious explanation for cessation in growth is a period of little or no rainfall above the cave, which prevents carbonate growth (e.g. Fleitmann et al., 2007). Other explanations can include a temporary blocking of fissures that feed drip-water to the speleothem (e.g. Fleitmann et al., 2004) or a change in drip water chemistry (i.e. drip waters become under-saturated in respect to Ca) (Baldini et al., 2006; Lachniet, 2009). Another important mechanism to consider is seismic activity in earthquake prone locations (Delaby, 2001; Kagan et al., 2005). Earthquakes can cause speleothems to break (or severed) (known as a speleoseismite), but they can also lead to rerouting of the cave drip water above the stalagmite or a shift in the location of the falling drip relative to the stalagmite, preventing future growth of the formation. Identify the existence and timing of a hiatus is important as this can have a major influence on the accuracy of the palaeoclimate record's age model and therefore the subsequent interpretation of the palaeoclimate information retrieved.

#### 4.1.8 Annual Growth Layers

Rhythmic variations in the stalagmite fabric may occur, forming laminae visible either macroscopically or microscopically depending on their frequency and the growth rate (Fairchild and Baker, 2012) and can be identified by changes in colour and physical appearance. The cause for these laminae may be variations in drip water chemistry or cave conditions occurring at regular intervals. The most common cause for this is distinct seasonal variations in rainfall and/or temperature each year, and where seasonal variations in climate is the cause, the laminae are known as annual growth layers. These are more likely in parts of the world with a highly seasonal climate, like Southwest Asia where there is a distinct wet and dry season. These will usually take the form of a couplet of darker and lighter calcite, much like the lighter and darker banding of tree rings. It is possible to study the number and width of these layers to help further understand changes in the growth rate and the age of the stalagmite (e.g. Flohr et al., 2017).

#### 4.2 Speleothems as Palaeoclimate Archives

Over recent decades it has become clear speleothems can be used to record changes in key aspects of climate which may include rainfall, annual temperature, vegetation changes and atmospheric circulation variability (McDermott, 2004). In fact, it has been suggested speleothems provide some of the most definitive archives of the global environmental system (Fairchild and Baker, 2012) and their potential to address climate and environmental questions led Henderson (2006, p. 622) to suggest that if “*the last two decades have been the age of the ice core. The next two may be the age of the speleothem*”. There are a number of characteristics of speleothems that make them valuable materials for palaeoclimate investigations:

- i) They can be precisely dated via U-Th dating.
- ii) They are a multi-proxy archive (McDermott, 2004; Fairchild and Treble, 2009; Lachniet, 2009),
- iii) They are a globally distributed archive, potentially present wherever karst environments exist, therefore they can be used not only to investigate regional climates around the globe,

but multiple speleothems for different locations can be used to make continental and inter-continental comparisons (Comas-Bru and Harrison, 2019).

- iv) Finally, both the ability to sample them at a very high resolution and the fact they are relatively protected from erosion and diagenesis by stable cave environments, it is potentially possible to investigate changes in environmental conditions and climate from a magnitude of days to millions of years (Fairchild and Baker, 2012).

In the following section of this chapter, the way in which speleothem are dated, using U-Th dating, will be summarised. After this, the key chemical proxies retrievable from speleothem carbonate and which will be employed in this investigation, will be explored, highlighting their value for palaeoclimate studies alongside the limitations and complications inherently involved in these types of analyses.

### **4.3 Dating Speleothems - U-Th Dating**

Palaeoclimate timeseries are only useful if real ages can be assigned to them which allows for the identification of the timing of climate fluctuations. While a number of methods are available to date speleothems, which includes  $^{14}\text{C}$  dating (e.g. Lechleitner et al., 2016) and annual layer counting (e.g., Proctor et al., 2000; Frisia et al., 2003), the most common way to date speleothem carbonate is through the uranium-thorium disequilibrium (U-Th) dating method. U-Th dating is now a common tool used in earth sciences, archaeology, and palaeontology, providing an alternative to, and exceeding the precision limits of,  $^{14}\text{C}$  and OSL dating. Speleothems provide the ideal material for the dating method as they are almost always a closed system, which means there is no leaching of U in or out the material following deposition (Hellstrom and Pickering, 2015). The development of analytical techniques has allowed for precise and accurate U-Th dates with relatively small samples, which has advanced from tens of grams of carbonate in the 1980s to milligrams today (Hoffmann et al., 2007). With the right sample, with low detrital contamination, the method that can provide a precision with errors of less than 1% (Hellstrom and Pickering, 2015). The development of U-Th dating has been cited as one of the fundamental reasons for the surge of speleothem investigations during the last couple of decades (Fairchild and Baker, 2012).

#### 4.3.1 Principles of U-Th dating

U-Th dating is based on the radioactive decay chain series of the uranium isotope  $^{238}\text{U}$  (Figure 11).  $^{238}\text{U}$  decays into a stable isotope of lead ( $^{206}\text{Pb}$ ) via intermediate radioactive daughter isotopes, including the thorium isotope  $^{230}\text{Th}$ . These isotopes decay at a known rate, recorded in terms of their half-life. In natural materials which have been left undisturbed for millions of years these elements are usually found in a state of 'secular equilibrium' where the daughter elements are decaying as fast as the parent uranium isotope and therefore the ratios of them, relative to one another, remain constant. However, U-Th dating is made possible because, through geochemical fractionation processes, this equilibrium can be broken, and a state of disequilibrium will exist (Schwarcz and Blackwell, 1992).

U-Th dating of speleothems is based on, and is made possible by, the extreme fractionation of the U parent isotope from the Th and other daughter isotopes in the hydrosphere as a result of their different solubilities (Richards and Dorale, 2003). Uranium is highly soluble, while Th is not soluble. As a result, cave drip waters which ultimately go on to form speleothems, will contain U, but Th concentrations should be essentially absent (unless transported in by detrital contamination).

Calculation of a U-Th age requires accurate measurement of the ratios  $^{230}\text{Th}/^{238}\text{U}$  and  $^{234}\text{U}/^{238}\text{U}$ , usually expressed as activity ratios, that is where secular equilibrium would be a ratio of 1 (Hellstrom and Pickering, 2015). The extent to which  $^{230}\text{Th}/^{238}\text{U}$  activity ratios have returned to unity will be a function of time because of the constant and known rate of U decay (Richards and Dorale, 2003). It is this information which can be used to identify how long ago the deposition of calcite occurred. U-Th dating limit is controlled by the time secular equilibrium between the two elements is reached once again, which is about 600,000 years (Hellstrom and Pickering, 2015).

Detrital input (Th and U that is transported in with organic matter, colloidal material and sediments) can potentially lead to age errors. To estimate the amount of detrital contamination and the need for correction, the ratio of  $^{232}\text{Th}$ , which is not radiogenic and is assumed to derive solely from detrital input is compared to the radiogenic  $^{230}\text{Th}$  isotope  $^{230}\text{Th}/^{232}\text{Th}$  and the parent U isotope  $^{232}\text{Th}/^{238}\text{U}$ . To mitigate against detrital contamination and subsequent age uncertainties, areas of clean, dense calcite should be targeted when sampling for U-Th dates.

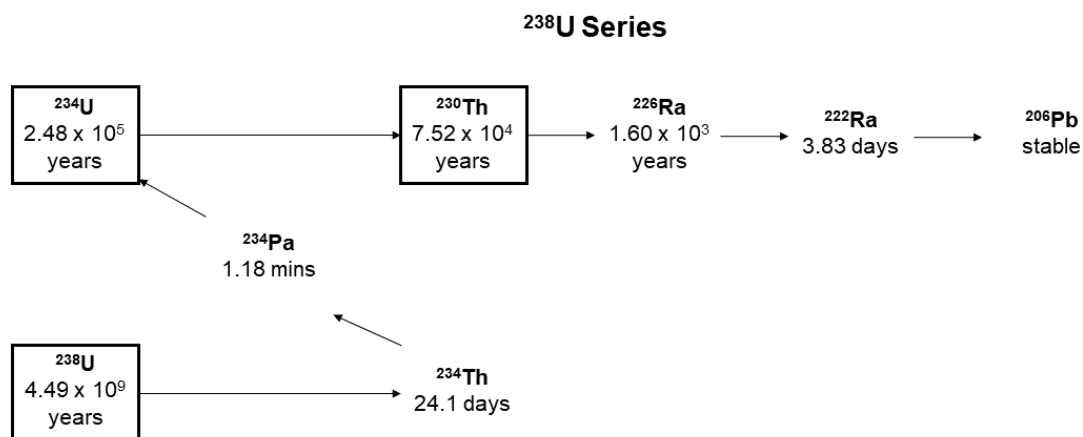


Figure 11: Decay chain series of  $^{238}\text{U}$ . The isotopes measured for U-Th dating are in bold boxes. After Hellstrom and Pickering (2015, p. 33).

#### 4.3.2 Combining U-Th and Annual Layer Counts

Where annual layers exist, combining U-Th dates with annual layer counts can be used to improve the uncertainties associated with radiometric analyses (Fleitmann et al., 2007). A series of U-Th dates through time along a continuously annually laminated speleothem can be tied to that lamina chronology (e.g., Liu et al., 2013; Flohr et al., 2017).

#### 4.4 Palaeoclimate Proxies

Most analysis of speleothems for palaeoclimate purposes involves studying how the chemical composition of the stalagmite changes through time (i.e. through the vertical growth axis of the speleothem). These chemical variables are known as proxies (as discussed in Chapter 3.2.1). One of the advantages of speleothems is that there are multiple different types of these chemical proxies that exist which can be examined, and as such they are a *multi-proxy* archive. These proxies may record past changes atmospheric input, vegetation and soil, the karst aquifer, speleothem growth and secondary alteration (Fairchild et al., 2006). The most investigated chemical proxies are the stable isotopes of oxygen and carbon, however the analysis of trace elements such as Mg and Sr is increasingly commonplace. In this section, the different proxies which will be analysed in this project will be discussed.

## 4.5 Stable Isotopes

Isotopes are variants of the same chemical elements (i.e. they have identical number of protons), but have different number of neutrons and, as a result, have different masses. Stable isotopes refer to the isotopes of elements which do not undergo radioactive decay, as opposed to radioactive isotopes. Most elements have multiple, naturally occurring stable isotopes. For speleothem studies, the most useful and commonly analysed stable isotopes for palaeoclimate investigations are those of oxygen (O), carbon (C) and, to a lesser extent, hydrogen (H).

A fundamental principle which makes the investigations of stable isotopes useful for palaeoclimate purposes is that there is a preferential fractionation of isotopes between phase changes (e.g. liquid to gas), with one phase preferentially incorporating the heavier or lighter isotope relative to the other phase (Sharp, 2007). Fractionation can be caused by either kinetic or equilibrium isotopes effects (Sharp, 2007). Importantly, the amount of fractionation that occurs between these phase changes can be related to changes in, directly or indirectly, environmental parameters (e.g. temperature or precipitation variability) and, consequently, variations in stable isotopes can be used to reconstruct past climatic conditions.

### 4.5.1 Oxygen Isotopes

The analysis of oxygen stable isotope ratios is the most widely employed proxy in speleothem palaeoclimate investigations. Oxygen isotope analysis is based on the varying concentrations of the heavier  $^{18}\text{O}$  isotope compared to the lighter, more common  $^{16}\text{O}$  isotope in the material being examined.

#### 4.5.1.1 Standards and notations

$^{18}\text{O}/^{16}\text{O}$  values are reported relative to a recognised standard and expressed in the *delta* ( $\delta$ ) notation, with the unit of  $\delta$  given as per mille (‰).

$$\delta^{18}\text{O} \text{ ‰} = \left( \frac{\frac{^{18}\text{O}}{^{16}\text{O}}_{\text{sample}} - \frac{^{18}\text{O}}{^{16}\text{O}}_{\text{standard}}}{\frac{^{18}\text{O}}{^{16}\text{O}}_{\text{standard}}} \right) \times 1000$$

The standards used for  $\delta^{18}\text{O}$  measurements are ‘Vienna Pee Dee Belemnite’ (VPDB) for carbonates and ‘Vienna Standard Mean Ocean Water’ (VSMOW) for sea, rain and drip water (Sharp, 2007). Where, the  $\delta^{18}\text{O}$  value of the standard materials arbitrarily equals 0.00‰. More positive  $\delta^{18}\text{O}$ ‰ values indicate a relative increase in the amount of the heavier  $^{18}\text{O}$  isotope relative to the lighter  $^{16}\text{O}$  isotope. To convert between the two standard scales, the relationship between the two scales can be expressed as (Coplen et al., 1983):

$$\delta^{18}\text{O}_{\text{VSMOW}} = 1.03091 \times \delta^{18}\text{O}_{\text{VPDB}} + 30.91$$

$$\delta^{18}\text{O}_{\text{VPDB}} = 0.97002 \times \delta^{18}\text{O}_{\text{VSMOW}} - 29.98$$

When comparing a  $\delta^{18}\text{O}$  value of one material to another, a sample which has a value higher (or lower) than another, should be described as having a ‘higher’ (or ‘lower’)  $\delta^{18}\text{O}$  value rather than the often employed, but mistakenly used terms such as ‘heavier’, ‘lighter’, ‘enriched’ or ‘depleted’ (Sharp, 2007).

#### 4.5.1.2 $\delta^{18}\text{O}$ of speleothems

Assuming equilibrium conditions (Hendy, 1971), the  $\delta^{18}\text{O}$  value of speleothem carbonate reflects two variables (Lachniet, 2009):

- The  $\delta^{18}\text{O}$  composition of cave drip-water which forms the stalagmite, which itself reflects the  $\delta^{18}\text{O}$  composition of precipitation above the cave.
- A fractionation which occurs during the liquid (drip water) to solid (calcite) phase change (*i.e.* calcite precipitation) which is temperature dependant (Tremaine et al., 2011).

Commonly, changes associated with the first of these variables cause much larger  $\delta^{18}\text{O}$  variations than those associated with temperature-dependent fractionation (Lachniet, 2009, pp. 412–413). Consequently, changes in speleothem  $\delta^{18}\text{O}$  variations are more than likely the result of changes in the  $\delta^{18}\text{O}$  composition of precipitation above the cave, discussed further here.

#### 4.5.1.3 $\delta^{18}\text{O}$ of Precipitation

Variations in the  $\delta^{18}\text{O}$  value of precipitation are well documented and are related to a number of so called ‘*effects*’ in the global water cycle. These effects include changes in the source of moisture, rain-out processes in the atmosphere related to *Rayleigh distillation*, and changes in the amount of precipitation (Figure 12) (Rozanski et al., 1993; Lachniet, 2009).

#### 4.5.1.4 The Source Effect

The original control on the  $\delta^{18}\text{O}$  value of rainwater is the  $\delta^{18}\text{O}$  of the oceanic or freshwater source of moisture. However, the  $\delta^{18}\text{O}$  value of different water bodies is not ubiquitous as the amount of evaporation of, freshwater input into, and precipitation over, a moisture source will modify its  $\delta^{18}\text{O}$  value. As a result, air masses originating from different moisture sources will often have distinct  $\delta^{18}\text{O}$  values (Lachniet, 2009). Consequently, when two or more significant moisture sources exist for a cave site, variations in cave drip water  $\delta^{18}\text{O}$  may reflect changes in the relevant dominance of the different moisture sources, providing an important proxy for past changes in the behaviour of atmospheric dynamics. For instance, in a study of speleothems from sub-tropical Brazil, variations in the  $\delta^{18}\text{O}$  value of carbonate were interpreted to reflect shifts in the relative balance between two rainfall systems that dominated the region (summer monsoonal and winter extratropical precipitation) (Cruz et al., 2005, 2007). Lower  $\delta^{18}\text{O}$  values were associated with increased influence of monsoonal rainfall sourced from the Amazon basin, while higher  $\delta^{18}\text{O}$  values were associated with an increased dominance of winter rainfall sourced from the North Atlantic.

Another related process to take into account is whether the  $\delta^{18}\text{O}$  value of an individual moisture source may have changed over time (Clark and Fritz, 1997). This is particularly important to consider when investigating records which cover long-millennial scale time periods and where the main moisture sources is especially susceptible to  $\delta^{18}\text{O}$  variation, such as enclosed water bodies. Main processes which can lead to changes in the  $\delta^{18}\text{O}$  value of oceanic water sources include (Lachniet, 2009):

- The ‘*ice volume effect*’ – This refers to the growth or melting of ice sheets, which have lower  $\delta^{18}\text{O}$  values than sea water. As ice sheets grow, they effectively lock-in water with low  $\delta^{18}\text{O}$  values and consequently, the  $\delta^{18}\text{O}$  value of the ocean will increase. Conversely, when ice sheets

melt, they release large amounts of freshwater into the oceans, lowering the  $\delta^{18}\text{O}$  value of sea water.

- Evaporation – Evaporation results in the preferential uptake of water with low  $\delta^{18}\text{O}$  values. Therefore, any increase in the rate of evaporation will result in higher, residual sea water  $\delta^{18}\text{O}$  values.
- Freshwater runoff – As evaporation of ocean water preferentially removes the lighter  $^{16}\text{O}$  isotope, freshwater derived from the subsequent atmospheric moisture will generally have lower  $\delta^{18}\text{O}$  values than seawater. Therefore, large increases in freshwater input from land (e.g., via rivers) into the oceans will decrease  $\delta^{18}\text{O}$  values of the seawater.

As an enclosed waterbody in a sub-tropical region, the Eastern Mediterranean (the main moisture source for the EFC) undergoes high amounts of evaporation, resulting in high salinity and high  $\delta^{18}\text{O}$  values relative to mean global ocean values. But it is also the outlet for the River Nile, a major and large source of freshwater, introducing water with lower  $\delta^{18}\text{O}$  values. Therefore, the  $\delta^{18}\text{O}$  value of the Eastern Mediterranean is likely to be very sensitive to changes in these two competing processes. For this reason, the influence of potential changes in the  $\delta^{18}\text{O}$  value of the Eastern Mediterranean and its impact on the  $\delta^{18}\text{O}$  value of speleothem carbonate in Southwest Asia is discussed more thoroughly in Chapter 5.

#### 4.5.1.5 Fractionation processes of Atmospheric Vapour

As an air mass moves away from a vapour source, it will cool and, in order to maintain thermodynamic equilibrium, the air mass will condense (i.e. form clouds) and lose vapour through precipitation, a process known as ‘rainout’ (Clark and Fritz, 1997, p. 47). During this process, the heavier isotope is preferentially removed from the vapor phase into the liquid phase, which is known as Rayleigh Distillation, as a result, as an air mass ‘rains out’, the residual water vapour becomes increasingly depleted in  $^{18}\text{O}$ , and thus rainfall  $\delta^{18}\text{O}$  from this air mass will have progressively lower  $\delta^{18}\text{O}$  values (Figure 12). Effects related to this process that influence the  $\delta^{18}\text{O}$  value of precipitation include the ‘continental’ and ‘altitude effect’.

The continental effect describes the decrease in rainfall  $\delta^{18}\text{O}$  values as it moves away from the moisture source further inland as a result of Rayleigh distillation, as  $^{18}\text{O}$  is preferentially rained out (Dansgaard, 1964; Rozanski et al., 1993; Clark and Fritz, 1997). However, the input of new inland moisture sources (e.g. inland lakes) or recycling of precipitation through evaporation, will lead to an influx of moisture with high  $\delta^{18}\text{O}$  that could counter the continental effect (Rozanski et al., 1993; Lachniet, 2009).

The altitude effect refers to the decrease in  $\delta^{18}\text{O}$  values as altitude increases, approximately 2 to 3 ‰ per  $\text{km}^{-1}$  (Lachniet, 2009). Orographic distillation of air masses as they traverse a high mountain range may result in a pronounced leeward-side “*isotopic rain shadow*” (Blisniuk and Stern, 2005). From a palaeoclimate perspective, while both the altitude, and continental location of a site will not change over the time periods considered in this thesis (unless significant shifts in sea level), these effects can sometimes be used to explain variations in  $\delta^{18}\text{O}$  values associated with changes in air mass trajectories.

#### 4.5.1.6 The Temperature Effect

Temperature performs a key role in the  $\delta^{18}\text{O}$  value of rainwater due to temperature-dependent equilibrium fractionation. The ‘temperature effect’ refers to the positive correlation between mean annual temperature (MAT) and rainwater  $\delta^{18}\text{O}$  at a site ( $d\delta^{18}\text{O}/dT$ ) (Lachniet, 2009). This relationship is related to the control temperature has on the amount of moisture an air mass can hold, where colder airmasses cannot retain as much moisture as warmer air masses. Therefore, as an air mass cools moisture will condense resulting in the preferential loss of the heavy isotope to the liquid phase (rain) in accordance with Rayleigh distillation, leaving the resulting air mass with a lower  $\delta^{18}\text{O}$ , moreover the amount of fractionation that occurs will increase at lower temperatures (Sharp, 2007). This effect is most significant in mid to high latitude regions due to increased temperature gradients (Dansgaard, 1964; Rozanski et al., 1993).

However, in low latitude regions, such as Southwest Asia, with lower temperature gradients there is an absence of correlation between  $\delta^{18}\text{O}$  values and mean annual temperatures (Dansgaard, 1964; Rozanski et al., 1993) and therefore the temperature effect is usually not a dominant control on the  $\delta^{18}\text{O}$  of

rainwater. However, in these regions seasonal differences in temperatures can have an important influence on the  $\delta^{18}\text{O}$  of rainfall during different times of the year.

#### 4.5.1.7 The Amount Effect

The 'amount effect' refers to the negative relationship between the amount, and the  $\delta^{18}\text{O}$  value, of precipitation, first observed by Dansgaard (1964). This relationship may be caused by multiple processes (Dansgaard, 1964; Rozanski et al., 1993):

- It could be associated with the rainout process described above. Increased rainout (higher amounts of rainfall) will progressively lead to lower  $\delta^{18}\text{O}$  values of precipitation. This is likely to be a more dominant process during periods of intense rainfall (Sharp, 2007).
- In low humidity conditions, rain water will evaporate and the lighter  $^{16}\text{O}$  isotope will be preferentially vaporised with a kinetic isotope effect, leaving the residual rainwater with higher  $\delta^{18}\text{O}$  values (Sharp, 2007). This process is exacerbated during periods of low rainfall where air temperatures are likely to remain relatively high, allowing more evaporation to take place (Sharp, 2007).
- In more humid conditions, equilibrium isotopic exchange can occur between water droplets and existing vapour below the cloud base. Rain droplets become enriched in the heavier  $^{18}\text{O}$  isotope simply because of the positive direction of the isotopic fractionation between liquid and vapor (Sharp, 2007; Lachniet, 2009). Like evaporation, this process is enhanced during low intensity rainfall events where rain droplets are smaller enabling greater exchange.

The amount effect is especially noticeable in tropical, sub-tropical and semi-arid regions, like Southwest Asia (Bar-Matthews et al., 2003; Fleitmann et al., 2007; Sinha et al., 2019). Importantly from a palaeoclimate perspective, when the amount effect can be shown to be a dominant control on  $\delta^{18}\text{O}$  variability of monthly or inter-annual rainfall (often through monitoring studies) it can provide evidence that the  $\delta^{18}\text{O}$  values of speleothem carbonate reflect past changes in precipitation amount. Moreover, theoretically, if the modern day relationship between rainfall amount and  $\delta^{18}\text{O}$  is known, it may be possible to quantify past rainfall from the  $\delta^{18}\text{O}$  values of speleothem calcite (Bar-Matthews et al., 2003).

#### 4.5.1.8 Seasonality

Fluctuations in environmental parameters related to seasonality can lead to changes in the mean annual  $\delta^{18}\text{O}$  values of precipitation and groundwaters (Lachniet, 2009; Baker et al., 2019), consequently when examining the  $\delta^{18}\text{O}$  value of speleothems from regions with a highly seasonal climate, such as the EFC, changes in seasonality should be considered as a possible cause for annual  $\delta^{18}\text{O}$  variability. Variations in  $\delta^{18}\text{O}$  values of rainfall/groundwaters related to changes in seasonality can often be attributed to one of four processes (Rozanski et al., 1993; Sharp, 2007; Baker et al., 2019):

- Seasonal differences in temperature provide a strong seasonal variation (i.e. intra-annual variability) in the isotopic composition of rainwater due to the temperature effect. In Southwest Asia, winter rainfall generally has lower  $\delta^{18}\text{O}$  values than spring rainfall. Consequently, any relative increase in rainfall during the colder winter months will result in lower annual  $\delta^{18}\text{O}$  values of precipitation, while a relative decrease in winter rainfall (this could include an increase in spring rainfall) will lead to higher annual  $\delta^{18}\text{O}$  values (e.g. Stevens et al., 2001, 2006; Dean et al., 2018).
- In seasonal, semi-arid regions the amount of recharge that occurs will be different during different parts of the year (Baker et al., 2019). Recharge of the karst aquifer will only occur if enough precipitation falls or falls at a high enough intensity, if it is not, groundwaters in the soil or shallow karst will be lost to the atmosphere through evaporation (Baker et al., 2019). Consequently, the annual averaged  $\delta^{18}\text{O}$  values of groundwaters in the karst system will have a seasonal bias toward the precipitation  $\delta^{18}\text{O}$  value of recharge periods (i.e. periods with higher amounts of rainfall) (Baker et al., 2019). Therefore, changes in the amount of recharge that occurs during different parts of the year could influence the  $\delta^{18}\text{O}$  values of groundwaters, and thus speleothem carbonate.
- As discussed previously, the main moisture source for a specific site may change between seasons. Therefore, variations in the seasonal distribution of rainfall will change the relative input from these different sources, leading to a greater component of the  $\delta^{18}\text{O}$  value of one source over the other (e.g. Wang et al., 2001; Cruz et al., 2007).

- Evapotranspiration is higher in summer, as a result more moisture is recycled and returned to the atmosphere. This, in effect, reduces the continental or altitudinal effects. Therefore, any increase in the amount of evapotranspiration (e.g. longer summers) will reduce these effects further (Rozanski et al., 1993).

#### 4.5.1.9 $\delta^{18}\text{O}$ variations in the soil zone and karst system

While the  $\delta^{18}\text{O}$  value of groundwater is largely determined by the  $\delta^{18}\text{O}$  of precipitation and the processes discussed above, there are mechanisms in the soil zone and epikarst which can lead to significant modifications of the  $\delta^{18}\text{O}$  of cave drip-waters (Bar-Matthews et al., 1997, 1999; Fleitmann et al., 2007; Baker et al., 2019), particularly in semi-arid and arid countries where high amounts of evaporation is more likely. Evaporative enrichment of soil moisture leads to the preferential loss of  $^{16}\text{O}$  into the atmosphere and as a result the  $\delta^{18}\text{O}$  value of the remaining moisture will become higher. As the water enters and travel through the vadose zone, it can go through further evaporative fractionation processes as well as mixing with other existing stored water above the cave, merging the  $\delta^{18}\text{O}$  value, potentially masking seasonal signals (Fairchild et al., 2006). Finally, as the drip water enters the cave and reaches the stalagmite, the water can be further altered by non-equilibrium fractionation processes (e.g. Flohr et al., 2017). However, in such scenarios where kinetic fractionation processes are present, evaporation causes residual waters to have higher  $\delta^{18}\text{O}$  values and wetter, more humid conditions result in lower  $\delta^{18}\text{O}$  values, therefore the fractionation process moves in the same way as ‘*the amount effect*’ and, in effect, rather than invalidating the signal, amplifies it (Bar-Matthews et al., 2003; Fleitmann et al., 2004, 2007). Therefore, where evaporative processes can be shown to be a major influence,  $\delta^{18}\text{O}$  can still be used as a palaeohydrological proxy (e.g. Flohr et al., 2017).

#### 4.5.1.10 Monitoring

It is now widely accepted within the speleothem science community that to fully understand the processes influencing the  $\delta^{18}\text{O}$  of speleothem carbonate and its effectiveness as a palaeoclimate proxy a comprehensive monitoring study is needed (Baker et al., 2019). These monitoring studies including taking measurements of drip water hydrology, drip water geochemistry, cave environment and calcite growth and geochemistry, as well as surface climate parameters, such as temperature or humidity (e.g.

Burstyn, 2013). However, the location of the cave, funding available and the time needed for such studies means that this is not always viable.

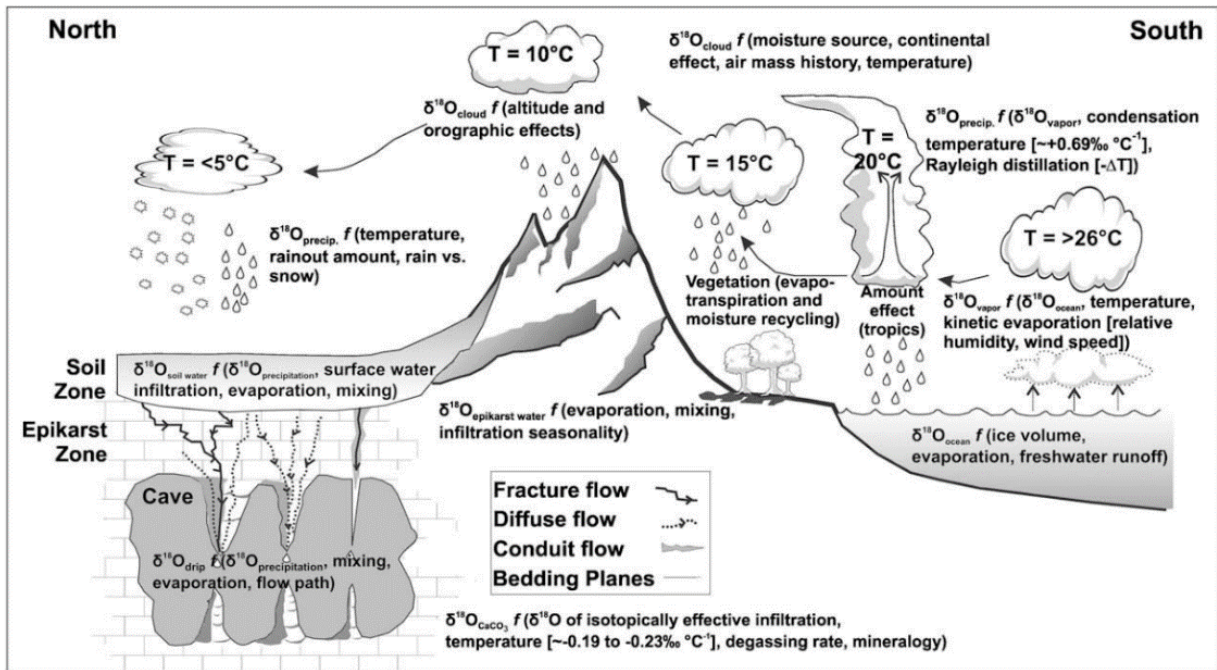


Figure 12: Schematic figure illustrating the many different processes which exist in the water cycle that can influence the  $\delta^{18}\text{O}$  value of rain and cave waters, and subsequently, speleothem calcite. From Lachniet (2009, p. 413).

#### 4.5.2 Deuterium, Meteoric Water Lines and Fluid Inclusions

Along with oxygen, isotopes of hydrogen in precipitation and cave drip water can also be used as a tracer for processes in the hydrological cycle. Deuterium ( $^2\text{H}$ , or D), or heavy hydrogen, is a stable isotope of hydrogen, containing one proton and one neutron in the nucleus; whereas the other, more common, stable isotope of hydrogen, protium ( $^1\text{H}$ ), or light hydrogen, contains a single proton in the nucleus without an accompanying neutron. The ratio of the two isotopes ( $\delta\text{D}$ ) in water, like oxygen, is reported relative to the standard, VSMOW. The processes that influences the  $\delta\text{D}$  values in water are largely determined by the same fractionation processes as  $\delta^{18}\text{O}$ , described in the previous section (Sharp, 2007; Lachniet, 2009). Therefore,  $\delta\text{D}$  and  $\delta^{18}\text{O}$  values in global meteoric waters are highly correlated and the linear relationship between  $\delta\text{D}$  and  $\delta^{18}\text{O}$  in global precipitation is known as the global

meteoric water line (GMWL) (Figure 13) (Dansgaard, 1964; Rozanski et al., 1993), which is defined as:

$$\delta D = 8.20 \times \delta^{18}O + 11.27$$

However, the isotopic composition of local and regional rainfall in a given area will have its own distinct waterline varying in slope and intercept, known as the local meteoric water line (LMWL) and in effect the GMWL is an average of different LMWL worldwide. The LMWL of a specific location will depend on different climatic factors, which can include the source of vapor, secondary evaporation and the seasonality of rainfall (Clark and Fritz, 1997, p. 51). Generally, all LMWL will have a slope <8 due to secondary evaporation processes. Because different air masses will potentially be characterised by different LMWL, the analysis of  $\delta D$  and  $\delta^{18}O$  can provide information on the origin of vapor and subsequent modifications by secondary processes (re-evaporation and mixing) as well as the dominance of different rainfall regimes (Clark and Fritz, 1997, p. 54; Heydarizad et al., 2019).

#### 4.5.2.1 The Eastern Mediterranean Water Line

The main source of moisture for the study region of this project, the EFC, is the eastern Mediterranean. Meteoric waters in the Eastern Mediterranean has a very distinct LMWL, known as the Eastern Mediterranean Water Line (EMWL), which is defined as:

$$\delta D = 8 \times \delta^{18}O + 22 \text{ (Gat, 1980, 1982; Gat and Carmi, 1987).}$$

As Figure 13 shows, the EMWL plots well above the GMWL. This is due to low humidity in the region resulting in greater kinetic (nonequilibrium) evaporation at the vapour source, ultimately leading to a greater fractionation of  $^{18}O$  than  $^2H$  (Clark and Fritz, 1997, p. 44). Due to the very distinct nature of the EMWL compared to the GMWL, the analysis of  $\delta D$  and  $\delta^{18}O$  in rainfall and groundwater from regions influenced by Mediterranean rainfall, like the EFC, can be used to distinguish between Mediterranean and other vapour sources relatively easily.

There have been little isotopic studies of precipitation carried out in the EFC. However, a local water line was produced after a comprehensive study of rainwater carried out on 55 precipitation events during the period December 2009 to June 2010 at the Bazian Meteorological Station in the Basara basin, 25

km west of Sulaymaniyah city in Iraqi Kurdistan (Hamamin and Ali, 2013, p. 2937; Seither, 2016). The LMWL produced with this data set, referred to here as the Bazian Meteoric Water Line (BMWL), is defined as:

$$\delta D = 7.7 \times \delta^{18}O + 14.4 \text{ ‰}$$

The BMWL plots between the EMWL and GMWL (Figure 13), demonstrating the influence of eastern Mediterranean as the major source of moisture for the EFC (Seither, 2016).

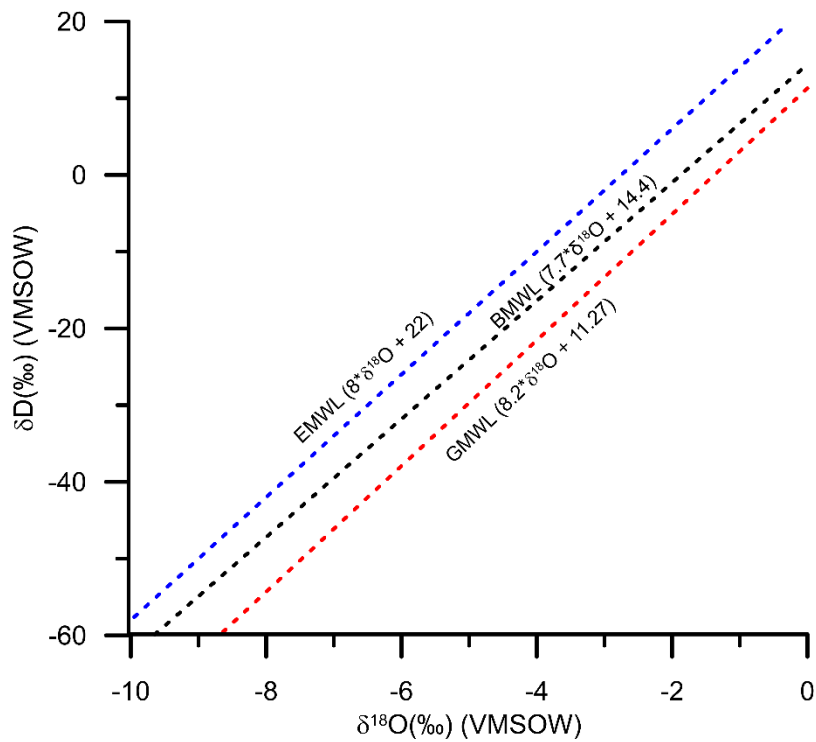


Figure 13: The Eastern Mediterranean Meteoric Water Line (Gat and Carmi, 1970) (blue dashed line), the Global Meteoric Water Line (Rozanski et al., 1993) (red dashed line), and the Bazian Meteoric Water Line (BMWL) which is local waterline produced from measurements on precipitation samples from north-east Iraq (Seither, 2016).

#### 4.5.2.2 Fluid Inclusions in Speleothems

As the analysis of the isotopic composition of modern-day precipitation and groundwater can provide an insight into hydrological climatic processes influencing present-day air masses, similar isotopic analysis of the palaeowaters can provide the same type of information. Palaeowaters are present in speleothems in the form of fluid inclusions, which are small volumes of water that are enclosed with the speleothem carbonate. In recent years, analytical advances has made it easier to extract and measure  $\delta D$  and  $\delta^{18}O$  values in speleothem fluid inclusion water (e.g. Affolter et al., 2014, 2019). By providing direct information on the isotopic composition of palaeoprecipitation, the  $\delta D$  and  $\delta^{18}O$  composition of fluid inclusions, in combination with the isotopic analysis of speleothem carbonate, can be used to calculate either paleotemperatures (e.g. Tremaine et al., 2011; Affolter et al., 2019) or to reveal changes in the source of moisture (e.g. Matthews et al., 2000; Fleitmann et al., 2003b; Rogerson et al., 2018). This makes the analysis of fluid inclusion a potentially powerful tool that can be used to help support the interpretation of stable isotope data retrieved from the carbonate itself.

#### 4.5.3 Carbon Isotopes

Carbon stable isotopes in speleothem carbonate are another retrievable proxy that can potentially provide information of past hydrological changes. They are routinely measured alongside  $\delta^{18}O$  and, therefore, are ordinarily a readily available dataset.  $\delta^{13}C$  analysis is based on the varying concentrations of the heavier  $^{13}C$  isotope compared to the lighter, more common,  $^{12}C$  isotope. Much like oxygen isotopes,  $^{13}C/^{12}C$  values are expressed as  $\delta^{13}C$  ‰ (per mille) values, where  $^{13}C/^{12}C$  values of a sample are measured relative to a known standard (usually V/PDB). The  $\delta^{13}C$  of speleothem carbonate reflects a mixture of the  $\delta^{13}C$  values of the two main sources of carbon into cave drip water, which are soil  $CO_2$  above the cave and the host rock carbonate (limestone or dolomite).

Soil  $CO_2$  mainly derives from atmospheric  $CO_2$  which has been extracted by plants where it is then fractionated by photosynthesis, after which it enters percolating soil water either through root respiration or the decomposition of organic material. A negligible amount of soil  $CO_2$  may also derive from direct absorption of atmospheric  $CO_2$  ( $\delta^{13}C = -8.2$ ‰) directly into rainwater droplets and ground water. Soil  $CO_2$   $\delta^{13}C$  values can range from between -10 to -28‰ depending on vegetation type above

the cave. The host rock, as a marine carbonate, will usually have a  $\delta^{13}\text{C}$  value which varies around 0‰ (Salomons and Mook, 1986). Consequently, the  $\delta^{13}\text{C}$  value of speleothem carbonate will usually fall somewhere between these two values.

#### 4.5.3.1 Variations in Speleothem $\delta^{13}\text{C}$

Variations in speleothem  $\delta^{13}\text{C}$  can be influenced by multiple factors which include vegetation type and density, soil microbial productivity, infiltration rates and water-rock interaction (Figure 14). As a result, it can often be challenging to disentangle these different mechanisms and makes it difficult to correctly interpret  $\delta^{13}\text{C}$  signals (Baker et al., 1997; Fohlmeister et al., 2020). For this reason,  $\delta^{13}\text{C}$  results are often neglected or omitted completely or discussion limited to very general conditions or vegetation trends and transitions (Fairchild and Baker, 2012; Fohlmeister et al., 2020). Furthermore, due to the many local factors influencing speleothem  $\delta^{13}\text{C}$ , each record needs to be treated on a site-to-site basis. However, they potentially provide a useful proxy for changes in vegetation and land use, especially in regions, such as Southwest Asia, where changes in vegetation usually involve shifts between the relative balance of C3 and C4 plants (Fairchild and Baker, 2012). Furthermore, they can be a useful proxy to investigate when other mechanisms are masking the climatic signal of the  $\delta^{18}\text{O}$  data (e.g. Fleitmann et al., 2009).

#### 4.5.3.2 C3 vs C4 plant types

As, the majority of  $\text{CO}_2$  in soil is derived from the decay of vegetation, the  $\delta^{13}\text{C}$  of soil  $\text{CO}_2$  will reflect the isotopic composition of the vegetation present. The  $\delta^{13}\text{C}$  of the vegetation will depend on the way in which the plant photosynthesizes for carbon fixation. There are three basic methods plants photosynthesize; these methods are known as C3, C4 and CAM pathways. The majority of land plants photosynthesize using the C3 (also known as the Calvin-Benson) pathway, where they produce a three-carbon compound (hence C3) called 3-phosphoglyceric acid. The majority of trees, woody bush and temperate grasses follow the C3 pathway. However, some plants (about 3% of species worldwide) have evolved to use the C4 (also known the Hatch-Slack) pathway, whereby plant produce a four-carbon organic acid (oxaloacetate) during photosynthesis, which have adapted to photosynthesize more

efficiently under conditions of higher temperatures and lower atmospheric CO<sub>2</sub> concentrations (Cerling, 1999). Consequently, C<sub>4</sub> plants are found more commonly in sub-tropical regions where they are more resilient to the hot and dry conditions than C<sub>3</sub> plants and include, amongst other species, the majority of sub-tropical grasses (Sharp, 2007).

These different photosynthetic pathways cause the plants to fractionate carbon differently and results in distinct  $\delta^{13}\text{C}$  values. C<sub>3</sub> plants will usually have isotope values of between -34 to -22‰ with an average of -28.5‰ (Diefendorf et al., 2010; Kohn, 2010). C<sub>4</sub> plants will have values between -16 to -10‰ (Cerling and Harris, 1999). As a result, in regions where these two different plant types are present, the speleothem  $\delta^{13}\text{C}$  signal can be used as a proxy signal for the relative abundances of the two types of plants, which can range from -14‰ to -6‰ for speleothems produced from C<sub>3</sub> plants and -6‰ to +2‰ in speleothems deposited from CO<sub>2</sub> produced from C<sub>4</sub> plants (Figure 14) (McDermott, 2004).

#### 4.5.3.3 Soil CO<sub>2</sub> Production

In semi-arid regions with high seasonality, such as Southwest Asia,  $\delta^{13}\text{C}$  variability has been linked to changes in soil CO<sub>2</sub> contribution to cave drip waters (Bar-Matthews and Ayalon, 2011; Cheng et al., 2015; Sinha et al., 2019). During wetter conditions, increased soil biogenic CO<sub>2</sub> production via plant respiration and microbial activity leads to enhanced CO<sub>2</sub> production in soils above cave, introducing more isotopically ‘light’ carbon, derived from organic material, into cave drip waters resulting in lower speleothem  $\delta^{13}\text{C}$  values. Furthermore, this process is enhanced because soil CO<sub>2</sub> has a higher pCO<sub>2</sub> content than initial water value, to achieve equilibrium between the two, higher soil pCO<sub>2</sub> content will allow for more isotopic exchange between the soil and solution introducing more isotopically light CO<sub>2</sub> in the water (Dreybrodt and Scholz, 2011). Whereas a decrease in soil CO<sub>2</sub> production during drier periods will lead to a relative increase in the amount of the heavier carbonate carbon from the host bedrock and therefore higher speleothem  $\delta^{13}\text{C}$  values (Baldini et al., 2005).

#### 4.5.3.4 Prior Calcite Precipitation

The effect of calcite precipitation is to release CO<sub>2</sub> and deposit CaCO<sub>3</sub>. During this process as a result of kinetic fractionation, the lighter <sup>12</sup>C isotope is preferentially released, leaving the residual isotopic

composition of the  $\text{HCO}_3^-$  in solution, which goes onto form the stalagmite, enriched in  $\delta^{13}\text{C}$  (Baker et al., 1997). Therefore, variations in the amount of degassing due to PCP can have a significant influence on speleothem  $\delta^{13}\text{C}$  values (Johnson et al., 2006; Van Rampelbergh et al., 2013). As PCP is enhanced during drier conditions due to longer residence time, higher speleothem  $\delta^{13}\text{C}$  values act as an aridity signal. However, determining the presence/extent of PCP can be difficult. The most common tool to investigate the existence of PCP is the identification of a strong positive correlation between variations in  $\delta^{13}\text{C}$  values and trace elements (Mg/Ca and Sr/Ca), which is discussed further in the next section.

#### 4.5.3.5 Local, Kinetic Effects in the Cave

If degassing in the cave occurs rapidly, kinetic fractionation can occur. This leads to the preferential loss of the lighter  $^{12}\text{C}$  isotope leaving the precipitated carbonate with higher  $\delta^{13}\text{C}$  values. which will lead to the loss of  $^{12}\text{C}$  and the precipitation of calcite of higher  $\delta^{13}\text{C}$  values (Hendy, 1971). Variations in drip rate can also have an influence on stalagmite  $\delta^{13}\text{C}$  values. During periods of lower drip rates, a longer residence time of the water on the surface of the stalagmite will allow for increased opportunity for  $\text{CO}_2$  degassing. As degassing results in the preferential loss of  $^{12}\text{C}$ , it will lead to higher calcite  $\delta^{13}\text{C}$  values (Hendy, 1971). Carbonate precipitation also leads to a temperature dependent carbon isotope fractionation processes which preferentially results in the incorporation of  $^{13}\text{C}$  into the solid, calcite phase. However, the effect of this is less significant than between the different oxygen isotopes.

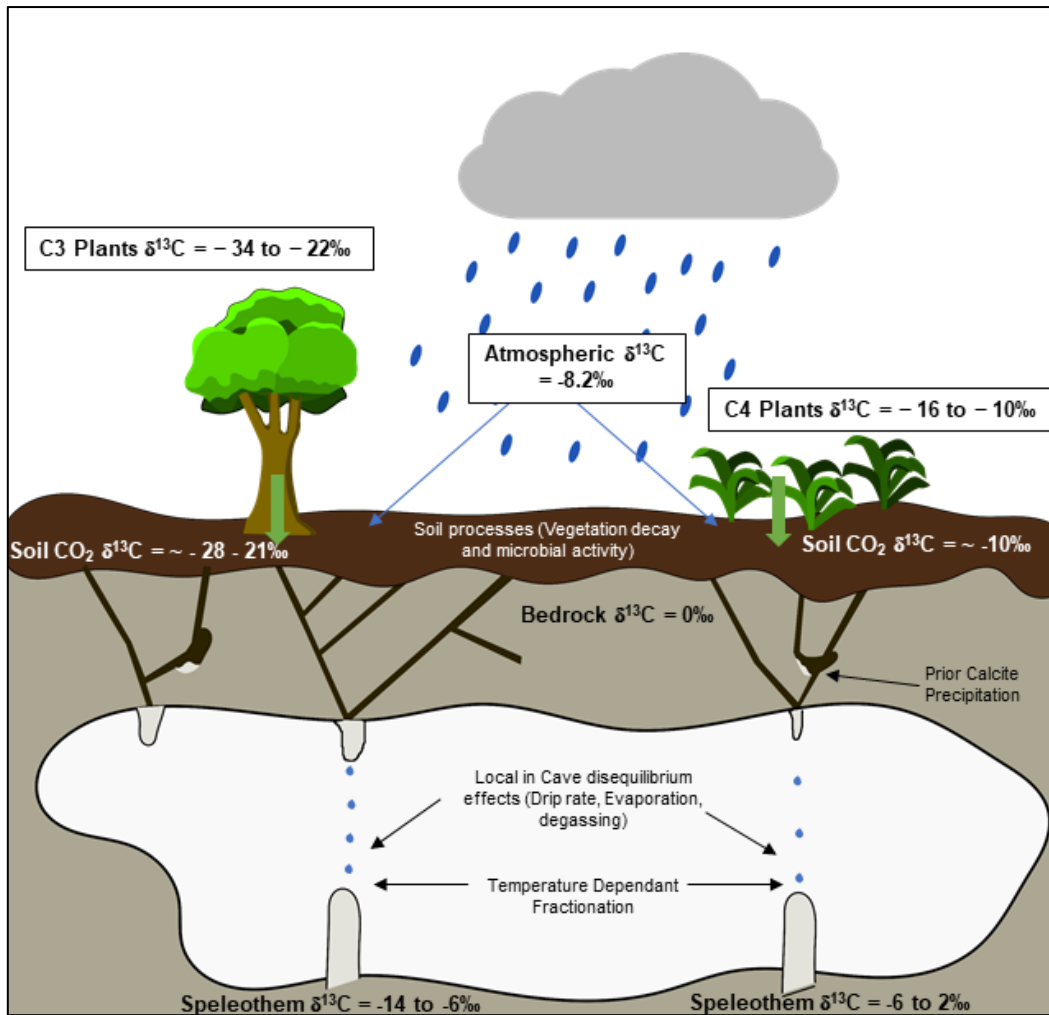


Figure 14: Schematic figure illustrating the different mechanisms above and in the karst system which can influence the  $\delta^{13}\text{C}$  composition of speleothem carbonate. Figure produced in InkScape.

## 4.6 Trace Elements

Trace elements within speleothem carbonate (elements found in much smaller quantities than Ca, C and O) are an alternative palaeoenvironmental proxy and represent a large proportion of retrievable information from speleothems (Fairchild and Treble, 2009). In the right conditions, certain elements have the ability to provide information about changes in temperature, effective moisture, vegetation coverage, atmospheric concentrations, volcanic and/or anthropogenic activity (Fairchild and Treble, 2009). They have been used independently as a palaeoclimate proxy for hydrological conditions (e.g Treble et al., 2003), but are perhaps more commonly employed to help provide support for, and compliment, the interpretation of stable isotope data (e.g Cruz et al., 2007).

The majority of work conducted on speleothem trace elements have focused on elements which form divalent ions in solution and substitute in for Ca in the crystal lattice, notably Mg, Sr and Ba. These are the elements that will be focused on, and studied, in this section and the thesis. These elements are incorporated into cave drip water disproportionately with respect to Ca, which is described as their distribution coefficient ( $K_{Tr}$ ). A simple equation exists that explains the relationship between the trace species (Tr) and Ca between solution and mineral phases:

$$K_{Tr} = (Tr/Ca)_{CaCO_3} / (Tr/Ca)_{solution}$$

The distribution coefficient of trace elements may vary due to changes in temperature, crystal morphology and solution composition, however, a key determinate is the difference in solubility between Mg, Sr, Ba, and Ca (Fairchild and Baker, 2012). The distribution coefficient of Mg, Sr and Ba relative to Ca is less than one and, as a result, their incorporation into calcite relative to Ca is suppressed.

### 4.6.1 Controls on Trace Element Concentrations

Much like carbon, the two major sources for trace elements in cave drip water and speleothems are the host bed rock and overlying soil components. There are many complex sets of processes which influence their incorporation into speleothem calcite which potentially make the interpretation of them complicated (Fairchild and Treble, 2009). This section will focus on the three major processes commonly employed to explain variations of trace element in speleothems:

- Prior Calcite Precipitation
- Dolomite Dissolution
- Aeolian Dust Input

#### 4.6.1.1 Prior Calcite Precipitation

The result of PCP is to remove cations from the water in proportion to which they are incorporated into the precipitate (Holland et al., 1964; Fairchild and Treble, 2009). Since the distribution coefficient of trace elements ( $K_{Tr}$ ) is often less than one, it has the effect that Tr/Ca values in the residual percolating solution is enhanced, which in turn will lead to increased Tr/Ca ratio in speleothem carbonates downflow (Figure 15). Because the effect of PCP on Mg, Sr and Ba concentrations relative to Ca is similar, strong Mg/Ca-Sr/Ca-Ba/Ca covariations in speleothems can be used to infer trace concentrations are a result of PCP (McMillan et al., 2005; Johnson et al., 2006). Furthermore, as PCP can impact  $\delta^{13}C$  (Chapter 4.5.3.4), correlations between trace element ratios and  $\delta^{13}C$  are another good indication of the presence of PCP (Johnson et al., 2006; Cheng et al., 2015). Since the PCP occurs where descending karst waters are able to degas, the process should be enhanced in dry climatic periods when there is decreased water storage and enhanced ventilation in the karst system (Fairchild et al., 2000). For this reason, covarying  $\delta^{13}C$ , Mg/Ca and Sr/Ca values, because of PCP, are used as proxies for moisture variability. Similarly, in tropical and sub-tropical regions where the ‘*amount effect*’ is thought to be the dominant control of  $\delta^{18}O$  variation, trace elements modified by PCP can also be expected to covary with  $\delta^{18}O$ , providing supporting hydrological evidence to compliment the interpretation of stable isotope data (e.g. Van Rangelbergh et al., 2013).

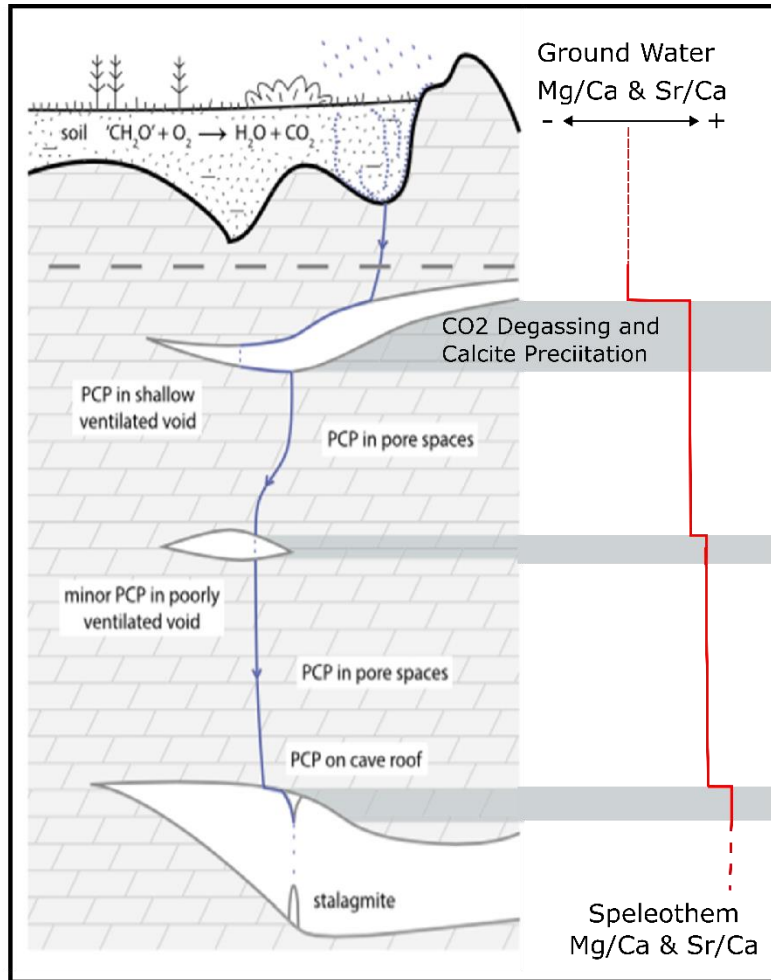


Figure 15: Schematic illustration of the effect Prior Calcite Precipitation has on Mg/Ca and Sr/Ca values. When percolating meets an area within the karst system with lower  $P_{\text{CO}_2}$  it will degas and precipitate  $\text{CaCO}_3$ , which results in the preferential removal of Ca over Mg, leaving the remaining drip water with higher Mg/Ca values. PCP has a similar effect on Sr/Ca and Ba/Ca ratios, as well as  $\delta^{13}\text{C}$  values. Figure modified from Owen et al., (2016).

While correlations between trace element concentrations internally, and with  $\delta^{13}\text{C}$ , have been used to suggest PCP as a driver for trace element ratio variability, there are other mechanisms which can cause covariations between different trace elements. Therefore, a number of studies have attempted to develop more empirical models to determine if PCP is the primary cause for Tr/Ca variations (Sinclair et al., 2012; Burstyn, 2013; Wassenburg et al., 2020). Sinclair et al., (2012) who, by using a collection of data from speleothem and cave water studies, suggested that a linear running through a log-log scatter plot of Mg vs Sr ( $\ln(\text{Mg}/\text{Ca})$  vs  $\ln(\text{Sr}/\text{Ca})$ ), should exhibit a slope of between 0.709 and 1.003. More recently, Wassenburg et al. (2020) developed this further. They suggested that the previous model was too strict and did not account for other factors that could influence trace element ratios, particularly the

dissolution of dolomite, at the same time. They found that when PCP was a dominant process, the slope could be between 0.709 and up to 1.45.

#### 4.6.1.2 Dolomite Dissolution

Dolomite ( $\text{CaMg}[\text{CO}_3]_2$ ) by its geochemical nature contains much higher levels of Mg than calcite, but also generally lower concentrations of Sr (Fairchild et al., 2000). At sites where both limestone and dolomite phases are present in the bedrock, variations in drip water trace element chemistry may be related to changes in the relative contribution of these two different carbonates. The main mechanism which causes variations in the contribution of these two different types of carbonates is associated with the differential rates of dissolution of dolomite and calcite (Fairchild and Treble, 2009). Dolomite dissolves much more slowly than calcite, and for this reason a greater influence of dissolved calcite will leave cave drip waters lower in Mg/Ca than the surrounding, bulk, bedrock. However, karst waters reach saturation in respect calcite than dolomite much quicker. Therefore, during periods of longer water residence time in the karst aquifer, where fluids have become saturated in respect to calcite (and thus cannot dissolve any further), there is more opportunity for dolomite dissolution and lead to increasing cave drip water Mg/Ca values (Roberts et al., 1998; Hellstrom and McCulloch, 2000). However, for this process to occur, residence time in the karst system must be necessarily long enough to allow calcite saturation (potentially months to years) (Fairchild et al., 2006).

If this mechanism can be shown to be occurring, high Mg/Ca values, associated with longer residence times, will correspond to drier conditions and therefore Mg/Ca can be used as an effective hydrological proxy. As dolomite phases are generally lower in Sr and Ba than associated calcite phases, the existence of an anticorrelation between Mg/Ca with Sr/Ca and Ba/Ca, in groundwaters and speleothems and can be a good indicator of this processes occurring (Roberts et al., 1998; Hellstrom and McCulloch, 2000).

#### 4.6.1.3 Aeolian Dust flux

The deposition of wind-blown (aeolian) dust in the overlying soil or directly into the cave has been suggested to be major contributor to trace elements variation in speleothems (Goede et al., 1998; Zhou et al., 2009, 2011; Rutledge et al., 2014; Carolin et al., 2019). These exogenic particulates may have significantly higher, or lower, Tr/Ca values relative to the local bedrock and soil, particularly dust

particulates with high components of dolomite (high Mg) (e.g. Carolin et al., 2019) and/or high Sr components (e.g. Zhou et al., 2009). Therefore, sites with high levels of atmospheric dust deposition, variations in the amount of dust flux can potentially significantly influence speleothem geochemistry, especially in arid or semi-arid location where aeolian dust activity is more common, thin existing soil profiles amplify any exogenic input and evaporation exceeds precipitation, resulting in salt accumulation in soil profiles (Rutledge et al., 2014).

Low vegetation cover and dry conditions provide ideal conditions for dust mobilisation. Therefore, several studies have used trace elements fluctuations related to dust activity as a major proxy for hydrological conditions. For instance, Zhou et al (2011) suggested increasing Sr/Ca and Ba/Ca from a speleothem in central China were related to enhanced atmospheric dust activity and deposition above the cave related to drier conditions during periods of a stronger Asian winter monsoon. Within Southwest Asia, Carolin et al., (2019) linked increasing Mg/Ca values in a speleothem from Iran to dolomitic dust activity in Mesopotamia during the middle to late Holocene, associated with enhanced summer aridity. Similarly, Ayalon et al., (1999) suggested higher trace-element concentrations in speleothems from Soreq Cave, Israel reflected periods of enhanced aeolian contributions during drier periods.

Dust mobilisation and activity in semi-arid regions of Southwest Asia is common, particularly in Iraq where a combination of hot, arid conditions during the summer and strong winds provide ideal conditions for dust storms (Nabavi et al., 2016). Dust storms in the region can be grouped into two main categories, called Shamal and Frontal dust storms (Hamidi et al., 2013). The Shamal refers to north-westerly winds that produce large sandstorms in Iraq and the Persian Gulf occurring once or many times during the summer. While Frontal storms refers to strong south-westerly winds caused by a high-pressure system over southern Iran and a low pressure system over the eastern Mediterranean Sea and Turkey, which leads to dust transport from the alluvial plains of the Tigris and Euphrates alluvial plains to northwest Iraq and Iran which are dust sinks (Hamidi et al., 2013; Nabavi et al., 2016). Therefore, this is an important mechanism to consider when investigating speleothems from the EFC.

However, the effect of dust deposition on speleothem geochemistry will be very site specific, dependant on the geochemical make up of dust particulates, the overlying soil and the local bedrock, it can be very difficult to establish without comprehensive monitoring studies. However, Sr isotopes are one relatively simple tool that have been used to help determine the influence of exogenic dust flux on speleothem trace element values (Goede et al., 1998; Frumkin and Stein, 2004; Zhou et al., 2009).

#### 4.7 Strontium Isotopes

The analysis of strontium isotopes are another, but less commonly employed, proxy used in speleothem palaeoclimate studies. There are four naturally occurring isotopes of Sr;  $^{84}\text{Sr}$  (0.56%),  $^{86}\text{Sr}$  (9.87%),  $^{88}\text{Sr}$  (82.53%) (all of which occur in constant relative proportions within earth materials), and  $^{87}\text{Sr}$  (7.04%), which is formed through the radioactive decay (*radiogenic*) of  $^{87}\text{Rb}$  (half-life 48.8 billion years), and as a result its abundance increases over time (Capo et al., 1998, pp. 199–201; Stewart et al., 1998).

As the abundance of the non-radiogenic isotopes remains constant, but the abundance of the radiogenic isotope changes over time in a mineral or rock, the ratio between one of these isotopes (usually  $^{86}\text{Sr}$ ) and the radiogenic isotope ( $^{87}\text{Sr}/^{86}\text{Sr}$ ) can be used as a chemical tracer for past geological processes as well as the age and date of geological materials (Capo et al., 1998). Old continental crust rocks, especially those rich in Rb, will have high  $^{87}\text{Sr}/^{86}\text{Sr}$  values ( $> 0.71$ ), due to the accumulation of  $^{87}\text{Sr}$  over time. While young, low Rb rich rocks such as basalts have low  $^{87}\text{Sr}/^{86}\text{Sr}$  values ( $< 0.705$ ) (Capo et al., 1998, p. 203). The  $^{87}\text{Sr}/^{86}\text{Sr}$  composition of ocean precipitates, such as carbonate rocks, reflect the isotopic composition of the ocean at the time of formation, with no fractionation during this process. The isotopic composition of sea water falls somewhere between older and younger rocks, and will change depending on the amount of sea spreading, which will introduce mantle derived material, lowering the  $^{87}\text{Sr}/^{86}\text{Sr}$  values or mountain forming, leading to the erosion of old, continental rocks, increasing  $^{87}\text{Sr}/^{86}\text{Sr}$  values (Fairchild and Baker, 2012).

##### 4.7.1 Strontium Isotopes in Speleothems

The  $^{87}\text{Sr}/^{86}\text{Sr}$  composition of speleothem carbonate will reflect the composition of drip water during the time of precipitation, with no fractionation occurring during this process (unlike for example  $\delta^{18}\text{O}$ ). Therefore,  $^{87}\text{Sr}/^{86}\text{Sr}$  can provide a useful insight into the sources and processes affecting the amount of

Sr in the cave drip water, which may reflect changes in environmental conditions. However,  $^{87}\text{Sr}/^{86}\text{Sr}$  analysis of speleothem calcite is still a relatively underdeveloped field. The  $^{87}\text{Sr}/^{86}\text{Sr}$  of speleothems are likely to be dominated by the Sr composition of the host bedrock. However, deviations from this will be as a result of a greater incorporation of an exogenic source(s) of Sr (Musgrove and Banner, 2004). The most likely alternative source of Sr are aeolian-derived silicates or carbonates into the soil above the cave (Fairchild and Treble, 2009)

Studies investigating  $^{87}\text{Sr}/^{86}\text{Sr}$  of speleothems have suggested that changes in the incorporation of exogenic source(s) of Sr may be related to changes in water-bedrock interaction associated with water residence time (Musgrove and Banner, 2004; Oster et al., 2010), the influence of terrestrial and atmospheric dust flux (Frumkin and Stein, 2004), changes in weathering intensity of soil and bedrock (Avigour et al., 1990; Banner et al., 1996), sea spray (Bar-Matthews et al., 1999) or a mixture of these effects.

Changes in water residence time can alter the amount of interaction between infiltrating cave waters and the bedrock that can have an influence on drip water  $^{87}\text{Sr}/^{86}\text{Sr}$  values. During periods of increased precipitation rapidly infiltrating water decreases the amount of water-bedrock interaction, as a result exogenic Sr will have a greater influence on the composition of cave drip waters, which will shift the  $^{87}\text{Sr}/^{86}\text{Sr}$  of drip water to values more similar to the exogenic Sr. However, during periods of increase water-residence time (drier periods) there is greater interaction between water and bedrock, and the drip water will be more heavily influenced by bedrock Sr and therefore have  $^{87}\text{Sr}/^{86}\text{Sr}$  values that more resemble the host rock (Oster et al., 2010).

Soil thickening or thinning may also lead to changes in the  $^{87}\text{Sr}/^{86}\text{Sr}$  values of speleothem carbonate (Cooke et al., 2003). Soil thickening will lead to a weaker (or stronger) presence of the underlying bedrock in the  $^{87}\text{Sr}/^{86}\text{Sr}$  signature of the soil zone. Variations in soil thickness might also be reflected in speleothem  $\delta^{13}\text{C}$  values, as thicker soils (higher  $^{87}\text{Sr}/^{86}\text{Sr}$  values) and lower  $\delta^{13}\text{C}$  values are likely to occur under warmer, wetter conditions (Ward et al., 2019; Utida et al., 2020). Other investigations have linked variations in  $^{87}\text{Sr}/^{86}\text{Sr}$  values to changes in aeolian dust flux, either directly into the cave or from the accumulation and subsequent dissolution of overlying soil above the cave. For instance, Frumkin

and Stein (Frumkin and Stein, 2004) were able to use  $^{87}\text{Sr}/^{86}\text{Sr}$  ratios in the speleothem to identify the amount of Sahara sourced dust flux, which was elevated in respect to  $^{87}\text{Sr}/^{86}\text{Sr}$  compared to the local bedrock. Increased dust flux is usually considered to be an indicator of drier conditions as aeolian dust mobilisation, input and accumulation occurs more often during drier periods (Frumkin and Stein, 2004).

The interpretation of each record will depend on the local bedrock  $^{87}\text{Sr}/^{86}\text{Sr}$  composition and the  $^{87}\text{Sr}/^{86}\text{Sr}$  composition of the soil and other exogenic sources of Sr (e.g. dust flux). Understanding the composition of these different possible inputs will help clarify which end-members are actually present and therefore help interpret the  $^{87}\text{Sr}/^{86}\text{Sr}$  signal more accurately. If only two significant end members are present, for instance the bedrock and overlying soil. A linear relationship between  $^{87}\text{Sr}/^{86}\text{Sr}$  ratios and the reciprocal of the Sr Concentrations ( $1/\text{Sr}$ ) should be present (Zhou et al., 2009).

#### 4.8 $^{234}\text{U}/^{238}\text{U}$ Activity ratios

$^{234}\text{U}/^{238}\text{U}$  activity ratios ( $^{234}\text{U}/^{238}\text{U}_0$ ) are measured as part of the process of generating Uranium Series dates, and are therefore a readily available (free), data source. There are now a number of studies which have suggested variability in  $^{234}\text{U}/^{238}\text{U}_0$  may be related to climate processes (Kaufman et al., 1998; Hellstrom and McCulloch, 2000; Frumkin and Stein, 2004; Göktürk et al., 2011).

Under conditions of radioactive equilibrium, the  $^{234}\text{U}/^{238}\text{U}_0$  of carbonates should be 1:1. Activity ratios of speleothem carbonate above one suggest an external source of excess  $^{234}\text{U}$ . There are two possible mechanisms that can cause  $^{234}\text{U}/^{238}\text{U}_0$  greater than unity in cave waters, both relate to the contribution of  $^{234}\text{U}$  atoms from soil components above the cave relative to the host carbonate rock (Hellstrom and McCulloch, 2000). Firstly, it can occur because  $^{234}\text{U}$  is easily leached from crystal lattice sites in soils by alpha particle ( $\alpha$ ) recoil after the radioactive degradation of  $^{238}\text{U}$ , where the daughter isotope ( $^{234}\text{U}$ ) is mobilised from its initial position directly (leached) into solution by the energy released by  $\alpha$  decay. Secondly, the preferential leaching of  $^{234}\text{U}$  from crystal lattice sites damaged by  $\alpha$  decay (Hellstrom and McCulloch, 2000). Where ground water residence time is increased, it provides more time for  $^{234}\text{U}$  to leach into solution, leading to increased  $^{234}\text{U}/^{238}\text{U}_0$  values in cave waters. Conversely, during wetter conditions, increased weathering of bedrock and soil, which does not lead to the preferential loss of

$^{234}\text{U}$ , results in lower  $^{234}\text{U}/^{238}\text{U}_0$  values (Ayalon et al., 1999). Furthermore, relatively fast rates of water flow will cause a decrease in  $^{234}\text{U}/^{238}\text{U}_0$  values as it limits the amount of leaching that can occur.

## 5 Interpretating $\delta^{18}\text{O}$ records from Southwest Asia

### 5.1 How speleothem $\delta^{18}\text{O}$ variability is interpreted

As discussed in Chapter 3 & 4, the investigation of  $\delta^{18}\text{O}$  values is the most widely employed proxy in speleothem palaeoclimate studies, as well as a commonly used proxy for lake sediment studies. However, the interpretation of  $\delta^{18}\text{O}$  variability in speleothems (and lake sediments) from Southwest Asia is not necessarily straightforward. In this chapter I first aim to further review the way in which variations in  $\delta^{18}\text{O}$  values from palaeoclimate records from the Southwest Asia have been interpreted, highlighting areas of disagreement and the cause for differing interpretations. In the second part of this chapter, I will explore the evidence for and an understanding of how the isotopic composition of the Eastern Mediterranean has changed during the Holocene, which is one fundamental reason for the differing interpretations of terrestrial  $\delta^{18}\text{O}$  records in the region.

In Southwest Asia, the way in which changes in  $\delta^{18}\text{O}$  values in speleothems have usually been interpreted has differed depending on the timescales investigated. On shorter timescales (sub-annual to centennial),  $\delta^{18}\text{O}$  variability has usually been interpreted to be responding to changes in the amount of precipitation (the amount effect) where lower  $\delta^{18}\text{O}$  values reflect wetter periods and higher  $\delta^{18}\text{O}$  values reflect drier periods (Bar-Matthews and Ayalon, 2011; Cheng et al., 2015; Sinha et al., 2019). These interpretations are supported by multi-annual seasons of monitoring at cave sites (Bar-Matthews et al., 1997, 2003) (e.g. Figure 16), comparisons with available instrumental data (Flohr et al., 2017; Sinha et al., 2019) and global climate models (Werner et al., 2011) which have exhibited a clear relationship between the amount of rainfall and speleothem  $\delta^{18}\text{O}$  variability. Therefore, on these shorter timescales  $\delta^{18}\text{O}$  values have usually provided a valuable climate proxy to investigate past changes in moisture availability.

On orbital timescales, it has been observed that speleothem  $\delta^{18}\text{O}$  records from the Levant display a strong similarity to Eastern Mediterranean planktonic (*G.ruber*)  $\delta^{18}\text{O}$  curves, which record the isotopic composition of sea surface waters ( $\delta^{18}\text{O}_{\text{EMSS}}$ ) (Frumkin et al., 1999; Bar-Matthews et al., 2003; Grant et al., 2012) (e.g. Figure 17) (See Figure 19 for locations). It is therefore generally accepted that  $\delta^{18}\text{O}$

values of speleothems on these longer timescales predominantly respond to changes in  $\delta^{18}\text{O}_{\text{EMSS}}$ , the main source of moisture for the region and therefore the source effect is the dominant control on speleothem  $\delta^{18}\text{O}$  values (Frumkin et al., 1999; Kolodny et al., 2005; Almogi-Labin et al., 2009; Rohling et al., 2015). The general influence of water vapour originating from the Eastern Mediterranean has on speleothem  $\delta^{18}\text{O}$  from Southwest Asia can be illustrated by their generally higher  $\delta^{18}\text{O}$  values than would be expected from their longitudinal position compared to European records (McDermott et al., 2011). This is related to the high-evaporation rate in the Eastern Mediterranean and resultant higher  $\delta^{18}\text{O}_{\text{EMSS}}$  values.

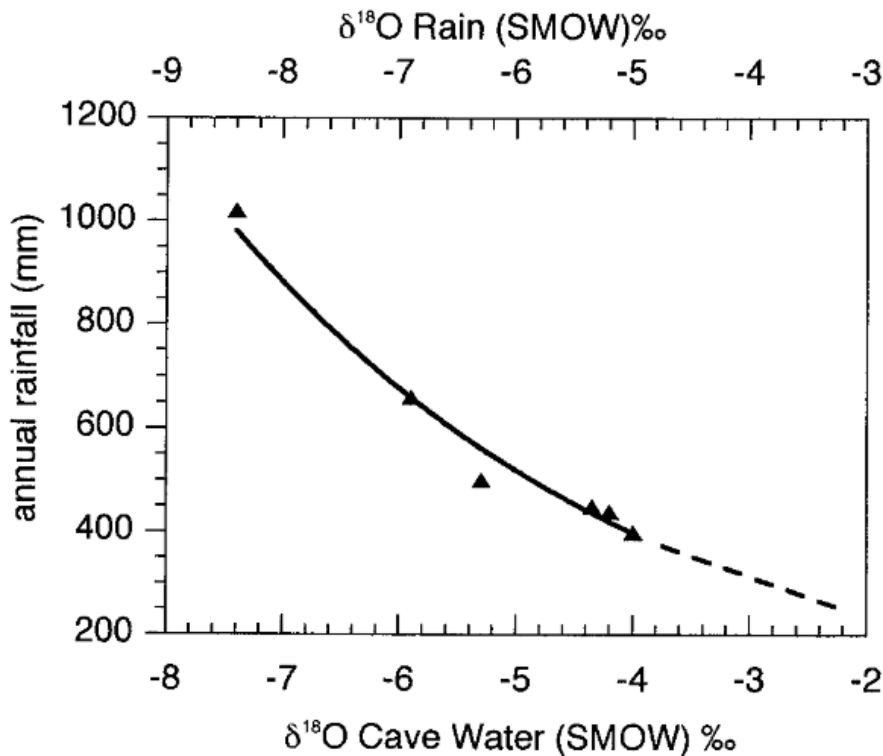


Figure 16: Monitoring data from Soreq Cave in Israel which shows a clear relationship between annual rainfall amount and the mean annual weighted  $\delta^{18}\text{O}$  value of rainwater and cave drip water between 1989 and 1995, which provides evidence that the amount effect is a dominant process on annual timescales. Figure from Bar-Matthews et al., (1997).

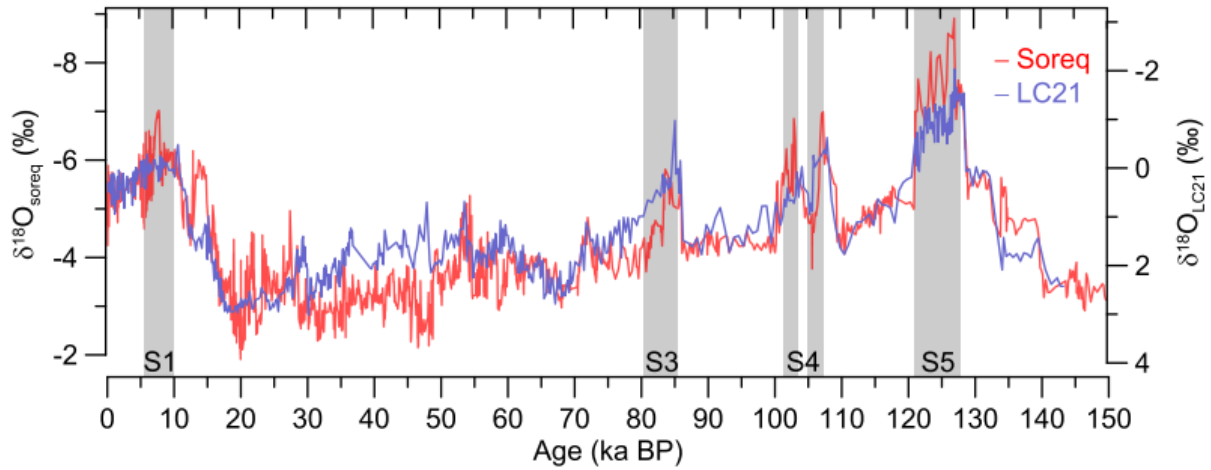


Figure 17: Comparison between  $\delta^{18}\text{O}$  profiles of an eastern Mediterranean marine sediment core (LC21 – blue line) (Grant et al., 2012) and the Soreq Cave speleothem record (red line) (Bar-Matthews et al., 2003). The two records show a strong similarity in millennial scale trends over the last 150,000 years demonstrating that the speleothem record is likely to be dominated by a source-water effect over this time frame. Figure from Rohling et al., (2015) after Grant et al., (2012).

However, for timescales between these two shorter and long periods (i.e. centennial – millennial timescales), the interpretation of  $\delta^{18}\text{O}$  variation is more complex as it becomes more difficult to disentangle the influence of the amount and source effects, as well as other mechanisms, controlling  $\delta^{18}\text{O}$  values of speleothems. Bar-Matthews et al. (2003) interprets  $\delta^{18}\text{O}$  variation of the Soreq Cave speleothem record during the Holocene in terms of rainfall amount (Figure 18), and in fact uses  $\delta^{18}\text{O}$  values to semi-quantitatively estimate the amount of palaeorainfall during the Holocene. While Bar-Matthews et al. (2003) acknowledged the possibility of source changes during the Holocene to influence  $\delta^{18}\text{O}$  values, they argued that there was little evidence for large amounts of fresh water input into the Eastern Mediterranean during the Holocene to influence speleothem  $\delta^{18}\text{O}$  values (Bar-Matthews et al., 2003; 3194), particularly any significant variation in global ice volume or temperature. A similar interpretation was made recently by an investigation on a recently published record from Katalakhor Cave in the Iranian Zagros, where millennial scale  $\delta^{18}\text{O}$  variability during the Holocene were interpreted in terms of rainfall amount (Andrews et al., 2020). They support this interpretation with comparable changes in speleothem diameter and  $^{234}\text{U}/^{238}\text{U}_0$  values. Although, little attention was given towards the contribution of changes in  $\delta^{18}\text{O}_{\text{EMSS}}$  values in this latter study.

On the other hand, a study on a speleothem from Jeita Cave, Lebanon, while displaying a very similar  $\delta^{18}\text{O}$  profile to both the Soreq and Katakhor Cave records identified a similarity between the speleothem  $\delta^{18}\text{O}$  profile and marine  $\delta^{18}\text{O}$  records from the Eastern Mediterranean and thus argued that  $\delta^{18}\text{O}_{\text{EMSS}}$  variations may have influenced Holocene  $\delta^{18}\text{O}$  values of speleothem carbonate through the source effect during the Holocene (Cheng et al., 2015) (Figure 18). For this reason,  $\delta^{13}\text{C}$  and Sr/Ca values were used as alternative proxies for hydrological variability. Cheng et al., (2015) proposed that that  $\delta^{18}\text{O}_{\text{EMSS}}$  was largely driven by changes in the amount of freshwater discharge from the River Nile and the influence of its isotopically low waters (Cheng et al., 2015), but do not explore this relationship much further.

This problem in interpreting centennial to millennial scale  $\delta^{18}\text{O}$  trends in Southwest Asia records does not only apply to speleothems. As mentioned in Chapter 3.3.4 similar challenges also face the investigation of  $\delta^{18}\text{O}$  values of lake sediment carbonates, which all show a similar trend, albeit with a higher amplitude, from lower to higher  $\delta^{18}\text{O}$  values during the Holocene (Stevens et al., 2001, 2006; Dean et al., 2018). This long-term trend has commonly been interpreted in terms of lake salinity and evaporation, and therefore a proxy for the balance between precipitation and evaporation (P:E) (Jones and Roberts, 2008). However, discrepancies between  $\delta^{18}\text{O}$  of lake sediments and other proxies (pollen, macrofossil, trace elements) in some lakes, particularly in or near the EFC has provided challenges to this view (Jones and Roberts, 2008; Stevens et al., 2006, 2001; Wasylkova et al., 2006). Stevens et al. (2001;2006) interprets  $\delta^{18}\text{O}$  in two lakes from Iran in terms of changes in seasonal distribution of rainfall, where lower  $\delta^{18}\text{O}$  values represent a relative increase in the amount colder, winter rainfall compared to warmer, spring rainfall with higher  $\delta^{18}\text{O}$  values. Similarly, Dean et al., (2018) in their investigation of  $\delta^{18}\text{O}$  values from Eski Acigöl in Turkey, indicated that seasonal changes may have influenced  $\delta^{18}\text{O}$  values of the lake, although in this latter study they suggested that seasonal changes alone were not enough to account for the amplitude of change observed in  $\delta^{18}\text{O}$  values and therefore variations in the P:E balance were also partly responsible, an interpretation which was supported by the analysis of other proxies (Dean et al., 2018). Geochemical studies of the Dead Sea and Yammouneh Lake proposed that changes in  $\delta^{18}\text{O}_{\text{EMSS}}$  values may have influenced the  $\delta^{18}\text{O}$  values of lake sediment

carbonates in the Levant during the Holocene (Kolodny et al., 2005; Develle et al., 2010), similar to the interpretation made by Cheng et al., (2015). However, Develle et al., (2010) argued that the amplitude of change identified in the Yammouneh Lake record could not be explained solely by source changes alone and P:E balance was an important secondary driver of  $\delta^{18}\text{O}$  values.

## **5.2 The Isotopic Composition of the Eastern Mediterranean Sea**

The discrepancy in how studies have interpreted  $\delta^{18}\text{O}$  values on centennial to millennial timescales during the Holocene is often related to the different views of investigators in whether the amplitude of change of  $\delta^{18}\text{O}_{\text{EMSS}}$  values during this time period were sufficiently large enough to explain the magnitude of change observed in terrestrial  $\delta^{18}\text{O}$  records. In this section, I take a closer look at the drivers behind  $\delta^{18}\text{O}_{\text{EMSS}}$  variation during the Holocene to provide an awareness of how  $\delta^{18}\text{O}_{\text{EMSS}}$  values may have influenced palaeoclimate  $\delta^{18}\text{O}$  records from Southwest Asia, and consequently the likelihood of it influencing the  $\delta^{18}\text{O}$  values produced in this thesis.

The Eastern Mediterranean Sea is nearly a completely enclosed entity, only connected to the Western Mediterranean by the narrow and shallow Strait of Sicily. Because of this restricted nature, the Eastern Mediterranean Sea is strongly influenced by evaporative processes, leading to enhanced water salinity, temperature and  $\delta^{18}\text{O}$  of the sea surface water (Figure 19) (Almogi-Labin et al., 2009). While evaporation leads to increasing salinity of the Eastern Mediterranean, the influx of fresh or less saline water has, logically, the opposite effect, which make the Eastern Mediterranean susceptible to relatively large  $\delta^{18}\text{O}$  variability. There are two main sources of significant amounts of fresh water into the Eastern Mediterranean:

- 1) The first is the addition of meltwater from ice sheet melting into the world's ocean during periods of deglaciation (i.e. the ice volume effect), ultimately feeding into the Mediterranean through the straits of Gibraltar. This also has the effect of increasing sea levels, resulting in an increased contribution of less saline Atlantic water, potentially amplifying the signal.
- 2) The second is enhanced freshwater runoff from the surrounding land, particularly from the River Nile and North Africa (during Green Saharan phases where sufficient amount of rainfall penetrate above the central Saharan watershed at  $21^\circ$ ) (Tzedakis, 2007) during periods of

enhanced African monsoon intensity (Rohling et al., 2015). The Nile is known to have a significant influence on the composition of waters in the south eastern Levantine basin of the Eastern Mediterranean and its influence reduces as you move away from the mouth of the Nile. However, during periods of enhanced outflow (up to 9 times the modern pre-Aswan Nile discharge during African Humid Periods; Amies et al., 2019 ) the influence of the ‘Nile Plume’ becomes more enhanced (Almogi-Labin et al., 2009).

Deglaciation after the Younger Dryas was minimal and therefore the ice volume effect is unlikely to have a major impact on EMSS waters during the Holocene (approx. up to 0.3 ‰; 10 m sea level rise equal 0.1 ‰ change in  $\delta^{18}\text{O}$ ). However, the insolation variability is known to have caused relatively large variations in African Monsoon intensity and position during the Holocene (Fleitmann et al., 2007), and it is therefore possible changes in the discharge rates of the Nile was likely to have influenced the composition of the Eastern Mediterranean (Hennekam et al., 2014).

$\delta^{18}\text{O}$  of planktonic foraminifera such as *Globigerinoides ruber* (*G.ruber*) in marine sediments can be used to track past changes in water salinity (e.g., Fontugne and Calvert, 1992; Essallami et al., 2007; Almogi-Labin et al., 2009; Grant et al., 2012) and can also be used to compare to terrestrial records to examine the relationship between the  $\delta^{18}\text{O}_{\text{EMSS}}$  and terrestrial  $\delta^{18}\text{O}$  records in the region (e.g. Figure 17).

There are now a number of orbital long marine sediment records which have tracked how the  $\delta^{18}\text{O}_{\text{EMSS}}$  has change over multi-millennial long-timescales (e.g., Fontugne and Calvert, 1992; Essallami et al., 2007; Almogi-Labin et al., 2009; Grant et al., 2012). Using these records, the link between multi-millennial scale changes in the  $\delta^{18}\text{O}_{\text{EMSS}}$  and speleothem  $\delta^{18}\text{O}$ , through the source effect, has been proposed a number of times and is well established (e.g., Frumkin et al., 1999; Bar-Matthews et al., 2003; Grant et al., 2012). In fact, the ocean-land link is so strong that speleothem age models (Soreq) have been used as a chronostratigraphic tool to tie chronologies to marine sediments which are much more difficult to precisely date (e.g., Grant et al., 2012). The cause for  $\delta^{18}\text{O}$  variability of the EMSS on glacial timescales has largely been explained in terms of the ice-volume effect, amplified by changes in evaporation, temperature and freshwater influx (Frumkin et al., 1999).

While, orbital scale  $\delta^{18}\text{O}_{\text{EMSS}}$  variability is generally well understood, there has been an absence of high-resolution marine records (most > 100 yrs per data point) to provide detailed information about how  $\delta^{18}\text{O}_{\text{EMSS}}$  has varied through the Holocene, which has made it difficult to reliably compare marine and terrestrial records from the region. Recently, however this has begun to change with the production of a few high resolution  $\delta^{18}\text{O}$  studies in the Eastern Mediterranean, particularly in the discharge area of the River Nile, which have sought to investigate how Nile discharge has changed during the Holocene (Hennekam et al., 2014; Hennekam, 2015) (Figure 19). One record in particular, PS009PC, is a marine sediment core from the southeast Levantine Basin (Figure 19) and provides the first marine  $\delta^{18}\text{O}$  record from the Eastern Mediterranean to match the resolution (c.10 yrs per data point) of speleothem records from Southwest Asia (Hennekam et al., 2014, 2015). In this study, the  $\delta^{18}\text{O}$  variations of *G.ruber* in the sediment core were interpreted to represent changes in the amount of freshwater discharge out of the River Nile during the Holocene. A trend from lower to higher values from 9,000 years BP to present indicates a shift from higher to lower discharge rates into the Eastern Mediterranean (Figure 18). Hennekam et al., (2014) suggested changes in the discharge rate of the Nile were largely driven by variations in the moisture contribution from the Indian Ocean Monsoon (IOM). During the early Holocene when the IOM was at its maximum intensity over East Africa, the contribution of isotopically light freshwater from the IOM into the Nile Basin increased resulting in increased freshwater output into the eastern Mediterranean from the Nile, resulting in lower  $\delta^{18}\text{O}_{\text{EMSS}}$  values. During the middle to later Holocene, the IOM weakened which resulted in less IOM derived freshwater entering into the Eastern Mediterranean, and lower Nile discharge rates, leading to higher  $\delta^{18}\text{O}_{\text{EMSS}}$  values. Hennekam et al., (2014) demonstrated the link between the IOM monsoon and  $\delta^{18}\text{O}_{\text{EMSS}}$  by comparing the  $\delta^{18}\text{O}$  profile of the PS0009PC marine sediment core to a speleothem  $\delta^{18}\text{O}$  record from Qunf Cave in Oman (Fleitmann et al., 2003a, 2007), which measured IOM monsoon intensity, and the two records displayed a strong positive correlation to one another. What this new marine record shows, from the perspective of the aims of this thesis, is that the influence of freshwater discharge from the Nile on the Eastern Mediterranean Sea is likely to be greater than previously thought. Moreover, the long-term trend during the Holocene from higher to lower values (Figure 18) is broadly like that identified in terrestrial records

from the region. This provides support to those studies which have suggested that terrestrial  $\delta^{18}\text{O}$  records during the Holocene were influenced by the source effect due to changes in Nile output.

Ultimately the influence of the source effect on Holocene  $\delta^{18}\text{O}$  values in palaeoenvironmental records from Southwest Asia is still a matter of ongoing debate and it is a process which is viewed by some researchers as a neglected mechanism (Tzedakis, 2007; Rohling et al., 2015). It has been suggested that the role of the source effect on terrestrial  $\delta^{18}\text{O}$  records may be neglected due to methodological difficulty in monitoring links between changes in source  $\delta^{18}\text{O}$  with variations in cave drip water or lake geochemistry, unlike the relatively simple methods employed to monitor relationships between  $\delta^{18}\text{O}$  values and rainfall amount or temperature. More specifically, this difficulty is because the time frame of monitoring studies is conducted on a sub-annual to decadal timescale at the most, a period in which the  $\delta^{18}\text{O}$  value of oceans remains virtually uniform, leading to biases in interpretations (Kolodny et al., 2005); however, the Eastern Mediterranean provides a unique case in which this statement is not necessarily true. During the 20<sup>th</sup> century, the construction of dams has significantly influenced the amount of freshwater entering the Eastern Mediterranean, particularly the construction of the high Aswan Dam in the Nile in 1964. Before the construction of the Aswan Dam, Nile discharge averaged  $8.4 \times 10^{10} \text{ m}^3 \text{ yr}^{-1}$  ( $4.5 \times 10^{10} \text{ m}^3 \text{ yr}^{-1}$  in low-flood years to  $15.0 \times 10^{10} \text{ m}^3 \text{ yr}^{-1}$  in high- flood years) (Rohling et al., 2015) and this has now dropped to a negligible amount. Due to the Eastern Mediterranean's enclosed nature this has had a significant impact on its salinity and should have also had an important influence on  $\delta^{18}\text{O}_{\text{EMSS}}$  values. Tracking how  $\delta^{18}\text{O}_{\text{EMSS}}$  values have changed since before and after the construction of these dams and comparing these results to precipitation data or high resolution palaeoclimate data (e.g., Jones et al., 2006; Flohr et al., 2017; Sinha et al., 2019) from Southwest Asia would provide a relatively simple way of testing the influence of the source effect on the isotopic composition of precipitation in Southwest Asia. However, as far as I am aware, exactly how  $\delta^{18}\text{O}_{\text{EMSS}}$  values have changed in response to dam building and other impacts on freshwater output during the 20<sup>th</sup> and 21<sup>st</sup> centuries is something which surprisingly has not be thoroughly examined.

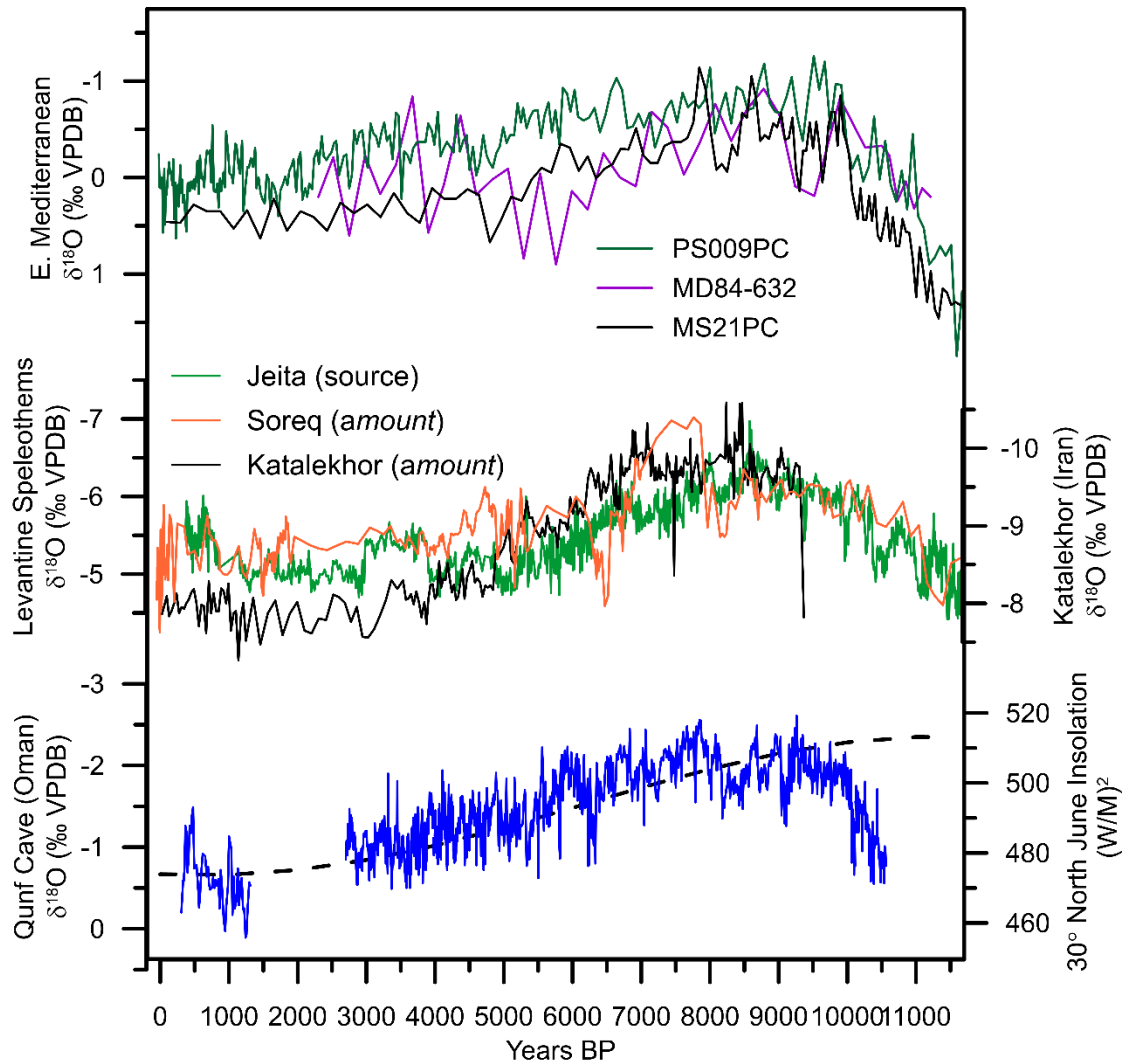


Figure 18:  $\delta^{18}\text{O}$  profiles of EMSS marine sediment cores (*G. ruber*) - PS009PC (top green line) (Hennekam et al., 2014, 2015), MS21PC (top black line) (Hennekam et al., 2015), MD84-632 (purple line) (Essallami et al., 2007), alongside Levantine and Iranian speleothem records (Bar-Matthews et al., 2003; Cheng et al., 2015; Andrews et al., 2020) as well as a speleothem record from Qunf Cave, Oman (Fleitmann et al., 2007). All records, both terrestrial and marine, show a general millennial scale trend from lower to higher  $\delta^{18}\text{O}$  values during the Holocene. Changes in the  $\delta^{18}\text{O}$  composition of the EMSS has been associated with changes in the IOM – measured by the Qunf Cave record linked to changes in summer insolation (dashed line). However, the way in which this trend has been interpreted in speleothems has been differed (in brackets next to speleothem names). Some have suggested the trend represents a trend from higher to lower rainfall amounts, while others suggest that given the broad similarity to EMSS  $\delta^{18}\text{O}$  profiles, the  $\delta^{18}\text{O}$  trend in speleothems may be related to changes in the  $\delta^{18}\text{O}$  composition of the EMSS during the Holocene, due to the so-called source effect.

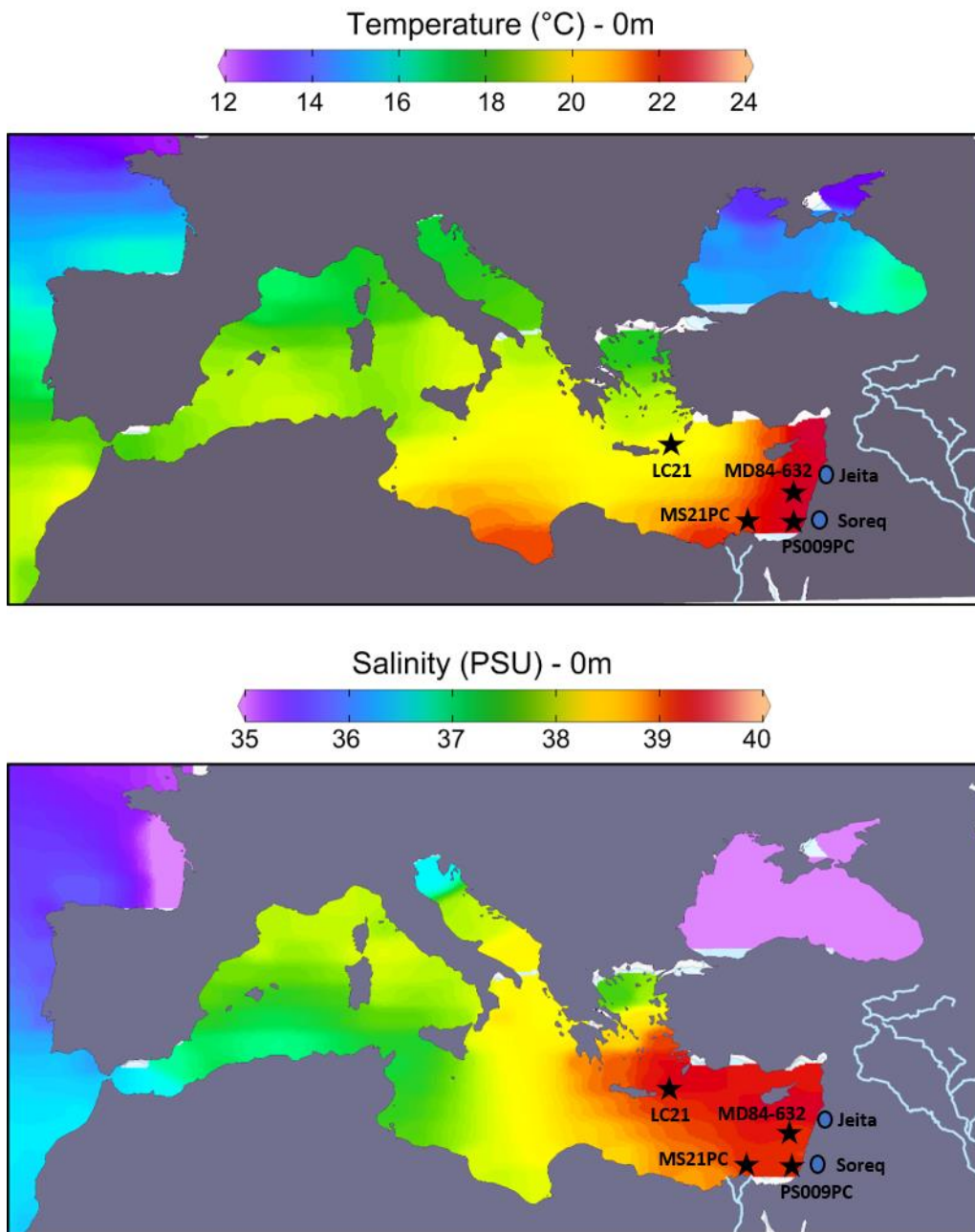


Figure 19: Annual temperature and salinity surface composition of the Mediterranean. The figure shows the clear west-east gradient in temperature and salinity, illustrating the susceptibility of the Eastern Mediterranean to evaporative processes.  $\delta^{18}O$  composition of the Mediterranean also closely follows the salinity gradient. Temperature and salinity data obtained from the World Ocean Atlas 2018 and plotted using the Ocean Data Viewer (ODV) and modified in ArcGIS pro. Key marine planktonic isotope records (black stars) and speleothem records (blue circles) discussed in this section are also shown.

### 5.3 Summary

In this chapter I have explored further the different mechanisms influencing  $\delta^{18}\text{O}$  values of speleothem records during the Holocene, specifically highlighting the debate centred around whether the amount or source effect has been a dominant driver for the observed millennial scale  $\delta^{18}\text{O}$  trend observed in many records from the region. While this chapter has not answered this debate, hopefully what it has shown is that interpreting  $\delta^{18}\text{O}$  values in Southwest Asia is a complex and challenging task and the proxy cannot be simply used as a ‘silver bullet’ for past climatic change in both speleothem and lake sediment records. An understanding of the different processes which influence the  $\delta^{18}\text{O}$  values on a site-site and archive-archive basis is probably needed, as well as integrating other types of proxies to support the interpretation. The recent production of high-resolution datasets from the Eastern Mediterranean Sea, such as the PS0009PC record, do fortunately now offer an opportunity to reliably compare marine and terrestrial records to explore the potential influence of the source effect, and these records should, and will, be used in this thesis to do make this comparison with the  $\delta^{18}\text{O}$  data produced in this thesis.

## 6 Site Selection, Geology and Shalaih Cave

Iraqi Kurdistan is host to many extensive cave systems which are located within the carbonate geology of the Zagros Mountains and surrounding foothills. Relatively recently (in 2002), the first systematic cave survey was carried out to record some of these systems and it identified the, albeit relatively rare, presence of caves with secondary carbonate formations in the region (Stevanović et al., 2009). Following these surveys, within the last decade a few studies have demonstrated the potential of speleothems from caves in the region to further our understanding of palaeoclimate conditions of northern Iraq and the broader EFC. These speleothem studies include work on samples from Shalaih Cave (Marsh et al., 2018; Amin Al-Manmi et al., 2019), Gejkar Cave (Flohr et al., 2017) and most recently Kuna Baa cave (Sinha et al., 2019).

The work of this PhD project is building on the early successes of these studies. New stalagmites from Shalaih Cave have been collected to further our understanding of Holocene climate change and variability. This chapter will provide information on the geology and summarise relevant past research of the cave in order to contextualise the interpretation of data produced in this project.

### 6.1 Shalaih Cave

Shalaih Cave (35.146°, 45.296°, 730masl) is a single entrance cave located in the Sangaw district, Sulaymaniyah province (c.50km southwest of Sulaymaniyah City), Iraqi Kurdistan, in the foothills of the Zagros mountains (Figure 20). The cave is located on the southern tip of the Ashdagh (or Aj-Dagh) anticline which runs north-west/south-east (Figure 20). The cave entrance is located in a large sinkhole within the anticline (Figure 21). The geology of the area is characterised by the exposure of 12 different formations dating from the late Eocene to late Miocene. Shalaih Cave itself is associated with the Bajawan (or Bajwan) formation in middle Oligocene rocks, deposited approximately 33.9 ma to 23 ma. The Bajawan formation has been described as a milky to white, thickly bedded and highly jointed limestone (Kharajiany, 2014, p. 27) and partially dolomitised (Ghafur, 2012, p. 41). The thickness of the Bajawan formation has been recorded as 16m at the nearby (deserted) village of Shalaih, from which the cave derives its name (Amin Al-Manmi et al., 2019). The cave is approximately 600 m long with

the ceiling height reaching nearly 30 m and less than 1 m in small passages in some locations, although it is likely the cave has not been fully explored. The main access tunnel of Shalaih Cave follows a N-E direction (Figure 22). The cave is mostly horizontal, with some areas filled with soil and collapsed rocks. There are two main galleries in the cave; a small gallery which is nearly 200 m away from the entrance where the monitoring work took place and a large gallery 30 m further into the cave which is filled substantially with both actively growing and fossil speleothems. The small gallery is filled with actively growing columns, stalactites, stalagmites and flowstones. The large gallery contains various types of speleothems which include rimstone dams, stalactites, stalagmites, columns, popcorn balls, flowstone, shelfstone and moonmilk. In both galleries, numerous stalagmites reach several metres in height. These passages have no running underground water flow but do have filled water pools (Amin Al-Manmi et al., 2019, p. 263)

Due to the semi-arid climate conditions vegetation above the cave is sparse and is mainly composed of steppe shrubland and grasses. Soil thickness is relatively thin with substantial areas of exposed limestone bedrock visible (Figure 20). During a 2018 survey of the site, evidence of pastoral activities above the cave (sheep/goat dung) could be identified and shepherds and flocks were seen nearby. Small plots of agricultural land were also identified close to the cave.

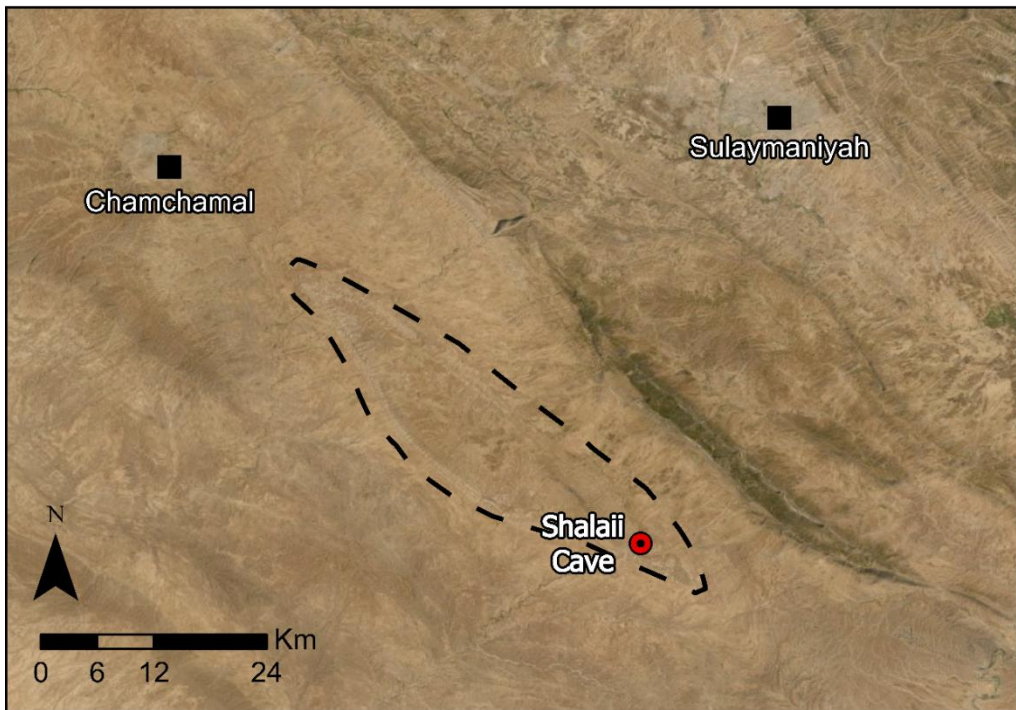


Figure 20: Top: Location of Shalaih Cave within wider Southwest Asia and its position within the EFC (red dashed line). Bottom: Zoomed in image, with locations of the Sulaymaniyah and Chamchamal. Dashed Black line represents the extent of the Ashdagh anticline within which Shalaih Cave is located.



Figure 21: Image of the sinkhole within which the entrance to Shalaih cave is located (red arrow) looking north-east. Vegetation is sparse, mostly composed of grasses, although the photo was taken at the very end of the dry season. The outcrops of bedrock (outside of the sinkhole) indicate a thin soil profile above the cave. Photo taken by author on October 2018.

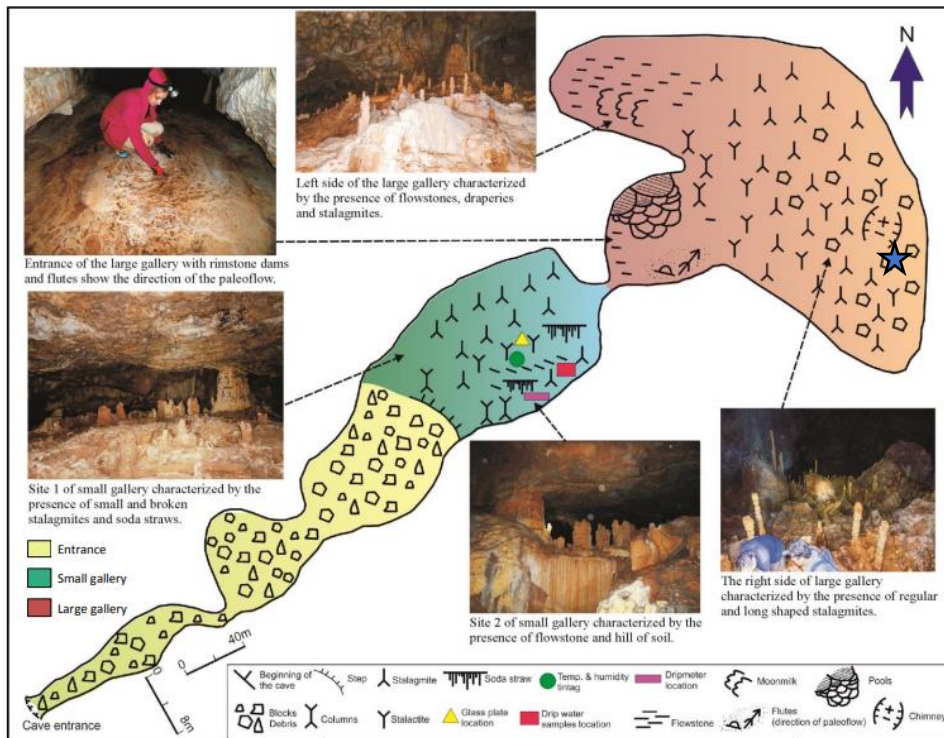


Figure 22: Schematic plan of Shalaih Cave with annotations. Green and red colouring indicate the smaller and large gallery within the cave respectively. The stalagmites collected for this project, SHC-03 and SHC-04, were found within the larger of the two galleries and the blue star marks the approximate location they both were collected from. Figure from Amin Al-Manni et al., (2019, p. 264).

## **6.2 Climate**

Average annual precipitation in Sangaw province is 463mm, recorded at the Chamchamal station measurements during 2000–2014 (Marsh et al., 2018, p. 956), however this is highly variable and often dependent on the amount of spring rainfall (Reuter et al., 2018) with the region experiencing high interannual rainfall variability of between 40 and 60% (Sinha et al., 2019). The wider regional area around the cave is locally known as ‘*Garmian*’, derived from the Kurdish word for ‘hot’. The average minimum monthly temperature occurs in January (7.1°C) and the average maximum monthly temperature is in August (33.2°C) (Marsh et al., 2018, p. 956).

## **6.3 Suitability of Shalaih Cave to Capture Regional Climate Change**

As explained in Chapter 2, the climate of Southwest Asia is highly heterogeneous and therefore it can be problematic to extrapolate palaeoclimate observations from one site to characterise another area. In order to identify to what extent the conditions around Shalaih, and how they have changed through time, are representative of the wider EFC, a precipitation correlation map was produced using the KMNI climate explorer (Figure 23) to illustrate how precipitation variability at Shalaih is likely to have correlated with precipitation variability in other areas throughout Southwest Asia between 1901 – 2015. The correlation map reveals that conditions at Shalaih Cave correlate strongly (p-value >0.6) with variability observed across most of the EFC, and therefore speleothems from this cave are likely to provide suitable records to characterise conditions for the wider EFC.

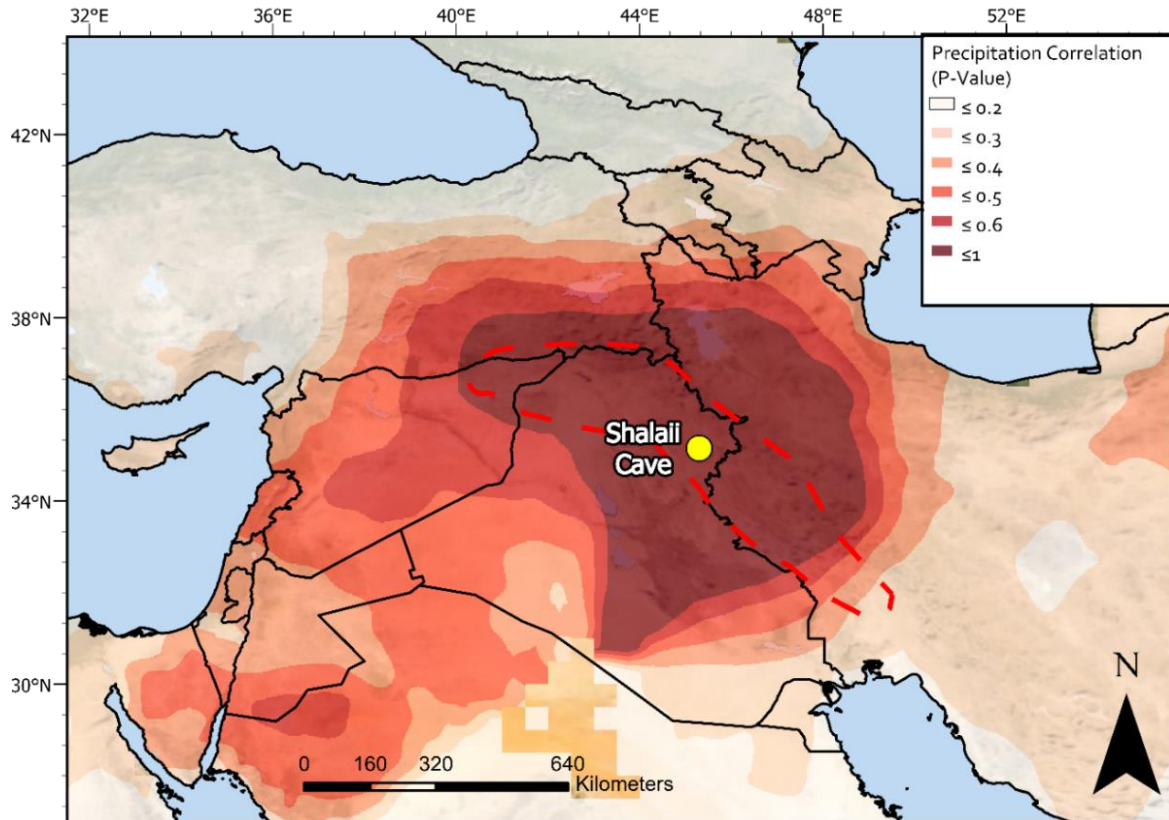


Figure 23: Map illustrating the correlation of precipitation variability between Shalaili Cave and other areas of Southwest Asia. Data CRU TS 4.01 gridded precipitation ( $0.5^\circ \times 0.5^\circ$ ) from summer (October to March) over the period 1901–2015 (Jones and Harris, 2008) via the KMNI climate explorer ([//climexp.knmi.nl](http://climexp.knmi.nl)) (Van Oldenborgh et al., 2009). It shows that precipitation variability within most of the EFC during this period correlates strongly ( $p$  value  $> 0.6$ ) with conditions around Shalaili Cave.

#### 6.4 History of Research

Fieldwork at the cave was initially carried out as part of an MSc programme at the University of Sulaimaniyah by Sozan Burhan Ismaeel. This work included mapping and monitoring the cave from June 2014 – June 2015. Monitoring methodology included using a smoker to determine air circulation, ten months of temperature and relative humidity readings and a drip meter was fixed to a stalagmite to measure the rate of drip, with measurements made every 12h. Furthermore, drip waters and rainwater above the cave were collected for stable isotope analysis. At the same time two small stalagmites were collected for analysis. The results of both the monitoring data and speleothem analysis have been published (Marsh et al., 2018; Amin Al-Manmi et al., 2019). I will summarise the findings in this section.

## **6.5 Monitoring Data Results**

### **6.5.1 Air Circulation**

The smoker used to determine air circulation showed no change in direction, therefore indicating that the cave has only one significant entrance and Shalaih is a closed system cave. The average cave air pCO<sub>2</sub> is 596 ppm. However, winter values were higher reaching 756 ppm and then falling to less than 484 ppm in mid-September, close to atmospheric levels. Seasonal variation in PCO<sub>2</sub> is suggested to be the result of reversals in chimney ventilation driven by temperature contrasts between the cave interior and exterior (Amin Al-Manmi et al., 2019, p. 267).

### **6.5.2 Minerology**

The analysis of the content of modern carbonate formation on a glass plate within the cave using a calcimeter showed that newly precipitated carbonate was 100% calcite (Amin Al-Manmi et al., 2019, p. 267).

### **6.5.3 Drip Rates**

Drip rates were measured daily in Shalaih Cave between July 2014 and May 2015 (Figure 24). This demonstrated that dripping occurred throughout the year, even during the arid summer months and therefore suggests relatively large storage capacity above the cave. Although, drip rates were considerably higher during the wetter winter months, reaching a maximum of 29,199 drips/day, compared to the summer where the lowest drip rates were identified with a minimum of 4408 drips/day. This variability reflects seasonal recharging of the aquifer and demonstrates that the drip rate within Shalaih Cave responds to changes in the amount of rainfall (Amin Al-Manmi et al., 2019, p. 266).

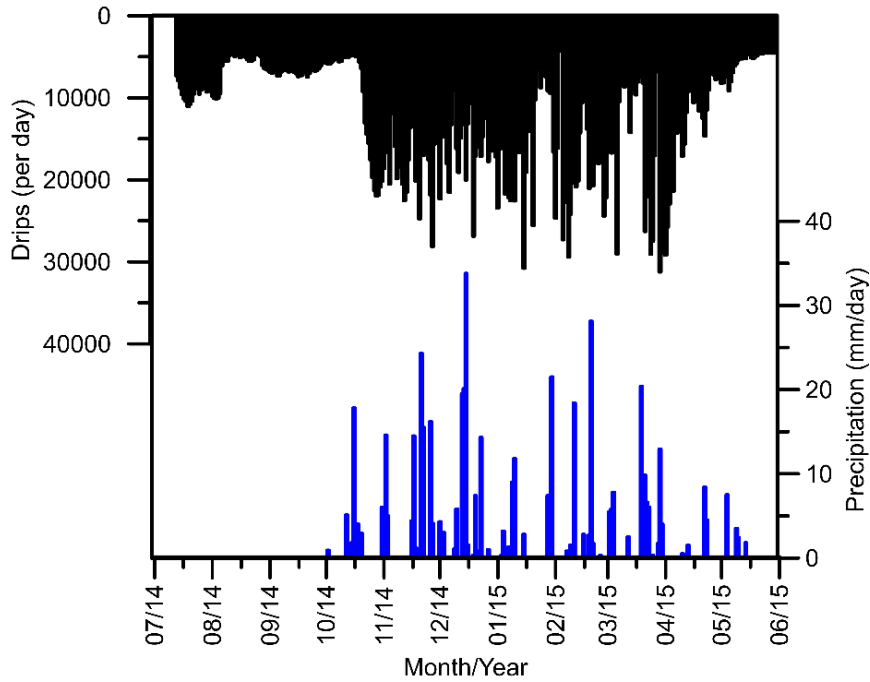


Figure 24: Drip rates from a location within Shalaih Cave compared to precipitation data recorded above the cave. It shows that dripping occurs throughout the year, even during the arid summer months, which indicates relatively large water storage above the cave. Modified after Al-Manmi et al. (2019).

#### 6.5.4 Temperature and Humidity

Temperature readings were collected at one per month over a ten-month period between 2014 and 2015 (Figure 25). The readings were taken above the cave, at the cave's entrance and within the cave gallery. They show that the cave maintains a stable temperature throughout the year of 20.18 °C, which is very similar to the mean annual outside temperature of 20.5 °C. This demonstrates that the rock and soil cover act as heat insulators which results in very little temperature variation. Humidity measurements within the cave demonstrate that the cave maintains a relative humidity of 100% throughout the year (Figure 26) (Amin Al-Manmi et al., 2019, p. 266). The high humidity within the cave minimises evaporation and therefore limits the amount of kinetic isotope fractionation of cave drip water (McDermott, 2004).

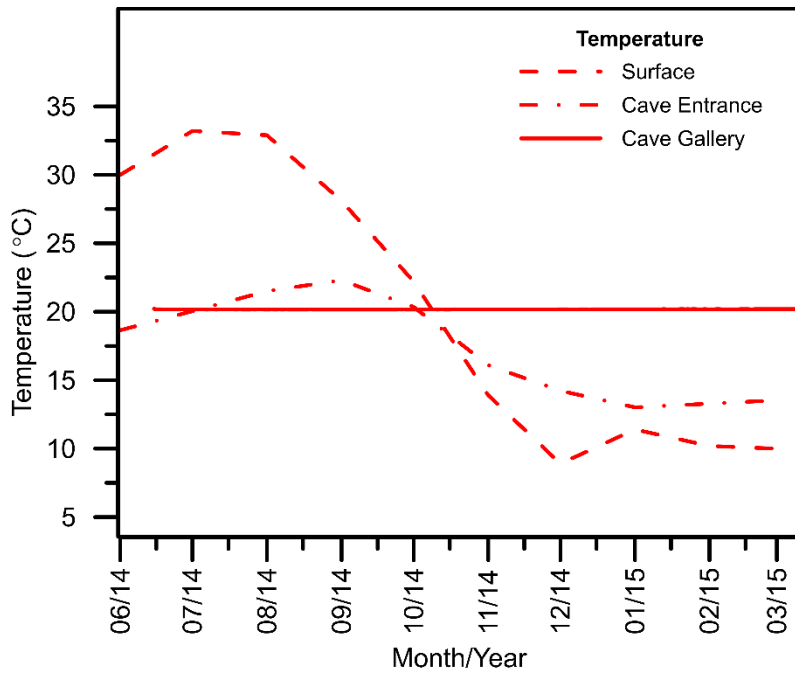


Figure 25: Temperature data recorded inside and outside Shalaih Cave. It shows that the temperature inside Shalaih Cave remains constant throughout the year. Modified after Al-Manmi et al. (2019).

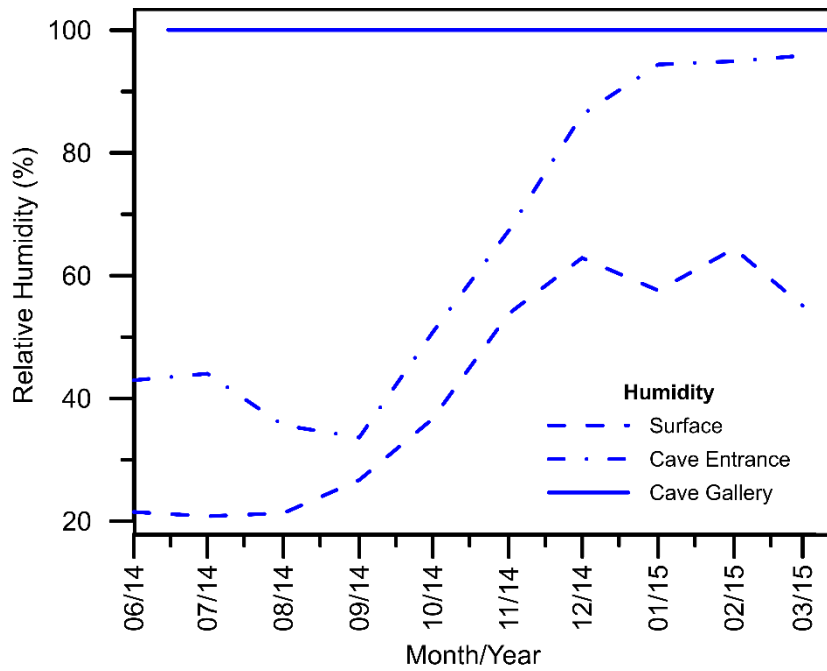


Figure 26: Humidity data recorded inside and outside Shalaih Cave. Like temperature, it shows that relative humidity inside Shalaih Cave remains constant, at 100%, throughout the year. Modified after Al-Manmi et al. (2019).

#### 6.5.5 $\delta\text{D}$ and $^{18}\text{O}$ of Rain and Drip Water

The hydrogen ( $\delta^2\text{H}$ ) and oxygen ( $\delta^{18}\text{O}$ ) isotopic composition of precipitation and drip water provides important fingerprint information which can help with the identification of moisture sources for precipitation, evaporated atmospheric moisture conditions, and air mass trajectory patterns (Heydarizad et al., 2019). As part of the previous investigations in Shalaih Cave, rainwater samples were collected for stable isotope analysis ( $\delta\text{D}$  and  $\delta^{18}\text{O}$ ) from Chamchamal meteorological station (Amin Al-Manmi et al., 2019). These samples were collected over a 5-month period from November to March 2014-2015 which represents the main wet season of the region. The isotopic values for precipitation range from  $-6.1\text{‰}$  and  $-4.01\text{‰}$  for  $\delta^{18}\text{O}$  and between  $-48\text{‰}$  and  $-34.7\text{‰}$  for  $\delta\text{D}$ . The rainwater results were used to construct a local meteoric water line, the Sangaw Meteoric Water Line (SMWL) (Amin Al-Manmi et al., 2019, p. 269), defined as:

$$\delta\text{D} = 6.312 \times \delta^{18}\text{O} - 9.45.$$

Similarly, 11 drip water samples from Shalaih Cave were collected once a month between June 2014 to April 2015. The average isotopic composition of the drip water samples is  $-5.611\text{‰}$  and  $42.102\text{‰}$  for the  $\delta^{18}\text{O}$  and  $^2\text{H}$  respectively and suggests a meteoric origin for the ground water (Amin Al-Manmi et al., 2019, p. 267).

To evaluate the precipitation and cave drip water data the results are compared to waterlines produced in other studies from the EFC as well as the EMWL and GMWL, which can act as references of the Shalaih Cave data. The SMWL line produced by (Amin Al-Manmi et al., 2019) is considerably lower than the 8.0 which characterises both the Global and Eastern Mediterranean water lines (GMWL and EMWL). This deviation from the GMWL to a slope below 8 is likely to be the consequence of local evaporative effects, particularly partial evaporation of water droplets below the clouds, a common process in semi-arid locations with low humidity (Gat and Dansgaard, 1972; Clark and Fritz, 1997) or evaporation after samples collection.

An alternative way to produce a local Meteoric Line is to use interpolated estimates from the GNIP (Global Network of Isotopes in Precipitation) database composed of monthly composite total rainfall data including  $\delta^2\text{H}$  and  $^{18}\text{O}$  values (Bowen et al., 2005; IAEA, 2009). These estimates are plotted in

Figure 27, The amount-weighted average value of modelled data falls very close to the BMWL, another recently constructed LMWL constructed from 55 precipitation events collected from nearby to Shalaih Cave. Therefore, this line (BMWL) is likely to be a more accurate fit for precipitation above Shalaih Cave.

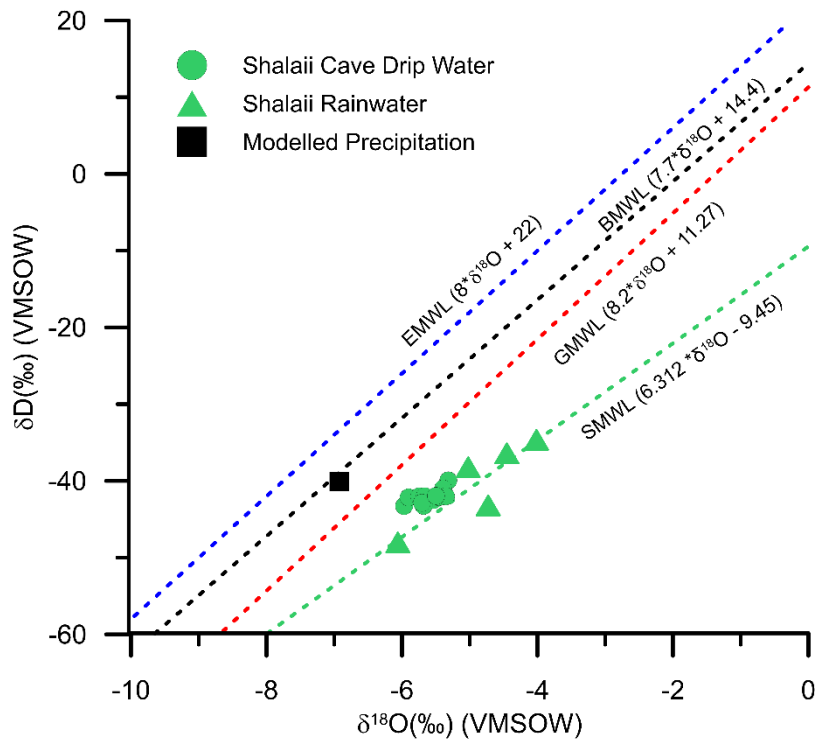


Figure 27: Rain (green open Squares) and drip water (green circles) δD and δ<sup>18</sup>O values from Shalaih Cave compared to local (BMWL – blue line), regional (EMWL – blue dashed line) and global water lines (GMWL – red dashed line). The Meteoric Water Line (SMWL - solid black line) for Shalaih Cave as observed by Al-Manmi et al. (2019) both fall well below the GMWL and indicate these have been heavily influenced by secondary evaporative processes below the cloud base. Supported by modelled data (Black square), the BMWL (black dashed line) is another LMWL produced recently from a site close to Shalaih cave arguably provides a better indicator of the source of moisture which suggests a strong influence of Eastern Mediterranean sourced moisture.

#### 6.5.6 Relationship between isotopic values and the amount of rainfall

Using the monthly isotopic values from rainwater samples, Amin Al-Manmi et al., (2019) suggested there was a relationship between rainfall amount and isotopic values as a function of the amount of rainfall. This current study argues that a comparison between the isotopic values and rainfall amount of these rainwater samples does not show a clear relationship, but this is likely due to the small number of rainfall samples used for isotopic analysis (five). However, by using isotopic values for precipitation at the cave site modelled using interpolated estimates from the GNIP database of long-term monthly values (OIPC) alongside observed and modelled precipitation amounts (Figure 28), a clear negative relationship between the amount of rainfall and isotopic values is clear. Therefore, this study still agrees that on a monthly scale, isotopic values for rainfall is likely to be a function of rainfall amount.

The values of  $\delta^2\text{H}$  and  $\delta^{18}\text{O}$  of drip water show very little variation over the eleven-month period (Ranging from c. -5.3 - -6 ‰) (Figure 29). This suggests a relatively large amount of mixing between groundwaters and recharge above the cave in the epikarst which dampens monthly isotopic variation. However, of the variation that does exist, a positive relationship exists between  $\delta^{18}\text{O}$  and  $\delta\text{D}$  values of drip water with rainfall amount, which is the opposite to the observed relationship between precipitation and isotopic values of rainwater. This is likely to be the result of a lagged response to changes in rainfall, most likely due to an increased hydraulic head and/or increased fracture flow with the onset of winter rainfall, forces through older, isotopically heavy (spring) rainwater that was stored in the epikarst for at least 1 month (Johnson et al., 2006). However, the, albeit delayed, isotopic response to the amount of rainfall above the cave does suggest that average transit time from precipitation to drip water is less than 1 year.

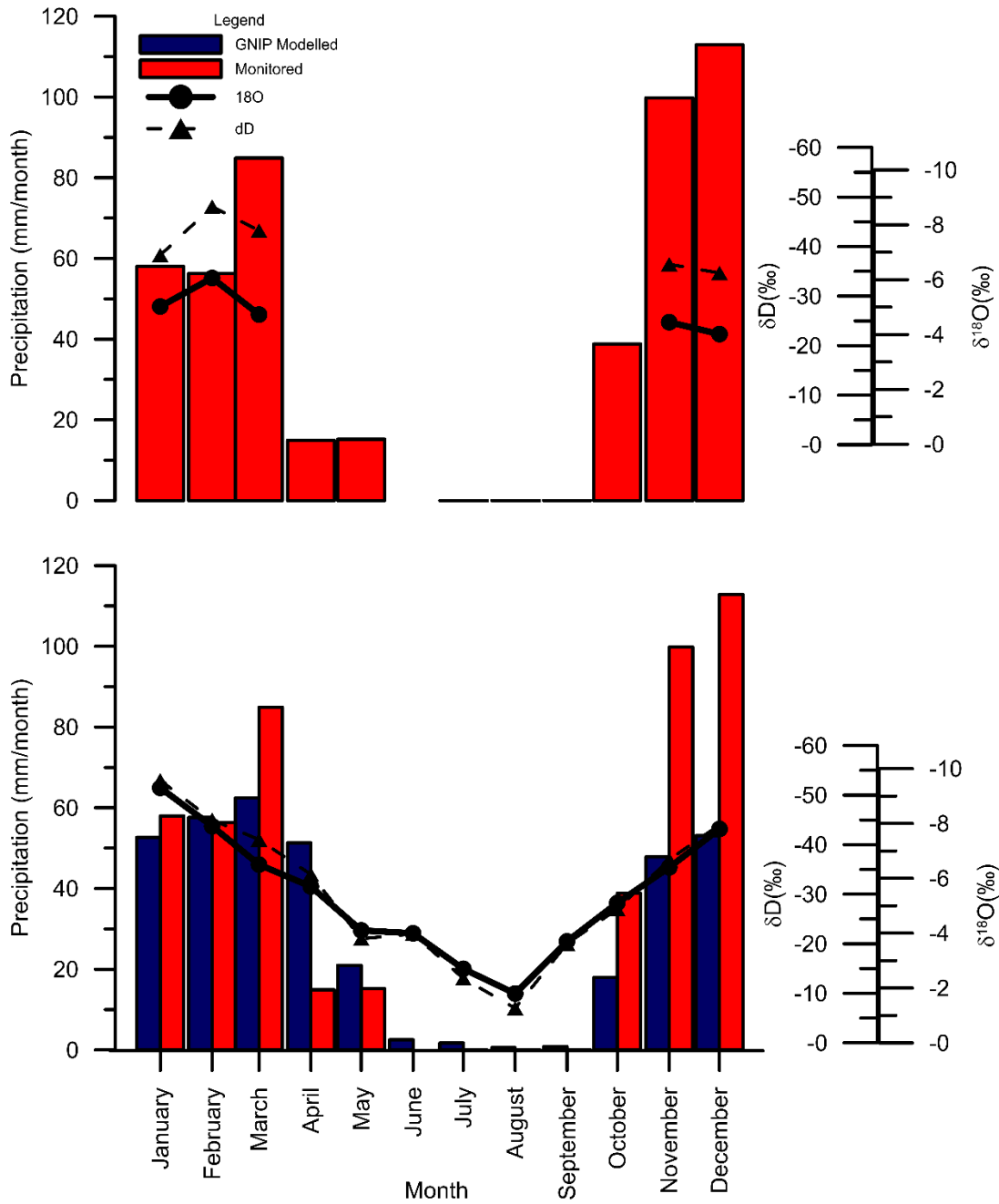


Figure 28: Top: Relationship between the isotopic composition and the amount of rainfall above Shalaih Cave using monitoring data from Al-Manmi et al. (2019). No clear relationship is observable, but this is likely due to the small number of samples used for the isotopic analyses. Bottom: Estimates of long-term seasonal variation in Shalaih Cave precipitation  $\delta D$  (dashed line and triangles) and  $\delta^{18}O$  (solid line and circles) values calculated using the Online Isotopes in Precipitation Calculator (OIPC) compared to the monitoring rainfall amount results from Shalaih Cave (red bar) (Al-Manmi et al. 2019), as well as long-term monthly average precipitation for the Shalaih Cave  $0.5^\circ$  grid cell, obtained from the KNMI climate explorer (<http://climexp.knmi.nl/start.cgi>), averaged over the years 1980 – 2019 . The plot clearly shows a clear negative correlation between the amount of rainfall and the isotopic composition of rainwater, and therefore the amount effect is likely to be a dominant driver of the isotopic composition of rainwater, at least on the long-term monthly scale.

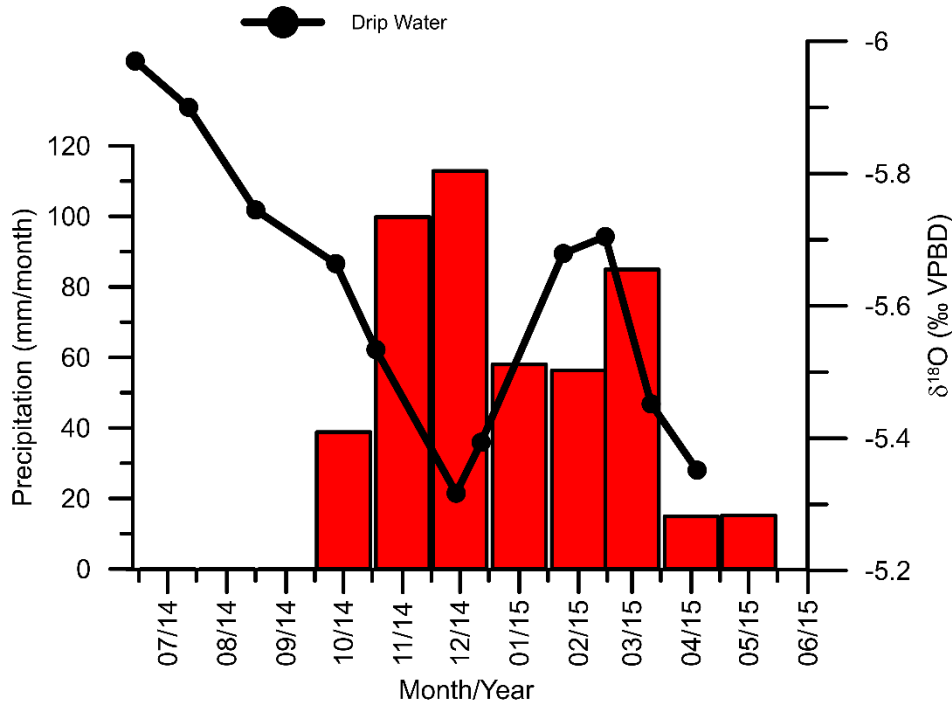


Figure 29: The isotopic composition of cave drip-water with Shalaih Cave alongside precipitation amount above the cave. It seems to show a positive relationship between rainfall amount and cave drip water  $\delta^{18}\text{O}$  (i.e higher rainfall amounts lead to more positive  $\delta^{18}\text{O}$  values), this is the opposite of what would be expected if the ‘*amount effect*’ is a dominant control. However, as Figure (27) shows, there is a clear negative relationship rainfall  $\delta^{18}\text{O}$  and rainfall amount. Therefore, it is likely that the drip-water  $\delta^{18}\text{O}$  values reflect a lagged response to variations in rainfall amount, where drip water represents water stored in the karst reservoir above the cave for multiple months. Modified after Al-Manmi et al. (2019).

## 6.6 Human and Animal Impact

Human impact can have an influence on cave environments, affecting both  $\text{pCO}_2$  and humidity levels within the cave that could potentially distort geochemical signals in speleothems. While there is some evidence of recent, low level temporary use of the cave entrance (e.g. as a shepherd shelter), there is no evidence of significant long-term occupation within the cave in the past that would significantly influence speleothem geochemistry. There is a high level of bat activity within the cave and therefore it is possible that mineral and organic (i.e. guano) bat deposits may influence the geochemistry of speleothems under roosts (Chang et al., 2010).

## 6.7 Previous Investigations

The cave has previously been the focus of palaeoenvironmental investigations (Marsh et al. 2018; Diary et al. 2019). Two stalagmites, SHC-01 and SHC-02 (Figure 30), were collected for a pilot study in 2014.  $\delta^{18}\text{O}$  and  $\delta^{13}\text{C}$  analysis were carried out by Prof. Dominik Fleitmann at the University of Reading on carbonate samples collected every 10mm through the stalagmites. Four U-Th samples, from the top and bottom of each stalagmite, were collected for analysis at the University of Minnesota.

The U-Th results indicated that SHC-01 is grew during the late Holocene ( $1012 \pm 42$  yr BP to  $494 \pm 29$  yr BP) and SHC-02 grew during the middle Holocene;  $8025 \pm 38$  yr BP to  $6977 \pm 219$  yr BP) (Marsh et al., 2018, p. 960) .

$\delta^{18}\text{O}$  values of stalagmite SHC-01 ranged from  $-6.34\text{‰}$  to  $-4.87\text{‰}$  around an average of  $-5.65\text{‰}$ .  $\delta^{18}\text{O}$  values of the older stalagmite SHC-02, ranged from  $-7.55\text{‰}$  to  $-5.77\text{‰}$  around a mean of  $-6.54\text{‰}$ , almost 1‰ more negative than SHC-01.  $\delta^{13}\text{C}$  values of stalagmites SHC-01 and SHC-02 range from  $-11.59\text{‰}$  to  $-9.07\text{‰}$  and from  $-10.05\text{‰}$  to  $-7.78\text{‰}$ , respectively. Mean  $\delta^{13}\text{C}$  values of stalagmite SHC-01 are  $-10.22\text{‰}$  compared with  $-8.94\text{‰}$  of sample SHC-02 (Marsh et al., 2018, p. 963; Amin Al-Manmi et al., 2019) (Figure 36).

$\delta^{18}\text{O}$  values from the stalagmites were interpreted in terms of rainfall amount. Therefore, the more negative  $\delta^{18}\text{O}$  values during the early Holocene were interpreted as an indication of wetter conditions, relative to the time period covered by the younger stalagmite, which showed more positive  $\delta^{18}\text{O}$  values and drier conditions (Amin Al-Manmi et al., 2019). The  $\delta^{13}\text{C}$  record provided more difficulty in interpreting as the more recent stalagmite had more negative  $\delta^{13}\text{C}$  values, potentially an indicator of wetter conditions. The authors suggest a number of mechanisms that influence  $\delta^{13}\text{C}$  could explain the contradiction which include vegetation density, recharge conditions and drip-rate and  $\text{CO}_2$  degassing within the cave (Amin Al-Manmi et al., 2019, p. 271).

These samples from the pilot study on stalagmites have demonstrated the potential for speleothems from the cave to produce palaeoclimate records. They also provide useful data to compare the results of this study to verify record replication within the cave.

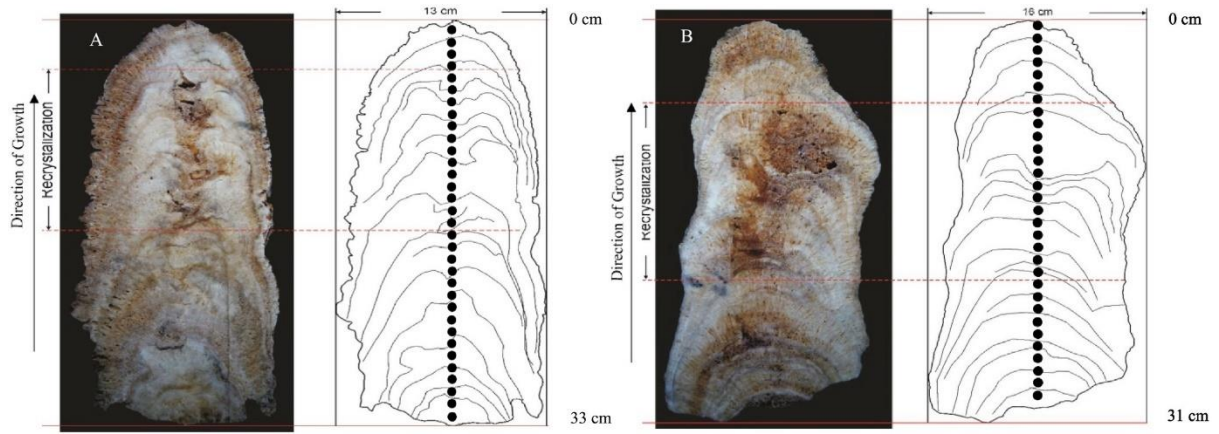


Figure 30: Images of the two previously investigated stalagmites from Shalaih Cave, SHC-1 (left) and SHC-2 (right). After Al-Manmi et al., (2019, p. 266).

## 7 Material and Methods

### 7.1 Sample Selection

#### 7.1.1 SHC-03

In 2016, following the success of the pilot studies at Shalaih Cave, researchers associated with this project returned to the cave to collect an actively growing stalagmite from Shalaih Cave that was likely to have grown throughout the entire Holocene. The stalagmite selected was a *c.*3.17m long columnar shaped stalagmite (SHC-03) (Figure 31 & Figure 32), found within the larger chamber of the cave (Figure 22).

To get the stalagmite out of the cave, it was cut into thirteen slabs (Slabs 1 – 13). Each of these slabs were later themselves cut in half through their vertical growth axis. The stalagmite fabric is composed of a creamy white porous calcite, however there is substantial post-depositional diagenesis throughout the centre of the sample, composed of a dark brown semi-transparent mosaic calcite. Although not verified, post-depositional diagenesis is likely to have been caused by solution ‘drilling’ of the stalagmite through the infiltration of unsaturated and acidic waters, particularly during periods of intense rainfall (Baldini et al., 2006; Lachniet, 2009) and a number of actively growing stalagmites within the cave show evidence of pooling on their tops (Figure 31). Areas of recrystallisation were avoided when sampling. SHC-03 has a clear hiatus visible at a depth of *c.*2,035mm as a thick layer of recrystallised calcite and this has been verified by U-series dates (Figure 33).

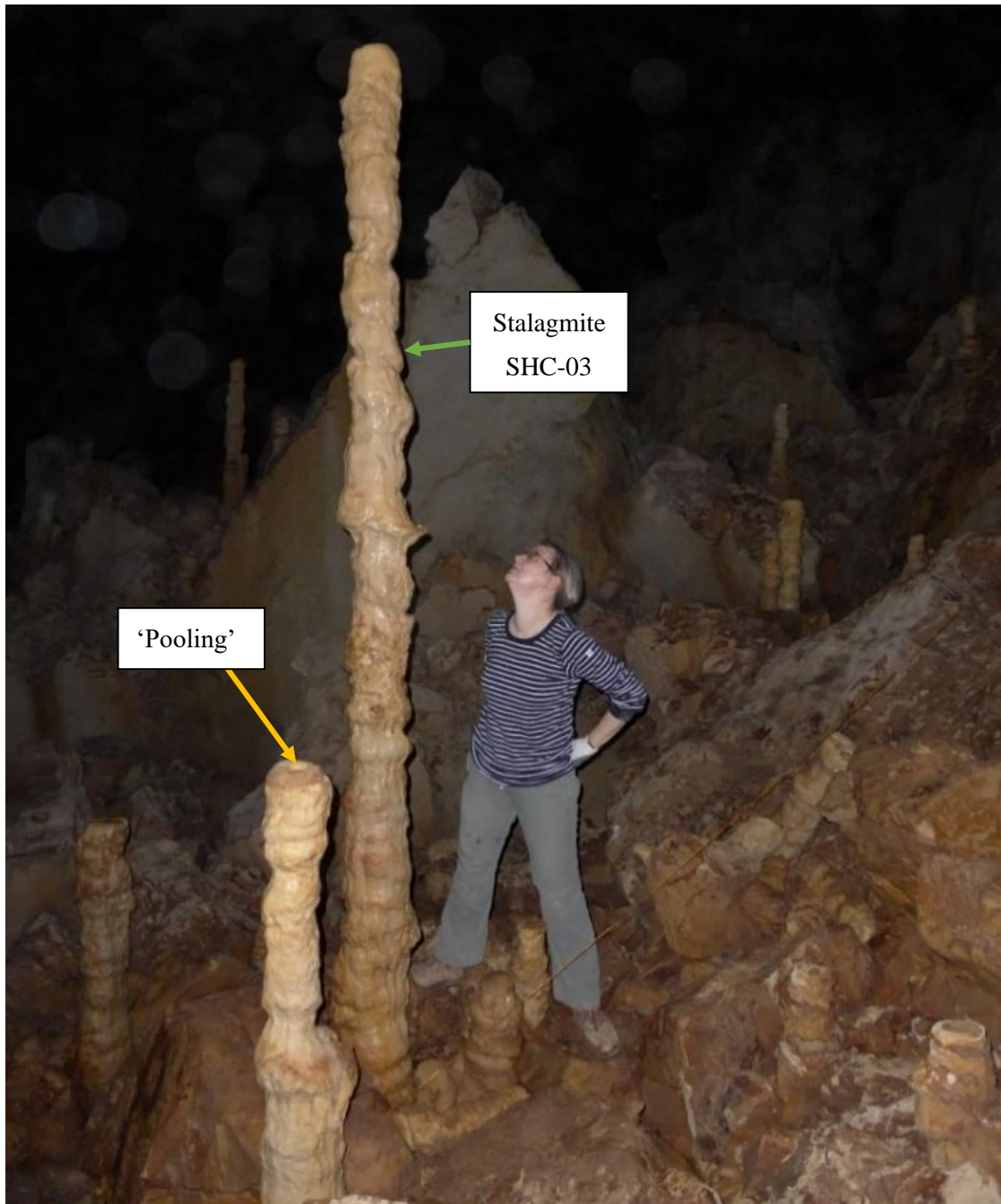
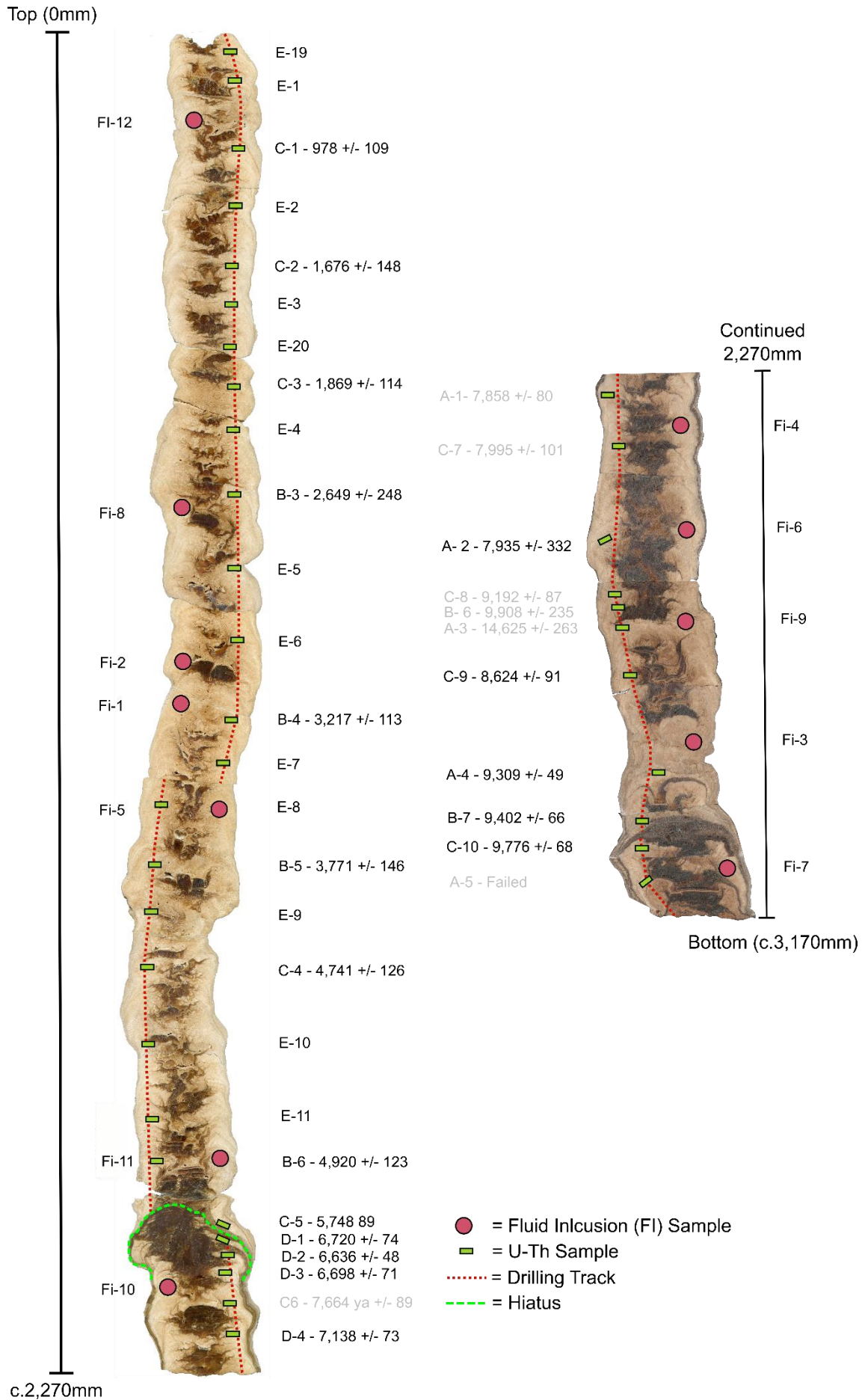


Figure 31: A colleague standing next to the stalagmite SHC-03 collected for this PhD study. Yellow arrow points to pooling at the top of a smaller, nearby stalagmite, the same mechanism might be the cause of recrystallisation in SHC-03.

Material and Methods



## Material and Methods

Figure 32: Scanned Images of stalagmite SHC-03, annotated with the location of samples collected for analysis in this study. Image on the left is the top c.2,270mm of the stalagmite and the image on the right hand side is the bottom c.1,200mm of the stalagmite. Red dashed line indicates location of the track where the stable isotope, trace element and strontium isotope samples were collected from. Green rectangles indicate location of samples collected for U-Th dating with their associated ages (as yr BP) adjacent. Greyed out text signifies dates excluded from the age model. Red circles indicate samples collected for fluid inclusion analysis. Green dashed line indicates location of the major hiatus in growth of the SHC-3 stalagmite (Figure 33). Text with no associated dates (e.g E-1) indicate locations where samples have been collected, but are yet to be analysed. Results of dating discussed in further detail in Chapter 8. The Figure also clearly shows the presence of recrystallised, dark mosaic calcite which runs along the central growth axis of the stalagmite which was avoided when sampling.

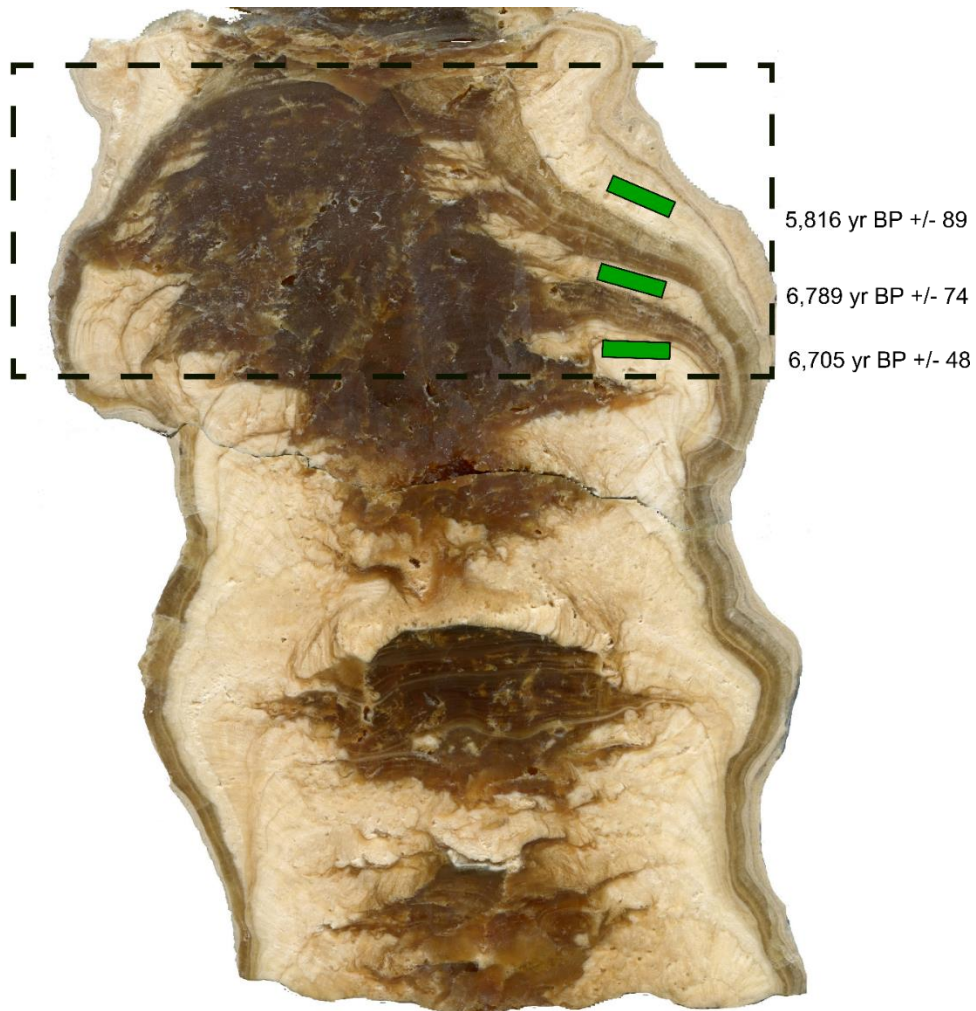


Figure 33: Zoomed in high resolution image of Slab 7. The figure highlights the major hiatus in growth present in the stalagmite, which is visible mineralogically and has also been identified by the U-Th dates (green rectangles).

7.1.2 SHC-04

In October 2018, a small team returned to the cave to collect another stalagmite sample. A c. 1.5m long stalagmite, SHC-04, was selected for further geochemical analysis. However, due to disruption related to the Covid-19 outbreak, it was unfortunately not feasible to conduct further analysis on this sample in the course of this project.



Figure 34: Scanned image of SHC-04, a second stalagmite collected for this project. Currently, no further work has been carried out on this stalagmite.

## 7.2 Analytical Methods

The following section explains the analytical procedures and methods used during this project to investigate proxies from the stalagmite SHC-03.

### 7.2.1 Uranium-Series Dates

23 carbonate samples (228mg – 744mg) for U-Th dates (Table 2) were collected and analysed in multiple stages between 2016 (CE) and 2019. The location of samples taken for U/Th dating are illustrated in Figure 32. Another 20 U-Th (E1-20) dates have been collected from the stalagmite which have not yet been analysed.

U-series dating was done within a class 100 HEPA filtered clean lab at the NERC Isotope Geosciences Laboratory Geochronology and Tracers Facility (NIGL-GTF), Keyworth following a similar method to Crémière et al. (2016). Sample powders were weighed (228mg – 744mg) and placed in Savillex vials, covered in high purity water, and dissolved by drop-wise addition of 15 M HNO<sub>3</sub> to ensure controlled and contained sample dissolutions. Samples were centrifuged and visually checked for complete dissolution and then spiked with a mixed high purity <sup>229</sup>Th/<sup>236</sup>U tracer. The U-Th tracer was calibrated against gravimetric solutions prepared from CRM 112a U metal, Ames Laboratory high purity Th metal, and blank checked ~2.5 M HNO<sub>3</sub> + trace HF. The gravimetric solutions, tracer stock and tracer working solution are all contained in Nalgene FEP bottles that were rigorously cleaned before use with ultrapure acids for a minimum of 3 months. Spike-sample equilibration was achieved through drying the dissolved samples down, re-dissolution in 15 M HNO<sub>3</sub>, and refluxing at ca. 100 °C for 24 hr. All samples went through two overnight oxidation steps in a mixture of 2 ml 16 M HNO<sub>3</sub> and 0.2 ml 30% H<sub>2</sub>O<sub>2</sub> followed by evaporation to dryness. After oxidation the samples were dissolved in 1 M HCl, approximately 5 mg Fe as FeCl was added, and U and Th pre-concentrated by Fe co-precipitation with ammonia. Initial separation on 0.6 ml columns using AG-1 × 8 anion exchange resin were done following the procedure of Edwards et al. (1987). Th fractions were further purified using a second pass through AG-1 × 8 resin and were filtered using 0.22-µm pore-size syringe filters to remove resin particles. Both U and Th fractions were oxidized twice in 2 ml 16 M HNO<sub>3</sub> and 0.2 ml 30% H<sub>2</sub>O<sub>2</sub>, and dissolved in 1 ml 0.1 M HCl and 0.035 M HF. Before mass spectrometry analyses, all samples were

filtered to remove particles originating from the perfluoroalkoxy alkane (FEP) beakers used for sample preparation.

Isotope ratio measurements were made on a Thermo Neptune Plus MC-ICP-MS with samples introduced via an Aridus II desolvating nebulizer using an ESI PFA nebulizer tip with an  $\sim 50 \mu\text{l min}^{-1}$  uptake rate. Typical operating conditions included the addition of  $4\text{--}8 \text{ ml min}^{-1}$  high-purity  $\text{N}_2$  to the sample-carrying Ar stream, to minimize U and Th oxide formation in the plasma. U measurements were made using a normal sample cone and X-skimmer cone, and a static multicollector data collection protocol with  $^{234}\text{U}$  measured on an axial secondary electron multiplier, and  $^{233}\text{U}$ ,  $^{235}\text{U}$ ,  $^{236}\text{U}$  and  $^{238}\text{U}$  measured on Faraday cups equipped with  $1011 \Omega$  resistors. Blocks of five samples were bracketed by analyses of CRM 112a U and CRM 112a U+IRMM 3636 spike. Exponential mass bias corrections were based on the measured values of the  $^{233}\text{U}/^{236}\text{U}$  ratio of the IRMM 3636 spike normalized to a value of 1.01906. Secondary electron multiplier/Faraday gain corrections were based on the  $^{234}\text{U}/^{235}\text{U}$  ratio of bracketing unspiked CRM 112a analyses. Hydride formation and tailing were monitored at the beginning of each analytical session, with measurements made at mass 237 and 239, while aspirating an unspiked CRM 112a solution, and were corrected during offline data reduction.

U-Th age calculations were performed in Isoplot v. 3.75 Excel 2010 add-in (See Ludwig, 2003). Activity ratios and ages were calculated using the decay constants of Cheng et al. (2013). Dates were corrected for detrital Th assuming an initial  $[^{232}\text{Th}/^{238}\text{U}]_{\text{activity}} = 1.2 \pm 0.6$ ,  $[^{234}\text{U}/^{238}\text{U}]_{\text{activity}} = 1.0 \pm 0.5$ , and  $[^{230}\text{Th}/^{238}\text{U}]_{\text{activity}} = 1.0 \pm 0.5$ . Dates are reported in Yr BP, where the Present is defined as the year 1950 CE.

### 7.2.2 Age Modelling

Growth behaviour of speleothems, which is non-linear, make them unsuitable for simple linear interpolation models. The predominant age model software used to create speleothem age models rely on Makrov Chain Monte Carlo simulations where age-depth relationships are built up from periods of defined deposition rates which allows for the production of an absolute timescale to attach proxy data to. For this project, the programme COPRA (Constructing Proxy-Records from Age Models) (Breitenbach et al., 2012) was selected to produce an age model for the SHC-03 stalagmite. COPRA

produces an age model by first scanning for age reversals and outliers which can then be ‘treated’ by the user. After this a number, selected by the user, of Depth Age Monte Carlo simulations are run and an age model produced. The uncertainty in the age model is defined by the 95% confidence intervals, derived using the  $\pm 2\sigma$  from the median (Breitenbach et al., 2012). For this project, the cubic interpolation procedure and computed 2000 Monte Carlo simulations were selected to produce the age model.

### 7.2.3 Stable Isotope Analysis

Carbonate samples for  $\delta^{18}\text{O}$  and  $\delta^{13}\text{C}$  analysis were obtained by collecting calcite every *c.*2.5mm through the stalagmite. This was done using a dremel hand drill and ethanol cleaned spatula and scalpel. As a result of recrystallisation in the central part of the stalagmite, samples were taken from a track adjacent to the central growth axis. These samples were weighed and analysed at the NERC Isotope Geosciences Laboratory, BGS, Keyworth. Approximately 60-100 micrograms of carbonate are used for isotope analysis using an IsoPrime dual inlet mass spectrometer plus Multiprep device. Samples are loaded into glass vials and sealed with septa. The automated system evacuates vials and delivers anhydrous phosphoric acid to the carbonate at 90°C. The evolved  $\text{CO}_2$  is collected for 15 minutes, cryogenically cleaned and passed to the mass spectrometer. Isotope values ( $\delta^{13}\text{C}$ ,  $\delta^{18}\text{O}$ ) are reported as per mille (‰) deviations of the isotopic ratios ( $^{13}\text{C}/^{12}\text{C}$ ,  $^{18}\text{O}/^{16}\text{O}$ ) calculated to the VPDB scale using a within-run laboratory standard calibrated against NBS-19. The Calcite-acid fractionation factor applied to the gas values is 1.00798. Due to the long run time of 21 hours a drift correction is applied across the run, calculated using the standards that bracket the samples. The Craig correction is also applied to account for  $\delta^{17}\text{O}$ . The average analytical reproducibility of the standard calcite (KCM) is 0.05‰ for  $\delta^{13}\text{C}$  and  $\delta^{18}\text{O}$ .

### 7.2.4 Trace Element Analysis

Trace element analysis was carried out at the School of Archaeology, Geography and Environmental Sciences (SAGES), University of Reading. 0.002g of powdered carbonate sample was diluted in 14.998g of ~2% trace element grade  $\text{HNO}_3$ , resulting in a dilution factor of 7,500. Samples were measured using Perkin Elmer 7300 Dual View ICP-OES. Samples were nebulised using a Meinhard Type C nebuliser

and introduced into the instrument using a cyclonic spray chamber. The plasma conditions were as follows: 15 litres/minute plasma gas flow, 0.2 litres/minute auxiliary gas flow, 0.4 litres/minute nebuliser gas flow, 1500W RF power and sample flow rate of 1ml/min. All of the elements were measured radially, with the exception of Ba. The lower detection limits were 0.64 ppb for Ca, 0.04 ppb for Mg, <0.04 ppb for Sr, 0.01 ppb for Ba. RSD % for all elements were usually below 2%, all were below 5%. Final trace element data were converted from ppm to molarity and presented as a ratio to Ca (Tr/Ca) as a millimoles per mole (mmol/mol) value.

#### 7.2.5 Strontium Analysis

Initial  $^{87}\text{Sr}/^{86}\text{Sr}$  analysis was conducted on 40 carbonate samples (*c.* 15mg) from stalagmite SHC-03 at the National Oceanography Centre, Southampton. These samples represented measurements every *c.* 40mm through the stalagmite before the hiatus and every *c.* 130mm during the latter half of the stalagmite after the hiatus.

For Sr separation with an ion-exchange resin column (0.2 mL Eichrom Sr resin; Horwitz et al., 1992), the  $\text{NO}_3^-$  concentration of sample solutions were adjusted to 3 M using 68%  $\text{HNO}_3$ . The resin column was pre-cleaned and conditioned with sub-boiled 3 M  $\text{HNO}_3$ . After loading the sample solution, 3-mL sub-boiled 3 M  $\text{HNO}_3$  was added to the column to elute cations such as Ca, Ba and Rb. The Sr fraction was collected by adding 1.5-mL of ultra-pure  $\text{H}_2\text{O}$ . Procedural Sr blanks during the column separation procedure contained less than 0.6 ng Sr, which is insignificant for isotopic analysis using 1  $\mu\text{g}$  Sr. Sr isotopic compositions were measured by thermal ionization mass spectrometer (ThermoFinniganTriton) using rhenium single filament method with tantalum oxide activator.  $\sim 1$   $\mu\text{g}$  of Sr in 1.0 $\mu\text{L}$  solution was dried on an evaporation filament. During the measurement, the intensity of  $^{88}\text{Sr}$  ion signal was maintained near  $4 \times 10^{11}\text{A}$ . The low  $^{85}\text{Rb}$  signal ensured that the interference of  $^{87}\text{Rb}$  on  $^{87}\text{Sr}$  signal was insignificant (*b*0.1%) for all analyses. 150 cycles of data were acquired in a single run. Instrumental bias was corrected using NIST987 standard, which yielded an average  $^{87}\text{Sr}/^{86}\text{Sr}$  value of 0.71024.

Following the first set of  $^{87}\text{Sr}/^{86}\text{Sr}$  analysis, a second batch of carbonate samples and a soil sample were collected for  $^{87}\text{Sr}/^{86}\text{Sr}$  analysis. For this set of analysis another 50 carbonate samples were collected to

improve the temporal resolution of the latter half of the stalagmite. These were analysed at the ALS Scandinavia AB laboratory in Sweden.  $^{87}\text{Sr}/^{86}\text{Sr}$  analysis was carried out after ion exchange separation as described above and prepared by closed vessel acid digestion. The samples were measured using an MC-ICP-MS (NEPTUNE Plus, ThermoScientific). A  $^{87}\text{Sr}/^{86}\text{Sr}$  ratio of NIST SRM 987 of 0.71034 was used for instrumental mass bias correction.

To correct for inter-laboratory differences between the two different sets of analyses, the results of the second run were corrected by subtracting the difference between the average NIST NBS 987 value between the two laboratories (i.e. 0.0001) (See Appendix D, Chapter 14.4).

### 7.2.6 Fluid Inclusions

11 carbonate samples were collected from the SHC-03 stalagmite for fluid inclusion analysis with rough dimensions: a length of ~30 mm (perpendicular to the growth axis), a thickness of ~4 to 5mm (parallel to the growth axis), and a weight between 3.8 and 6.2g (mean 4.85g).

Speleothem fluid inclusion water isotopes were analysed at the Physics Institute, University of Bern, Switzerland, following a recently developed laser cavity ring-down spectroscopy (CRDS)-based method (Affolter et al., 2014), with further improvements (Affolter et al., 2015). Interlaboratory comparison with isotope ratio mass spectrometry-based speleothem fluid inclusion isotope measurements showed a very good agreement for hydrogen ( $\delta\text{D}_{\text{fi}}$ ) values (Meckler et al., 2015). Oxygen ( $\delta^{18}\text{O}_{\text{fi}}$ ) and hydrogen ( $\delta\text{D}_{\text{fi}}$ ) isotope ratios are given in permille (‰) using the standard delta notation and are reported against Vienna Standard Mean Ocean Water (VSMOW).

To sum up the measurement procedure, a calcite block was placed in a copper tube connected to the line that was continuously heated to 140°C and crushed using a hydraulic press. The released sample water was instantaneously vaporized and directly flushed with nitrogen gas to a L2140-i Isotope and Gas Concentration Analyzer and measured with the CRDS technology without any prior water treatment. Analytical precision of measurements is typically 0.2 and 1.0‰ for  $\delta^{18}\text{O}_{\text{fi}}$  and  $\delta\text{D}_{\text{fi}}$ , respectively.

### 7.2.7 Monitoring

Monitoring at the Cave site was conducted before the start of this thesis (Amin Al-Manmi et al., 2019).

All Rain, pool and dripwater  $\delta^{18}\text{O}$  and  $\delta\text{D}$  samples collected from Shalaih Cave were measured using PICARRO cavity ring spectrometer L2120-I in the Department of Archaeology at the University of Reading.

## 8 Results and Proxy Interpretation

### 8.1 Uranium Series Dating

Table 2 displays the U, Th, radiogenic isotopic ratios, and calculated ages with errors reported to 2 standard deviations ( $2\sigma$ ) for the 23 U/Th ages measured in this study. The chronology of the SHC-03 stalagmite age model (Figure 35) was based on 17 of these U-Th dates, the other 6 dates from the older part of the stalagmite displayed age inversions and were consequently excluded. As the stalagmite was actively growing when collected, an artificial age of -66 yr BP was also included within the age model to anchor the youngest part of it to the date of collection (2016 CE). Sample errors for the dates used in the age model range between 48 and 248 years. The U-Th dates also revealed evidence of a hiatus between dates D-2 ( $6,636 \pm 48$  yr BP) and C-5 ( $5,747 \pm 89$  yr BP), supporting macroscopic visual evidence of a hiatus in growth in the same location (*c.* 2,045mm depth from top) (Figure 33). As a result, the hiatus function in COPRA was used to input a break in the age model at this point (Breitenbach et al., 2012).

The resulting age model indicates that the stalagmite grew between 10,560 yr BP and present (-66 yr BP/2016 CE) with a hiatus between *c.* 6,540 and *c.* 5,780 yr BP. Thus, the age model shows that the stalagmite does not quite cover the entire Holocene, but does encompass the majority of it and is comparable in length to another recently produced speleothem record from Katalakhor Cave, western Iran (Andrews et al., 2020), the only other near-Holocene long high-resolution record from the wider region.

#### 8.1.1 Cause for Age Inversions

The age inversions present during the early part of the stalagmite are potentially caused by open system behaviour post precipitation causing diagenetic alteration of the carbonate. The effect of diagenesis is that U is commonly mobilized from the site of diagenesis, leading to an increase in the  $^{230}\text{Th}/^{238}\text{U}$  isotopic ratio, which results in older-than-true U-Th ages (Bajo et al., 2016). While care was taken to avoid areas of recrystallisation when sampling, it is possible and likely the stalagmite contains areas of “*cryptic*” diagenesis, which is not visible to the naked eye (Bajo et al., 2016).

### 8.1.2 Cause for the Hiatus

There are a number of mechanisms which exist that can cause a hiatus in stalagmite growth. These factors can include climate related processes such as aridity, cooling or biologic changes (Breitenbach et al., 2012), but also non-climate related mechanisms such as seismic activity may be responsible, which may break the stalagmite or alter the location of the drip site. There seems to be a slight change in the growth direction before and after the hiatus (Figure 32), which further indicates that seismic activity is a plausible cause. Large earthquakes are common in the region, with the last major earthquake occurring in 2017 (<https://www.bbc.co.uk/news/world-middle-east-41972338>).

Results and Proxy Interpretation

Lab ID	Sample ID	dft (mm)	Measured, Tracer-Corrected									Detrital-Corrected				Date corr (ka)	±2s (abs)	Initial 234U/238U AR	±2s (abs)
			U ppm	232Th ppm	230/232 AR	232/238 AR	±2s (%)	230/238 AR	±2s (%)	234/238 AR	±2s (%)	230Th/238U AR	±2s (%)	234U/238U AR	±2s (%)				
143-16	C1	190	0.09	0.001	6.5	0.002076	0.14	0.01355	1.23	1.2397	0.14	0.0118	10.36	1.2401	0.16	1.046	0.109	1.2408	±0.002
143-17	C2	380	0.11	0.001	7.8	0.002849	0.14	0.02217	1.14	1.2498	0.13	0.0198	8.46	1.2503	0.16	1.744	0.148	1.2516	±0.002
143-18	C3	580	0.09	0.001	10.9	0.002167	0.14	0.02370	1.06	1.2451	0.17	0.0219	5.85	1.2455	0.18	1.937	0.114	1.2468	±0.002
137-3	B3	760	0.10	0.001	7.2	0.004798	0.12	0.03463	0.49	1.2475	0.14	0.0308	9.05	1.2485	0.21	2.717	0.248	1.2504	±0.003
137-4	B4	1130	0.10	0.001	17.9	0.002147	0.12	0.03849	0.47	1.2372	0.14	0.0368	3.40	1.2377	0.16	3.285	0.113	1.2399	±0.002
137-8	B8	1395	0.11	0.001	16.2	0.002799	0.12	0.04534	0.42	1.2443	0.15	0.0431	3.75	1.2449	0.17	3.839	0.146	1.2475	±0.002
143-19	C4	1600	0.08	0.000	27.6	0.001997	0.15	0.05516	1.42	1.2401	0.14	0.0536	2.58	1.2405	0.16	4.809	0.126	1.2438	±0.002
137-5	B5	1810	0.10	0.001	24.7	0.002333	0.12	0.05754	0.44	1.2435	0.13	0.0557	2.42	1.2440	0.15	4.988	0.123	1.2474	±0.002
143-20	C5	2025	0.08	0.000	50.9	0.001297	0.15	0.06608	0.97	1.2504	0.15	0.0651	1.50	1.2506	0.16	5.816	0.089	1.2548	±0.002
152-13	D1	2045	0.09	0.000	59.6	0.001291	0.04	0.07701	0.46	1.2566	0.12	0.0760	1.06	1.2569	0.13	6.789	0.074	1.2619	±0.002
152-14	D2	2070	0.07	0.000	103.1	0.000729	0.04	0.07516	0.41	1.2483	0.17	0.0746	0.68	1.2485	0.17	6.705	0.048	1.2532	±0.002
152-15	D3	2095	0.09	0.000	61.8	0.001240	0.04	0.07656	0.44	1.2538	0.13	0.0756	1.02	1.2541	0.14	6.767	0.071	1.2590	±0.002
143-21	C6	2140	0.10	0.000	82.6	0.001060	0.13	0.08750	0.87	1.2634	0.13	0.0867	1.11	1.2637	0.14	7.732	0.089	1.2695	±0.002
152-16	D4	2200	0.09	0.000	64.0	0.001289	0.04	0.08248	0.42	1.2713	0.12	0.0815	0.98	1.2716	0.13	7.207	0.073	1.2772	±0.002
124-26	A1	2310	0.10	0.000	96.4	0.000932	0.07	0.08981	0.77	1.2681	0.13	0.0891	0.97	1.2684	0.13	7.924	0.080	1.2744	±0.002
143-22	C7	2410	0.11	0.001	58.4	0.001577	0.11	0.09204	0.73	1.2711	0.13	0.0908	1.21	1.2715	0.14	8.063	0.101	1.2777	±0.002
124-27	A2	2560	0.12	0.002	14.8	0.006347	0.05	0.09371	0.75	1.2523	0.15	0.0889	4.05	1.2536	0.26	8.001	0.332	1.2594	±0.003
143-23	C8	2640	0.12	0.000	169.0	0.000615	0.22	0.10391	0.83	1.2671	0.12	0.1035	0.89	1.2672	0.12	9.260	0.087	1.2743	±0.002
137-6	B6	2660	0.13	0.002	25.0	0.004591	0.12	0.11466	0.32	1.2679	0.15	0.1113	2.28	1.2689	0.21	9.976	0.235	1.2766	±0.003
143-24	C9	2785	0.15	0.000	103.5	0.000949	0.14	0.09823	0.84	1.2693	0.14	0.0975	1.00	1.2695	0.14	8.692	0.091	1.2762	±0.002
124-29	A4	2920	0.17	0.000	254.8	0.000415	0.05	0.10564	0.44	1.2748	0.13	0.1053	0.49	1.2749	0.13	9.375	0.049	1.2823	±0.002
137-7	B7	2980	0.20	0.001	92.6	0.001164	0.12	0.10783	0.29	1.2819	0.13	0.1070	0.66	1.2822	0.13	9.470	0.066	1.2898	±0.002
143-25	C10	3040	0.16	0.000	118.4	0.000947	0.10	0.11217	0.46	1.2871	0.12	0.1115	0.65	1.2873	0.13	9.844	0.068	1.2954	±0.002

Table 2: Measured U/Th isotope activity ratios and calculated ages for stalagmite SHC-3. Ages which show age inversions are shaded grey were rejected from the age model. Activity ratios and ages were calculated using the decay constants of Cheng et al., (2013).

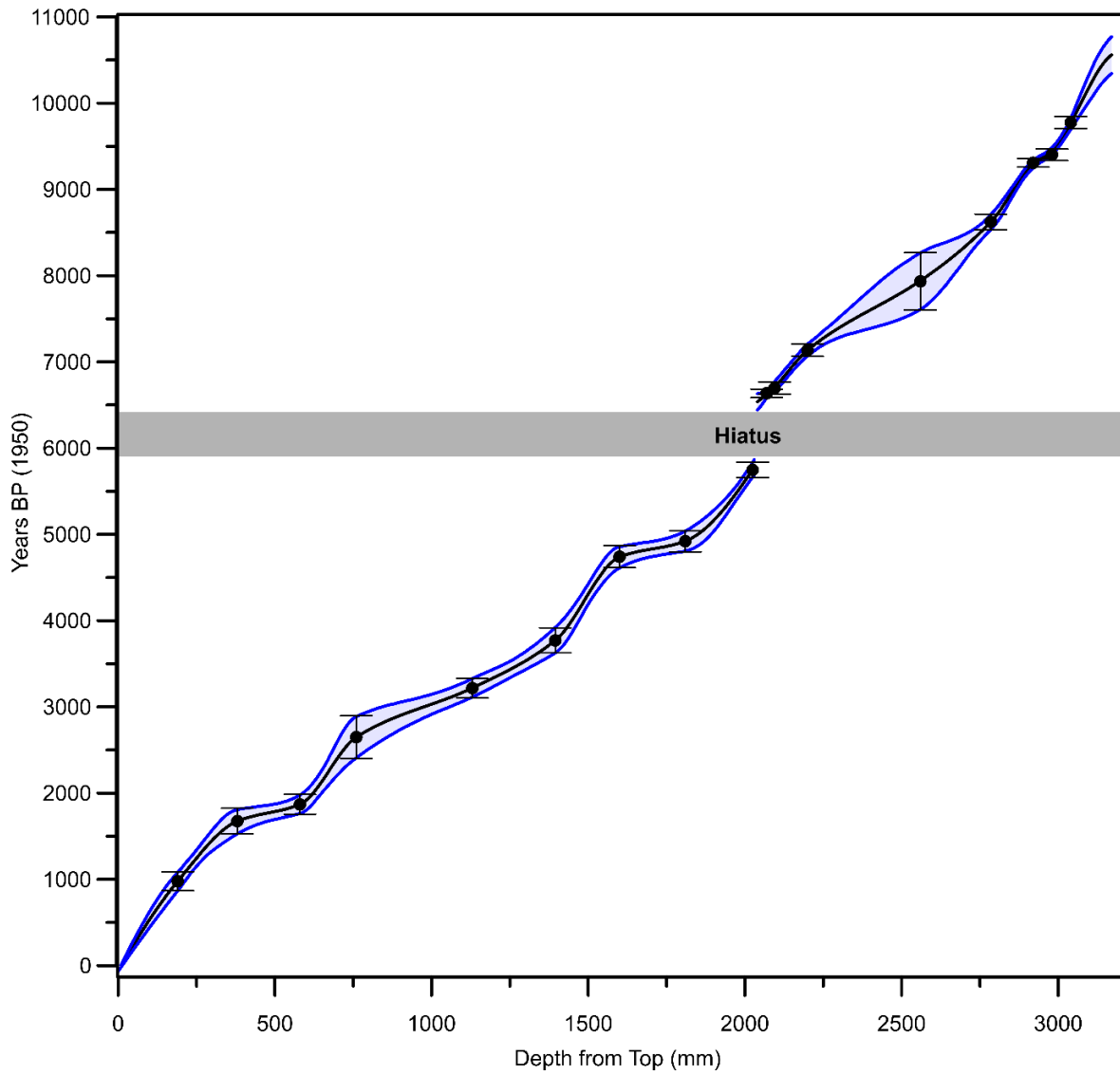


Figure 35: Age model (black line) produced in COPRA (Breitenbach et al., 2012) for stalagmite SHC-03. Black circles are U-series dates used to produce the age model with their associated error bars ( $2\sigma$ ). Blue lines indicate the 95% confidence interval for the age model. Age model also shows a hiatus in growth between 6,540 and 5,780 yr BP (grey bar).

## 8.2 Stable Isotope ( $\delta^{18}\text{O}$ & $\delta^{13}\text{C}$ ) Analysis

### 8.2.1 Sampling Strategy

To begin with, carbonate samples for  $\delta^{18}\text{O}$  and  $\delta^{13}\text{C}$  analysis were collected every 10mm through the growth axis of the stalagmite. The drill track was slightly away from the centre of the sample to avoid the recrystallised area (Figure 32). Once these samples were analysed; further samples were taken every 2.5mm through the growth axis (excluding the samples already taken) to increase the temporal resolution. In total, the  $\delta^{18}\text{O}$  and  $\delta^{13}\text{C}$  records are based on 1201 isotope measurements. The temporal resolution of the stable isotope measurements ranges from 2 to 18 years between data points providing a near-annual temporal resolution. Differences in the resolution of data points were dependent on the growth rate at the particular location and gaps in sampling location because of recrystallised areas which were avoided.

### 8.2.2 $\delta^{18}\text{O}$ Results

$\delta^{18}\text{O}$  values exhibit a range from -7.53‰ to -4.20‰ (Figure 36) around a mean  $\delta^{18}\text{O}$  value of -5.76 ‰. The  $\delta^{18}\text{O}$  values in stalagmite SHC-03 decrease abruptly between 10,560 – 10,280 yr BP, from -6.11 ‰ to -6.93‰. After this phase, the  $\delta^{18}\text{O}$  values are low, but begin a steady, slow trend towards higher values culminating *c.* 2,200 yr BP, from -6.93‰ to -4.56‰. After this period, values increase relatively abruptly to *c.* -5.50‰ at *c.* 700 yr BP and then there is a trend toward higher values until the present, with the measurement from the most recent (i.e. youngest) part of the stalagmite exhibiting the highest value of the whole record (-4.20‰). Superimposed on these longer-term trends are decadal to centennial periods of variability.

### 8.2.3 $\delta^{13}\text{C}$ Results

The  $\delta^{13}\text{C}$  values display a range from -10.48‰ to -3.88‰ (Figure 36), around a mean  $\delta^{13}\text{C}$  value of -8.23 ‰. Like the  $\delta^{18}\text{O}$  data, at the start of the  $\delta^{13}\text{C}$  profile values are high and then it exhibits an abrupt shift from lower values from -4.72‰ to -8.01‰ at *c.* 10,280 yr BP. After this shift, the  $\delta^{13}\text{C}$  profile remains remarkably stable for the remainder of the record, exhibiting no long-term trends and varying around a mean state of -8.28‰. However, like the  $\delta^{18}\text{O}$  data, superimposed on this stability are shorter

periods of relatively large variability of *c.* 4‰. These periods of variability also potentially show a quasi-cyclical nature of about 1,000 – 1,500 years, particularly noticeable between *c.* 5,000 – 1,000 yr BP (Figure 36).

#### 8.2.4 $\delta^{18}\text{O}$ Interpretation

$\delta^{18}\text{O}$  values of speleothem calcite are the most widely employed proxy in speleothem based palaeoclimate research. However, as discussed in Chapter 4.5.1 there are a number of well-known, potentially competing, controls on  $\delta^{18}\text{O}$  values of speleothem carbonate which include changes in the source of moisture, atmospheric path trajectories, temperature, amount of rainfall and local kinetic processes (Rozanski et al., 1993; Lachniet, 2009). These different processes need to be considered to understand the factors causing  $\delta^{18}\text{O}$  variability in the SHC-03 stalagmite. Here, by employing monitoring data, comparisons with previous speleothem investigations from Shalaih Cave and palaeoclimate records elsewhere in the region, this section seeks to understand the principle controls of SHC-03  $\delta^{18}\text{O}$  variability to identify what climatic/environmental or other non-climate related mechanisms may be responsible for the observed variation.

##### 8.2.4.1 Tests for Isotopic Equilibrium

First, in order to establish whether the stable isotope data predominantly reflects changes in the isotopic composition of meteoric water, rather than the consequence of kinetic processes (e.g. evaporation) within the cave, tests can be performed to assess whether calcite precipitated under conditions of isotopic equilibrium. To assess whether speleothem carbonate was deposited in isotopic equilibrium many speleothem studies conduct a ‘Hendy Test’ (Hendy and Wilson, 1968). To perform this test, carbonate  $\delta^{18}\text{O}$  and  $\delta^{13}\text{C}$  samples are collected and analysed from across the same growth layer. A positive covariation between  $\delta^{18}\text{O}$  and  $\delta^{13}\text{C}$  along this growth layer is thought to be indicative of evidence of kinetic fractionation. Unfortunately, the recrystallised nature and absence of visible growth layers in the SHC-03 stalagmite made this difficult to carry out reliably and therefore was not performed in this project. However, there are three other types of tests which are available which will be applied here which may be as, or even more effective, than the Hendy Test (Dorale and Liu, 2009):

8.2.4.1.1 Replication

High levels of agreement between the isotopic values observed in different stalagmites from within the same cave provides some evidence of conditions of isotopic equilibrium (Dorale and Liu, 2009). Previous investigations on stalagmites SHC-01 and SHC-02 from Shal'ai Cave provide an opportunity to conduct this test. Figure 36 shows the new isotopic data from the SHC-03 stalagmite alongside these existing datasets from Shal'ai Cave (Marsh et al., 2018; Amin Al-Manmi et al., 2019). The different datasets overlap each other well (particularly for  $\delta^{18}\text{O}$ ) and demonstrates that the values of the different stalagmites are in good agreement with one another. Replication, therefore, between these samples provides some evidence that calcite precipitated under conditions of isotopic equilibrium.

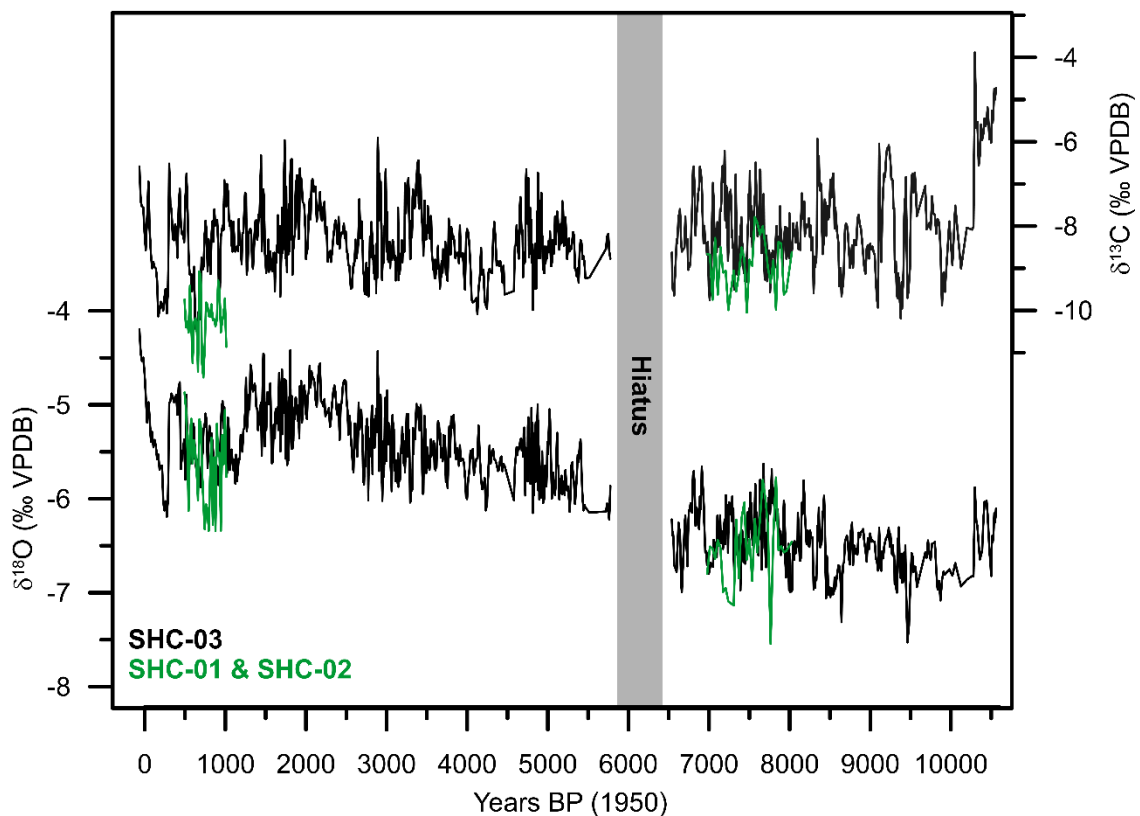


Figure 36:  $\delta^{18}\text{O}$  and  $\delta^{13}\text{C}$  measurements from the SHC-03 stalagmite (black line) alongside results from previous investigations on speleothems from the same cave (SHC-01 and SHC-02 - green line) on the same y-axes. The SHC-03  $\delta^{18}\text{O}$  profile displays a clear trend from lower to higher values during Holocene, in contrast the  $\delta^{13}\text{C}$  profile remains stable throughout much of the record, albeit with shorter periods of variability super imposed on it. The new SHC-03 and old SHC-01 and SHC-02 data show very good agreement with one another, demonstrating good replication within the cave, evidence that calcite precipitated under conditions of isotopic equilibrium (Dorale and Liu, 2009).

8.2.4.1.2 Correlation

A strong positive correlation between the  $\delta^{18}\text{O}$  and  $\delta^{13}\text{C}$  values measured along the growth axis of the stalagmite can be indicative of kinetic fractionation as kinetically driven changes influencing the two isotopes similarly (Mickler et al., 2006). Correlation tests between  $\delta^{18}\text{O}$  and  $\delta^{13}\text{C}$  values from the SHC-03 stalagmite show no correlation ( $r^2 < 0.01$ ) (Figure 37), and further suggests that kinetic fractionation likely did not affect isotope variability in the stalagmite (When the measurements are separated between groups before and after the hiatus there is a more positive correlation between them, but these are still very weak ( $r^2 = 0.1$  &  $r^2 < 0.25$ )).

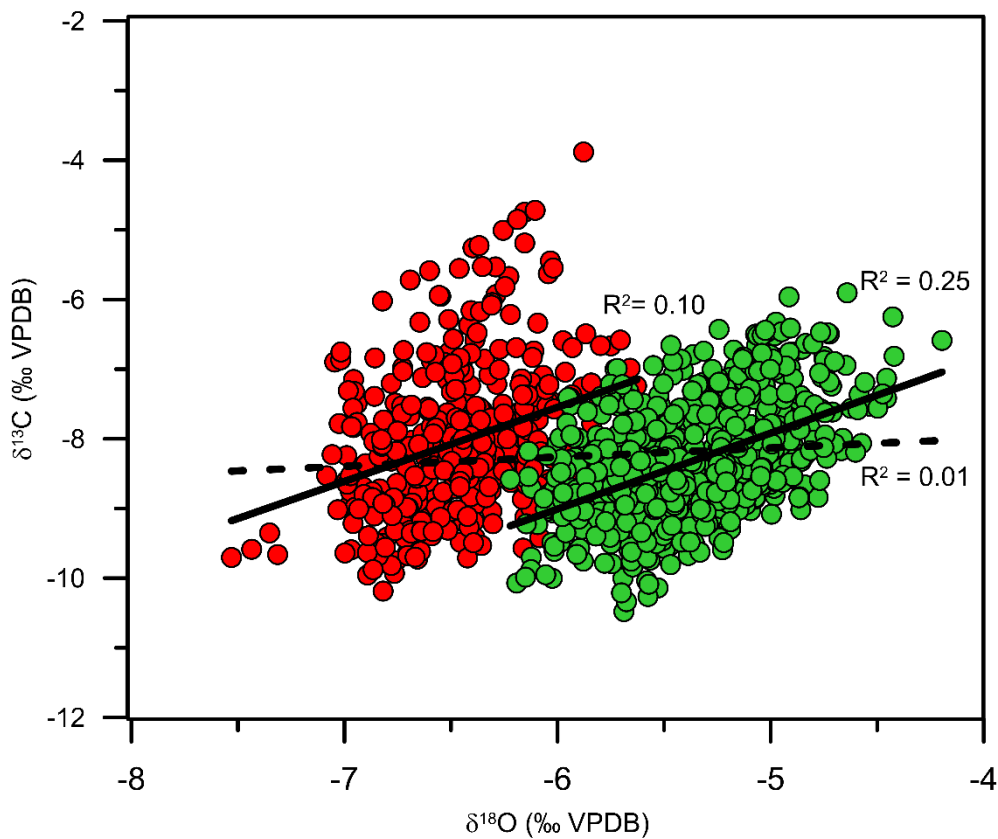


Figure 37: Scatter of the  $\delta^{18}\text{O}$  and  $\delta^{13}\text{C}$  data which shows no clear relationship between the two sets of data that would indicate disequilibrium fractionation processes were a dominant cause for isotope variability. Red circles are data points before the hiatus (c.10,560 – 6,540 yr BP) and green circles are data points after the hiatus (5,780 yr BP – Present). Dashed line is the linear regression trendline for the whole data ( $r^2 < 0.01$ ), while black lines represent the trendlines for the subsets of data ( $r^2 = 0.1$  &  $r^2 < 0.25$ ).

#### 8.2.4.1.3 Temperature Dependant Isotopic Equilibrium Calculations

An additional test for isotopic equilibrium deposition is to calculate the expected theoretical calcite  $\delta^{18}\text{O}$  values for equilibrium conditions using drip water  $\delta^{18}\text{O}$  values, and to assess how well these theoretical values correspond with the measured modern calcite  $\delta^{18}\text{O}$  data. When calcite precipitates from cave drip water, even under equilibrium conditions, there is a preferential incorporation of  $^{18}\text{O}$  into the solid phase (Kim and O'Neil, 1997; Tremaine et al., 2011). The degree of this fractionation that occurs between drip water and calcite is temperature dependant (temperature dependant fractionation factor). There have been a number of studies which have tried to calculate what the temperature dependant  $\delta^{18}\text{O}$  fractionation factor between drip water and calcite, which began with laboratory-based experiments (O'Neil et al., 1969; Kim and O'Neil, 1997; Kim et al., 2007).

The most recently published calculation was made by Tremaine et al. (2011), who developed their new calculations after identifying previous equations and laboratory experiments regularly predicted calcite values that were much lighter than in situ cave observations. They developed a new equation by running through a best fit line through a large collection of calcite/drip water relationships from laboratory studies and in-situ cave experiments:

$$1000\ln\alpha = (16.1 \pm 0.65) \times (10^3\text{T}^{-1}) - (24.6 \pm 2.2)$$

Where T is temperature of the cave in Kelvin and  $\alpha$  is the fractionation factor ( $\alpha = (1000 + \delta^{18}\text{O}_{\text{Calcite}}) / (1000 + \delta^{18}\text{O}_{\text{Drip}})$ ).

Provided that the isotopic composition of drip water and calcite, as well as cave temperature are known, these equations can be used to determine whether calcite precipitated in isotopic equilibrium, where the modelled calculation should match or be close to the observation data. Monitoring studies have collected drip water and temperature information from Shalaih Cave, so it is possible to calculate the theoretical temperature and calcite at deposition and compare these values to the real observation (Table 3).

### *Results and Proxy Interpretation*

Table 3: Monitored and modelled isotopic and temperature data from Shalaih Cave using the temperature dependant fractionation factor equation from Tremaine et al. (2011). Calculations used to examine SHC-03 calcite  $\delta^{18}\text{O}$  values averaged over the last 300-year period were used. Drip water measurements averaged over the months with the highest drip rates (Oct – May).

<b>Drip Water (VMSOW)</b>	<b>Drip Water (VPDB)</b>	<b>Calcite (VPDB)</b>	<b>Fractionation Factor (1000ln<math>\alpha</math>)</b>	<b>Modelled Temperature (K)</b>	<b>Modelled Temperature (°C)</b>	<b>Observed Temperature (°C)</b>	<b>Modelled Calcite (VPDB)</b>
-5.49	25.43	-5.32	30.61	291.49	18.49	20.2	-5.62

Based on the data available, the estimated isotopic value for the speleothem calcite (-5.62 ‰) and temperature (18.49°C) are slightly lower than observed values (-5.32 ‰ and 20.2°C) and suggests that some level of isotopic disequilibrium maybe influencing isotope values from the cave. However, this is common in most speleothems, particularly in those forming in caves in arid and semi-arid regions, and the difference observed here is in a similar range to most records from across Southwest Asia and Europe (McDermott et al., 2011) (Figure 38), from records where disequilibrium processes are thought to be negligible and are usually offset from their theoretical equilibrium value by  $1.0 \pm 0.5\%$ , which SHC-03 also does. Therefore, fractionation of  $\delta^{18}\text{O}$  due to kinetic processes is a negligible factor in Shalaih Cave.

Therefore, all three tests performed here therefore suggest that the calcite of SHC-03 precipitated under conditions near to isotopic equilibrium and consequently, the  $\delta^{18}\text{O}$  values of the stalagmite SHC-03 predominantly reflects changes in the isotopic composition of meteoric waters (precipitation) above the cave rather than local kinetic processes within the karst system.

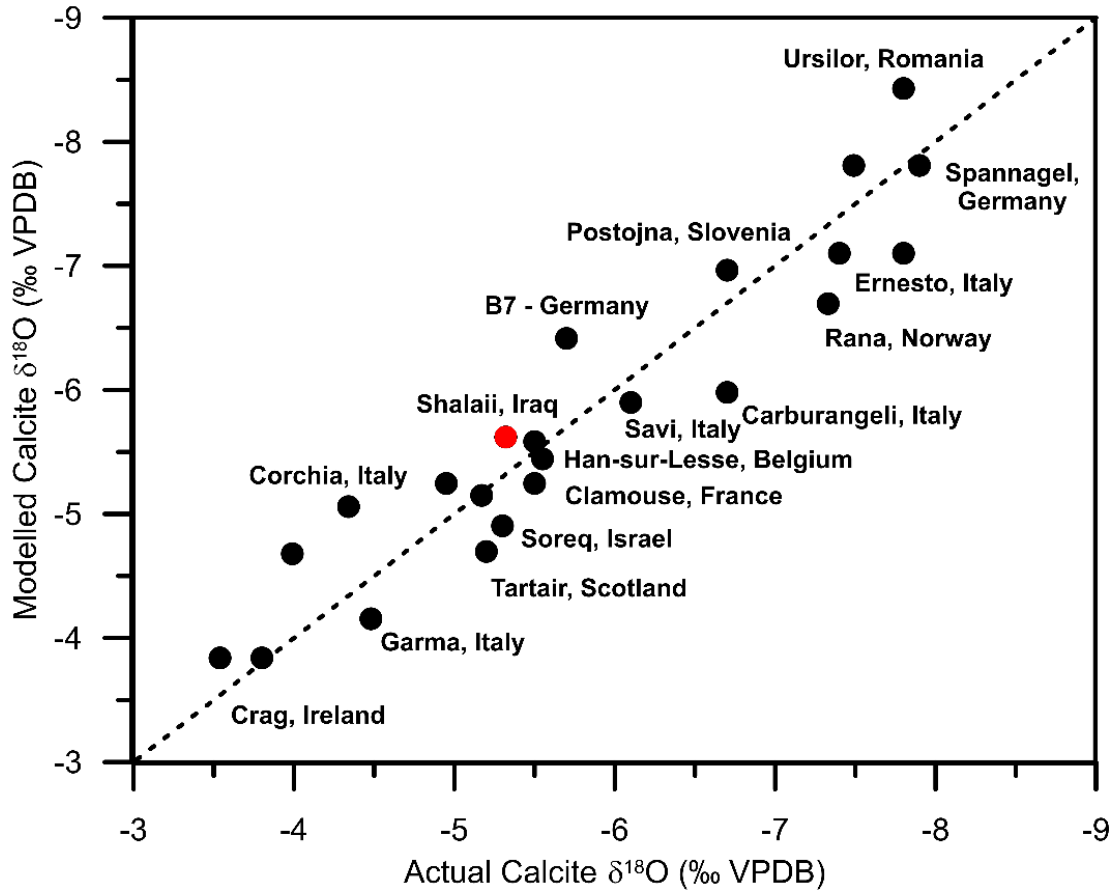


Figure 38: Modelled vs actual  $\delta^{18}\text{O}$  value plot for pre-existing speleothem studies from Europe and Southwest Asia (black circles) and the new SHC-03 record (red circle). Calculated using the isotope-temperature fractionation relationship developed by Tremaine et al (2011) with known drip water  $\delta^{18}\text{O}$  and cave temperature values. Black line represents the 1:1 relationship of perfect isotopic equilibrium conditions. All pre-existing records shown here are thought to have precipitated under conditions close to isotopic equilibrium. The calculated SHC-03 fits well within the expected range of isotopic equilibrium behaviour based on the observations made on these other speleothem studies. Data for European and Southwest Asian cave drip-water  $\delta^{18}\text{O}$ , speleothem  $\delta^{18}\text{O}$  and cave temperature obtained, and figure modified, from McDermott et al. (2011). See Appendix A 14.1 for calculations and site references.

#### 8.2.4.2 Interpretation of Annual to Centennial $\delta^{18}\text{O}$ Variability

To identify the cause for short-term variations in speleothem  $\delta^{18}\text{O}$  values, long-term cave monitoring studies are often employed which can be used to examine the relationship between drip-water  $\delta^{18}\text{O}$  with possible controlling mechanisms such as rainfall amount, temperature or humidity (e.g. Burstyn, 2013; Baker et al., 2019). Unfortunately, monitoring data from Shalaih Cave covers a period of less than a year (Chapter 6.5) and therefore is not long enough to capture multi-annual relationships between drip water  $\delta^{18}\text{O}$  and calcite  $\delta^{18}\text{O}$ . However, based on the limited monitoring data available, there seems to be a negative, but lagged, relationship between the amount of rainfall and drip water  $\delta^{18}\text{O}$  on a monthly timescale (Figure 29) (Amin Al-Manmi et al., 2019), this is also supported by modelled isotopic and precipitation data above Shalaih Cave, which show a clear relationship between rainfall amount and the  $\delta^{18}\text{O}$  composition of precipitation (Figure 28). Consequently, previous studies on stalagmites from the cave interpret the  $\delta^{18}\text{O}$  in terms of rainfall amount, where low  $\delta^{18}\text{O}$  values reflect periods of increased rainfall, while drier conditions result in more positive  $\delta^{18}\text{O}$  values (Marsh et al., 2018; Amin Al-Manmi et al., 2019). This interpretation is in agreement with the way in which short-term  $\delta^{18}\text{O}$  variability in other speleothems from within Southwest Asia have been understood (e.g. Bar-Matthews and Ayalon, 2011; Sinha et al., 2019; Andrews et al., 2020).

Many speleothem studies also attempt to make comparisons between calcite  $\delta^{18}\text{O}$  values with instrumental data/instrument-derived precipitation models to assess whether there is a relationship between calcite  $\delta^{18}\text{O}$  and rainfall amount (e.g. Flohr et al., 2017; Sinha et al., 2019). Unfortunately, the current resolution and dating uncertainty of the youngest part of the SHC-03 stalagmite makes it impossible to reliably make comparisons with instrumental data in this study. However, a comparison between the SHC-03  $\delta^{18}\text{O}$  record and the Kuna Ba Cave  $\delta^{18}\text{O}$  record (Figure 39), which was able to show a link between  $\delta^{18}\text{O}$  variability and instrument-derived precipitation model variability, exhibit a broad similarity which would suggest they are responding to similar controlling mechanisms (i.e. rainfall amount).

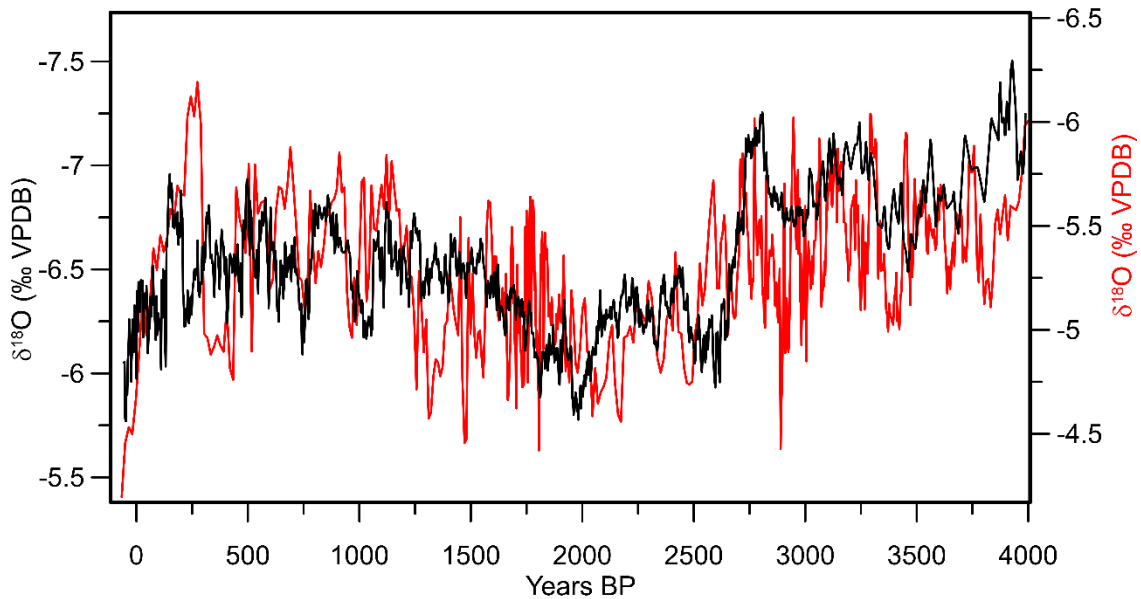


Figure 39: Comparison between the recently produced Kuna Ba composite  $\delta^{18}\text{O}$  record (black line) (Sinha et al., 2019) and the SHC-03  $\delta^{18}\text{O}$  record (red line). The two records show a broad similarity which suggests they are controlled by similar mechanisms. Given that the Kuna Ba record has been closely linked to modelled instrumental data, this provides further support that short-term  $\delta^{18}\text{O}$  oscillations of the SHC-03 record is a function of rainfall amount.

Therefore, based on the evidence available, this study suggests, like previous investigations from the cave, that short-term  $\delta^{18}\text{O}$  variability in the SHC-03 record is a function of rainfall amount and can therefore be used as a proxy for hydrological changes. This interpretation is also supported by similar fluctuations in both the  $\delta^{13}\text{C}$  and Mg/Ca datasets (Figure 45). Obviously, in the future, further monitoring studies, a more refined chronology, and enhanced sampling resolution will improve and verify the understanding of short-term  $\delta^{18}\text{O}$  variability.

#### 8.2.4.3 Interpretation of Centennial to Millennial Change

On longer-timescales, the SHC-03  $\delta^{18}\text{O}$  record displays a shift from lower values during the early Holocene (10,280 yr BP) and then after exhibits a clear millennial scale trend toward higher values culminating at *c.*2,200 yr BP (Figure 36). Comparisons of the isotopic profiles of the SHC-03  $\delta^{18}\text{O}$  record with other speleothem  $\delta^{18}\text{O}$  records from Southwest Asia including Jeita, Soreq and Katalekhor Cave records show similar profiles during the Holocene (Figure 40) which also broadly follows the northern hemisphere summer insolation curve. The similarity between the SHC-03  $\delta^{18}\text{O}$  profile to speleothems from the same cave and records from the wider region suggest they are all responding to similar climate and environmental fluctuations on centennial to millennial timescales. However, as discussed in Chapter 5, the way in which this Holocene long trend has been interpreted has differed between studies, with some interpreting in terms of rainfall amount (Bar-Matthews et al., 2003; Andrews et al., 2020), while others suggest a large influence of the source effect (Cheng et al., 2015; Rohling et al., 2015; Reuter et al., 2018) and this problem is still a matter of debate in palaeoclimate studies in the region.

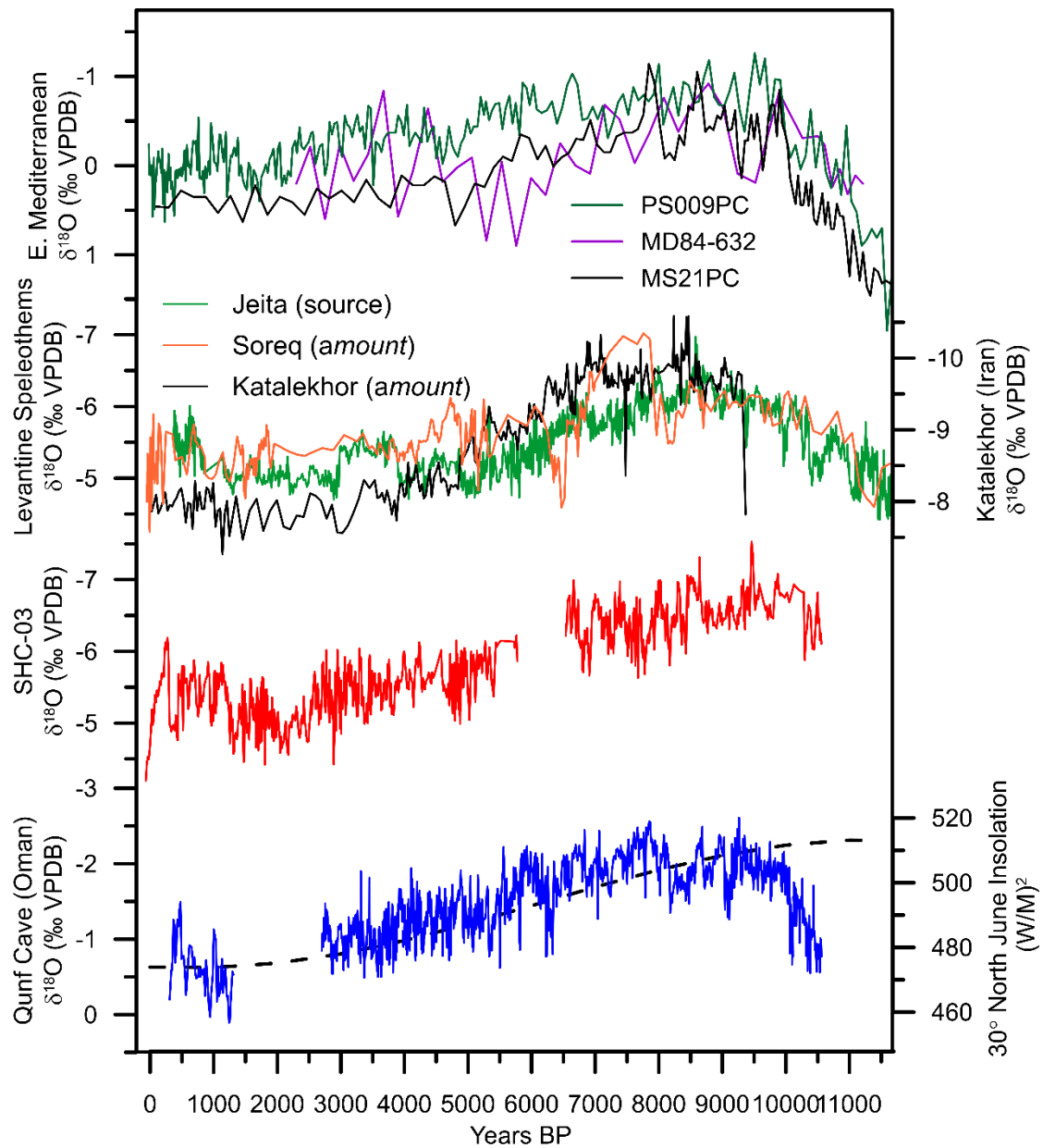


Figure 40: Key Holocene long speleothem and marine  $\delta^{18}\text{O}$  from Southwest Asia (Bar-Matthews et al., 2003; Essallami et al., 2007; Hennekam et al., 2014; Cheng et al., 2015; Andrews et al., 2020) and Oman (Fleitmann et al., 2007) alongside the new SHC-03 data (Red line). All speleothem records from Southwest Asia exhibit a similar long-term, millennial scale trend during the Holocene from lower to higher  $\delta^{18}\text{O}$  values, between *c.*10,000 – 2,000 yr BP, which broadly follows the Northern Hemisphere Summer Solar Insolation curve (black dashed line). However, how this long-term trend has been interpreted in speleothem records from the region has differed between studies, which are shown in brackets next to record label (source = source effect, amount = amount effect).

## *Results and Proxy Interpretation*

In order to rule out and test the hypothesis that (Eastern Mediterranean) source  $\delta^{18}\text{O}$  variability during the Holocene influenced SHC-03  $\delta^{18}\text{O}$  values sufficiently enough to cause this shift, it is necessary to compare records between the two areas. This has, until recently, been difficult due to the absence of high-resolution planktonic-derived  $\delta^{18}\text{O}$  datasets studies from the Eastern Mediterranean Sea. However, the recent production of a high-resolution Holocene marine sediment record from the southeast Mediterranean Sea (PS0009PC) (Hennekam et al., 2014), on the periphery of the Nile Delta, offers a very useful record to test this hypothesis and allows us to more accurately examine to what extent changes in the isotopic composition of the source of moisture may have influenced speleothem  $\delta^{18}\text{O}$  during the Holocene.

To compare the marine  $\delta^{18}\text{O}$  record ( $\delta^{18}\text{O}_{\text{EMSS}}$ ) with the SHC-03  $\delta^{18}\text{O}$  record, both records were averaged into bins of 100 yr intervals to place them on a common timescale and to remove short-term variability. A Pearson correlation coefficient was computed to assess the relationship between the two records which showed a statistically significant and moderately strong positive correlation between them ( $r^2 = 0.51$ ) (See Appendix B 14.2). Moreover, to compare long-term trends, their values were standardised by their average and standard deviation (i.e.  $\text{mean}/1\sigma$ ) (Figure 41) and when these transformed datasets are visually compared they show virtually identical trends (Figure 41), which indicates their relative rate of change through the Holocene was the same (See Appendix B 14.2). Similar trends and relationships are also present with other speleothem records from Southwest Asia. While this similarity does not provide a definitive causal link, it does provide a large amount of support that Holocene millennial scale  $\delta^{18}\text{O}$  in Southwest Asian speleothems may have been largely driven by changes in the isotopic composition of surface waters in the Eastern Mediterranean rather than rainfall amount. At the very least, it is not possible to rule out source isotopic changes as a major driver of speleothem  $\delta^{18}\text{O}$  variability and this limits the reliability of  $\delta^{18}\text{O}$  as a proxy for changes in effective moisture, unless other proxies from the speleothem support it (e.g. Cruz et al., 2007).

The identification of a strong similarity between  $\delta^{18}\text{O}_{\text{EMSS}}$  and speleothem  $\delta^{18}\text{O}$  variability provides motivation to further explore this relationship in order to fully understand the fundamental cause for  $\delta^{18}\text{O}$  variability in the SHC-03 record. Hennekam et al., (2014) demonstrated the  $\delta^{18}\text{O}_{\text{EMSS}}$  composition

### *Results and Proxy Interpretation*

was largely driven by changes in the discharge of the (isotopically light) River Nile, freshwater runoff elsewhere in North Africa and increased precipitation into the Eastern Mediterranean. By comparing their sediment  $\delta^{18}\text{O}$  record to a speleothem  $\delta^{18}\text{O}$  record from Qunf cave, Oman (Figure 41) they demonstrated that Nile discharge rates were largely responding to fluctuations in the position and intensity of the IOM over east Africa, due to changes in northern hemisphere solar insolation, with increased monsoon rainfall during the early Holocene (Fleitmann et al., 2007). Therefore, if the interpretation that the SHC-03  $\delta^{18}\text{O}$  profile is influenced by changes in freshwater runoff into the Eastern Mediterranean, a relationship between the SHC-03 and the Qunf cave speleothem  $\delta^{18}\text{O}$  records should be present as well. When the two records are compared, they display a statistically strong positive correlation ( $r^2 = 0.63$ ) (See Appendix B 14.2) (Figure 41), providing further support to this hypothesis. Consequently, the long-term trend of the SHC-03  $\delta^{18}\text{O}$  record seems to be largely changing, indirectly, in response to variations in the intensity of the IOM and the impact the Monsoon had on freshwater runoff into the Eastern Mediterranean, rather than changes in rainfall amount. This relationship is schematically illustrated in Figure 43.

## Results and Proxy Interpretation

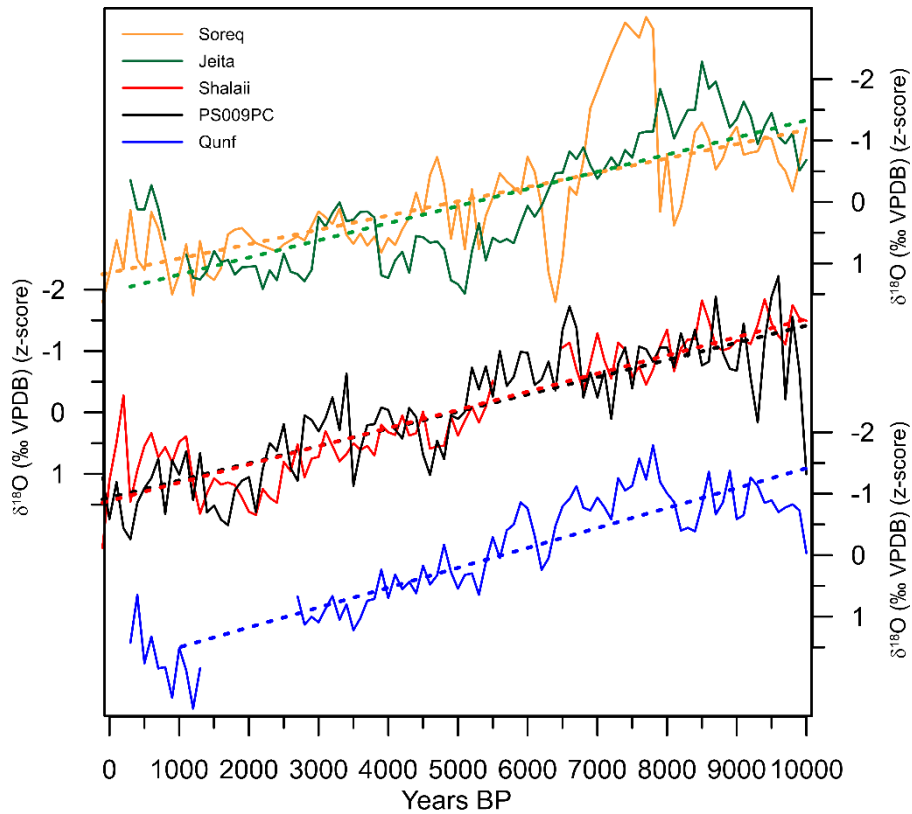


Figure 41: Standardised  $\delta^{18}\text{O}$  Records from Southwest Asia and the Eastern Mediterranean Sea. The plot shows that the relative change of each record from lower to higher  $\delta^{18}\text{O}$  during the Holocene is very similar. In particular, the rate of change between the Nile discharge (Hennekam et al., 2014) and SHC-03  $\delta^{18}\text{O}$  records is almost identical. This, therefore, does not rule out that changes in the EMSS  $\delta^{18}\text{O}$  may have influenced Speleothem  $\delta^{18}\text{O}$  during the Holocene (i.e. ‘the source effect’), and in fact provides further support that it does, in agreement with Cheng et al., (2015). Dashed lines are linear regression to highlight long-term trends.

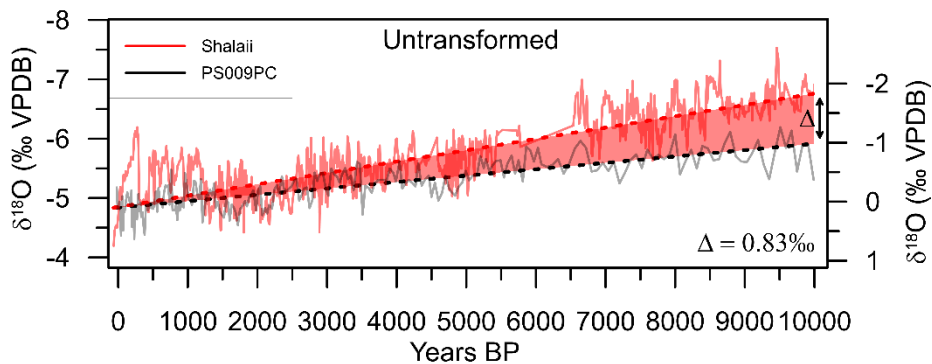


Figure 42: A comparison between long-term trends of SHC-03 and PS009PC (Original data that has not been standardised). While the relative rate of change might be identical (Fig.41) the absolute amplitude of change is different ( $\Delta$ ), with SHC-03 displaying a shift of  $0.83\text{‰}$ . greater than PS009PC. Consequently, the source effect cannot explain all of the observed  $\delta^{18}\text{O}$  change in the SHC-03 record.

Results and Proxy Interpretation

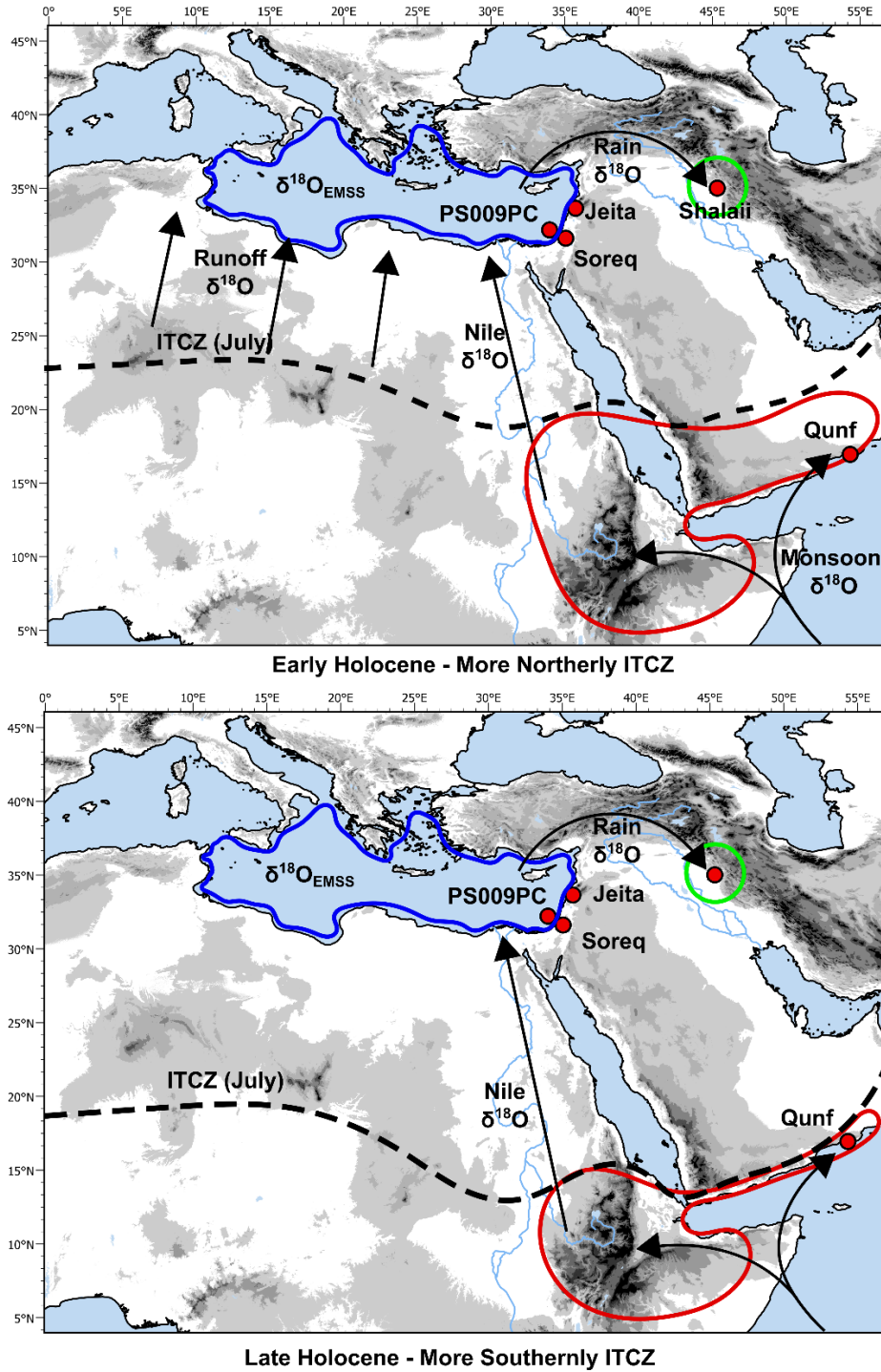


Figure 43: Schematic figure explaining the relationship between  $\delta^{18}\text{O}$  records from Southwest Asia, the EMSS and Oman. The black arrows represent the transport of moisture (and associated  $\delta^{18}\text{O}$  value of the moisture) to explain how these records, located in different climate regions, might display similar  $\delta^{18}\text{O}$  profiles. During periods of more intense monsoon and more northerly positioned ITCZ (top figure) higher amounts of precipitation in the Nile Basin of eastern Africa results in increased monsoon derived, isotopically light, moisture entering the Mediterranean, as well the initiation of freshwater runoff from North Africa at times when the ITCZ cored the central Saharan watershed ( $\sim 21^\circ\text{N}$ ), which leads to lower  $\delta^{18}\text{O}_{\text{EMSS}}$  values which in turn results in lower  $\delta^{18}\text{O}$  values of precipitation sourced from the EMSS.

There is an important caveat to this source effect explanation for long-term  $\delta^{18}\text{O}$  changes in the SHC-03 record. It must be highlighted that, while the relative changes (i.e. when standardised) in the  $\delta^{18}\text{O}$  records are almost identical, there is a difference in the absolute amplitude of change between the  $\delta^{18}\text{O}_{\text{EMSS}}$  and speleothem  $\delta^{18}\text{O}$  calcite. Specifically, the  $\delta^{18}\text{O}_{\text{EMSS}}$  record exhibits a general shift of around *c.* 1.08‰, while the SHC-03  $\delta^{18}\text{O}$  record exhibits a larger amplitude of change of *c.* 1.91‰ during the Holocene (Figure 42), leaving a difference of *c.* 0.83‰ between the two records unaccounted for. Therefore, the source effect alone cannot explain all the variability identified in the SHC-03 speleothem  $\delta^{18}\text{O}$  record. This disparity in the amplitude of change has been observed by some studies before, particularly in the investigation of lake sediments which often exhibit an even greater difference (Jones and Roberts, 2008; Develle et al., 2010; Dean et al., 2018; Reuter et al., 2018). Therefore, other mechanisms must be considered as additional factors to explain the difference between EMSS and speleothem  $\delta^{18}\text{O}$  variability. Here are some potential processes that could lead, not necessarily exclusively (e.g. Dean et al., 2018), to the observed discrepancy between the marine and terrestrial  $\delta^{18}\text{O}$  records, which should be considered when interpreting the  $\delta^{18}\text{O}$  profile from the SHC-03 stalagmite:

1. Changes in annual rainfall amount/P:E Balance

This is perhaps the most commonly employed and simplest reason provided to explain the observed difference between  $\delta^{18}\text{O}_{\text{EMSS}}$  values and terrestrial  $\delta^{18}\text{O}$  records from Southwest Asia (Jones and Roberts, 2008; Develle et al., 2010; Burstyn et al., 2019). Increased annual rainfall amount would lead to lower speleothem  $\delta^{18}\text{O}$  values due to the amount effect. Therefore, the relatively low  $\delta^{18}\text{O}$  values observed in the SHC-03 record during the early to middle Holocene might be associated with wetter conditions alongside the source effect. However, this explanation cannot be tested using the  $\delta^{18}\text{O}$  data alone and therefore it is usually supported by other hydrologically sensitive proxies. For example, at Jeita Cave low speleothem  $\delta^{13}\text{C}$  values also suggested conditions were generally wetter during the early to middle Holocene, when the  $\delta^{18}\text{O}$  values was thought to be heavily modified by source isotopic changes (Verheyden et al., 2008; Cheng et al., 2015). Similarly, Develle et al., (2010) suggested that the difference between the amplitude of change between  $\delta^{18}\text{O}_{\text{EMSS}}$  and the Yammouneh Lake  $\delta^{18}\text{O}$

record was the result of wetter conditions during the early Holocene, supported by observations made with pollen data from the Levant.

## 2. Changes in seasonal distribution of rainfall (Seasonality)

Another common reason provided for the difference between EMSS and terrestrial  $\delta^{18}\text{O}$  records is changes in the seasonal distribution of rainfall (i.e. seasonality). Due to the difference in the isotopic composition of rainfall during different seasons, where winter rainfall has lower  $\delta^{18}\text{O}$  values relative to spring precipitation, changes in the seasonal distribution of precipitation can potentially explain changes in  $\delta^{18}\text{O}_{\text{carbonate}}$  (Stevens et al., 2001, 2006; Dean et al., 2018).

Another, slightly more complex, mechanism related to seasonality which could lead to changes in  $\delta^{18}\text{O}$  values of speleothem carbonate is the timing and amount of recharge, previously discussed in Chapter 4.5.1.8. Only precipitation events with a high enough amount or intensity will result in the recharging of an aquifer with water that will go on to form speleothem carbonate, this threshold is known as selective recharge. If rainfall events are not of sufficient quantity, groundwaters will be lost to the atmosphere through evaporation in the soil or shallow karst (Baker et al., 2019). Consequently, the isotopic composition of karst waters, and associated speleothem  $^{18}\text{O}$  values, are likely to be seasonally biased towards the value of recharge periods (i.e. periods with higher amounts of rainfall) (Baker et al., 2019), which in the case of Shalaih Cave is winter, leading to lower  $\delta^{18}\text{O}$  values of karst waters relative to the annual weighted  $\delta^{18}\text{O}$  value of precipitation. Therefore, changes in seasonality resulting in an increased amount of winter rainfall will lead to a greater proportion of recharge occurring in the winter contributing waters with relatively low  $\delta^{18}\text{O}$  values, while reduced spring rainfall will make spring groundwaters at this time more susceptible to evaporation and thus will have less of an influence on the  $\delta^{18}\text{O}$  values of karst waters, resulting in a smaller contribution of relatively high  $\delta^{18}\text{O}$  values. However, this process could also be countered by increased evaporative fractionation of post-infiltration water in the karst system, which would lead to higher  $\delta^{18}\text{O}$  values (Baker et al., 2019).

Seasonality in southwest Asia is thought to be strongly modulated by the position and intensity of the monsoon system to the south. A stronger monsoon system will lead to a more northerly position of the sub-tropical Jet earlier in spring and later in autumn, this has the effect of blocking moisture laden

westerlies form reaching the region (Djamali et al., 2010). Like changes in rainfall amount, this should be possible to test; any decrease in spring rainfall is likely to exhibit itself as a drying trend in other hydrologically sensitive proxies. Importantly, from a hydrological perspective, a decrease in spring rainfall in the EFC is likely to be accompanied by longer and more intense summer aridity and could have important environmental consequences.

### 3. Greater influence of the Nile and freshwater runoff across the Mediterranean Sea:

This final point is an extension of the source effect and is one which has been less commonly explored and is also much harder to test than the previous two explanations. Changes in the discharge of the Nile would lead to a variations in its influence on the isotopic composition of surface water further away from the mouth (i.e. changes in the size of the Nile plume) (Almogi-Labin et al., 2009). During periods of enhanced discharge, it has a greater effect on Mediterranean surface water further away from the mouth of the river. Whereas, during periods of weakened discharge, its influence becomes less. Therefore, during periods of enhanced discharge it is possible than more rainfall sourced from the Mediterranean will be modified by  $\delta^{18}\text{O}$  variability of the EMSS. This is much more difficult to test than the other points, however it is an explanation which does not require changes in precipitation behaviour above the cave, unlike the previous too.

#### 8.2.4.4 Summary

By using monitoring data and comparisons with other palaeoclimate records, on shorter timescales, it is very likely that, like most speleothem records from Southwest Asia, the  $\delta^{18}\text{O}$  value of speleothem carbonate reflects changes in rainfall amount. Therefore, short-term fluctuations in  $\delta^{18}\text{O}$  are likely to be a suitable proxy for hydrological changes. However, on longer timescales, the similarities between the trend of the SHC-03 record and a marine  $\delta^{18}\text{O}$  record from the eastern Mediterranean Sea suggest that source changes could be a significant control on speleothem  $\delta^{18}\text{O}$ . Thus, this limits the ability of  $\delta^{18}\text{O}$  to be used as a palaeohydrological proxy, unless other proxies which are sensitive to hydrological change within the speleothem support suggestions that amount effect are superimposed on these source changes.

### 8.2.5 $\delta^{13}\text{C}$ Interpretation

There are a number of potentially competing controls on speleothem  $\delta^{13}\text{C}$  (Fairchild et al., 2006; Fohlmeister et al., 2020). These mechanisms can be difficult to disentangle and can make the interpretation of the data complex and, for this reason,  $\delta^{13}\text{C}$  data from speleothem investigations are often less discussed compared to  $\delta^{18}\text{O}$ . However,  $\delta^{13}\text{C}$  can potentially provide an important alternative hydrological proxy, especially in cases, such as here, where the interpretation of the  $\delta^{18}\text{O}$  data is not straightforward (e.g Genty et al., 2003; Mischel et al., 2017). In this section, I consider the different mechanisms potentially influencing the SHC-03  $\delta^{13}\text{C}$  data. Again, as with the  $\delta^{18}\text{O}$  data, it is likely that the speleothem formed under conditions near to isotopic equilibrium and thus local kinetic effects within the cave as a major cause for  $\delta^{13}\text{C}$  variation are rather unlikely. Unfortunately,  $\delta^{13}\text{C}$  data from soil, host rock and vegetation above the cave to aid with the interpretation of the data is not available.

#### 8.2.5.1 Centennial – Millennial Variability

During the earliest part of the  $\delta^{13}\text{C}$  record (c.10,560 – 10,280 yr BP) values range between c.-4.00‰ and -6.00‰ (Figure 36), characteristic of a C4 dominated landscape above the cave (McDermott, 2004). At c.10,280 there is a rapid shift to lower  $\delta^{13}\text{C}$  values that vary around c.-8.00‰, characteristic of a mixed C3/C4 mixed landscape (McDermott, 2004). Therefore, a change in vegetation type above the cave is a reasonable explanation for the change observed at c.10,280 yr BP. This is the only time in the record that a shift of this magnitude occurs, and therefore it probably represents the only time during the Holocene that a major change in the proportion of C3 vs C4 plant type vegetation above the cave occurred. Since C4 vegetation is typically more drought and extreme temperature tolerant than C3 vegetation, the shift from a C4 to C3/C4 mixed landscape likely represents a time of significant climate amelioration to warmer, wetter conditions and perhaps represents a boundary change between environmental zones, moving from a more to less arid state. The shift is contemporary to similar trends observed in the  $\delta^{18}\text{O}$  and trace element data (Figure 49) that supports the interpretation that this is climate related.

After this abrupt shift, the SHC-03 is remarkably stable for most of the record varying around a mean value of -8.28‰ between c.10,280 years and present, which suggests that a mixed C3/C4 landscape

above the cave persisted for this whole period and while I do not have any isotopic data to support this interpretation, the present-day shrub/grassland that exists above the cave today would support this. This is unlike other speleothem  $\delta^{13}\text{C}$  records from Southwest Asia which display millennial scales trends (e.g. Cheng et al., 2015). The long-term stability of the  $\delta^{13}\text{C}$  record during the last *c.* 10,280 years would suggest that the dominance of the vegetation type (i.e. C3 vs C4) on the  $\delta^{13}\text{C}$  signal masks any other centennial – millennial trends in the  $\delta^{13}\text{C}$  data, somewhat limiting its use to observe longer term trends in moisture variability. However, it would seem to indicate that moisture did not change severely enough during this period to cross a threshold required to cause a major change in vegetation type, either toward drier or wetter conditions, like that observed at *c.* 10,280 yr BP providing broad hydrological information in itself.

#### 8.2.5.2 Decadal to Centennial Variability

However, superimposed on this  $\delta^{13}\text{C}$  long-term stability is a large range of decadal to centennial scale variability of *c.* 4‰. These short-term periods of change correspond to similar fluctuations in both the  $\delta^{18}\text{O}$  and Mg/Ca datasets (Figure 45). Therefore, it is plausible these coeval periods of variability represent some type of local hydrological change. There are multiple different mechanisms that could be the potential cause of this short term  $\delta^{13}\text{C}$  variability, which are considered here.

As I interpret the long-term stability of the SHC-03 as an indication of little vegetation change above the cave between C3 and C4 plant species, I rule this out as a likely process for short-term variability, along with local kinetic factors within the cave.

PCP is often-cited process for  $\delta^{13}\text{C}$  variability (e.g., Baker et al., 1997; Johnson et al., 2006; Van Rampelbergh et al., 2013). The effect of PCP is to preferentially release the lighter  $^{13}\text{C}$  during  $\text{CO}_2$  degassing, leaving the remaining cave drip water with higher  $\delta^{13}\text{C}$  values. Therefore, during periods of enhanced PCP (i.e. periods of enhanced ventilation and negative water balance during drier periods) speleothem  $\delta^{13}\text{C}$  will be higher, and lower during wetter periods (Fairchild and Treble, 2009). One way to test the influence of PCP on  $\delta^{13}\text{C}$  is by comparing the  $\delta^{13}\text{C}$  values to trace element data from the same record, where a strong positive correlation between  $\delta^{13}\text{C}$  and trace element values can often be a good indication of PCP influencing the proxies (Johnson et al., 2006; Cruz et al., 2007). While the  $\delta^{13}\text{C}$  and

Mg/Ca datasets from SHC-03 show a moderately strong correlation during the latter part of the record (Spearman correlation coefficient 0.57) (Table.4), there is no clear relationship between  $\delta^{13}\text{C}$  and Sr/Ca, which would indicate that PCP is not a dominant control on  $\delta^{13}\text{C}$  values.

While changes in the proportion of vegetation type (i.e. C3 vs C4) above the cave are unlikely to be the cause, short term variability in soil biogenic  $\text{CO}_2$  production might be a plausible explanation for short term variability. Biogenic  $\text{CO}_2$  production can be influenced by changes in microbial activity or vegetation density and has been shown to be an important influence on speleothem  $\delta^{13}\text{C}$  in warm regions (Fohlmeister et al., 2020). During warmer and wetter conditions, microbial activity and/or vegetation density increases leading to an increased input in the amount of isotopically light  $\text{CO}_2$  into soil moisture which results in more negative speleothem  $\delta^{13}\text{C}$  values, while drier conditions leads to reduced  $\text{CO}_2$  production and higher speleothem  $\delta^{13}\text{C}$  values (Baldini et al., 2005; Fleitmann et al., 2009; Mischel et al., 2017; Fohlmeister et al., 2020). Therefore, during periods of low respiration rates (drier conditions) and less productive soils the  $\delta^{13}\text{C}$  values are higher, reaching values above -7‰, and conversely when respiration rates increase (wetter conditions),  $\delta^{13}\text{C}$  reaching values below -9‰. To support this, during the latter half of the record, there is a moderately strong anti-correlation between  $\delta^{13}\text{C}$  and Ba (further discussed later in this chapter), Ba become more hydrologically mobile in acidic conditions (Hellstrom and McCulloch, 2000), and therefore will be more mobile when soil respiration increased soil  $\text{pCO}_2$ . A similar interpretation of  $\delta^{13}\text{C}$  was made by a recently published record from a speleothem record from Iraqi Kurdistan (Sinha et al., 2019). An attempt was made in this project to support these interpretations by investigating organic matter content of the speleothem, however the organic content of the speleothem was too low to achieve this (M. Leng personal communication) (Appendix 14.5).

#### 8.2.5.3 Summary

The multiple different controls on  $\delta^{13}\text{C}$  make it difficult to provide a definitive answer of which of these is the dominant controlling mechanism without further monitoring data. However, here it is suggested that the SHC-03  $\delta^{13}\text{C}$  values are controlled predominantly by changes in vegetation type (C4 vs C3/C4 mixed environments) on millennial timescales, which as the proportion of C3 vs C4 vegetation remains fairly constant for much of the record seems to make it less sensitive to millennial scale trends in

### *Results and Proxy Interpretation*

climate. On shorter, decadal to centennial timescales the  $\delta^{13}\text{C}$  is mainly controlled by soil  $\text{CO}_2$  production which is related to vegetation density and soil microbial activity, both enhanced during period of enhanced moisture. Therefore, variability superimposed on the long-term trend is likely to provide a useful hydrological proxy. As the  $\delta^{13}\text{C}$  correlates with Mg/Ca, I cannot completely rule out the influence of PCP on the  $\delta^{13}\text{C}$ , although the relationship between Sr/Ca and Ba/Ca is not would be expected and suggests this is unlikely (Table 5). However, even if it does, the interpretation of the  $\delta^{13}\text{C}$  data would remain the same as drier conditions would act in the “same direction”, i.e. less soil microbial activity and vegetation density, more PCP, lower drip rates and enhanced fractionation. Thus, this study is confident that stalagmite  $\delta^{13}\text{C}$  values are sensitive proxies for shorter-term climate variability, more specifically moisture availability associated with rainfall fluctuations.

### 8.3 Trace Element Analysis

#### 8.3.1 Sampling Strategy

447 trace element (Mg/Ca, Sr/Ca, Ba/Ca) samples were collected and measured from the SHC-03 stalagmite. These measurements mostly represent one sample every 10mm, although in a few targeted locations the resolution was increased to one sample per 2.5 mm to match the resolution of the stable isotope data.

#### 8.3.2 Results

The results of the trace element analysis are shown in Figure 44. The mean value for Mg/Ca (mmol/mol) is 3.40 and the values range from 1.85 to 9.11. The mean value for Sr/Ca (mmol/mol) is 0.08 and the values range from 0.05 to 0.40. The mean value for Ba/Ca is 0.012 and the values range from 0.004 to 0.026 (Table 4).

	Min	Max	Mean
Mg/Ca (mmol/mol)	1.85	9.11	3.40
Sr/Ca (mmol/mol)	0.05	0.40	0.08
Ba/Ca (mmol/mol)	0.004	0.026	0.012

Table 4: Statistics for trace element measurements.

Between *c.*10,530 and *c.*10,260 yr BP, both Mg/Ca and Sr/Ca values are at their highest of the entire record, averaging 8.58 and 0.38 respectively during this time. At 10,260 yr BP, both Mg/Ca and Sr/Ca exhibit an abrupt shift to lower, but still relatively high, values corresponding to a similar shift observed in the stable isotope data. The Ba/Ca data also exhibit their highest values during this period, but show a slight increase at 10,260 yr BP. After this early part of the record, both Mg/Ca and Sr/Ca, exhibit a long, steady trend toward lower values until approximately the hiatus (6,540 yr BP) from 6.48 to 2.49 and 0.21 to 0.06 respectively. The trend of the Ba/Ca profile is slightly different to the Mg/Ca and Sr/Ca profiles, but generally still shows a trend from higher to lower values during this period. After the hiatus (5,780 yr BP – Present) the Mg/Ca data exhibits a quasi ‘U-shaped’ trend from low values at the end of the hiatus (Mg/Ca = 2.67), to higher values reached around 1,800 yr BP (Mg/Ca = 4.27), before a shift toward lower values again, with centennial to decadal scale variability superimposed on this long-term

trend. The Sr/Ca remains constant throughout this later period and show only minor fluctuations around a mean of 0.06. The Ba/Ca data is also relatively stable but exhibits a slight trend toward higher values between 5,780 yr BP – Present.

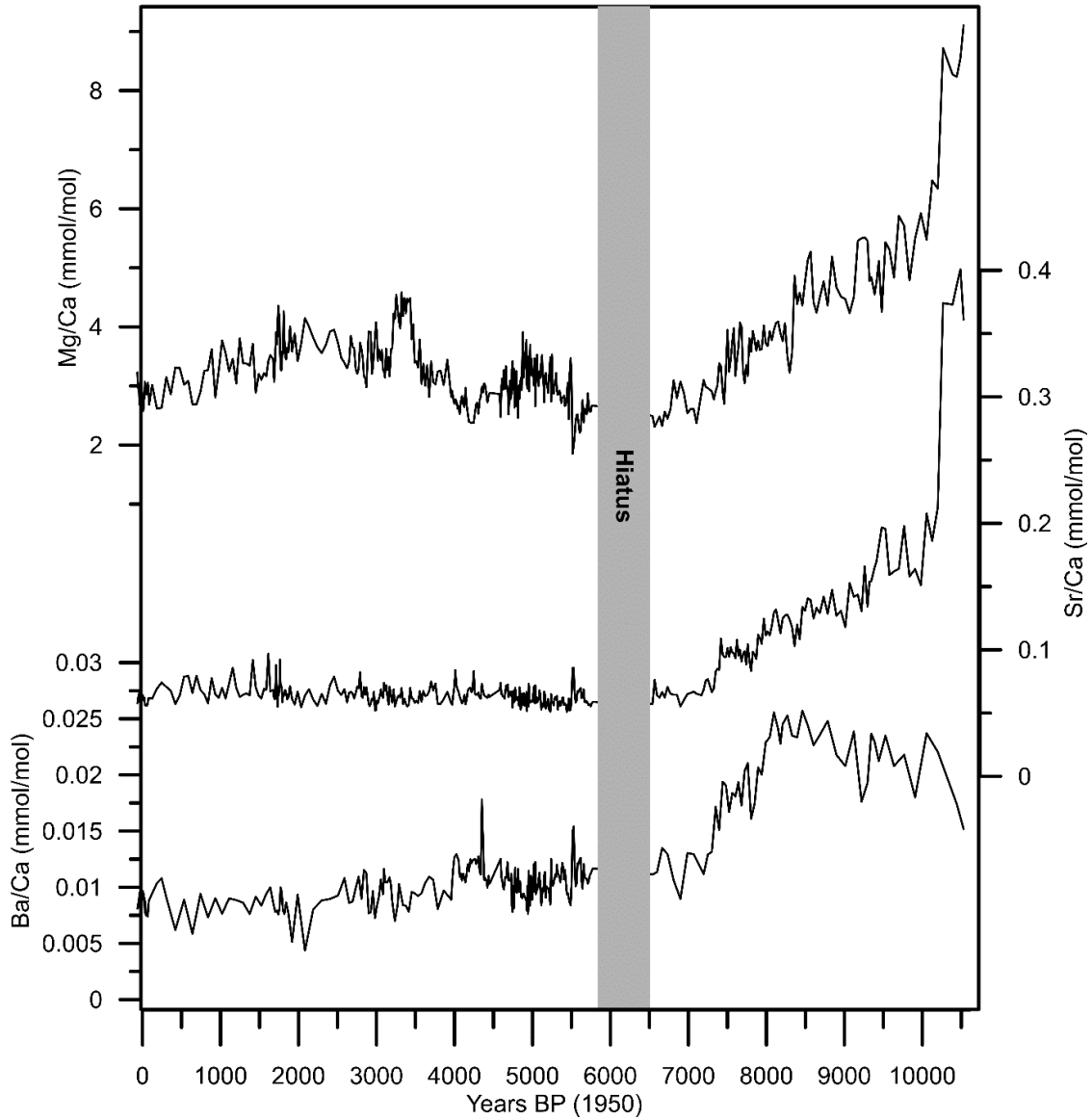


Figure 44: Trace element (Mg/Ca, Sr/Ca, Ba/Ca) data from the SHC-03 stalagmite. All three trace elements profiles show a clear trend from higher to lower values during the early part of the record before the hiatus (c.10,560 - 6,540 yr BP). However, after the hiatus there is less similarity between them, although they are all relatively stable during this later period.

*Results and Proxy Interpretation*

Table 5 displays the statistical relationship between the different trace elements for the whole record and sub-divided into the periods before and after the hiatus. While the Mg/Ca and Sr/Ca data only exhibit a weak to moderate positive correlation for the entire record (Spearman correlation coefficient 0.31, p-value = <0.001), they exhibit a very strong, positive correlation (Spearman correlation coefficient 0.91, p-value = <0.001) during the first half of the record before the hiatus (c.10,560 - 6,540 yr BP). During the second half of the record after the hiatus (5,780 yr BP – Present) no statistical relationship between the two trace elements is observable. Similarly, both Mg/Ca (Spearman correlation coefficient 0.55, p-value = <0.001) and Sr/Ca (Spearman correlation coefficient 0.7, p-value = <0.001) show a positive relationship with Ba/Ca during the early half of the record. While after the hiatus, Ba/Ca exhibits only a weakly positive relationship with Sr/Ca (Spearman correlation coefficient 0.43, p-value = <0.001), and a strong negative correlation with Mg/Ca (Spearman correlation coefficient -0.64, p-value = <0.001).

Table 5: : Correlation coefficients for the isotopic and geochemical proxies from SHC-03. Coefficients are provided for the whole record as well as sub-divided into two periods, representing intervals before and after the hiatus in the SHC-03 record.

Spearman's rho	Time period (yr BP)	Mg/Ca	Sr/Ca	Ba/Ca	$\delta^{13}\text{C}$	$\delta^{18}\text{O}$
<b>Mg/Ca</b>	All	1.00**				
	10,560 - 6,540	1.00**				
	5,780 - Present	1.00**				
<b>Sr/Ca</b>	All	.31**	1.00**			
	10,560 - 6,540	.91**	1.00**			
	5,780 - Present	-0.10	1.00**			
<b>Ba/Ca</b>	All	-.12*	.66**	1.00**		
	10,560 - 6,540	.55**	.7**	1.00**		
	5,780 - Present	-.64**	.43**	1.00**		
<b><math>\delta^{13}\text{C}</math></b>	All	.46**	0.01	-.18**	1.00**	
	10,560 - 6,540	.34**	0.13	-0.06	1.00**	
	5,780 - Present	.51**	-.16**	-.46**	1.00**	
<b><math>\delta^{18}\text{O}</math></b>	All	-0.04	-.48**	-.68**	.16**	1.00**
	10,560 - 6,540	-.29**	-.48**	-.31*	.30**	1.00**
	5,780 - Present	.47**	0.05	-.43**	.43**	1.00**
*. Correlation is significant at the 0.05 level (2-tailed). **. Correlation is significant at the 0.01 level (2-tailed).						

8.3.2.1 Relationship Between Stable Isotopes and Trace Elements

The trend observed in the trace element profiles between *c.* 10,560 - 6,540 yr BP is the reverse to that observed in the  $\delta^{18}\text{O}$  profile, with all trace elements exhibit a weak – moderate negative correlation with  $\delta^{18}\text{O}$  (Table 5). During this early period, only Mg/Ca shows a weak positive relationship with  $\delta^{13}\text{C}$  (Spearman correlation coefficient 0.34, p-value = <0.001), while Sr/Ca and Ba/Ca exhibit no relationship with  $\delta^{13}\text{C}$ . However, after the hiatus (5,78 yr BP – Present) the Mg/Ca data exhibits a strong relationship with both isotope datasets, exhibiting a moderately strong correlation with  $\delta^{13}\text{C}$  (Spearman correlation coefficient 0.51, p-value = <0.001) and still moderately strong, but slight weaker relationship with  $\delta^{18}\text{O}$  (Spearman correlation coefficient 0.47, p-value = <0.001). Notably, there are several coeval periods of abrupt changes observed in both the Mg/Ca and the isotopic data in the record, this included a particularly prolonged and sharp multi-centennial shift to more positive values between *c.* 3,600 – 3,300 yr BP, where  $\delta^{13}\text{C}$  shifts from *c.* -9‰ to -6.4‰ and Mg/Ca from 3.0 to 4.5 mmol/mol. Sr/Ca data does not exhibit any correlation to the stable isotope data after the hiatus, while the Ba/Ca data exhibits moderately strong negative correlations to both stable isotope during the period after the hiatus (*c.* 10,560 - 6,540 yr BP) (Spearman correlation coefficient -0.43, p-value = <0.001 and Spearman correlation coefficient -0.46, p-value = <0.001, for  $\delta^{18}\text{O}$  and  $\delta^{13}\text{C}$  respectively).

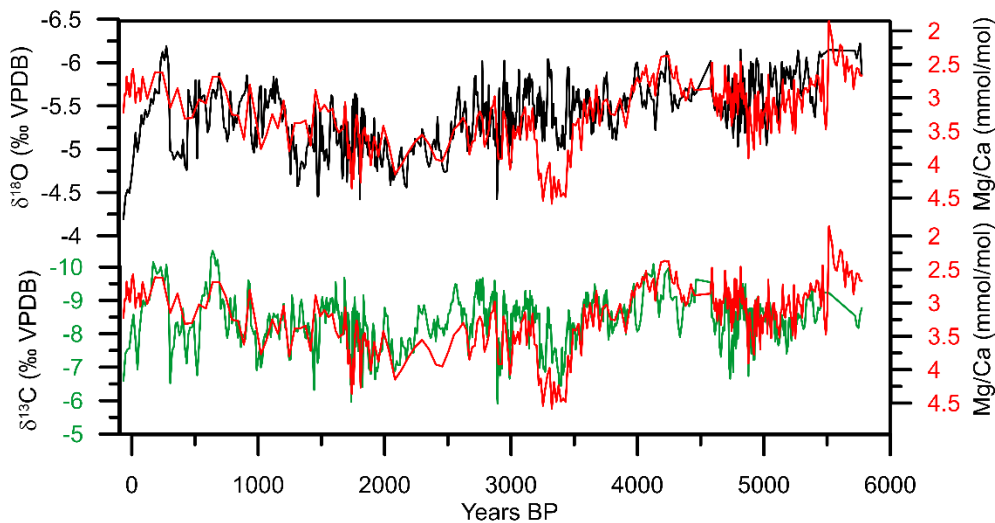


Figure 45: The Mg/Ca profile (red line) superimposed on the stable isotope profiles. A clear visual similarity between the datasets is clear for the period after the hiatus (5,780 yr BP – Present), including coeval periods of shorter abrupt shifts and suggests they are all responding similarly to climatic variability.

### 8.3.3 Interpretation

The earlier sections of this chapter have shown that there are some limitations and uncertainties of the  $\delta^{18}\text{O}$  and  $\delta^{13}\text{C}$  datasets to record millennial scale trends in moisture availability during the Holocene, which is a major objective of this project. Therefore, the concentration of trace elements (Mg/Ca, Sr/Ca and Ba/Ca) within the stalagmite have been investigated as potential alternative sources of palaeohydrological information. However, like the analysis of stable isotopes, there are many different and complex mechanisms that can influence trace element variability within speleothems which need to be considered.

#### 8.3.3.1 Possible Mechanisms for Trace Element Variation

Changes in the degree of PCP occurring in the unsaturated zone of the karst system overlying the cave is often cited as a major cause for trace element variation in speleothems when a positive correlation exists between the different trace element ratios (Fairchild et al., 2000; Johnson et al., 2006; Cruz et al., 2007) as all elements in cave drip waters are all similarly modified by PCP. Monitoring studies from Shalaih Cave have shown year-long dripping (Figure 24) and lagged isotopic responses (Figure 29) which demonstrate water residence times above Shalaih Cave are likely to be long enough (multiple months) for groundwater in the vadose zone to undergo PCP. The covarying trend between the trace elements in the SHC-03 record, particularly between Mg/Ca and Sr/Ca, observed between (c. 10,560 - 6,540 yr BP) could therefore be caused by changes in the amount of PCP occurring. However, other mechanisms can also result in similar relationships between trace elements and, therefore, positive correlations alone are not diagnostic of PCP.

Attempts have been made to develop diagnostic tools to more accurately determine whether PCP is a dominant influence on trace element variation in cave drip waters (Fairchild et al., 2000; Sinclair et al., 2012; Wassenburg et al., 2020). Sinclair et al., (2012) used a combination of mathematical models, trace element concentrations of existing speleothem studies and data from cave drip water studies to show that the slope of a trend line through log-log plot of Mg/Ca vs Sr/Ca ( $\ln(\text{Mg/Ca})$  vs  $\ln(\text{Sr/Ca})$ ) should fall between 0.709–1.003 if PCP is to be considered a dominant controlling processes on trace element variability. Following on from this study, Burstyn (2013) set out two conditions which need to

be fulfilled if PCP is to be considered a plausible mechanism for trace element variation in the SHC-03 stalagmite:

- 1) The linear relationship slope is within the range of values determined by Sinclair et al., (2012).
- 2) The linear correlation coefficient ( $r^2$ ) for the slope is above 0.70.

This criteria for the first condition has recently been updated by Wassenburg et al., (2020) who conducted a similar study, but suggested that the range should be widened, so that a slope between 0.709 up to 1.45 could indicate the influence of PCP, which allows for greater uncertainties and other mechanisms acting at the same time influencing speleothem trace element concentrations. Therefore, using these conditions set out by these different studies, the potential influence of PCP on SHC-03 trace elements can be examined.

Figure 46 shows the  $\ln(\text{Mg}/\text{Ca})$  vs  $\ln(\text{Sr}/\text{Ca})$  plot for the SHC-03 stalagmite. It shows that the relationship between the measurements before the hiatus (c. 10,560 - 6,540 yr BP) fall within the criteria needed to consider PCP as a plausible mechanism for trace element variability, with a correlation coefficient ( $r^2$ ) value of 0.86 and a slope of 1.33, within the upper level of the range set out by Wassenburg et al. (2020). This would indicate that PCP is likely to be the driving mechanism for the broad trend observed during this period. As PCP is enhanced during periods of longer water residence times, this trend is consequently likely to represent a shift from drier to wetter conditions. The same plot also clearly shows that the measurements after the hiatus (5,780 yr BP – Present) display no relationship to one another. Therefore, PCP should not be considered as the dominant mechanism for trace element variation during this later time period and indicates water residence time remained relatively constant.

PCP and associated degassing also often leads to a rise of  $\delta^{13}\text{C}$  values of cave drip water (Fairchild and Treble, 2009), but as discussed in earlier in this chapter there is little evidence that  $\delta^{13}\text{C}$  is influenced by PCP. This might indicate that other mechanisms that control  $\delta^{13}\text{C}$  variation masks the influence of PCP making it less sensitive to the process than trace elements and this would explain why  $\delta^{13}\text{C}$  does not exhibit the same long-term trend during the early to middle Holocene.

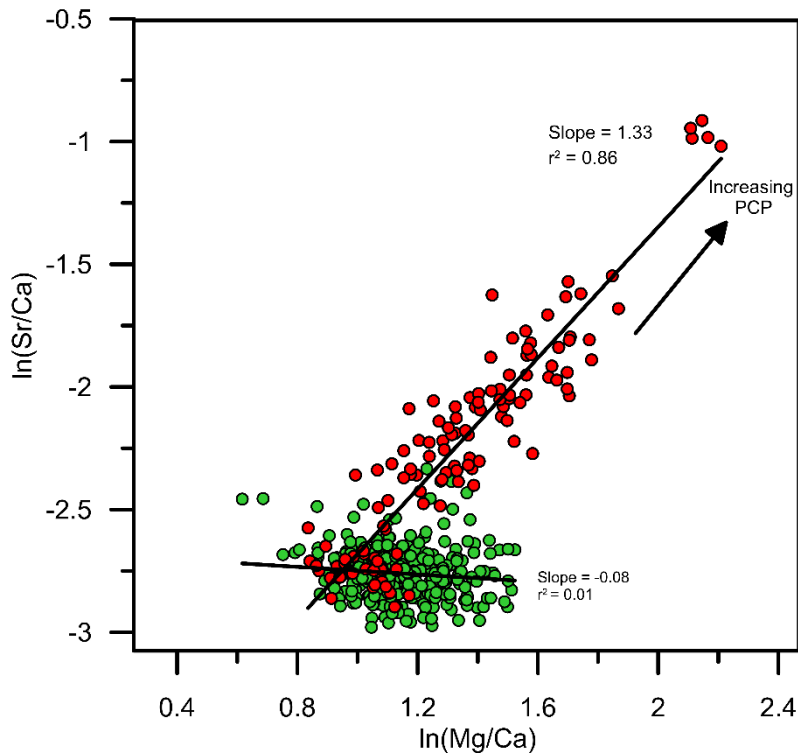


Figure 46:  $\ln(\text{Mg}/\text{Ca})$  vs  $\ln(\text{Sr}/\text{Ca})$  plot to test the influence of PCP on SHC-03 trace element data. Red circles are data point before the hiatus (10,560 – 6,540 yr BP) and green circles are data points after the hiatus (5,780 yr BP – Present). The plot shows that before the hiatus the slope of the trace element data falls within the criteria needed for PCP to be considered as a plausible mechanism for trace element variation. Values after the hiatus show no clear relationship and PCP can be ruled out during this period.

The variability and change of  $\text{Mg}/\text{Ca}$  observed after the hiatus, which does not occur in the  $\text{Sr}/\text{Ca}$  profile, may largely be explained by changes in the dissolution of dolomite ( $\text{CaMg}[\text{CO}_3]_2$ ) as the mineral is rich in Mg but has negligible Sr concentrations. Dolomite dissolution can influence speleothem geochemistry via two primary ways, either by the dissolution of dolomitic bedrock or the dissolution of dolomite dust above the cave.

The host bedrock of Shalaih Cave (Bajawan Formation) is a partially dolomitised limestone (Kharajiany, 2014) and, as a result, the influence of dolomite bedrock dissolution on trace element incorporation into the SHC-03 speleothem should be considered. As discussed in Chapter 4.6.1.2, dolomite dissolution is enhanced during periods of longer residence time, and consequently drier conditions, as cave waters become saturated in regards to calcite much faster than dolomite (Fairchild et al., 2000; Fairchild and

Treble, 2009). If dolomite dissolution is a mechanism influencing Mg/Ca variability during the latter half of the SHC-03 record, high Mg/Ca values should reflect drier conditions and low Mg/Ca values reflect wetter conditions. However, while this mechanism is plausible, as changes in dolomitic bedrock dissolution occurs due to changes in water residence time, the amount of PCP which occurs should also vary causing Sr/Ca variability, which is not observed.

Alternatively, another potentially important source of trace elements into speleothem carbonate is through the deposition of aeolian dust above or directly into the cave which is subsequently leached into cave drip water<sup>2</sup> (Goede et al., 1998; Frumkin and Stein, 2004; Zhou et al., 2011; Carolin et al., 2019). Dust mobilisation is common in Iraq (Nabavi et al., 2016; Attiya and Jones, 2020) and Shalaih Cave is located downwind from important dust sources in Iraq and Syria, therefore it is an important mechanism to consider in this case. Mineralogical studies of dust deposits in the Iranian Zagros have shown they contain, dolomite, and other Mg rich minerals such as palygorskite (Hojati et al., 2012). For this reason, the deposition of dolomite rich dust has recently been cited as an important influence for Mg/Ca variation in a stalagmite from the Iranian Zagros (Carolin et al., 2019), where increased dust deposition is likely to result in a greater Mg/Ca ratio in drip waters through dissolution of the dust particulates in the soil above the cave. Dust activity in Iraq is most common in spring and summer, strongly related to arid conditions (Attiya and Jones, 2020), consequently changes in the amount of dust deposition may act as a useful proxy for hydrological conditions in these seasons (e.g. Carolin et al., 2019).

Unfortunately, this project does not yet have a detailed understanding of the trace element composition of the host rock, overlying soil or potential dust sources. This absence of data it difficult to reliably assess the influence of dust input as a cause for trace element variation in the SHC-03 stalagmite using the trace element data alone and will make any interpretation rather speculative. However, one

---

<sup>2</sup> Buringh (1960:95) observed leaching behaviour in soils within Iraq, where thin aeolian dust layers accumulated during the summer months and observed that they had completely leached from the surface during the winter rains.

important tool which is available is  $^{87}\text{Sr}/^{86}\text{Sr}$  analysis of carbonate samples from the stalagmite.  $^{87}\text{Sr}/^{86}\text{Sr}$  analysis has previously been shown to help to better understand to what extent trace elements are derived from exogenic sources (e.g. aeolian dust) versus trace elements derived from the host bedrock rock (Oster et al., 2010; Riechelmann et al., 2012; Weber et al., 2017). Nevertheless, whether the dissolution of dolomitic bedrock and dolomitic dust is the correct interpretation, from a climatic perspective they influence Mg/Ca in the same direction, more specifically during drier conditions dolomite dissolution increases (higher Mg/Ca values) while it is reduced during wetter conditions (lower Mg/Ca values). Moreover, the broad co-variation between Mg/Ca with  $\delta^{13}\text{C}$  and  $\delta^{18}\text{O}$  would support suggestions that Mg/Ca variability during the middle to late Holocene is related to climate variability.

#### 8.3.3.2 Ba/Ca

While focus on trace elements in speleothem investigations has predominantly been on Mg/Ca and Sr/Ca, Ba/Ca values also provide a similar important means to understanding past changes in cave and local environment. The behaviour of the Ba/Ca data in the SHC-03 record is similar to the other trace elements during the first half of the record and therefore the above discussion of the factors which control Sr/Ca and Mg/Ca values in the SHC-03 record probably applies equally well to the Ba/Ca concentrations (i.e. PCP). However, during the second half of the record the Ba/Ca displays a negative correlation to the Mg/Ca,  $\delta^{18}\text{O}$  and  $\delta^{13}\text{C}$  data, while exhibiting no relationship to the Sr/Ca data (Table 5).

Some studies have linked speleothem Ba concentrations to its limited mobilisation in soils above the cave (Hellstrom and McCulloch, 2000; Wu et al., 2012; Mischel et al., 2017). Ba is relatively insoluble because of the high cation exchange selectivity for  $\text{Ba}^{2+}$ . It becomes more soluble in acidic environments and therefore an increase in soil carbonic acid linked to enhanced  $\text{CO}_2$  production will lead to enhanced Ba dissolution. In semi-arid regions like Iraq, enhanced  $\text{CO}_2$  production, as already explained earlier on this section, is most likely linked to wetter conditions (Wu et al., 2012). Therefore, during wetter conditions increased leaching of soil cations by more concentrated carbonic acid will lead to enhanced  $\text{Ba}^{2+}$ . Because soil  $\text{CO}_2$  production is the same process that influences  $\delta^{13}\text{C}$ , this explains the negative

correlation between the two datasets, as enhanced CO<sub>2</sub> leads to higher Ba, but lower δ<sup>13</sup>C values, providing further support for our interpretation of the δ<sup>13</sup>C data as a sensitive hydrological proxy.

#### 8.4 Strontium Isotope (<sup>87</sup>Sr/<sup>86</sup>Sr) Analysis

##### 8.4.1 <sup>87</sup>Sr/<sup>86</sup>Sr Results

In total 90 <sup>87</sup>Sr/<sup>86</sup>Sr measurements were made on carbonate samples from the SHC-03 stalagmite alongside one soil sample collected from above the cave, with the results displayed in Figure 47. There was a small, but systematic difference between values obtained from different laboratories (See Appendix.D 14.4) therefore, to correct for inter-laboratory variation, the measurements made on the second set of analysis were adjusted by subtracting the difference between the value of (the same) standards measured at the two facilities (see Material and Methods). <sup>87</sup>Sr/<sup>86</sup>Sr variability is small with a range between  $0.70814 \pm 0.000035$  and  $0.70835 \pm 0.000039$ , and a mean of 0.70821. There is a clear decreasing trend from more radiogenic (higher) to less radiogenic (lower) <sup>87</sup>Sr/<sup>86</sup>Sr values from 0.708287 to 0.708186 between 10,200 and 6,700 yr BP, similar to the trace element profiles. After the hiatus, the <sup>87</sup>Sr/<sup>86</sup>Sr profile shows higher levels of variability, but still displays a similar long-term trend as the Mg/Ca profile (Figure 47), except for a period between *c.*2,500 – 4,200 yr BP where the <sup>87</sup>Sr/<sup>86</sup>Sr data exhibit both the highest and lowest values of the record. The soil sample collected from above the cave exhibited a <sup>87</sup>Sr/<sup>86</sup>Sr value of 0.7086.

##### 8.4.2 <sup>87</sup>Sr/<sup>86</sup>Sr Interpretation

<sup>87</sup>Sr/<sup>86</sup>Sr analysis was employed in this project to reduce some of the uncertainties in the interpretation of the SHC-03 trace element data. In particular, it was used to identify the potential influence of dust deposition on the trace element concentration of the SHC-03 stalagmite, in a similar way to previous speleothem studies (Frumkin and Stein, 2004; Musgrove and Banner, 2004; Zhou et al., 2009; Oster et al., 2010).

The geology of the Shalaih Cave bedrock is a middle-late Oligocene formation which dates from 33.9 to 23 Ma (Amin Al-Manmi et al., 2019). Based on previous studies examining the <sup>87</sup>Sr/<sup>86</sup>Sr value of Oligocene formations, <sup>87</sup>Sr/<sup>86</sup>Sr composition of the carbonate bedrock should be around 0.7081

(DePaolo and Ingram, 1985; Miller et al., 1988), although further monitoring data is needed to verify this. The analysis of soil collected from above the cave showed that it has a much higher  $^{87}\text{Sr}/^{86}\text{Sr}$  value of 0.7086 than this estimated carbonate bedrock value. Therefore, if the bedrock and overlying soil can be considered to be the two main end members for Sr for the SHC-03 stalagmite, lower  $^{87}\text{Sr}/^{86}\text{Sr}$  values in the SHC-3 record are likely to be indicative of increased bedrock sourced Sr, while elevated  $^{87}\text{Sr}/^{86}\text{Sr}$  values are indicative of exogenic soil derived Sr.

The elevated  $^{87}\text{Sr}/^{86}\text{Sr}$  values of the soil above Shalaih Cave are in broad agreement with the values observed in previous  $^{87}\text{Sr}/^{86}\text{Sr}$  studies of modern atmospheric dust in Iraq (Cullen et al., 2000; Mustafa et al., 2016) and indicate that the high soil  $^{87}\text{Sr}/^{86}\text{Sr}$  value is likely to be the consequence of exogenic dust deposition. Consequently, dust deposition could be a plausible mechanism for  $^{87}\text{Sr}/^{86}\text{Sr}$  variation in the SHC-03 stalagmite, where higher levels of dust deposition would lead to higher speleothem  $^{87}\text{Sr}/^{86}\text{Sr}$  values. As exogenic dust is thought to be rich in Mg, a positive relationship between Mg/Ca and  $^{87}\text{Sr}/^{86}\text{Sr}$  in the SHC-03 stalagmite should be observed if dust deposition is also a cause of Mg/Ca variation in the stalagmite. When the two proxies are compared, it is clear that they visually show a clear positive relationship throughout most of the record, with an exception between c.2500 – 4,000 yr BP (Figure 47).

As discussed in Chapter 4.4.6.1.3, dust mobilisation in northern Iraq is most common in spring and summer, related to increased aridity and temperature in the region (Nabavi et al., 2016; Attiya and Jones, 2020). Therefore, a plausible interpretation would be that an increase in dust deposition, and higher  $^{87}\text{Sr}/^{86}\text{Sr}$ , reflects periods of longer and more intense summer aridity creating ideal conditions for dust erosion and mobilisation, conceptually illustrated in Figure 52. The relatively low variability and observed values of the  $^{87}\text{Sr}/^{86}\text{Sr}$  suggests that the end members are likely to be carbonate derived sources, therefore other more distant non-limestone sources, such as the Sahara ( $^{87}\text{Sr}/^{86}\text{Sr} = >0.71$ ) or Arabia ( $^{87}\text{Sr}/^{86}\text{Sr} = >0.7088$ ) (Palchan et al., 2019), which would have contributed much higher  $^{87}\text{Sr}/^{86}\text{Sr}$  values can be discounted as a significant contributor, indicating that the dust sources are likely to be relatively local, and therefore the climatic signal is likely to be a local one as well.

The observation that  $^{87}\text{Sr}/^{86}\text{Sr}$  values display a broadly long-term trend to Mg/Ca during the early Holocene suggests that part of the Mg/Ca profile during this period may also be influenced by dust deposition alongside PCP. As discussed in Chapter 4.7.1 water residence time can also be an important influence on  $^{87}\text{Sr}/^{86}\text{Sr}$  values (e.g. Utida et al., 2020) due to enhanced dissolution of the bedrock, however if influenced by water residence time, it should display an negative correlation to Mg, which is the opposite to that observed and would seem to suggest that the influence of exogenic dust masks the impact of changes in water residence time on  $^{87}\text{Sr}/^{86}\text{Sr}$  values, although this later mechanism is likely to be acting as a secondary, competing processes which may dampen the  $^{87}\text{Sr}/^{86}\text{Sr}$  dust signal.

The only exception where Mg/Ca and  $^{87}\text{Sr}/^{86}\text{Sr}$  do not show good agreement is a period between c.2500 – 4,000 yr BP (Figure 47), where the  $^{87}\text{Sr}/^{86}\text{Sr}$  data displays relatively high levels of variability which also clearly negatively correlates with Mg/Ca variations, the opposite pattern to the rest of the record. The cause for this behaviour is currently unclear, although anthropogenic influences, such as the intensification of grazing activities (e.g. Zerboni and Nicoll, 2019) or other intensive agricultural activities leading to soil erosion and dust mobilisation, cannot be ruled out.

## 8.5 Uranium Isotopes

$^{234}\text{U}/^{238}\text{U}_0$  values of the SHC-03 speleothem were determined through the process of U-series dating and are displayed in Figure 47 and also presented in Table 2, using only the  $^{234}\text{U}/^{238}\text{U}_0$  data from the 17 U-Th dates used in the age model. The  $^{234}\text{U}/^{238}\text{U}_0$  values are all above unity and range from (1.2399) to (1.2954). Interestingly, they show a similar long-term trend of higher to lower values identified in the trace element and  $^{87}\text{Sr}/^{86}\text{Sr}$  data during the earlier half of the record before the hiatus.

### 8.5.1 $^{234}\text{U}/^{238}\text{U}_0$ Interpretation

Increased  $^{234}\text{U}/^{238}\text{U}_0$  may relate to an increased contribution of U leached from soil components above the cave linked with increased residence time in the soil zone. Lower  $^{234}\text{U}/^{238}\text{U}_0$  values are associated with increased weathering of soil components and host rocks, normally enhanced during periods of high dissolution, aggressive regimes (wetter periods). Therefore, they can provide a potentially important proxy that can be used to support our current interpretation of the trace element and  $^{87}\text{Sr}/^{86}\text{Sr}$  data.

### *Results and Proxy Interpretation*

The  $^{234}\text{U}/^{238}\text{U}_0$  data of the SHC-03 stalagmite exhibits a similar long-term shift to the Sr isotopes and trace elements ratios during the early to middle Holocene, from higher to lower values, which would suggest that they are responding to similar, potentially climate related, mechanisms. The clear trend in the SHC-03  $^{234}\text{U}/^{238}\text{U}_0$  would suggest a change in the contribution of soil vs host rock U. High values exhibited during the early Holocene represent a period of a greater influence of leaching of  $^{234}\text{U}$  from soils above the cave. Whereas the shift to lower  $^{234}\text{U}/^{238}\text{U}_0$  values represents a trend to an increased contribution of U from the weathering and dissolution of the host carbonate rock. Greater contribution of soil components during the early Holocene may have occurred due to longer residence time in the overlying soil during drier periods which led to enhanced leaching (Ayalon et al., 1999) or dust deposition above the cave (Frumkin and Stein, 2004), as suggested by the Sr data, either way both processes would suggest that the trend is the result of a shift from drier to wetter conditions. Therefore, this data can be used as additional support the interpretation of the shift in the trace element data as a palaeohydrological signal.

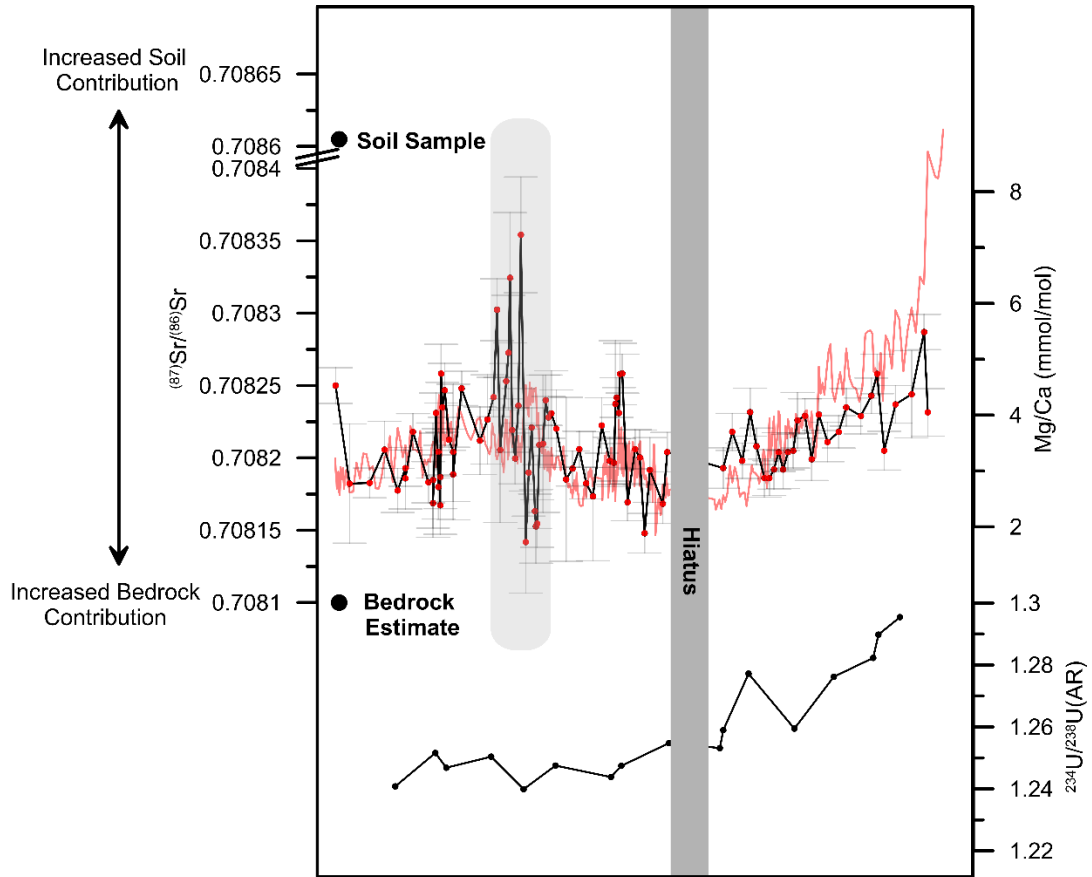


Figure 47: The  $^{87}\text{Sr}/^{86}\text{Sr}$  and  $^{234}\text{U}/^{238}\text{U}_0$  data from SHC-03. Both show similar long-term trend during the early Holocene (illustrated with the use of a black arrow) that is similar to that observed in the Mg/Ca (and Sr/Ca) data. Mg/Ca and  $^{87}\text{Sr}/^{86}\text{Sr}$  also show a similar long-term trend after the hiatus which would indicate a similar controlling process. Faded grey area highlights a period of high  $^{87}\text{Sr}/^{86}\text{Sr}$  variability and where the relationship between the Mg/Ca and the  $^{87}\text{Sr}/^{86}\text{Sr}$  data is the reverse of that seen in the rest of the record, the cause for anti-correlation is unknown. The error bars (faded) for the strontium data is to 2 standard deviations.

## 8.6 Fluid Inclusion Analysis

### 8.6.1 Results

The results of the fluid inclusions analysis are summarised in

Table 6 and Figure 48. Only 6 of the 11 samples released <0.3µl of trapped moisture and therefore are the only samples to have released enough water for reliable results. These six fluid inclusion samples fall below the global meteoric water line (GMWL). The slope (6.87) and intercept (2.08) of the linear fit for the fluid inclusions data is above that of the GMWL (8 and 10 respectively). This suggests a strong influence of kinetic fractionation (evaporation) on the samples as evaporation results in a greater relative enrichment of  $\delta^{18}\text{O}$  than  $^2\text{H}$  in ground water, which influences the  $^2\text{H}$ - $^{18}\text{O}$  relationship (Clark and Fritz, 1997). The samples also show an enrichment in both  $\delta^{18}\text{O}$  and  $^2\text{H}$  compared to isotopic analysis on cave drip water from Shalaih Cave (Amin Al-Manmi et al., 2019).

### 8.6.2 Interpretation

Investigations of speleothem fluid inclusion from Southwest Asia have previously enabled a better insight into the influence of different moisture sources on the isotopic composition of cave drip water (Matthews et al., 2000; Fleitmann et al., 2003b; Rogerson et al., 2018). Therefore, investigating the isotopic composition of fluid inclusions from the SHC-03 stalagmite could provide additional supporting evidence that  $\delta^{18}\text{O}_{\text{carbonate}}$  was strongly influenced by source  $\delta^{18}\text{O}$  variations during the Holocene. To explore this, this study selected 11 carbonate samples throughout the stalagmite for fluid inclusion analysis. Unfortunately, the amount of water recovered from the SHC-03 samples were low, with only six of the eleven samples releasing a volume of water greater than 300µl, with samples below 0.3µl too small to have confidence in their values. While, the fluid inclusion results are generally well clustered, they display values consistently higher  $\delta\text{D}$  values (by about 10 - 20‰) than expected based on present day drip water and precipitation values identified by monitoring studies. Unfortunately, the combined evidence of low fluid recovery and higher than expected  $\delta\text{D}$  values suggest that fluid inclusions within the stalagmite may have been exposed to, and modified by, evaporation post-deposition, possibly as a consequence of the stalagmite's porous carbonate texture. For this reason, further study of the fluid inclusion data is of limited value.

Results and Proxy Interpretation

Sample ID	dft	$\delta^{18}\text{O}$ (‰ VSMOW)	$\delta\text{D}$ (‰ VSMOW)	$\mu\text{l}$ released
Fi-8	79	-3.05237	-17.5105	0.33934
Fi-2	106.5	-3.03287	-22.0321	0.663229
Fi-1	116	-3.73003	-21.4577	1.067977
Fi-5	148	-4.0517	-27.406	0.393062
Fi-11	192	-3.15989	-18.2354	0.418545
Fi-10	213	-2.35228	-24.6424	0.295221
Fi-4	240.5	-3.04209	-23.3514	0.283759
Fi-6	256.3	-3.71233	-23.4639	1.107656
Fi-9	270.8	-3.59294	-26.5698	0.241644
Fi-3	289.3	-2.0955	-22.2975	0.206843
Fi-7	309.3	-1.45679	-21.5115	0.198541

Table 6: Results from the fluid inclusion analysis conducted on samples from stalagmite SHC-03. Only the samples unshaded released the required 300 $\mu\text{l}$  of trapped moisture needed for reliable results.

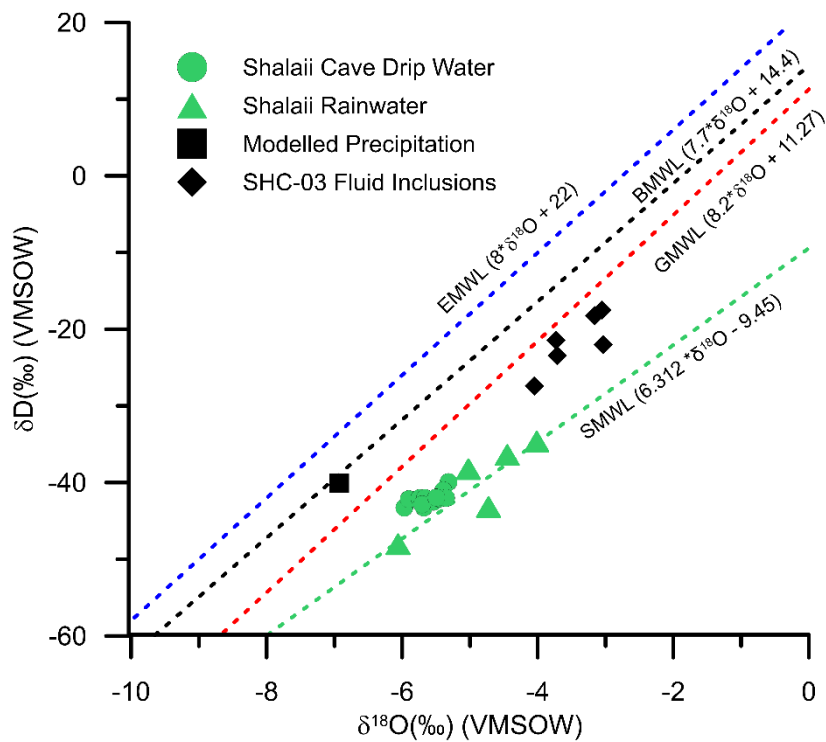


Figure 48:  $\delta^{18}\text{O}$  vs  $\delta\text{D}$  versus plot of fluid inclusions samples from SHC-03 (black diamonds) and drip water samples from monitoring data collected in 2014 (green circles). Also shown are  $\delta^{18}\text{O}$  vs  $\delta\text{D}$  relationships for precipitation above the cave (green triangles), GMWL = Global meteoric water line (red dashed line), SMWL = Sangaw meteoric water line. The fluid inclusion  $\delta^{18}\text{O}$  and  $\delta\text{D}$  values are much more positive compared to drip water observations which suggests a large influence of evaporative effects on fluid inclusions post deposition, limiting their value for this project.

## Summary

By examining the proxy data from stalagmite SHC-03 this chapter has assessed what processes are likely to be influencing their variation over time and consequently, to what extent they are responding to past climatic and environmental changes:

- Due to a strong correlation between  $\delta^{18}\text{O}$  variability of the Eastern Mediterranean Sea Surface and the SHC-03 stalagmite during the Holocene this study suggests, that on centennial to millennial timescales,  $\delta^{18}\text{O}$  is largely modified by the source effect limiting its ability to record long-term trends in moisture availability, unless supported by other proxies.
- Long-term  $\delta^{13}\text{C}$  values are likely to be controlled by the dominant vegetation type above the cave (i.e. C3/C4 vs C4), which seems to have only changed once throughout the whole record. The relative stability of vegetation type above the cave seems to have masked other long-term trends in climate variability.
- The strong correlation between Mg/Ca and Sr/Ca during the early Holocene suggest that they are likely to be controlled by the amount of PCP occurring within the vadose zone above the cave, associated with changes in water residence time, consequently these can be used as proxies for long-term changes in moisture availability. Additionally, a broad correlation between  $^{87}\text{Sr}/^{86}\text{Sr}$  and Mg/Ca, suggest that dolomite dust deposition, also associated with climate aridity, may be acting as a second order mechanism super-imposed on this long-term trend.
- On shorter timescales, coeval fluctuations in the  $\delta^{18}\text{O}$ ,  $\delta^{13}\text{C}$  and Mg/Ca data suggest they are all responding to changes in moisture availability; the  $\delta^{18}\text{O}$  responding to changes in rainfall amount, the  $\delta^{13}\text{C}$  responding to changes in soil biogenic  $\text{CO}_2$  production and vegetation density, and Mg/Ca likely responding to changes in dolomite dust deposition.

Therefore, a number of proxies from the SHC-03 stalagmite are likely to be responding to hydrological variability, both on longer and shorter timescales, demonstrating that the new record can be used to reconstruct past hydrological conditions in the EFC during the Holocene, explored in the next chapter.

## 9 Palaeoclimate Interpretation and Implications of the SHC-03 Record

Based on the interpretation of the proxy data of the SHC-03 speleothem record (Figure 49) as outlined in Chapter 8, alongside comparisons with pre-existing palaeoclimate datasets, this chapter will summarise Holocene climate conditions in the EFC. The first section will focus on long-term change while the second section will look at evidence for short-term variability.

### 9.1 Long-Term Trends

#### 9.1.1 10,560 – 10,280 yr BP: Arid continental conditions

At the very beginning of the record (*c.* 10,560 – 10,280 yr BP) the Mg/Ca and Sr/Ca data exhibit their highest values of the record. Based on the current interpretation of the trace element data, these values indicate high amounts of PCP in the vadose zone above the cave, associated with dry conditions. Similarly, the  $\delta^{13}\text{C}$  data also display the highest values during this period, between -4‰ and -6‰, which are indicative of vegetation above the cave dominated by more drought resilient C4 plant species and sparser vegetation, rather than C3 type vegetation (McDermott, 2004). The absence of speleothem growth before *c.* 10,560 could imply conditions too dry for speleothem formation (most likely <300 mm yr<sup>-1</sup>), and there are still currently no speleothem records from the EFC that extend further back than this time.

Consequently, both the trace element and  $\delta^{13}\text{C}$  data provide evidence that the earliest part of the SHC-03 record was associated with conditions which were at their most arid for the Holocene, but still very likely to be wetter than the preceding glacial period. Dry conditions during this period could be associated with a period of recovery following the end of the Younger Dryas or related to the shorter pre-boreal oscillation dry event which has been identified in other records from Southwest Asia around this time (Verheyden et al., 2008; Asouti, 2017).

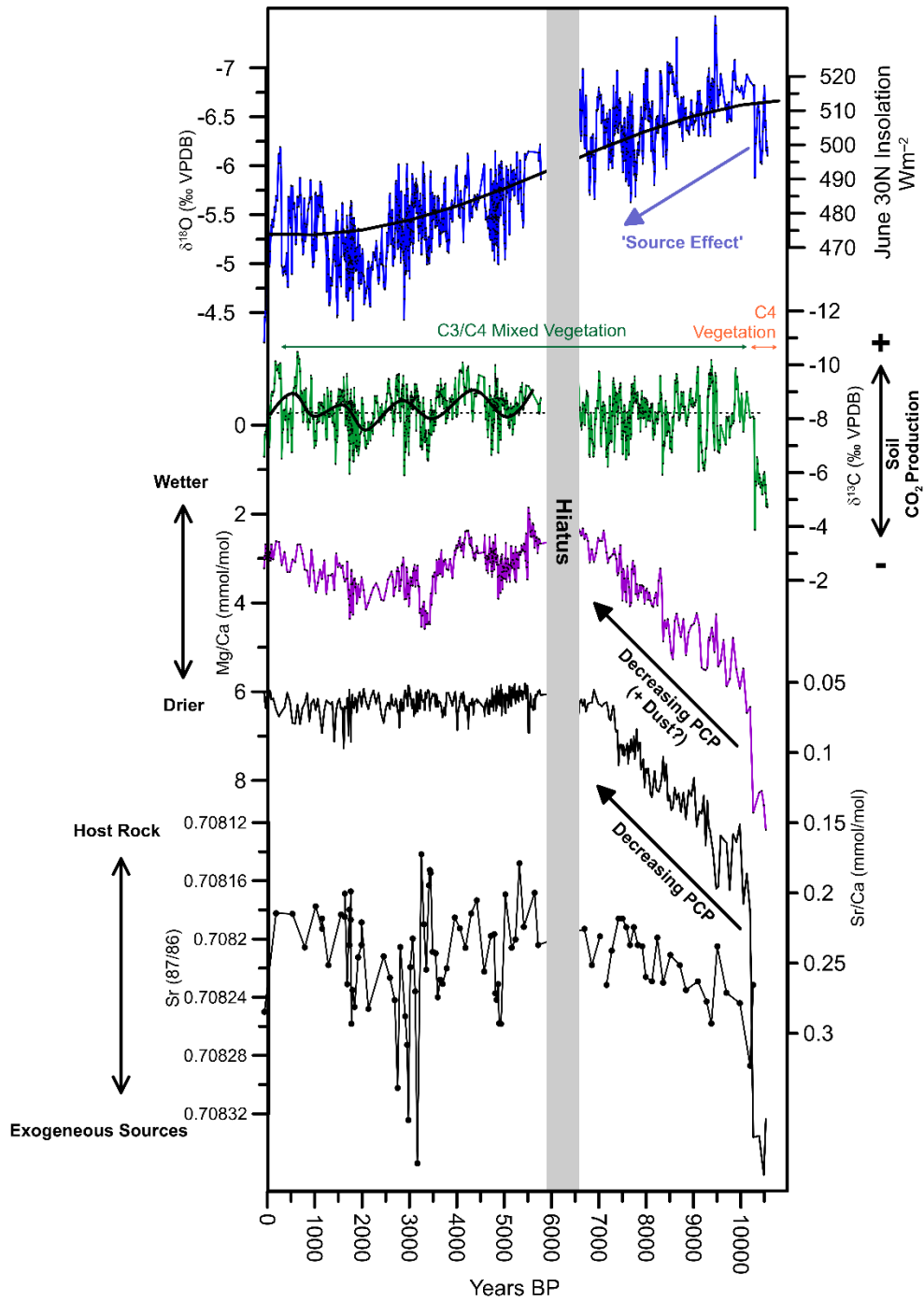


Figure 49: Key geochemical proxies from stalagmite SHC-03, annotated with their associated interpretations. Trace element (Mg/Ca, Sr/Ca) and  $^{87}\text{Sr}/^{86}\text{Sr}$  all show a coeval trend from higher to lower values during the early to middle Holocene which this study suggests represents a shift from drier to wetter conditions.  $\delta^{13}\text{C}$  data indicates little fluctuations in vegetation type (C3 vs C3/C4) above the cave for most of the record, except for the shift at c.10,280 yr BP. The long-term  $\delta^{18}\text{O}$  is likely to be significantly masked by the source effect. Shorter-term variability is superimposed on these longer-term trends.

At c.10,280 yr BP, all proxies (Mg/Ca, Sr/Ca,  $\delta^{13}\text{C}$ ,  $\delta^{18}\text{O}$  and  $^{87}\text{Sr}/^{86}\text{Sr}$ ) exhibit an abrupt and marked shift to lower values. The  $\delta^{13}\text{C}$  data displays a change from a mean of c.-5‰ to c.-8‰, which is likely to represent a shift in vegetation above and around the cave from an environment dominated by C4 plant types to a C3/C4 mixed regime. Based on modern analogues, this perhaps reflects a change in the environment from one dominated by steppe shrubland species such as *Chenopodiaceae* and *Artemisia* to one which included (still relatively drought tolerant) C3 grasses along with the pre-existing C4 steppe species, characteristic of the local environment today. The timing of this vegetation change broadly coincides with an increase in grass and *Pistacia* pollen values, and the decline in steppe shrubland species, in lake sediment records from the Iranian Zagros (van Zeist and Bottema, 1977). Therefore, this  $\delta^{13}\text{C}$  shift could represent a regional shift in vegetation development associated with wetter and warmer conditions. The magnitude and speed of change of all the proxy values indicate that this was likely to be the single largest shift in moisture availability during the Holocene. Similar changes in proxy data reflecting wetter conditions around the same time are observed in other records from wider Southwest Asia, including stalagmites from Jeita Cave in Lebanon (Verheyden et al., 2008; Cheng et al., 2015).

#### 9.1.2 10,280 – 6,540 yr BP

After this abrupt shift at c.10,280 yr BP, the Mg/Ca and Sr/Ca datasets, alongside the  $^{87}\text{Sr}/^{86}\text{Sr}$  data, still display relatively high values compared to the long-term mean of the entire SHC-03 record. These high values suggest conditions were still comparatively dry, enabling high levels of PCP, as well as relatively high amounts of atmospheric dust deposition. However, from the start of this period (c.10,280 yr BP) until the hiatus in the SHC-03 record (c.6,540 yr BP) the trace elements and  $^{87}\text{Sr}/^{86}\text{Sr}$  data display a slow and steady trend to lower values, representing decreasing levels of PCP and dust deposition due to increasing moisture availability. A gradual shift from drier to moister conditions is additionally supported by the  $^{234}\text{U}/^{238}\text{U}_0$  data which exhibit a trend from higher to lower values, indicating increasing dissolution of the carbonate host rock relative to leaching of weathered soil components. Therefore, the SHC-03 record suggests that this early to middle Holocene period was characterised by relatively dry conditions, but these conditions became increasingly wetter overtime. Trace element values eventually

reach the long-term Holocene mean and by the start of the hiatus (*c.* 6,540 yr BP) Mg/Ca and Sr/Ca are at some of their lowest values of the record, marking a period when the wettest conditions of the Holocene may have been reached.

It is important to mention here that similar trends in trace elements during the early to middle Holocene were recently observed in the Katakhor Cave speleothem record from western Iran (Andrews et al., 2020). However, in this study this trend was associated with flushing of epikarst water with a legacy of bedrock regolith which had built up during the drier late Pleistocene (Andrews et al., 2020) rather than direct changes in climatic conditions, in contrast to the interpretation made in this thesis. One cause for these differing interpretations is opposing  $^{234}\text{U}/^{238}\text{U}_0$  trends (Figure 50), with the Katakhor Cave record displaying a shift from lower to higher values, while the trend of the SHC-03 record is from higher to lower values (alongside the  $^{87}\text{Sr}/^{86}\text{Sr}$  data). Confirming the cause for the observed changes in trace elements in these records is certainly something that warrants future investigation.

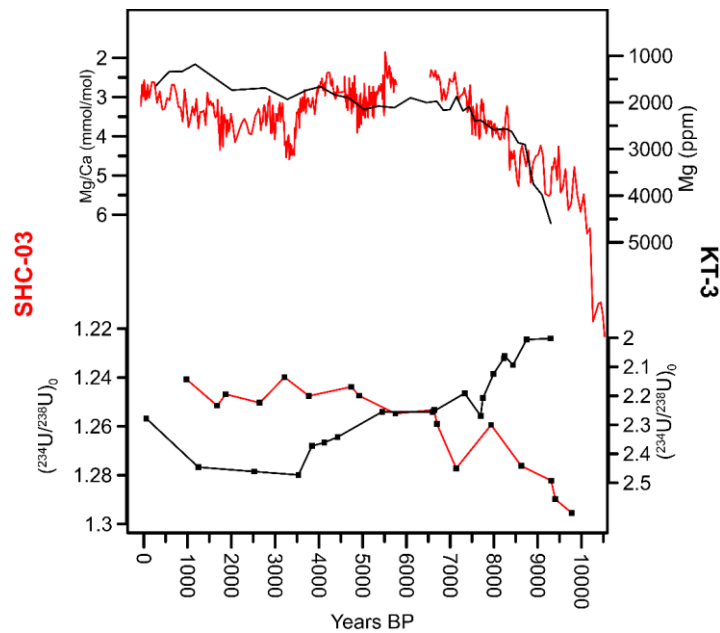


Figure 50: Comparisons between trace element and  $^{234}\text{U}/^{238}\text{U}_0$  proxies from the Katakhor Cave (black line) and Shalaih Cave (red line) records. The long-term trend of the trace element data during the early to middle Holocene is broadly similar in the two records (i.e. a trend from higher to lower values), however the way in which this trend is interpreted differs between these studies. One cause for these contrasting interpretations is the differing  $^{234}\text{U}/^{238}\text{U}_0$  trends, with the Katakhor Cave record exhibiting a trend from lower to higher values, while the Shalaih Cave record displays a trend from higher to lower values.

As discussed in Chapter 8.2.4, while  $\delta^{18}\text{O}$  values of the speleothem carbonate are at their lowest throughout the period discussed here (10,280 – 6,540 yr BP), this study suggests this is largely related to changes in the  $\delta^{18}\text{O}$  value of the main source of moisture (the Eastern Mediterranean) rather than local hydrological conditions. The  $\delta^{13}\text{C}$  data remains constant throughout this period which suggests that the proportion of C3 vs C4 plant types and vegetation density remained fairly constant, perhaps providing some evidence that absolute long-term changes in moisture availability were never great enough to cause significant vegetation change around Shalaih Cave.

This time period (10,280 – 6,540 Yr BP) overlaps with a period known as the ‘*Holocene Climate Optimum*’, where a number of studies from around the Mediterranean and Southwest Asia have suggested relatively wet conditions persisted (Rohling and De Rijk, 1999; Robinson et al., 2006; Weninger et al., 2009; Clarke et al., 2016; Andrews et al., 2020). Consequently, given the SHC-03 seems to indicate relatively dry conditions, this study provides somewhat of a challenge to this consensus. However, this is not the first study to suggest relatively dry conditions were present during the early to middle Holocene, particularly in the EFC. Most notably, and as discussed in Chapter 3.3.4, this includes pollen investigations from the Iranian and Turkish Zagros which have proposed that a delay in the expansion of oak woodland into the region during the early Holocene was a consequence of relatively low effective moisture (van Zeist and Bottema, 1977; Wick et al., 2003). This interpretation was more recently supported by plant macrofossil data from these lakes which have provided evidence of low lake levels during this period related to warm and long summers, resulting in increased evaporation (Wasylikowa et al., 2006). Furthermore, high levels of charred fragments in both Lake Van and Lake Zeribar found during the early Holocene may indicate an increase in natural fires associated with climatic dryness, (Wick et al., 2003; Wasylikowa et al., 2006).

Interestingly, if the new SHC-03 trace element data is visually compared to the pollen data from lake sediment records from the EFC (Figure 51) there is a broad similarity between the long-term trends during the early to middle Holocene. Oak/tree pollen percentages are low or non-existent during the earlier part of the Holocene before exhibiting a steady trend to higher values peaking around 6,000 yr BP, mirroring the trend observed in the SHC-03 Mg/Ca data. Additionally, a comparison against the

Mg/Ca profile from Lake Van, which reflects changes in lake-water salinity, and consequently the P:E balance of the lake (Wick et al., 2003), also displays a striking long term visual similarity to the SHC-03 data (Figure 51).

Stevens et al., (2001, 2006), Tzedakis (2007) and Djamali et al., (2010) have offered similar explanations for relative aridity in the EFC during the early Holocene. They all suggest that it is related to the seasonal distribution of rainfall in the region, associated with changes in the intensity and the position of the ITCZ and ISM. During the early Holocene, increased northern hemisphere summer solar insolation resulted in a greater differential between land and sea surface temperatures, which caused an increase in intensity and a poleward shift of the ITCZ (Fig.53) (Fleitmann et al., 2003a, 2007). The intensification of the ISM and northward displacement of the ITCZ in spring would have caused the establishment of a stable and relatively high pressure system (ridge) over the Iranian Zagros earlier in spring (Djamali et al., 2010). This high pressure system would have blocked moisture bearing westerlies from reaching the region and therefore reduced the amount of, or potentially completely prevented, spring rainfall creating a winter-only rainfall regime. This would have extended the duration and intensity (as a result of increased summer temperatures) of the arid summer months (Tzedakis, 2007). The weakening and retreat of the ITCZ further south and the associated high-pressure system over the EFC as solar insolation decreased in the middle Holocene would have increased the frequency of storm tracks in the region, re-establishing a winter-spring rainfall regime, which is present in the climate of the region today. Increased seasonality during the early Holocene in mid latitude, continental regions of the northern hemisphere, like the EFC, have also been identified by climate modelling studies (Brayshaw et al., 2011b).

Additional support for the interpretation can be provided by observing conditions in other regions of the Mediterranean located at similar latitudinal positions, and therefore similarly situated in between monsoonal and westerly systems. Lake sediments from Sicily (Figure 51) and southern Spain also exhibit evidence of a delay in the expansion of woodland alongside higher rates of natural fires during the early Holocene (Sadori and Narcisi, 2001; Pantaléon-Cano et al., 2003; Tinner et al., 2009), which these studies also link to an intensified and northward shift of the ITCZ. Moreover, there is less evidence

of human activity at these other Mediterranean locations during the early Holocene that would significantly influence vegetation, providing further support that the vegetation development identified in the EFC during the early Holocene was related to changes in the position and influence of major climate systems rather than anthropogenic activities.

The interpretation of the SHC-03 trace element data would support these previous explanations for early Holocene aridity; reduced spring rainfall would have reduced the amount of recharge of the karst system during spring, increasing water residence time in the vadose zone enabling higher amounts of PCP, while longer-periods of summer aridity may have also provided more suitable conditions for dust mobilisation. These relationships are schematically explained in (Figure 52).

Another implication of the identification of heightened seasonality during the early Holocene is its potential influence on rainfall  $\delta^{18}\text{O}$  values. Increased seasonality would lead to a relative increase in winter rainfall compared to spring rainfall, both because of a reduction/cessation of spring precipitation and, perhaps, an increase winter rainfall amount. Because winter rainfall has lower  $\delta^{18}\text{O}$  than spring rainfall, these changes in seasonality would lead to lower speleothem  $\delta^{18}\text{O}$  values. Moreover, as discussed in Chapter 8.2.4.2, reduced spring rainfall would have led to less or negligible recharge of the karst system in spring (Figure 52), resulting in a seasonal bias of cave drip waters towards the value of winter rainfall (Baker et al., 2019), where the majority of recharge occurs, further exacerbating the seasonality  $\delta^{18}\text{O}$  effect. Consequently, these processes could explain the larger magnitude of change observed in the SHC-03  $\delta^{18}\text{O}$  compared to the  $\delta^{18}\text{O}_{\text{EMSS}}$  during the Holocene if source  $\delta^{18}\text{O}$  changes were only accounted for.

These findings have important implications for the *early Holocene precipitation paradox*, one of the largest outstanding problems in paleoenvironmental studies in the region, referring to the discrepancy between pollen and  $\delta^{18}\text{O}$  data of lake sediments and speleothems. The SHC-03 record offers support to the pollen and other studies which have suggested hydrological conditions, particular highly seasonal and dry conditions, were the cause for the delay in the expansion of oak woodland in the EFC during the early Holocene (van Zeist and Bottema, 1977; Stevens et al., 2001; Djamali et al., 2010), rather than other processes (e.g. anthropogenic activities) proposed by other investigations (Roberts, 2002; Asouti

and Kabukcu, 2014). Importantly, this study also offers alternative explanations for  $\delta^{18}\text{O}$  variation during the Holocene rather than solely rainfall amount.

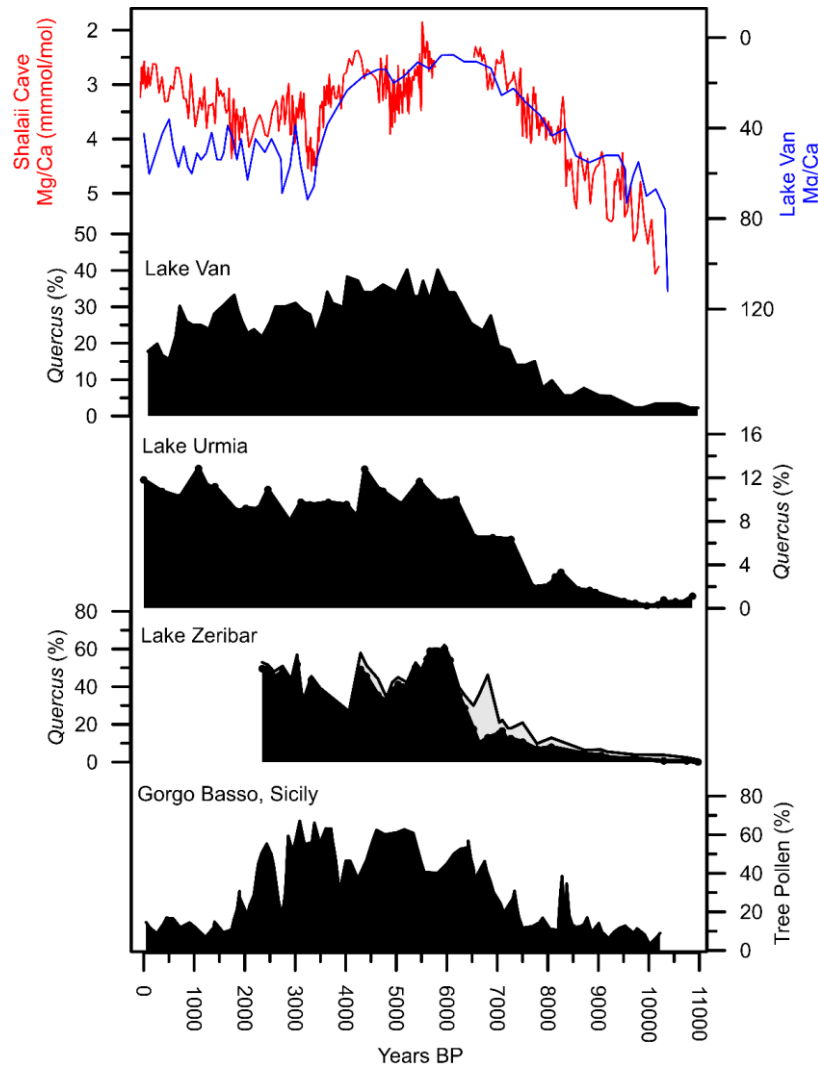


Figure 51: Comparison between the SHC-03 Mg/Ca data (red line) with selected pollen data from the EFC and Sicily. (Van Zeist and Bottema 1977; Wick et al., 2003) and Sicily (Tinner et al., 2009), alongside geochemical data from Lake Van (blue line) (Wick et al., 2003). The similarity between the long-term trends of the SHC-03 Mg/Ca data and the EFC pollen percentages suggest that increased seasonality and drier conditions were the cause of the delay in the expansion of oak woodland during the early Holocene. The similar trend observed in the Sicily tree pollen curve provides further support that the delay is the consequence of shifts in the position of major regional climate systems rather than local anthropogenic activities. Faded grey area represents total tree pollen percentages in the Zeribar record.

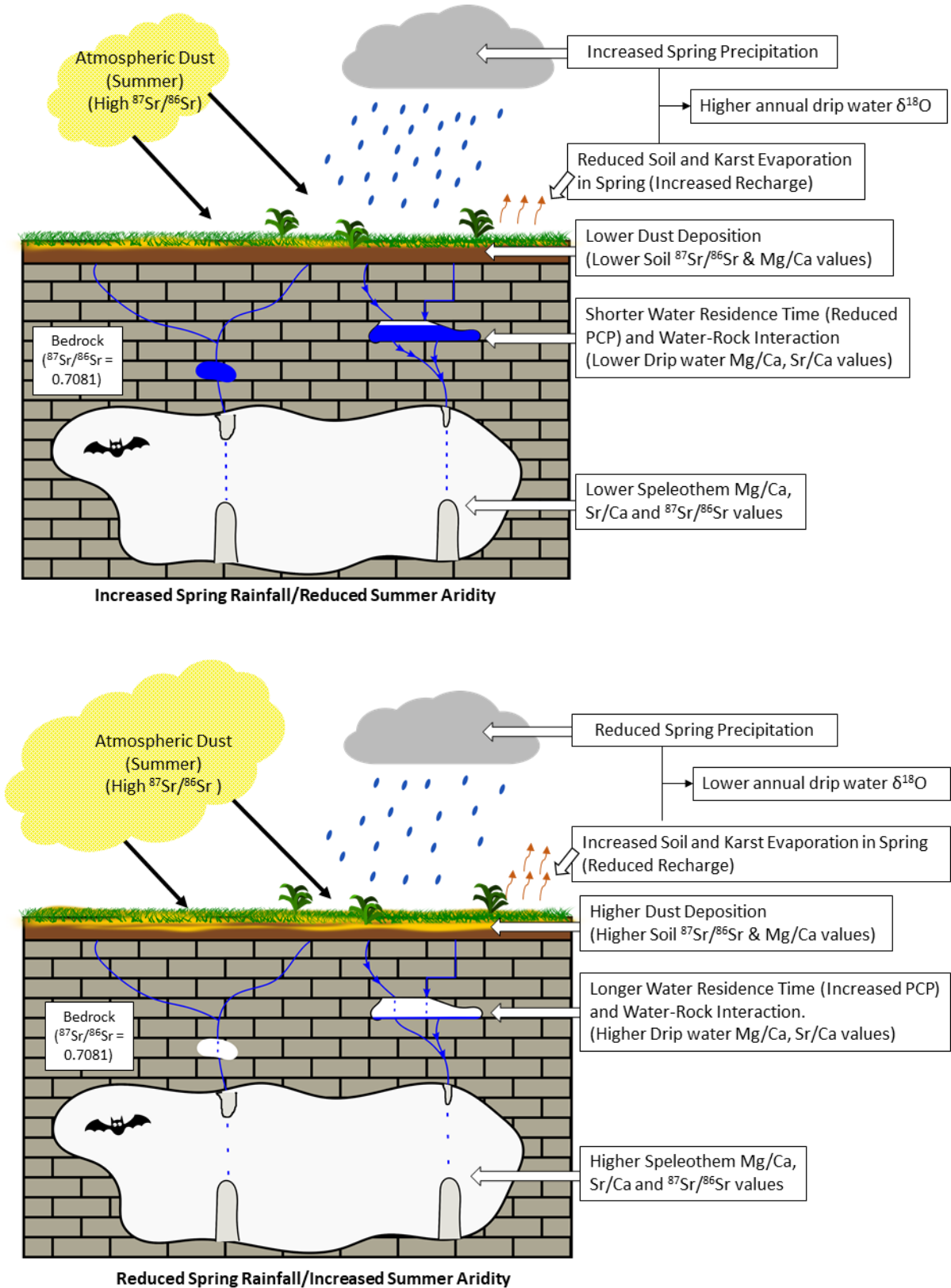


Figure 52: Schematic illustration of how different proxies change in response to changes in the amount of spring rainfall to explain the current interpretation of these proxies.

9.1.3 5,780 yr BP – Present: Relative Stability

After the hiatus, and like the observations made just before it, the Mg/Ca, Sr/Ca and  $^{87}\text{Sr}/^{86}\text{Sr}$  proxy data exhibit their lowest values of the record. This suggests wetter conditions, lower water residence time and reduced dust deposition above the cave and lower seasonality likely to be associated with a weakening monsoon system. Peak humidity during the middle Holocene is in agreement with peak oak pollen concentrations from lake sediments from the EFC as well as trace element and isotopic data from Lake Van (Wick et al., 2003). However, once again this is somewhat in opposition to the general consensus for conditions in wider southwest Asia, where the middle Holocene is often interpreted as a transitional phase to drier conditions (e.g. Weninger et al., 2009; Roberts et al., 2011; Clarke et al., 2016).

For the rest of the record, the different trace elements no longer exhibit a positive correlation to one another and remain relatively stable compared to the trend observed during the early Holocene. This would suggest that the mechanism that led to the correlation and long-term trend during the early Holocene (i.e. water residence time) remained relatively similar for the latter half of the Holocene, which may indicate a time of relative long-term climatic stability. Moreover, this would further imply that the position and influence of the climate systems causing seasonality changes (i.e. monsoon strength) remained relatively similar for this period.

However, variations in Mg/Ca during this period are consistent with simultaneous shifts in the  $\delta^{13}\text{C}$  and  $\delta^{18}\text{O}$  data, and maintain a broad similarity to the  $^{87}\text{Sr}/^{86}\text{Sr}$  values. Therefore, this study argues fluctuations in Mg/Ca data are still likely responding to hydrological variability, which could be the result of dolomite dust deposition above the cave, similar to Carolin et al. (2019). The Mg/Ca profile exhibits a quasi-U-shaped trend (Figure 49) during this period (5,780 yr BP – present) which is also visible in the  $\delta^{18}\text{O}$  profile. Between 5,780 and c.4,000 yr BP, relatively wet conditions persist and then there was a shift to drier conditions centred around 4,000 – 2,000 yr BP followed by a period of recovery. This U-shaped pattern broadly follows the northern hemisphere summer solar insolation curve and could therefore represent changes in the strength of North Atlantic westerlies reaching the region. Similar U-shaped trends in the middle to late Holocene climate are observable in Kuna Ba cave in Iraqi

Kurdistan (Sinha et al., 2019) as well as other records from wider Southwest Asia, including Jeita Cave (referred to as a w-shaped trend in the publication).

A recent speleothem study from the EFC has previously identified a clear drying trend covering the last c.1000 Years (Flohr et al., 2017). In the SHC-03 there is no clear trend present to support this observation, however the resolution and chronological constraints of this period in the Shalaih Cave record are relatively poor. Future work should aim to increase the resolution and chronological constraints across this period, and the fast growth rates of the speleothem should make this relatively straightforward. However, both  $\delta^{18}\text{O}$  and  $\delta^{13}\text{C}$  exhibit large shifts to higher values during the last c.100 years which could represent a drying trend identified in both the Gejkar Cave and Kuna Ba cave records (Flohr et al., 2017; Sinha et al., 2019).

## 9.2 Short-term climate variability

The existence and investigation of short-term climate variability during the Holocene is a major focus for many palaeoclimate studies, particularly when examining the influence of past climate change on human societies (Mayewski et al., 2004; Staubwasser and Weiss, 2006; Weninger et al., 2009). As discussed in Chapter 8, the Mg/Ca,  $\delta^{13}\text{C}$  and  $\delta^{18}\text{O}$  proxy data from SHC-03 are all likely to some extent reflect short-term changes in effective moisture. Therefore, covariations of these different proxies are likely to be a good indication of short-term (multi-decadal to multi-centennial scale) climate fluctuations.

To semi-empirically identify wetter and drier period, a similar approach taken by Regattieri et al., (2014) was used to create a mean anomaly index (MAI). An MAI is a similar, but alternative method of identifying co-variations between different proxies to principal components analysis (PCA), which statistically combines different proxies to create a ‘master’ record. To create the MAI record for the SHC-03 data, long term trends from the proxies were detrended by applying a 5<sup>th</sup> order polynomial spline to the data and subtracting it, the data was then normalised to produce z-scores (where deviations from a zero-mean expressed in standard deviation units) (See Appendix C 14.3). Secondly, to place the different isotopic and trace element data on a common x axis value, the data was binned into 30-year increments. Standard scores of the three series were then averaged for each time increment to produce

a mean anomaly (MA) time series (Figure 53) where low (high) average standard scores correspond to relatively wetter (drier) intervals. However, as highlighted by Regattieri et al., (2014), it is possible for one anomalous large excursion in one of the proxies to skew the MA value therefore, anomalous wet (dry) excursions should not only have relatively low (high) mean anomalies, but those means should also have low variability (i.e. agree internally). To account for this possibility, a ‘filtered index’ (FI) was created to identify statistically significant ‘wetter and ‘drier’ periods. To do produce the FI, the standard deviation (SD) of the three different scores for each time increment were calculated and a SD threshold of one was set, where any SD over one was given a score of 0 (essentially ignored). Values with a SD under one were then given arbitrary thresholds to identify significantly drier or wetter conditions. An adapted approach than that taken by Regattieri et al., (2014) was taken here to act as a more sensitive index in which multiple thresholds were set, where values were given to mean anomaly scores that deviated from the mean by 0.25, 0.5 and 1, where positive excursions represent wet intervals and negative excursions represent dry intervals. FI Scores of 1 or -1 represent more extreme events, whereas scores of 0.25 or -0.25 represent still statistically significant, but less extreme events. These scores were then plotted using a step plot (Figure 53). The resulting combined MA and FI series shows different wetter and drier events which can be set in the wider regional context of climatic changes during the Holocene (Figure 55).

The resulting timeseries of this transformed data reveals the presence of abrupt, multi-decadal events alongside longer centennial-millennial scale trends in climate. The FI plot highlights especially dry multi-decadal events at *c.*35, 400, 2,100, 3,400, 6,800, 7,500, 8,400, 9,200, 10,400 yr BP and wetter events at *c.*200, 650, 4,200, 5,500, 6,600, 7,000, 9,400, 10,200 yr BP. Additionally, the MAI data presents some evidence of a quasi-cyclical trend between wetter and drier conditions over a 1500 – 2000-year period, particularly during the latter half of the SHC-03 record. This pattern is also clearly visible in the original  $\delta^{13}\text{C}$  data which is not masked by long-term trends (Figure 49). This data can be used to make comparisons with other regional and inter-regional records which will allow these shorter scale events and trends to be placed within the context of climate variability seen elsewhere, and offers a chance to investigate and contribute to the discussion for the cause(s) for short-term variability

identified in the SHC-03 record. For the purposes of this study, the focus will be on the variability identified over the last 6,000 years.

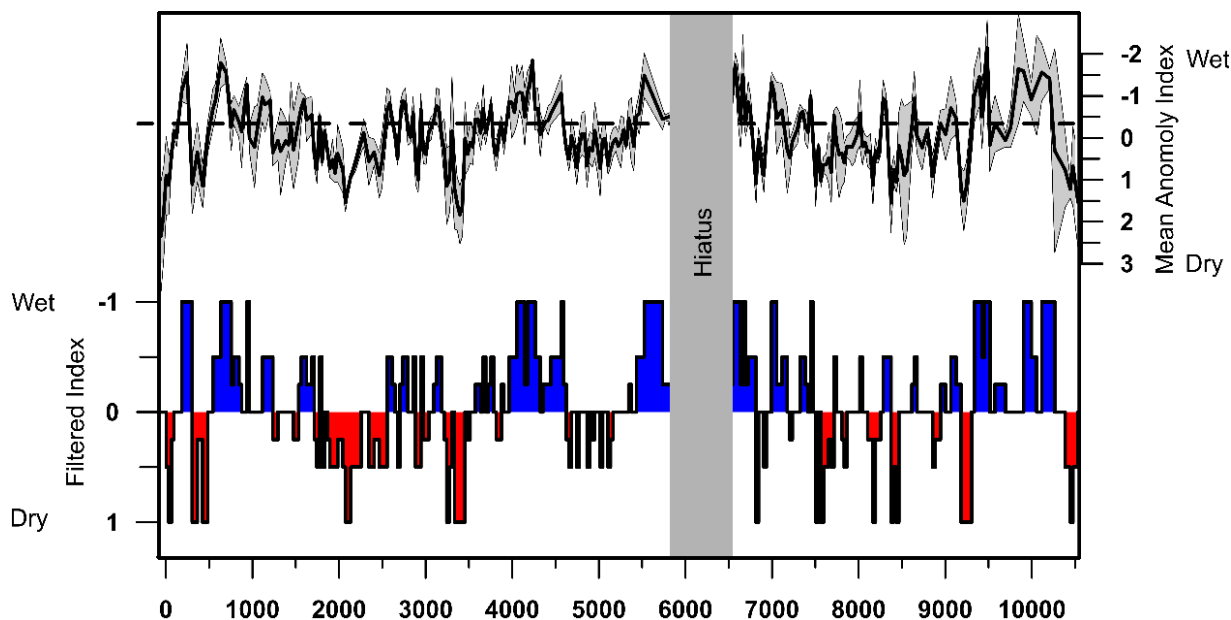


Figure 53: The combined mean anomalies (referred to as MAI in the main text) of Mg/Ca,  $\delta^{13}\text{C}$  and  $\delta^{18}\text{O}$  (black line) (See Appendix.C 14.3). Error bars (grey) are expressed as standard deviation units. Also presented is the step plot of filtered anomalies where positive and negative excursions indicate statistically significant wetter and drier conditions (blue = wet, red = dry). Method adapted slightly from Regattieri et al., (2014) to be more sensitive, where mean anomalies which deviate 0.25, 0.5 and 1 away from the long-term mean are displayed to illustrate less and more extreme conditions.

The identification of a *c.*1,500 year sinusoidal cycle between wetter and drier conditions is a pattern which has also been identified in a number of records from Southwest Asia, including Soreq Cave (Bar-Matthews and Ayalon, 2011), Jeita cave (Cheng et al., 2015) and Lake Neor (Sharifi et al., 2015) as well as records elsewhere around the globe (Mayewski et al., 2004; Isono et al., 2009; Smith et al., 2016). Cyclical variations such as this have previously been linked to ice-rafting, ocean cooling, events in the North Atlantic (Bar-Matthews and Ayalon, 2011). These ice-rafting events are known as Bond events and are thought to have occurred every *c.*1500 years associated with variations in solar activity (Bond et al., 2001). Since rainfall in Southwest Asia is predominantly associated with storm tracks originating in the North Atlantic, studies have suggested that North Atlantic cooling, associated with

Bond events, led to drier conditions in Southwest Asia (Bar-Matthews and Ayalon, 2011; Cheng et al., 2015). However, when the SHC-03 MAI and FI data are compared to the record of hematite-stained grains (HSGs) from North Atlantic deep-water sediments where higher amounts of hematite-stained grains reflect increased drift ice and, thus, reflect cool phases in the North Atlantic (Bond et al., 2001), there is no clear evidence of a relationship between them.

Other records from Southwest Asia have proposed alternative explanations for 1,500-year periodicities detected in their records. For instance, a sediment study from Lake Neor, on the coast of the Caspian Sea in Iran, exhibited a similar quasi-cyclical variation (a ~1550 year cycle) (Sharifi et al., 2015). The authors identified a correlation between fluctuations in Ti,  $\delta^{13}\text{C}_{\text{TOC}}$  and TOC, proxies for moisture availability, to variations in  $\text{K}^+$  ion concentrations in the GISP2 ice core (Figure 55). The latter is used as a proxy for the strength of the Siberian High-pressure system (Mayewski et al., 1997), a dominant synoptic system in north east Eurasia which is thought to strengthen during periods of reduced solar irradiance and insolation. Therefore, Sharifi et al., (2015) suggested that moisture availability largely responded to changes in the strength and influence of the Siberian High.

The SHC-03 and Lake Neor proxies exhibit a broad similarity that might also suggest that changes in the strength and position of the Siberian High may have had an important influence on the climate of the EFC during the Holocene. However, an important and interesting observation is that this relationship is inverse, that is to say drier periods in the Lake Neor correspond to wetter periods in the SHC-03 record and *visa versa* which given the relatively close proximity of the two records, is somewhat of a puzzle. Here a possible explanation is provided. While the expansion of the Siberian High would lead to blocking of moist westerlies from reaching Neor Lake and likely lead to colder and drier conditions to dominate Northern Iran (Figure 54). The area around Shalaih is further south and west and consequently is less likely to be directly influenced by the Siberian High than the Caspian Sea coast. Therefore, it is possible that the expansion/strengthening of the Siberian High caused the displacement of cyclonic storm tracks further south, over the Zagros region, leading to more rainfall over the EFC, although future exploration of the behaviour of these climate dynamics is needed to verify this.

Another interesting observation can be made through the comparison between a reconstruction of the NAO index (Olsen et al., 2012) and the SHC-03 FI data (Figure 55). As explained in Chapter 2.2.3 the NAO refers to the north-south dipole and relative difference of atmospheric pressure at sea level between the Icelandic Low and the Azores High pressure systems situated above the North Atlantic. NAO positive (negative) events are usually linked to dry (wet) conditions in southern Europe and the western Mediterranean. However, its influence on Southwest Asia, perhaps with the exception of Anatolia, is still largely uncertain. The NAO reconstruction and the SHC-03 show a generally broad similarity from about 2,500 years onwards, but unlike western European records, wetter (drier) conditions seem to reflect NAO positive (negative) conditions. Furthermore, significant dry events in the SHC-03 FI record correspond to large negative excursions in the NAO reconstruction (Figure 55) further suggesting a teleconnection between the two datasets. This would seem to indicate the EFC and parts of Southwest Asia respond differently to the rest of the Mediterranean region to NAO variation. An anti-phase relationship between Southwest Asia and the rest of the Mediterranean to the NAO has previously been reported by palaeoclimate reconstructions (Roberts et al., 2012), referring to it as the Mediterranean Oscillation, an observation also supported by modelling studies (Black, 2012) and tentatively, the new SHC-03 record would seem to show this relationship.

The observations between these different systems with the SHC-03 provides an initial clue into potential causes for shorter-term climate variability in the EFC during at least the latter half of the Holocene. It should also be highlighted that the similarity between these systems and the SHC-03 record seems to change over time, where the SH (GISP2 +) record shows a generally good similarity between 6,000 – 2,500 years BP, whereas the NAO reconstruction shows little similarity to the SHC-03 record before 3,500 years BP. This might indicate non-stationary behaviour and that the relative influence of these systems on the EFC may not have been uniform over time. Moreover, while this was an initial attempt to identify major influences, ultimately, the cause for short-term climate variability in regions distant from the North Atlantic is likely to be the consequence of number of complex factors and interactions between North Atlantic, Monsoon and Siberian climate dynamics that make it hard to pinpoint the exact nature and drivers of these events.

Where the SHC-03 record starts to show a close similarity to multi-centennial trends also marks a period where the similarity between the SHC-03 records and the GISP+ data weakens, similarly identified by Sharifi et al. (Sharifi et al., 2015). Therefore, this could indicate that the influence of different systems is non-stationary over time. To fully understand this goes beyond the scope of this project. However, it does demonstrate the complex nature of the behaviour of atmospheric dynamics in the past, and the need to utilise well dated, high resolution palaeoclimate to capture heterogenous behaviour which may provide a better insight to how these systems could behave in the future.

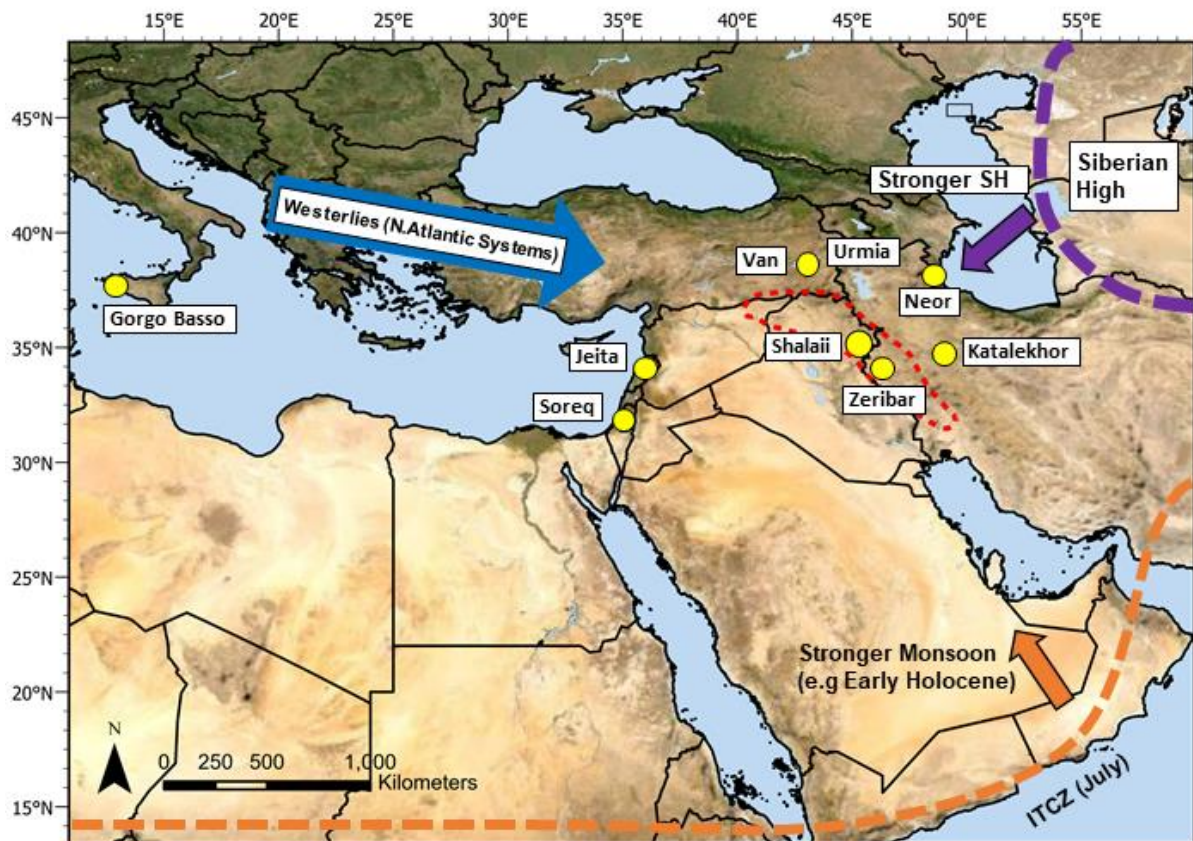


Figure 54: Schematic position of major synoptic systems and location of key records (yellow circles) discussed in this chapter. Dashed Orange and Purple line mark the current maximum extent of the climate systems (ITCZ and Siberian High), whilst, the arrows drawn off from these systems illustrate their direction of movement if they were to become stronger as they may have done in the past, potentially having a greater influence on the climate of the EFC in response to changes in solar insolation.

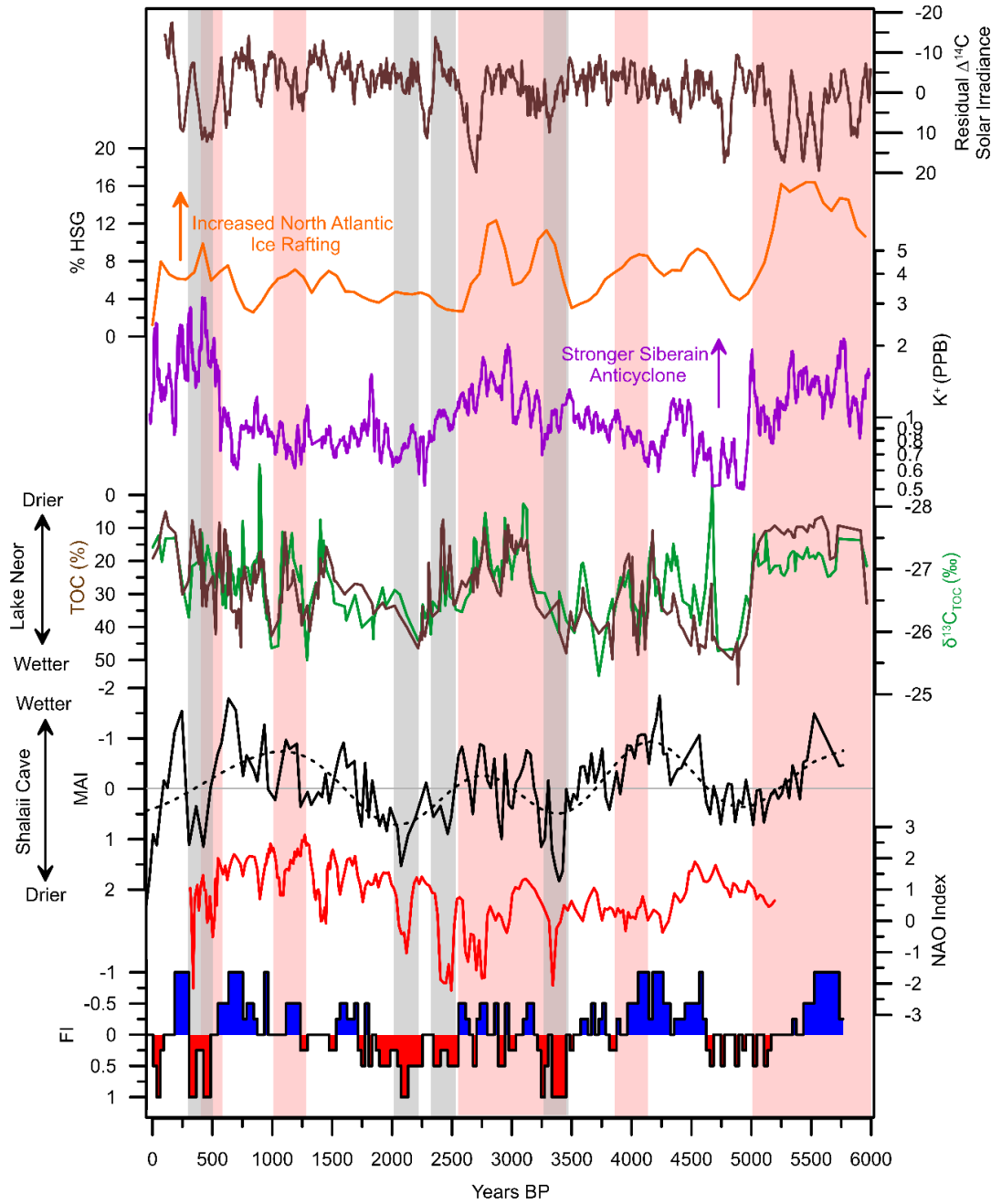


Figure 55: Comparison between the SHC-03 MAI and Fi data with the Neor Lake record (Sharifi et al., 2015), regional climate indices (Bond et al., 2001; Mayewski et al., 2004; Olsen et al., 2012) and solar irradiance (Stuiver et al., 1998) covering the last 6,000 years. The cyclical variation (schematically highlighted with dotted line) identified in the SHC-03 MAI record correspond well with similar fluctuations in the nearby Lake Neor record. However, the relationship is inverse, so wetter periods at Shalaih correspond to drier conditions at Lake Neor. Fluctuations in Lake Neor were related to shift in the Siberian anti-cyclone, records by the GISP2 K+ record. There is also a broad similarity to the NAO reconstruction (Olsen et al. 2012), particularly the last c.2,500 years. Moreover, major dry events identified in the SHC-03 record (grey bars) match negative excursions in the NAO reconstruction. Finally, there seems to be no clear link between events identified in the SHC-03 record with rapid climate change events (RCCs) identified by Mayewski et al., (2004) (pink bars).

### 9.3 Summary

The multi-geochemical proxy approach undertaken in this project has uncovered both millennial long changes and shorter multi-decadal to centennial scale variability in hydrological conditions in the EFC during the Holocene, providing the first high resolution record from the EFC to cover the majority of the Holocene.

For long-term, millennial scale changes, trace element (Mg/Ca, Sr/Ca), U and Sr Isotope data have been employed to reconstruct past changes in water residence time and dust deposition above Shalaih Cave, which this study argues is linked to the length and intensity of summer aridity, a major influence on the annual moisture balance of the region. If this interpretation is correct, the record indicates that the early Holocene was characterised by a highly seasonal climate, with extended periods of summer aridity than present with little or inconsistent spring rainfall. This finding displays a strong similarity to, and supports the interpretation of, existing pollen data from lake sediment records from the region, indicating low levels of tree pollen present in lake sediments during the early Holocene were the consequence of climate aridity, rather than other mechanisms. For this reason, this study provides an important contribution to ongoing discussion into the reasons behind the *early Holocene precipitation paradox*. The cause of increased summer aridity during the Holocene was likely to be the result of increased summer insolation which led to the northward displacement of the ITCZ, resulting in the establishment of high pressure systems over the EFC earlier in spring than present, blocking spring rainfall as suggested by a number of studies already (Stevens et al., 2001; Tzedakis, 2007; Djamali et al., 2010). From c.5,780 yr BP, trace elements values display less evidence of multi-millennial scale trends which would suggest the position and influence of these major dynamics remained relatively stable throughout this latter period.

Superimposed on this long-term trend, co-variations between Mg/Ca,  $\delta^{13}\text{C}$  and  $\delta^{18}\text{O}$  indicate periods of shorter-term variability in the hydroclimate. By combining these proxies and producing a mean anomaly index and filtered index, this project has been able to semi-empirically identify the timing of wetter and drier multi-decadal to multi-centennial events and trends. Focusing on the last 6,000 years, multi-centennial scale trends in climate oscillating between wetter and drier periods broadly follow a quasi-

cyclical 1,500-year pattern. This longer-term cyclical trend is broadly similar, but inverse, to that observed at Lake Neor, related to changes in the strength of the Siberian anti-cyclone. From about 2,500-year the SHC-03 seems to show a good fit with a reconstruction of the NAO, where more negative (positive) conditions lead to drier (wetter) conditions. Moreover, the timing of shorter multi-decadal abrupt dry events during the latter half of the Holocene coincide with negative excursions in the NAO which might indicate some type of teleconnection between conditions in the North Atlantic and conditions in the EFC, which would be interesting to further explore, but would go beyond the scope of this project.

This new record provides an updated understanding of palaeoclimate conditions in the EFC which allows the investigation and testing of existing and new hypotheses concerning human-environmental relationships during the Holocene, which will be the focus of the subsequent chapters of this thesis.

## **10 Human-Environmental Relationships: Theoretical Considerations & Archaeo-Demographic Proxies**

The second smaller section of this thesis will explore how past human societies in the EFC responded to climate change and variability, integrating the palaeoclimate information retrieved from the SHC-03 stalagmite (Chapter 9). To do this, I have chosen to focus on one archaeological case study which covers an important period of cultural transformation. Specifically, Chapter 11 will investigate what impact climate variability may have had on the development and sustainability of early urban settlements in Northern Mesopotamia during the middle Holocene (c.6,350 – 4,200 yr BP). But first, in this current chapter, I will briefly explore how human-environmental relationships are more generally approached in archaeological investigations from a theoretical and methodological perspective and the inherent challenges involved in these types of studies. I will discuss the development and use of archaeo-demographic proxies, which have become an increasingly common way of correlating societal change with palaeoclimate datasets. By providing this background, it should provide some context for the objectives of, methodological considerations needed, and the approaches I take in Chapter 11.

### **10.1 Studying Human-Environmental relationships**

Understanding how past societies responded to climate and environmental change, as well as the impact of human activities on the surrounding environment (e.g. Lewis and Maslin, 2015), has always been a key topic of interest in archaeological, palaeoenvironmental and geographical investigation around the globe. In fact, the investigation of human-environmental interaction/relationships is regarded as one of the 5 main topics which cover major grand challenges in current archaeological research as outlined by Kintigh et al., (2014a). While the level of interest fluctuated during the 20<sup>th</sup> century (Judkins et al., 2008, pp. 19–20), the last 30 years has witnessed an exponential rise in investigations examining historical and pre-historical human-environmental relationships (Coombes and Barber, 2005; Carleton and Collard, 2020, pp. 114–115), fuelled by increasing concern associated with how anthropogenic climate change will affect present and future societies (Van De Noort, 2011) as well as the development of modern analytical techniques in palaeoenvironmental and archaeological sciences which have made human-environmental studies simpler to conduct. However, the study of human-environmental

interactions, particularly the impact of climate change on societies, has been and remains a somewhat controversial and hotly debated topic within archaeology and related disciplines (e.g. Coombes and Barber, 2005; Judkins et al., 2008; Contreras, 2016; Arponen et al., 2019). Historically, this debate has been polarised between two schools of thought which broadly represent ‘*systems centered*’ vs ‘*actor-centered*’ perspectives (Stanton, 2004, p. 30), one which focuses on top-down processes in which humans have to respond to external factors vs one which focuses on bottom up processes where decisions from individuals are given priority for reasons behind historical processes.

On one side of this debate have been archaeologists, usually working from an environmental perspective and *materialist* position (Arponen et al., 2019), who have emphasized the fundamental role climate and environmental change and conditions must have had on past human societies and cultural development. These types of studies usually framed their argument around observed climate changes in palaeoclimate data occurring synchronously with socio-cultural change identified in the archaeological record (Wossink, 2009), often arguing that the synchronous nature of the event was likely to be evidence of a causal link (Coombes and Barber, 2005). Proponents of this position are cited, often as a term of reproach, as climate or environmental determinists (e.g. Judkins et al., 2008). Critiques of this position often argue that these types of studies often provide oversimplistic explanations and ‘*ignore many complex, interacting, non-environmental factors that influence social processes and decision making*’ (Butzer, 1997; Brooks, 2012, p. 94).

On the other hand and at the other extreme of the debate, are archaeologists who have given cultural processes, particularly human agency, priority as an explanation for societal change and are likely to reject, ignore or diminish the potential influence of climatic and environmental change as a causal mechanism for modifications in socio-cultural systems (Van De Noort, 2011). This position is itself criticised for discussing human societies in a context which is somehow detached from their environmental surroundings (Contreras, 2016, p. 7) and also for equating any explanation that involves environmental change with climate determinism (Brooks, 2012, p. 94).

I would argue that, to some extent, the true nature of this polarisation is somewhat exaggerated. There are likely to be very few archaeologists who would argue that human agency has performed no role in

the trajectories of societies in the face of environmental stress, while equally, there are likely to be few who would argue that changes in the environmental context of, and resources available to, human societies played no importance in their successes or failures. Besides, both archaeologists and palaeoenvironmental scientists, particularly as the amount of inter-disciplinary work has increased, have begun moving away from this polarised debate towards more nuanced middle ground stances in which both environmental conditions and human agency are accepted as possible simultaneous and interconnected major drivers for societal change (Wossink, 2009; Riehl et al., 2012, p. 116), and that human-environmental interactions should be considered on a case to case basis. Nevertheless, one of the reasons for the theoretical dichotomy is the inherent challenges involved in demonstrating, in a quantifiable manner, causal relationships between climate and societal changes.

The major way in which climate and environmental change has been, and still is, linked to societal change has been achieved by identifying evidence of changes in palaeoclimate or palaeoenvironmental data and then identifying synchronous changes in the archaeological record (known as *parallelism*) (Arponen et al., 2019). Clearly, identifying a correlation of this type is essential if any causal relationship between societal change and the environment is to be asserted.

But, there are two major challenges with this strategy (Contreras, 2016, p. 9):

- 1) *“Problems of spatial and temporal scale and resolution. (Correlation)*
- 2) *Problems of articulation of mechanism.” (Causation)*

The first of these problems is an analytical issue. Historically, because of analytical limitations, it was challenging to establish the precise chronologies or proxy resolution needed in both palaeoenvironmental and archaeological datasets to provide robust, reliable correlative links between them (i.e. identifying synchronous changes). However, the development of new analytical techniques over the last couple of decades has made it increasingly possible to overcome the challenge. The advent of AMS <sup>14</sup>C dating (Brock et al., 2010), U-Th dating (Hoffmann et al., 2007), application of Bayesian statistics (Ramsey, 2009) and improved archaeo-demographic datasets (e.g., Lawrence et al., 2012; Flohr et al., 2016; Palmisano et al., 2021) have provided more precise and reliable archaeological and palaeoenvironmental chronologies. The latter of these developments will be explored further in this

chapter. These analytical developments now permit for more reliable correlations to be made between environmental and cultural changes, while they have also resulted in the review and questioning of pre-existing assumptions related to the influence of climate change on human societies (Maher et al., 2011; Flohr et al., 2016). This is not to say that reliably identifying correlations is not a challenge anymore, it very often is, but as these analytical developments continue to improve, the ability to determine such correlative links will become increasingly straightforward.

The second problem is arguably more challenging and the main cause for the polarisation of debate regarding human-environmental relationships. Simply identify synchronous fluctuations, however reliable, in both the archaeological and palaeoclimatological data does not prove a causal relationship, (to quote Contreras' (2017) Chapter title - '*Correlation is not enough*'). It is now widely accepted that investigators must go further and provide explanatory mechanisms which link the detected climate/environmental change with the archaeological observations, and as mentioned already, one of the main criticisms of aimed at climate determinists is that they fail to do this, relying predominantly on parallel shifts in the climate and archaeological proxies as evidence for their arguments. However, providing explanatory mechanisms is far from straightforward (Coombes and Barber, 2005). As Southwest Asia is a water stressed region an assumption is often made that other factors remaining constant, increased aridity will negatively affect soil moisture, and therefore vegetation, food production and human population. This is also an assumption this thesis will make in Chapter 11. However, this relationship is not straightforward, and is mitigated by human responses to environmental change including social and technological adaptation and population movement (Palmisano et al., 2021).

## **10.2 Archaeo-Demographic Proxies**

Understanding how populations have grown/declined in the past is an important research theme within archaeology (Kintigh et al., 2014a; Carleton and Collard, 2020) and it is widely seen as vital to our understanding of past cultural and environmental change at a range of temporal scales (Palmisano et al., 2017, 2021). Historically, research into demographic change has been driven by an interest into whether population growth may have acted as a driver for cultural transformation in the past, including

shifts in subsistence strategies (Binford, 1968; Shennan, 2000), socio-economic complexity (Feinman and Neitzel, 1984), technological development (Cohen, 1975; Coombes and Barber, 2005), conflict (Carneiro, 1972), and migration (Binford, 1968). However, more recently and importantly from the perspective of this thesis, there has been a growing amount of studies which have used temporal trends of demographic change as a proxy for societal trajectories which can then be compared to palaeoclimate data to address questions regarding human-environmental relationships (e.g., Blockley and Pinhasi, 2011; Borrell et al., 2015; Flohr et al., 2016; Lawrence et al., 2016, 2021; Roberts et al., 2017; Palmisano et al., 2021). The recent rise in these types of studies is likely to be partly the result of academic fashion due to current interest into the impact modern climate change will have on societies. However, there has also been a number of recent methodological developments which have allowed for the production of more chronologically precise and accurate demographic datasets, resulting in more precise comparisons with existing palaeoclimate records, the importance of which has already been highlighted in this chapter (Contreras, 2016).

Estimating past demographic trends is a notoriously problematic task to achieve. But there have been several different methods developed which have attempted to provide empirical reconstructions of past population sizes. These reconstructions evaluate trends on local, regional and/or inter-regional spatial scales, providing either absolute or relative demographic estimates (Müller, 2015). Archaeo-demographic methods include data from burial sites (e.g., number of burials, age at death ratios of burials) (Bocquet-Appel, 2002; Bocquet-Appel, 2008), counts of dwelling structures within settlements (Parsons et al. 2000), counts of single object types (Castro et al., 1998), ethnographic and ecological based estimations (Hassan, 1981; Binford, 2019), and genetic studies (Brotherton et al., 2013; Fu et al., 2016).

However, the two most commonly employed archaeo-demographic proxies are settlement data (Adams, 1981; Wilkinson et al., 2014; Lawrence and Wilkinson, 2015; Lawrence et al., 2016, 2021) and counts of radiocarbon dates (Blockley and Pinhasi, 2011; Borrell et al., 2015; Flohr et al., 2016; Palmisano et al., 2017, 2021). In this chapter I have chosen to focus and critically evaluate these two demographic proxies. I will also explore how these approaches have been employed in Southwest Asia, where a

number of demographic studies have emerged over the last decade examining the role short-term (e.g., Blockley and Pinhasi, 2011; Borrell et al., 2015; Flohr et al., 2016; Lawrence et al., 2021; Palmisano et al., 2021) and longer-term (Lawrence et al., 2016; Roberts et al., 2017; Palmisano et al., 2021) climate change had on human populations during the Holocene. By undertaking this review, it might be possible to identify datasets which can be used to make comparisons with climate data produced in this thesis and to support, or challenge, any hypotheses made.

#### 10.2.1 Archaeological Settlement Data

The use of settlement data as a proxy for population estimates has a relatively long history in archaeological research, particularly within Southwest Asia (Adams, 1965, 1981; Whitmore et al., 1990; Wilkinson, 2000; Menze and Ur, 2012; Wilkinson et al., 2014; Lawrence and Wilkinson, 2015; Lawrence et al., 2016; Allcock, 2017). Settlement data used for demographic purposes can take the form of raw site counts, calculations of settlement size and density, and aggregate settled area. These calculations can be used to reconstruct relative populations estimates or, using assumptions about population densities, produce estimations of absolute population numbers. Settlement data is usually retrieved through archaeological field investigations such as landscape survey, excavations, site mapping or remote sensing methods (e.g., aerial photography, satellite imagery).

Using survey information to examine settlement patterns and, associated demography has several benefits. Firstly, it is possible to address a number of archaeological research questions simultaneously, which include relationships between settlement and the environment, political organisation, urbanisation, occupations of transitory nomadic and sedentary settlements, recognition of long-distance communications, and of course demographic trends (Wilkinson, 2000). Surveys can gather large amounts of information over substantial areas, allowing examination of settlement patterns on local, regional or inter-regional spatial scales (Lawrence et al., 2016). Moreover, over the last couple of decades computational approaches, such as remote sensing using aerial photography (including the use of aerial drones), satellite imagery and GIS software, have allowed areas to be surveyed at unprecedented temporal and spatial resolutions leading to the identification of thousands of previously unidentified sites (Menze and Ur, 2012; Lawrence et al., 2016).

However, demographic estimations based on settlement data need to be treated with some caution as a number of limitations exist with the method (Wilkinson, 2000). Populations estimates based on raw site counts could result in population overestimations if many small sites exist within a particular area, and the reverse is possible where only a few, previously densely settled, large sites are present. Surveys can miss sites which are buried under deposits such as colluvium or alluvium, a particular problem in riverine landscapes like Southern Mesopotamia. Survey projects usually rely on typological dating methods (e.g. ceramics) which are, most of the time, not as chronologically accurate or precise as radiometric dating techniques. Moreover, sites with no pottery or other dateable artefacts are often underrepresented or missed by surveys, this can include sites occupied by pastoral nomadic communities (Wilkinson 1990).

The use of settlement data to map population trends extends relatively far back in the Fertile Crescent. Perhaps most importantly, this included the pioneering work carried out by Robert McCormick Adams (Adams, 1965, 1981) in Mesopotamia which laid the methodological and interpretive framework of landscape archaeology in Southwest Asia and elsewhere (Stone, 2007). A key element of his approach was to use surveys to examine long-term settlement patterns, not just to identify previously unidentified sites. Following the work of Adams, there have been several surveys which have examined long-term regional settlements patterns in Northern Mesopotamia (e.g., Meijer, 1986; Stein et al., 1990; Wilkinson and Tucker, 1995; Lyonnet, 1996; Wilkinson, 2000), as well as surveys which have carried out more local, site focused studies (e.g., Eidem and Warburton, 1996; Ur, 2002; Stein and Wattenmaker, 2003; Ur and Wilkinson, 2008; Ur and Gibson, 2010). As a result of all these different studies, there is a relatively large amount of available settlement data from Northern Mesopotamia overlapping with the geographic scope of this thesis.

Building upon these settlement surveys a recent 'big data' study, the Fragile Crescent Project (FCP), collated and reviewed these existing datasets from Mesopotamia and the wider Fertile Crescent (Lawrence et al., 2012; Menze and Ur, 2012; Wilkinson et al., 2014; Lawrence and Wilkinson, 2015). They also revised and added to the survey data using new accessible remote sensing and ground survey information to improve the spatial resolution and accuracy of the old datasets (Lawrence et al., 2012,

2016; Wilkinson et al., 2014). Moreover, to overcome the issues of ceramic chronologies, Lawrence (2012) developed a method that modelled absolute chronologies for survey data by transforming differing site, period-based chronologies and placing these on a common calendar-based timescale (binned in to 100 year-time blocks). By producing this chronological framework, it allows for a time-series visualisation of broad temporal trends in settlement patterns and trajectories. This method not only allows for more direct comparisons between the different surveys and regions (e.g. Northern Mesopotamia vs Southern Mesopotamia) (Lawrence et al., 2012), it also provides a more suitable, robust way to compare regional settlement trends with timeseries of climate data in order to explore human-environmental relationships.

Using these available and updated settlement datasets, Lawrence et al., (2016) compared settlement trajectories, as aggregate settled area (ha/km<sup>2</sup>), in the Fertile Crescent with palaeoclimate data to examine long-term relationships between settlement trajectories and climate change over the last 8,000 years. In this study, the authors argued that a period of initial settlement development and population growth, between *c.* 7,500 and 4,200 years BP coincided with a period of relatively moist conditions. Consequently, they suggested that increasing settled areas during this period may have been partly linked to increased resource surpluses related to higher rainfall (Lawrence et al., 2016). However, after about 4,000 years BP Lawrence et al., (2016) contended that relationships between settlement trajectories and climate variability become decoupled, where there is no obvious relationship between atmospheric moisture and settlement. It should be highlighted that these correlations were made using only two climate datasets from Southwest Asia; Soreq Cave and Lake Van, due to the sparsity of palaeoclimate records in the region. The heterogenous nature of climate conditions in Southwest Asia and proxy uncertainties, which have been discussed in this thesis already, means that any human-environmental observations made should be treated with some caution and more high-resolution records from the region are needed to test the hypotheses made in these types of studies. The SHC-03 record found within the Fertile Crescent can be used to do this.

### 10.2.2 Radiocarbon Date Counts

Radiocarbon date counts have become an increasingly common proxy used to examine past demographic trends, where variations in the frequency of radiocarbon dates over time act as a proxy for human population levels. The method assumes that larger populations living in a certain area or region will produce more archaeological deposits, including organic remains, that can be dated which results in more radiocarbon dates from that particular time. Put simply, the higher the population, the more radiocarbon dates from that period there should be.

The use of radiocarbon dates as a proxy for population changes is not new, and can be traced back to the 1970s (e.g. Deacon, 1974). Rick (1987) was the first to propose using summed date distributions as data ('dates as data') for the purpose of reconstructing spatial-temporal variation in coastal-highland settlement practices during the Peruvian preceramic period. These summed date distributions are produced by summarising multiple radiocarbon distributions (Ramsey, 2017) and are commonly referred to as summed probability distributions (SPDs) of radiocarbon dates. This method is the most common way in which radiocarbon dates are now used and presented for past demographic reconstructions. The last two decades has seen an explosion in the number of studies using this method due to the emergence of large and accessible radiocarbon datasets and the development and ready access to radiocarbon calibration programs (such as Oxcal and CALIB) which make the statistical calculations needed for the method relatively straightforward.

SPDs of radiocarbon dates provide valuable empirical datasets to estimate past population trends and the method has a number of benefits over other more traditional demographic proxies. Through their very nature as chronological datasets, SPDs provide more accurately dated population reconstructions than other archaeo-demographic proxies which are often dated through typological techniques. SPDs are presented as a probability distribution curve through time, providing a through time curve that has the chronological precision and resolution needed to make more precise comparisons with environmental datasets. SPDs are a particularly common and useful method employed in prehistoric studies where radiocarbon dates are the predominant technique used to date archaeological remains (Rick, 1987; Weninger et al., 2009; Shennan et al., 2013; Palmisano et al., 2021), and where other

evidence commonly used for demographic estimations, such as written evidence, settlement data, or burial evidence is less likely to be present or survive. Similarly, as radiocarbon dating is the most common way to date archaeological remains, it is possible to gather large amounts of data to examine patterns over large areas (e.g. Palmisano et al., 2021).

However, much like settlement data, there are a number of important methodological limitations of this proxy which need to be considered when employing it for demographic estimations (Shennan et al., 2013; Timpson et al., 2014; Carleton and Groucutt, 2020). Collection biases (e.g. strategically collected for research agendas or cost constraints) and taphonomic processes can lead to biases in how many dates are collected from different areas, therefore radiocarbon datasets are not necessarily a true population numbers. The interference effect of wiggles in the calibration curve causes spurious fluctuations to exist on a scale below c.200 years, this renders this method quite inadequate for any time-series shorter than a few thousand years for demographic purposes (Timpson et al., 2014). By summing radiocarbon date distributions together, the method also combines the different instrumental and calibration errors of the dates. Consequently it is argued that what this proxy actually reveals is the summed chronological uncertainty rather than through time variation in radiocarbon samples, and thus population (Carleton and Groucutt, 2020). Unlike settlement data and other archaeo-demographic proxies, SPDs of radiocarbon dates cannot provide estimates of absolute numbers of a population, only able to provide relative estimates. Finally, certain chronological periods are more likely to be sampled for radiocarbon dates than others: if datable coins, documents or fine-ware pottery exist, for instance, there is typically greater reliance on these forms of chronological evidence and less interest in paying for expensive radiocarbon dates. A good example of this problem is highlighted by Palmisano (2017). In this study SPDs severely underestimated populations levels in 1<sup>st</sup> Century AD imperial Italy, a period of massive economic and demographic growth by all other accounts.

There have been studies which have developed methods to correct for some of these limitations, for instance employing statistical methods to correct for collection biases and calibration curve effects as well as taking standardised approaches when it comes to sample selection (Blockley and Pinhasi, 2011; Shennan et al., 2013; Timpson et al., 2014). However, due to the uncertainties that do exist it is usually

accepted that the proxy needs to be compared to other archaeo-demographic reconstructions to support any observations made (e.g. Palmisano et al., 2017). There have been some papers which have been highly critical of the method (Contreras and Meadows, 2014; Carleton and Groucutt, 2020) and it has been suggested that alternative methods, which still use radiocarbon dates as data and are in development, avoid the major issues of SPD and should be used instead (Carleton and Groucutt, 2020).

In southwest Asia the use of SPDs of radiocarbon dates had been limited until relatively recently. However, the last decade has witnessed a relative explosion in the number of studies which have used the method to reconstruct demographic trends within the region (Weninger et al., 2009; Blockley and Pinhasi, 2011; Borrell et al., 2015; Flohr et al., 2016; Roberts et al., 2017; Palmisano et al., 2019, 2021). Importantly from the perspective of this thesis, all of these studies have used these demographic reconstructions to compare to palaeoclimate datasets in order to make human-environmental inferences, predominantly focusing on the Pleistocene-Holocene transition and the impact early Holocene rapid climate change events may have had on human populations. Many of these studies were able to identify correlations between cultural and environmental change. Blockley and Pinhasi (2011) employed SPDs to show that population growth associated with the PPNA coincided with the Younger-Dryas-Holocene transition, the author therefore argued that the onset of the Holocene was a key event for the emergence of the Neolithic, providing support for the most prevalent theory in regards to the emergence of Neolithic societies in the region (e.g., Richerson et al., 2001; Willcox et al., 2009). Borrell et al. (2015) found a pronounced break in settlement in the northern Levant coinciding with a climate change event at c.10,000 years BP. On the other hand, in a similar study, Flohr et al. (2016) examined the human response to the 9.2 and 8.2 ka rapid climate change events and argued populations within Southwest Asia were resilient to both, challenging a number of long standing assumptions about the impact of these events on human societies. Notwithstanding the limitations of SPD methodology, these studies were also limited by the available palaeoclimate data in the region covering this period, the scarcity and uncertainties of which were outlined in Chapter 3 of this thesis. New palaeoclimate records, such as the SHC-03 record are vital if the hypothesis made in these studies are going to be tested. Unfortunately,

as shown in the previous chapter, the temporal coverage and chronological uncertainties of the SHC-03 record makes it difficult to reliably test the observations of these studies in this thesis.

However, an important paper has recently been published which collated 10,653 radiocarbon dates from 993 sites from across Southwest Asia in order to examine longer-term demographic trends throughout much of the Holocene (Palmisano et al., 2021). In the Palmisano et al. (2021) study, the radiocarbon datasets were separated regionally, recognising that the nature of demographic change and the impact of environmental change is likely to be different over these regions. Importantly from the perspective of this thesis, one of these regions was Northern Mesopotamia, again partly overlapping with the geographical scope of this thesis. These trends were compared to palaeoclimate data to assess long-term relationships between the regional SPDs of radiocarbon dates and environmental change. While the paper looked at multiple regions across Southwest Asia, in Northern Mesopotamia the results of the study suggested a clear relationship between population and climate in the Late Pleistocene and Early Holocene (14,000 - 8000 years BP) with population increasing with wetter climatic conditions. After 8,000 years BP, the paper argues that the population initially declined coinciding with a shift to drier conditions, again indicating some synchronicity between environmental conditions and population numbers. However, after about 5,500 years BP during the Late Chalcolithic and the Early Bronze Age, Mesopotamia witnessed rapid population growth which occurred, according to the paper, during a relatively arid climate, suggesting that by this time the relationship between population growth and climate had become decoupled as societies became more adaptive to climate change through technological advancements (Palmisano et al., 2021).

Palmisano et al., (2021) also employed settlement data from the Fragile Crescent Project to identify how well the two different archaeo-demographic datasets agreed with one another to help test the accuracy of both. They found that there was some similarity between the two datasets, including a generally increasing population from the Neolithic to the Early Bronze Age (8,400 and 4,000 years BP). However, settlement data suggests higher population levels during the Late Chalcolithic, between c.6,000 and 5,500 years BP than the SPD data, and after 4,000 years BP, the SPDs display a sharp decline in population, while the settlement data indicate a slower, gradual decline followed by periods

of rapid population growth in certain periods which are not present in the SPD dataset. Palmisano et al., (2021) indicates that, at least in part, the underrepresentation of population by the SPDs of radiocarbon dates after *c.*4,000 years BP reflects a lack of a systematic collection of radiocarbon samples. However, the inconsistency between the two datasets shows the importance of looking at multiple lines of evidence as well as using other forms of archaeological data, before coming to conclusions about relationships between demographic trends and climate.

However, both studies identified synchronous peaks in population during the Early Bronze Age, centred around *c.*4,400 years BP. Interestingly, Lawrence et al. (2016) and Palmisano et al., (2021) perceive different climate conditions during this time, with Lawrence suggesting it coincides with wetter conditions, while Palmisano et al., (2021) suggests conditions were more arid during this time. This highlights that even when demographic datasets are in agreement, inconsistencies with how climate records are interpreted or the use of different records, can lead to contrasting findings regarding the relationship between the environment and human societies and demonstrates the need for up to date high resolution records from the region to address these inconsistencies. In the subsequent chapter, I concentrate on a time period and region which overlaps with the scope of these two demographic studies, consequently these studies provide useful datasets that can be used to support or challenge any observations I make. Similarly the new, high resolution palaeoclimate record can be used to test the findings these studies came to.

### 10.3 **Summary**

This chapter has attempted to introduce some broad theoretical considerations needed when studying human-environmental relationships, as well as introducing some methods and datasets which can help address these questions. I began this chapter by outlining how linking cultural and environmental change has been, and to some extent, remains a hotly debated topic within archaeological studies, with debate divided between those who cite climate or cultural mechanisms as the dominating causes for changes in human society in the past. One of the causes for the theoretical dichotomy is the inherent challenges involved in demonstrating, in a quantifiable manner, correlative and causal relationships between climate and societal changes.

There have been several methodological developments over the last few decades which have made the ability to establish correlations simpler and more chronologically precise. These developments include AMS <sup>14</sup>C dating, U-Th dating, and the application of Bayesian statistics (Ramsey, 2009). However, in this chapter I have focussed on how archaeo-demographic datasets have become an increasingly used proxy to make human-environmental comparisons. There have been several studies from Southwest Asia which have employed settlement data and radiocarbon date counts as proxies for demographic fluctuations and while there are a number of limitations to both of these methods, they provide useful empirical proxies which can be used to help test hypothesis regarding human-environmental relationships. From the perspective of this thesis, important datasets exist for both these methods from Northern Mesopotamia which can be used to test any findings made in the following chapter. Similarly, the new SHC-03 record also provides an important, high-resolution record that can help review the findings of these previous archaeo-demographic studies.

## 11 Complex Societies and Urbanisation in Northern Mesopotamia

During the middle Holocene, between approximately 6,400 years BP and 4,200 years BP, Mesopotamia witnessed a shift in the scale and nature of settlement. This development was characterised by increasing social integration, from largely egalitarian, self-sufficient agricultural villages to large, socially stratified urban-scale settlements. This process is often referred to as urbanisation or urbanism. The transition marks a major shift in how human society functioned and ultimately resulted in the largely urban city-based lives humans inhabit in the modern world. As a result, the process of urbanism, and why and where it first occurred, has long been a focus of archaeological research and forms a central pillar in the understanding of the developments of Mesopotamian civilisation (Wilkinson et al., 2014). Historically, investigations into early urbanism focused on Southern Mesopotamia, in the alluvial floodplains of southern Iraq (Algaze, 2001). These investigations often highlighted the unique environmental advantages Southern Mesopotamia had relative to other locations in Southwest Asia and the world, which made it the ideally suited location for the pristine development of complex, urban societies. However, new data collected over the last few decades, from sites such as Tell Brak (Oates et al., 2007) and Hamoukar (Ur and Gibson, 2010), have revealed that Northern Mesopotamia, and more specifically the Khabur drainage basin in north-eastern Syria and northern Iraq (Figure 56), witnessed its own initial phase of urban development independently of those in the south. However, the environment and landscape of the northern region is vastly different from that of the south. Populations in Northern Mesopotamia would have been heavily dependent on rainfall, as oppose to irrigation technologies, as a means to grow crops and produce the food surpluses needed to provision large and growing urban populations. For this reason, it is likely that Northern Mesopotamian societies would have been much more susceptible to climate variability and/or change, particularly in rainfall amount.

The role, both positive and negative, variability in environmental conditions had on the development of urban centres in Mesopotamia has been examined numerous times. Perhaps the most well-known way in which this has been done, albeit controversially, has been by linking periods of societal decline, or 'collapse', to periods of climate deterioration (drier conditions) in the region (Weiss and Bradley, 2001; Staubwasser and Weiss, 2006; Charles et al., 2010). However, some studies have also linked periods of

growth and success of societies in the region to wetter conditions (Charles et al., 2010; Lawrence et al., 2016). Most studies examining the influence of climate variability on Northern Mesopotamian societies, along with the wider EFC, have had to rely on palaeoclimate records from Levant and Turkey, in a region known to have a highly heterogenous climate (Burstyn et al., 2019). Furthermore, there is not a complete consensus about climate conditions during the middle Holocene, perhaps as a result of climate heterogeneity, which limits the ability to reliably compare the palaeoclimate data to the archaeological record. The new SHC-03 speleothem record, produced in this project, provides the first high resolution record from the region and offers an important tool with which to test existing hypotheses regarding human-environmental relationships during this period.

There is no definitive criteria for what defines an urban settlement and distinguishing what an urban settlement looks like has troubled archaeologists for decades, Matthews (2003) describes this issue as the '*complexity of complexity*'. The use of the term to describe late chalcolithic settlements in Northern Mesopotamian settlements is still contentious, for instance, Algaze (2008) argues that Northern Mesopotamian settlements during the Late Chalcolithic often lack intermediate centres in a proper settlement hierarchy to be truly considered 'urban', but there are others suggest that a more liberal approach should be taken and settlements can be characterised by a cluster of variables that are best accepted along an axis of variability rather than simple presence or absence (Oates et al., 2007; Ur, 2010). For the purposes of this chapter, I broadly accept the conditions laid out by McMahon (2019) in which urban settlements can be defined by four physical and function elements, which include: (1) A large and diverse population when compared to average site size in a region and the range of professions or identities represented therein. (2) The presence of urban infrastructure, or elements of the built environment, such as public space, access routes, and industrial zones, that reflect and amplify frequent social and economic interactions. (3) They affect the surrounding region, through ideology, attraction of population, or resource drain; cities are capitals or focal points, whether this is of religious spheres, economic zones, or political units. (4) The presence of authority or institutions as materialized in highly visible public buildings. Similar, but alternative, definitions are also outlined in Matthews (2003) and Ur (2010).

In this chapter I will first provide the environmental and geographical context for the topic. Secondly, I will explore the development of urban societies in Northern Mesopotamia to provide the archaeological context needed to examine human-environmental relationships, closely following the structure and chronological framework devised by Ur (2010). Thirdly, I will critically review the existing evidence and arguments for relationships between climate and societal change during the middle Holocene. Finally, I will integrate the new data from the SHC-03 data and examine how the new record can contribute to the existing understanding of human-environmental relationships during this important period.

### **11.1 Geographic Scope and Environmental Context**

Mesopotamia, by the very nature of its name (*'Land between Rivers'*), is defined by its proximity to the Euphrates and Tigris River systems. Both rivers begin in the Taurus Mountains in Turkey and flow south into Syria and Iraq (Figure 56). They flow toward each other near Baghdad before converging in southern Iraq to form the Shatt al-Arab River which feeds into the Persian Gulf. The Euphrates has several tributaries within Syria: notably the Balikh and Khabur. The Tigris is fed by additional rivers that flow southwest from the Zagros Mountains: including the Greater and Lesser Zab, Adhaim, and Diyala rivers.

Mesopotamia encompasses the modern countries of Iraq, north-eastern Syria, south-eastern Turkey and the very southwest of Iran. While this contains a range of geographical and environmental zones (Chapter 2), it can be broadly separated into a southern and northern region at a dividing line near Baghdad (Figure 56). Northern Mesopotamia (also referred to as *'Upper Mesopotamia'*) is a broad area of hilly plains dissected by the river valleys of the Euphrates and Tigris and their associated tributaries in northern Iraq and Syria. The rivers in the region initially flow down a relatively high gradient leading to high energy flows, causing downcutting and deep valleys. Most Mesopotamian settlements were likely to have been situated on the elevated hilly plains surrounding these valleys, making the irrigation of these rivers (gravitationally) difficult (Ur, 2010). Most Northern Mesopotamian archaeological settlements of the middle Holocene are found in areas which today receive enough rainfall to support rainfed agriculture (<250mm a<sup>-1</sup>). However, sharp precipitation gradients exist in a relatively small area

(Figure 56), with rainfall broadly increasing as you move north and decreasing as you move south. These gradients are not static, and will move further north or south during drier and wetter years (Sinha et al., 2019). This feature makes the region highly susceptible to inter-annual variation in rainfall amount and episodic drought, where rainfall is 100 – 200mm lower than the long-term mean, which would bring a significant proportion of the region into a rainfall isolate that would be unsuitable, or highly limiting, for agriculture and lead to crop failures (Riehl, 2008).

Southern Mesopotamia is characterised by flat, alluvial plains. Here, the rivers (particularly the Euphrates) run at a much lower energy level than in the hillier north. Contrary to the situation in the North, this leads to a large amount of silt deposition and over time has raised river bed levels to an extent where they flow on broad levees slightly elevated compared to the surrounding land which makes irrigation from these rivers relatively straightforward (Ur, 2010). In contrast to the north, rainfall in Southern Mesopotamia is very low ( $<100\text{mm a}^{-1}$ ) and makes rainfed agriculture impossible, and leads to the region to be solely reliant on irrigation for agricultural production (McMahon, 2019). The geography of low-lying Southern Mesopotamia during the Holocene has been significantly influenced by the rate of sea level rise. Rapid sea level rise during the early Holocene caused the inundation of the sea much further inland, perhaps as much as 100km, than present and the formation of an extensive marine estuary in the location of the present delta area (Kennett and Kennett, 2006), which has meant that many sites in Southern Mesopotamia which are found some distance away from the sea or river systems now were located much closer or were even coastal settlements. Since the middle Holocene, slower sea level rise has caused silt deposition from the low energy rivers to fill the estuary and sea with silt causing land reclamation and pushing back the coast line (Kennett and Kennett, 2006).

## **11.2 Archaeological Background**

Historically, research into the earliest urban-scale settlements in Southwest Asia has focused on Southern Mesopotamia. Many of these investigations cited the unique environmental advantages the landscape offered the region which provided the ideal context for the indigenous development of urban centres. These advantages included the agricultural potentials of irrigated lacustrine environments as well as the logistical advantages closely braided water channels would have provided to the transport

of goods and people (Adams, 1981; Wilkinson et al., 1994; Algaze, 2001, 2005). In particular focus was, and to some extent still is, the site of Uruk (Figure 56), which is widely regarded as the world's first city (Liverani, 2006) and also gives its name to the chronological periods of its cultural dominance in Southern Mesopotamia and its associated material culture, in the 6<sup>th</sup> millennium BP.

Initial urbanism in Northern Mesopotamia has been historically approached and researched as a secondary phase of urbanisation, in the form of Southern Mesopotamian colonies, during the so called 'Uruk expansion', during the second half of the 6<sup>th</sup> millennium BP, in which southern societies colonised areas rich in strategic and luxury resources unavailable in the relatively homogenous, alluvial plains of the south (Algaze, 1993), or sites providing control over trade routes to and from resource rich areas. However, archaeological excavations and surveys in Northern Mesopotamia during the last few decades, particularly in the Khabur basin in Syria and plains around the Jebel Sinjar in northern Iraq, have demonstrated a form of urbanism may have been occurring in the north simultaneously during the 6<sup>th</sup> millennium BP independently of the developments in the south (Oates et al., 2007). Recently, there have been a number of review papers which have attempted to readdress the simple narrative of southern dominance (Oates et al., 2007; Ur, 2010; Lawrence and Wilkinson, 2015; Algaze, 2018; McMahon, 2019).

*Complex Societies and Urbanisation in Northern Mesopotamia*

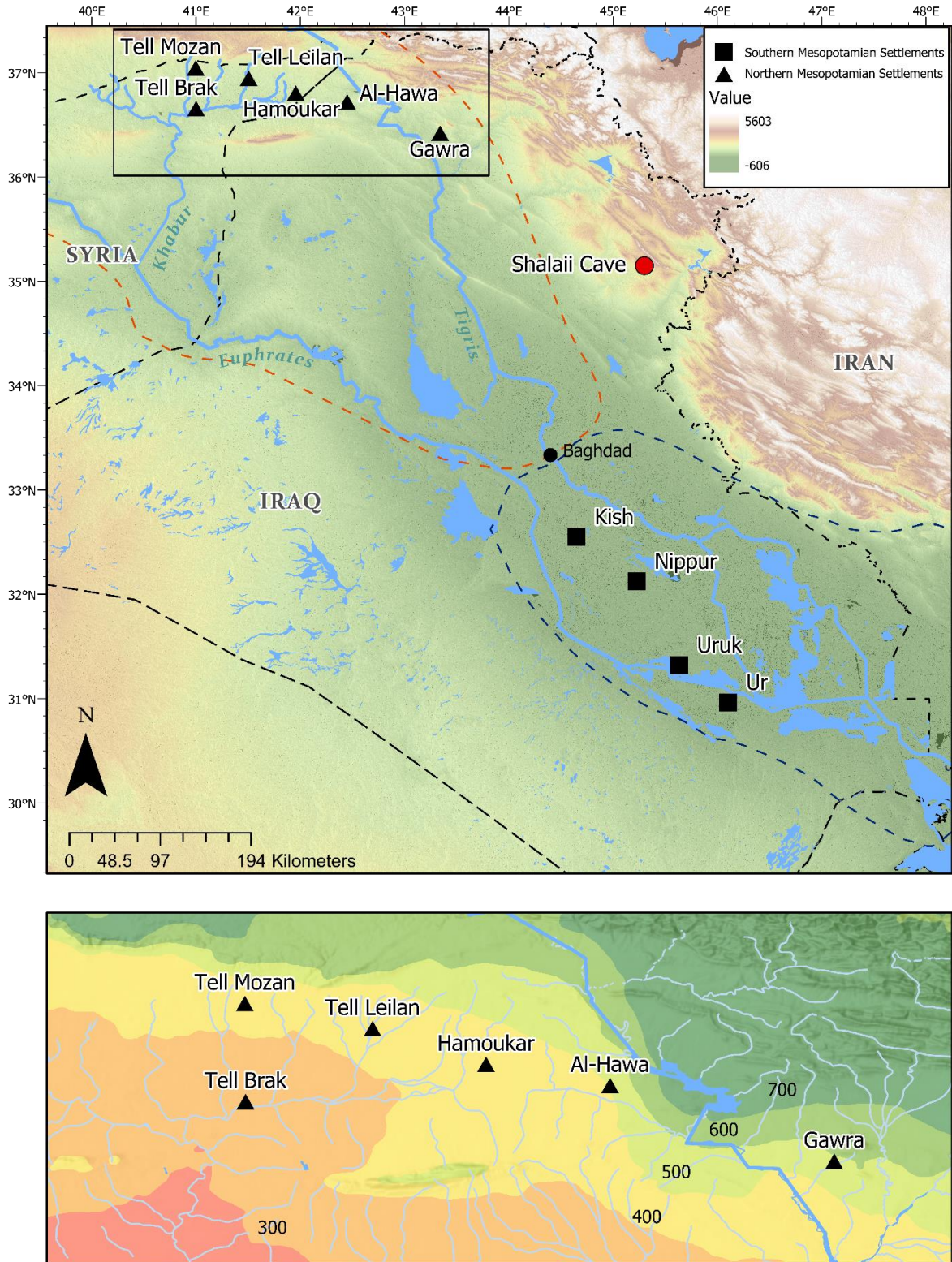


Figure 56: **Top:** Location of key Late Chalcolithic and Early Bronze Age sites in Northern Mesopotamia discussed in this text and a selection of Southern Mesopotamian sites. Also shown is the location of Shal'aii Cave. Boxed area represents the upper Khabur river basin and north Jazira, the geographic focus of this chapter. Red and dark blue dashed line indicate approximate location of northern and Southern Mesopotamia. **Bottom:** Zoomed in on Northern Mesopotamian sites, coloured map indicates precipitation gradients.

11.2.1 Chronological Framework

Chronologically, the development of urban societies in Northern Mesopotamia covers a period between the late 7<sup>th</sup> millennium BP to the end of the 5<sup>th</sup> millennium BP, which encompasses the archaeological Late Chalcolithic and Early Bronze Age. Two chronological frameworks specific to Northern Mesopotamia have been devised to provide common labels to work within when examining sites from the region. Rothmann (2001) divided the Late Chalcolithic of the 7<sup>th</sup> and 6<sup>th</sup> millennium BP into 5 subdivisions, LC1 – LC5. LC1 corresponds to the (Southern Mesopotamian term) terminal Ubaid and LC5 finished with the end of the Uruk period. Similarly, the Early Bronze Age during the 5<sup>th</sup> millennium BP has been divided into seven “Early Jazira” phases (EJ 0 through EJ V, with EJ IIIa and EJ IIIb subdivisions) (Lebeau 2000). These labels and their associated dates are summarised in Table 7.

<b>Years BCE</b>	<b>Years BP (1950)</b>	<b>Northern Mesopotamian Phase</b>	<b>Southern Mesopotamian Equivalent</b>	
4400 - 4100	6350 - 6050	LC1	Late Ubaid	Late Chalcolithic
4100 - 3800	6050 - 5750	LC2	Early Uruk	
3800 - 3500	5750 - 5450	LC3	Early Middle Uruk	
3500 - 3300	5450 - 5250	LC4	Late Middle Uruk	
3300 - 3000	5250 - 4950	LC5	Late Uruk	
3000 - 2900	4950 - 4850	EJ 1	Early Dynastic Periods I - III	Early Bronze Age
2900 - 2600	4850 - 4550	EJ II		
2600 - 2500	4550 - 4450	EJ III	Early Dynastic Period IIIa	
2500 - 2300	4450 - 4250	EJ IV	Early Dynastic Period IIIb	
2300 - 2100	4250 - 4050	EJ V	Akkadian	

Table 7: Chronological Framework used in this chapter for the Late Chalcolithic and Early Bronze Age for Northern and Southern Mesopotamia. Modified from Ur (2010).

### 11.2.2 Urbanism in Northern Mesopotamia: A Review

During much of the 7<sup>th</sup> millennium BP, societies in Northern Mesopotamia were largely characterised by egalitarian and communally orientated small communities (Ur, 2010). Until recently, this was thought to have continued into the 6<sup>th</sup> millennium BP and only significantly changed once Southern Mesopotamian influences delivered new elements of their more complex, urban culture (Algaze, 1993). However, it is now becoming clear that many sites in Northern Mesopotamia exhibited hallmarks of urban society (Box-1) before this. Moreover, it is also argued that the trajectory towards urbanism on the north was not a linear process, and it actually witnessed fluctuations and even cycles of periods of growth and decline (Ur, 2010). This next section will summarise the main evidence for societal developments in Northern Mesopotamia between the late 7<sup>th</sup> millennium BP and 5<sup>th</sup> Millennium BP, closely following the framework outlined by Ur (2010).

#### 11.2.2.1 LC1 & LC2 (c.6,350 – 5,750 Years BP)

During the earliest phases of the Late Chalcolithic, a few sites in Northern Mesopotamia display elements which might be considered evidence of proto-urban development. This includes monumental architecture, organised long distance trade, specialised craft industries and population agglomeration (Ur, 2010). Perhaps the best evidence until recently of this, during LC1 and LC2, came from the small site of Tepe Gawra in north-east Iraq (Figure 56). In layers associated with LC1 (6,350 – 6,050 Years BP), a wide distribution of clay sealings were recovered from areas within the sites which were thought to be extended family compounds. By LC2 (6,050 – 5,750 Years BP) specialised temple institutions are identified and the use of clay sealings seems to have been utilised for more specialised activities. By the end of LC2, the site, although small, contained a temple, public building and sophisticated resource administration (implied by container sealings). These elements are thought to demonstrate, to an extent, the indigenous development of complex administrative practices, and could represent the emergence of a class structure (Ur, 2010).

More recent excavations at other sites in Northern Mesopotamia also support evidence of increasing social complexity during this period, most notably in the form of monumental architecture. For instance, at the Syrian site of Tell Brak (Figure 56) archaeologists recovered the north-corner of a building with

walls 1.85m thick with an enormous basalt stone door threshold (McMahon et al., 2007; Oates et al., 2007, pp. 588–589). Next to this structure was a building in which a large number of industrial tools were found; this has been used to suggest the existence of specialised craft industries in the settlement as well as an economic function of the monumental building, instead of a religious one (McMahon et al., 2007, p. 155; Oates et al., 2007). For this reason, it has been argued this building could be the earliest secular monumental building yet discovered in Southwest Asia (Oates et al., 2007, p. 589). Furthermore, within this structure, a 16cm high chalice made of obsidian, marble and bitumen was found (McMahon et al., 2007, pp. 151–152), strongly implying the existence of a high ranking individual(s) and the existence of some form of class structure. Evidence of craft production beyond the basic household level is also evident at the site of Khirbat al-Fakhar (the southern extension of Hamoukar, Figure 56). Here, large quantities of obsidian in all stages of production from cores to finished tools are found suggesting direct access to the material source in the Taurus Mountains, with the settlement acting as a focal point for the manufacture and redistribution of the tools throughout Northern Mesopotamia (Khalidi et al., 2009), also demonstrating the existence of a highly developed and organised trade network.

Furthermore, while the majority of settlements in Northern Mesopotamia during LC1 and LC2 were small, both Tell Brak and Khirbat al-Fakhar show evidence of rapid settlement and demographic expansion. Khirbat al-Fakhar is thought to have reached a maximum extent of 300ha (Ur, 2002). However, this extent seems to have been relatively short lived and some have argued the large size might be explained by horizontal stratigraphy, where much smaller settlements periodically shifted locations within a small area over time (Algaze, 2001). Tell Brak is thought to have encompassed an area of at least 55ha by LC2 (Ur et al., 2011, p. 6). However, during this time both sites were of low density and were far in excess of the size of any of their neighbours, which did not exceed 5ha.

#### 11.2.2.2 LC3 (c.5,750 – 5,450 Years BP)

Further and more complex societal developments were followed into LC3 (5,750 – 5,450 Years BP). Tell Brak continued its demographic growth from 55ha in LC2 to a densely population settlement covering 130ha in LC3 (Oates et al., 2007, p. 597). However, in LC3 it seems to have evolved into a

central site in a four tier settlement hierarchy, which include towns of 5 – 7ha, villages of 2 – 3ha and smaller villages of 1ha or less (Wright et al., 2006), which is a more typical model for an urban settlement, like those observed later in Southern Mesopotamia, rather than the isolated settlements during LC1 and LC2. Other evidence of substantial nucleated settlements during LC3 are observed at Tell al-Hawa (Figure 56) in the Iraqi north Jazira, measuring between 33-50ha (Ball et al., 1989, p. 32), as well as Hamoukar and Leilan (Figure 56), both measuring around 15ha during this period (Ur, 2010, p. 396).

The shift to large, more densely populated settlements was accompanied by other societal developments in LC3 and the beginning of LC4. At Tell Brak, there is considerable evidence of institutionalised religion, in the form of the monumental eye temple (Mallowan, 1947). This building located at one of the highest positions within the settlement, contained hundreds of small stone figurines with oversized eyes. There is also further advancement of complex administration. For instance, at Tell Brak there is evidence of substantial sealing activities. At Tepe Gawra, the administrative developments seen in LC1 and LC2 are expanded further with the establishment of a central warehouse and tighter administration, reflecting centralised control of resources and hierarchical structures (Rothman and Peasnell, 2002; Rothman, 2004).

#### 11.2.2.3 LC4 and LC5 (5,450 – 4,950 Years BP) – ‘The Uruk Expansion’

Toward the latter half of the 6<sup>th</sup> millennium BP there is evidence of increasing influence of Southern Mesopotamian culture into and over the North which has become known as the Uruk expansion (Algaze et al., 1989). This began in LC4 and intensified in LC5, this is characterised by the influx of Southern Mesopotamian (Uruk) material culture into northern settlements and the founding of Uruk ‘colony’ sites such as Jerablus Tahtani, Habuba Kabira, Jebel Aruda (Rothman, 2004; Ur, 2010, p. 399). These relatively small settlements were located in strategic locations and follow the southern settlement model. This is thought to show an informal Southern Mesopotamian economic empire that exploited the asymmetric trade relationship between the south and north (Algaze, 1993).

The intrusion of Southern Mesopotamia into the north seems to have caused social and economic disruption to the indigenous settlements in Northern Mesopotamia. The expansion of indigenous

settlement sites, such as Tell Brak, stalls and even contracts in size. At Tell Brak, there is evidence the outer town of the settlement was abandoned and the eye temple was reorganised into a southern fashion. There is also evidence of destruction layers at both Tell Brak and Hamoukar (McMahon, 2019). The contraction and depopulation after 5,450 years BP mirrors the growth in urban populations of Southern Mesopotamia at sites such as Uruk (Kouchoukos and Wilkinson, 2007, p. 18). Different suggestions have been proposed for these contrary demographic trends toward the end of the 6<sup>th</sup> millennium BP. Kouchoukos (1998) suggested that populations in the north turned to more rural occupation such as Pastoralism, to feed the growing demand of Southern Mesopotamian markets for items like woolen cloth. Whereas others, have suggested that migration from north to south is a plausible explanation (Algaze, 2018).

#### 11.2.2.4 EJI – EJII – c.4,950 – 4,550 Years BP – Deurbanisation and Regionalisation

Following the societal developments of the Late Chalcolithic, the end of the 6<sup>th</sup> millennium BP marks an apparent downturn in societal complexity in Northern Mesopotamia. The expansion of Uruk culture in the north ‘collapses’ around 5,200 – 5,000 Years BP. The Uruk colony sites of Habuba Kabira, Jebel Aruda were abandoned. Many larger indigenous settlements in Northern Mesopotamia are replaced by small, tell based villages (Wilkinson, 2000; Ur, 2010). The ceramic material culture of Northern Mesopotamia, which had previously included styles from both the north and southern pottery, reverted back to solely local styles and suggests a reduction in interregional interaction (Ur, 2010). The use of tokens and sealed bullae as administrative technology disappeared. Some large sites do seem to maintain some urban form, including Tell Brak, however the size of the settlement was significantly reduced and had retreated onto the high mound with a small temple (Matthews, 2003). There is also little evidence of economic specialisation or powerful political institutions (Akkermans and Schwartz, 2003; Ur, 2010).

This period of decline or ‘devolution’ is in complete contrast to the situation in Southern Mesopotamia. It is during this period that Southern Mesopotamian society witnesses a ‘takeoff’ in settlement trajectory to much more intense urbanism (Ur calls this ‘hyperurbanism’ (Ur, 2010, p. 214)), complex socio-political institutions and the emergence of Sumerian city states (Algaze, 2005).

11.2.2.5 Reurbanisation (4,550 – 4,000 Years BP)

By the end of EJ II (2,600 years BP), the upper Khabur Basin and adjacent areas of northern Iraq witnessed a period of rapid resurgence of urban settlements, what Ur (2010) describes as *'the most pervasive phase of urban settlements prior to the 20<sup>th</sup> century'*. New cities quickly emerged, developing out of earlier settlements, such as Tell Leilan, Tell Beyder and Tell Brak. The pace and nature of urbanisation in this second phase was in a much different form to those observed in the 6<sup>th</sup> millennium BP; it was sudden, geographically widespread and archaeologically simultaneous (Ur, 2010). Tell Leilan, Tell Mozan, and Hamoukar all grew from around 15 ha to 90–120 ha within a century and Tell Brak expanded to 65–70 ha (Ur, 2010). The plains of Iraqi North Jazira supported a three-tiered hierarchy of settlements size, with Tell al-Hawa as the prime centre (Wilkinson et al., 1994). These urban centres show evidence of increased specialisation in the production of pottery and metals as well as the development of administrative organisation. Furthermore, there is evidence of the intensification of agricultural practices, to help support the growth of these large urban centres. The intensification and expansion of agricultural land during this period has left trackways, where people and animals moved across between agricultural plots. These trackways are visible from the air and space and have been mapped and help to provide some indication on the limits and use of land for agricultural purposes (Wilkinson, 1993; Altaweel, 2003; Ur, 2003; Altaweel and Palmisano, 2019). Further evidence of agricultural intensification is provided by the extensive low-density scattering of pot sherds over land, thought to be vestiges of elements related to manuring practices (Wilkinson et al., 1994). The largest sites during this period reached or exceeded the settlement size ceiling of c.100–120ha, which was limited by crop yield in their immediate hinterlands and labour availability (Wilkinson et al., 1994). Crop yield itself was largely related to rainfall amount (Wilkinson et al., 1994).

At the end of the 5<sup>th</sup> Millennium BP, Northern Mesopotamia entered another phase of decline and depopulation. The speed, extent and reason for this decline is still a matter of archaeological debate. Some have claimed the speed of decline represent a complete breakdown and collapse of society between 4,200 and 3,900 years BP (Weiss et al., 1993; Weiss and Bradley, 2001; Staubwasser and Weiss, 2006). While, other are more critical of this collapse model and suggest the decline was slower

and less homogenous in nature than the collapse model would suggest, as well as evidence of settlement continuity in places (Akkermans and Schwartz, 2003; Wossink, 2009; McMahon, 2012). This chapter does not seek to address the exact nature of societal decline in this period. But what is clear is that the end of the 5<sup>th</sup> millennium BP witnessed a general reduction of urban settlement in Northern Mesopotamia and marked the end of the second phase of early urbanism.

#### 11.2.2.6 Summary

This section has briefly summarised the development of urban settlement in Northern Mesopotamia between the 7<sup>th</sup> and 5<sup>th</sup> millennium BP. It is apparent that the region witnessed two phases (or cycles) of urban growth (Figure 57). The first occurred during the late 7<sup>th</sup> and 6<sup>th</sup> millennium BP and observed the slow and non-linear indigenous emergence of Urban settlement at sites such as Tell Brak and Hamoukar. The second phase, which was more rapid and homogenous, occurred during the second half of the 5<sup>th</sup> millennium BP. Both phases were followed by a period of population decline and ruralisation, in contrast with contemporary continued urban growth in Southern Mesopotamia. These general trends provide a useful archaeological framework to compare to palaeoclimate data from the region in order to investigate human-environmental relationships during this time.

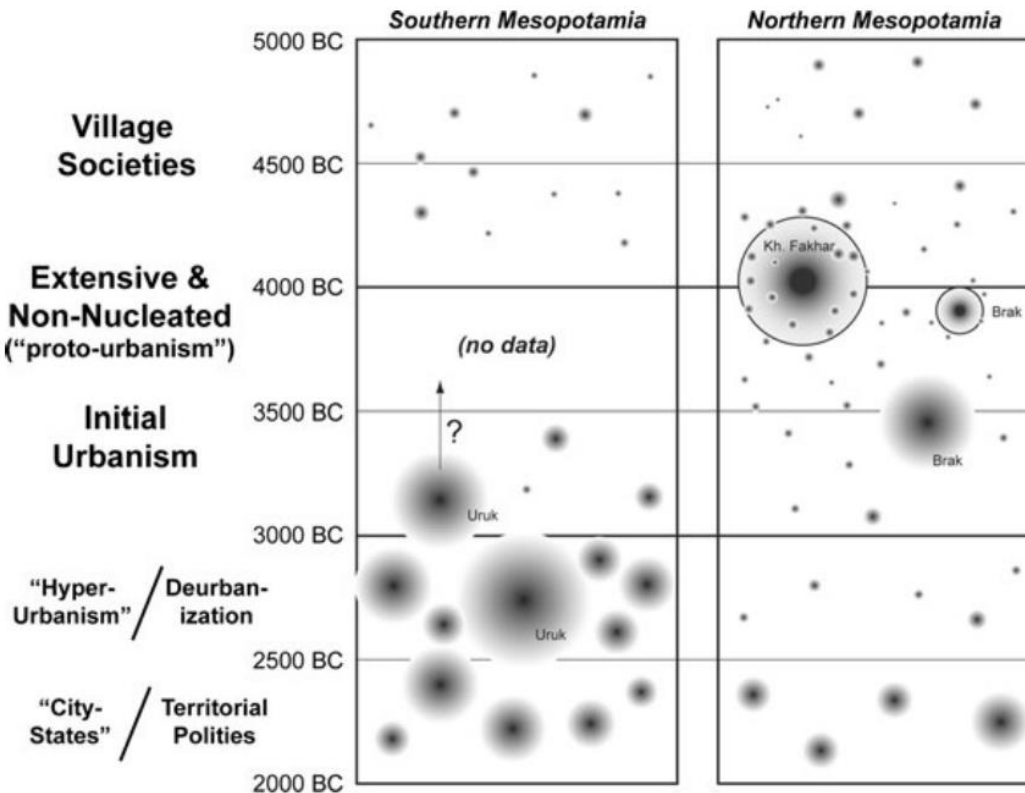


Figure 57: Schematic illustration of the scale and distribution of urban settlements in Southern and Northern Mesopotamia, 5000-2000 BC. Points with solid outlines are extensive proto-urban settlements. Figure from Ur (2010).

### 11.3 The Role of the Environment on Urbanisation: Current Understanding

From a palaeoclimate perspective, Northern Mesopotamia provides an ideal location to investigate human-environmental relationships. Societies in the region would have been sensitive to moisture variability for two reasons:

- 1) The heavy reliance of Northern Mesopotamian agrarian-based societies on rainfall to support crop production.
- 2) Their location in marginal rainfall areas (Figure 56).

Consequently, an assumption which is often made is that any decrease in rainfall will lead to decreased moisture availability, and thus crop production (food) will be negatively affected which will go on to have an impact on the societies economic output (e.g., Sinha et al., 2019; Palmisano et al., 2021)

providing a relatively simple causal explanation if parallel fluctuations between environmental and archaeological datasets are identified.

However, high resolution palaeoclimate records from Southwest Asia which cover the middle Holocene are sparse. No records exist from Mesopotamia itself, in a region known to have a highly heterogeneous climate (Burstyn et al., 2019) and this makes reliable human-environmental comparisons challenging. Nevertheless, using the palaeoclimate data available, which includes speleothems from the Levant (Bar-Matthews and Ayalon, 2011; Cheng et al., 2015) and lake sediment records from Turkey (Wick et al., 2003), there have now been several studies which have attempted to link settlement trajectories in Northern Mesopotamia with climate variability. The most well-known studies have been those which have linked climate deterioration, in the form of ‘dry events’ to periods of social decline.

The first of these is thought to have been a rapid climate change event that occurred approximately 5,200 years BP (‘the 5.2 ka event’). The event has been identified in records from Soreq Cave (Bar-Matthews and Ayalon, 2011), Jeita Cave (Cheng et al., 2015), Lake Van (Wick et al., 2003) and marine sediments from the Gulf of Oman (Cullen et al., 2000). It is thought to have resulted in increased aridity throughout Southwest Asia. There have been a number of studies which have linked this event to societal change in Mesopotamia. For instance, Charles et al. (2010) linked the event to the decline of settlement at the end of the Late Chalcolithic in Northern Mesopotamia. Perhaps more notably, there have been several studies which have linked the event to the decline, or ‘collapse’, of Uruk cultural influence, and its colony settlements, in Northern Mesopotamia during this period (Brooks, 2006; Staubwasser and Weiss, 2006; Bar-Matthews and Ayalon, 2011).

The second event is a period of climate deterioration which occurred approximately between 4,200 – 3,900 years BP (‘the 4.2 ka event’). The event is seen in a number of paleoclimate records both in Southwest Asia (Cullen et al., 2000; Bar-Matthews and Ayalon, 2011; Carolin et al., 2019) and worldwide (Drysdale et al., 2006). The event, which took the form of a multi-century long drought, has been cited as the main causal factor for the collapse of the Akkadian political system in Mesopotamia (Weiss et al., 1993; Weiss and Bradley, 2001; Staubwasser and Weiss, 2006) due to its impact on the agricultural carrying capacity of Northern Mesopotamia. These studies argue that it was this event

which led to the complete abandonment of Northern Mesopotamia at the end of the 5<sup>th</sup> millennium BP, as well as similar decline observed elsewhere around southwest Asia.

However, like the archaeological evidence for ‘collapse’, the nature, extent and even existence of these climate events is still a matter of palaeoenvironmental debate; and the studies which link the events to societal change have been critiqued many times (Coombes and Barber, 2005; Wossink, 2009; McMahon, 2012). Without high-resolution and precisely dated palaeoclimate data from the region itself, the true nature of these events and their influence on societies will remain uncertain.

While, most investigations have focused on the influence of short-term abrupt events on societies, there have been a few recent studies which have attempted to examine the role long-term trends may have had, as well as also highlighting the potential impact favourable environmental conditions may have had on settlement trajectories in Northern Mesopotamia. Lawrence et al. (2016) employs long-term settlement data and compares this to the palaeoclimate data from Soreq Cave and Lake Van. The study identified that the emergence of urban settlement in Northern Mesopotamia coincides with relatively high moisture availability and tentatively suggest that urbanisation may be linked to increases in production surpluses associated with increased moisture availability (Lawrence et al., 2016), a similar finding was made by Charles et al. (2010).

Finally, palaeoenvironmental variability has often been employed to explain the dichotomies of settlement trends between northern and Southern Mesopotamia during the middle Holocene. Where, during phases of settlement decline in Northern Mesopotamia, Southern Mesopotamia witnessed a continuation or an increase in urban growth. The different trajectories have been explained as the result of the relative resilience of the south to climate variability because of its reliance on irrigation over rainfall for crop production. Moreover, the demographic contrast is the result of people moving from areas affected by climate deterioration (Kennett and Kennett, 2006).

#### **11.4 SHC-03: Correlations with Settlement Trajectories in Northern Mesopotamia**

The new stalagmite (SHC-03) record from Shalaih Cave provides the closest high resolution palaeoclimate record to the Khabur basin, the heartland of urban development in Northern

Mesopotamia. Therefore, it offers a more useful record to make human-environmental comparisons than any record that yet exists and for this reason it can be used to test existing hypotheses about how urban settlement in the region was influenced by palaeoclimate variability during the 6<sup>th</sup> and 5<sup>th</sup> millennium BP.

Nevertheless, it is important to acknowledge that Shalaih Cave is still located c.350 km from the Khabur basin. However, there are two observations which make us confident that climate variability as identified in the speleothem also provides a useful proxy for conditions in Northern Mesopotamia. Firstly, when the amount of modelled precipitation variability that has occurred in the two areas over the last 100 years is compared, they correlate significantly well, which suggests that relative moisture variability over time is similar (Figure 58). Secondly, the cave is found in an area with a mean annual rainfall of c.470mm which is similar to much of Northern Mesopotamia and suggests that the range of variability occurring in the two locations is also likely to be comparable.

As discussed in Chapter 9.1, the generally low Mg/Ca values from the SHC-3 stalagmite between 7,000 and 4,000 years BP suggest the wettest conditions of the Holocene were apparent in EFC during this period. This is in strong agreement to the existing interpretation of Mg/Ca data from Lake Van (Wick et al., 2003) and pollen records from the EFC. This suggests that the cultural developments during this period are occurring during a period of relatively high moisture availability. Within this long-term trend, and identified in the SHC-03 MAI record, there is evidence of short-term variability. As discussed in Chapter 9.2 this short-term variability follows a quasi-cyclical nature. Two phases of wetter conditions can be observed between 5,780 – 5,500 Years BP and 4,550 – 4,000 years BP. This is separated by a drier period centred around 4,800 years BP, which is part of a slightly longer drying trend that begins c.5,500 years BP. The timing of this drying trend is broadly consistent with the observation of dry event around 5,200 years BP (the so called 5.2 ka event'). Similarly, a millennial long drying trend is observed after c.4,100 years BP, ending with an extremely dry period centred around 3,400 years BP (Figure 58), which is remarkably like an observation made in the Lake Van Mg/Ca record. This is approximately coincidental to the '4.2 ka event' but represents a much slower decline to drier conditions during the late 5<sup>th</sup> millennium BP, rather than a sudden, abrupt event.

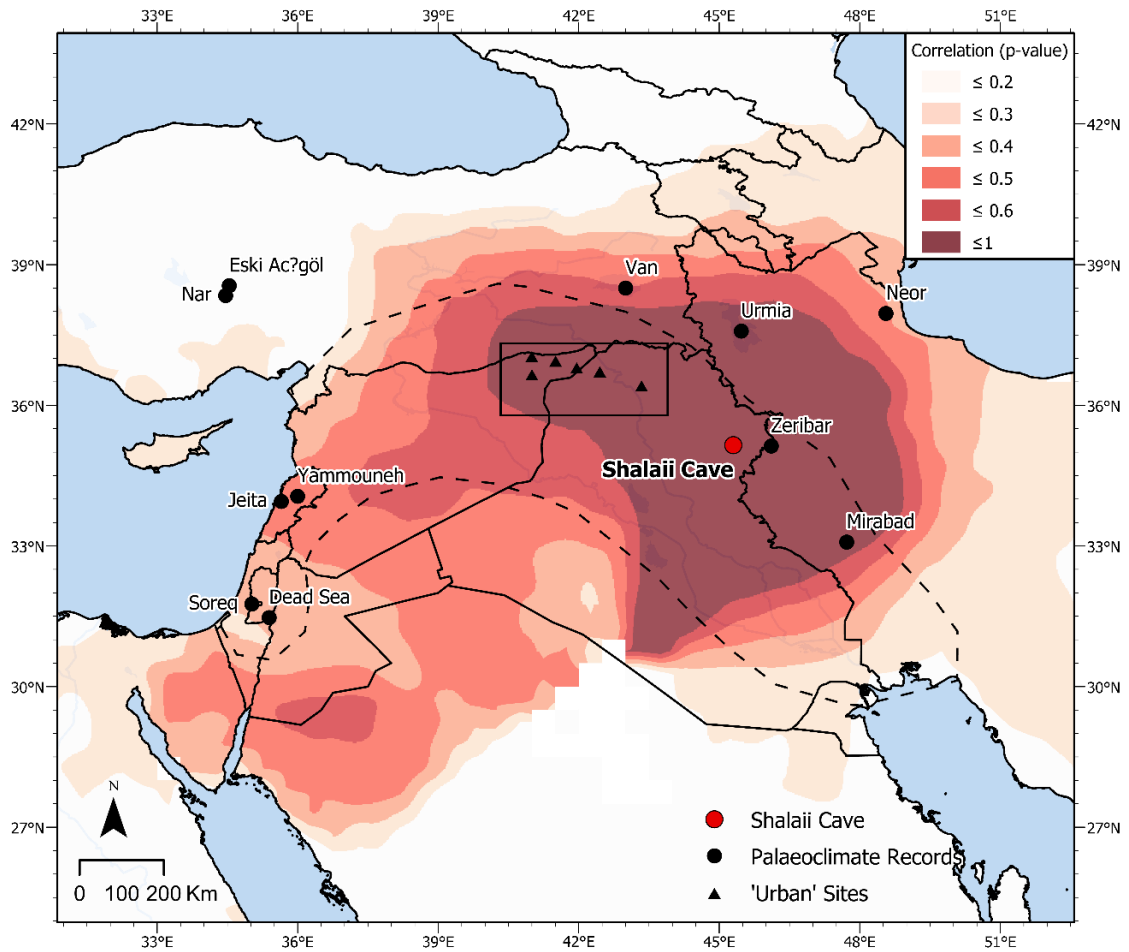


Figure 58: Map showing the location of Shalaih Cave relative to sites in the Khabur Basin and North Jazira (in rectangle). Colour represents the modelled precipitation correlation between Shalaih cave and other regions in the Middle East (KMNI climate explorer) that illustrates that precipitation variability around the cave and Northern Mesopotamia show a strong correlation (p values = >0.6).

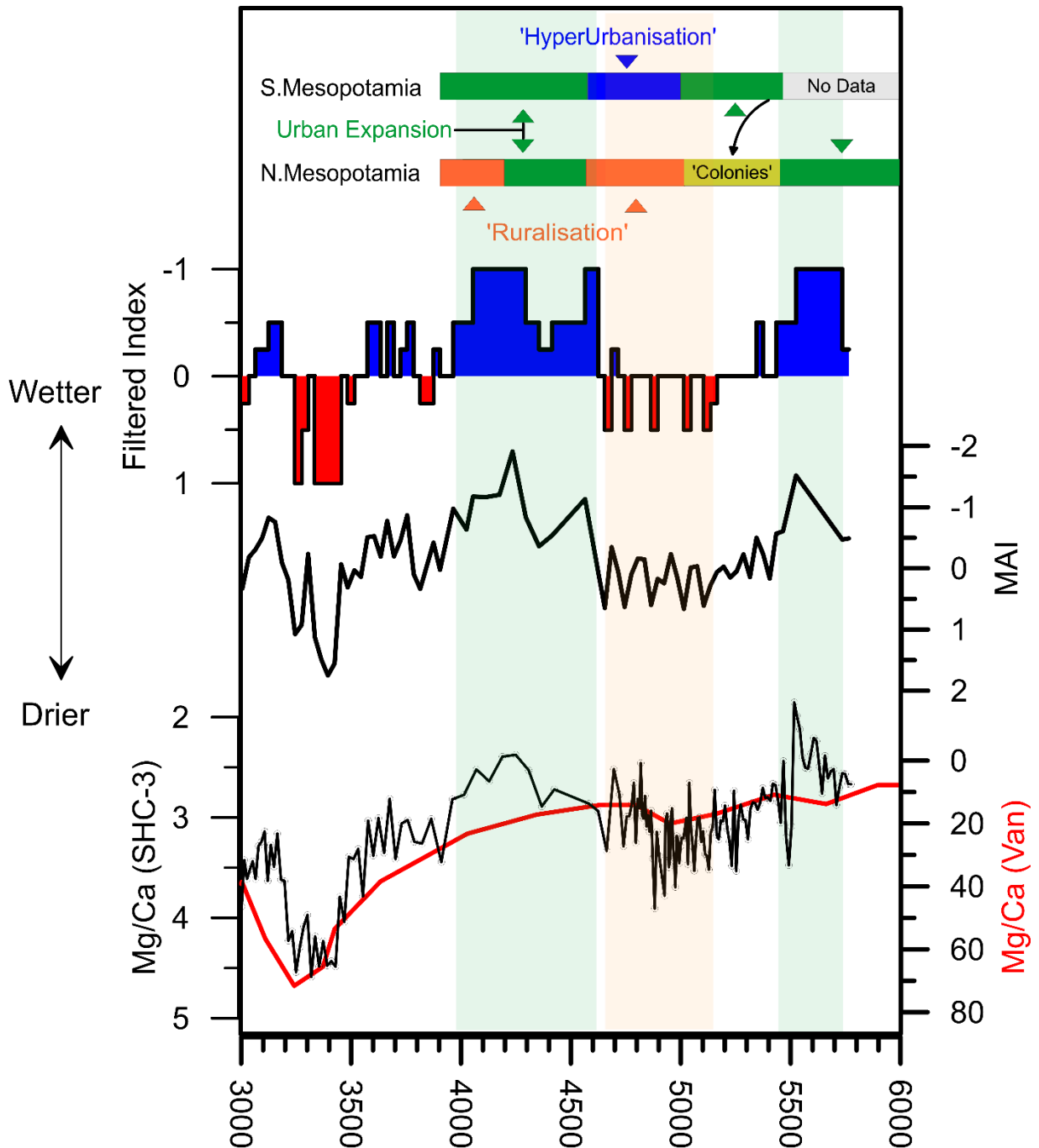


Figure 59: Graph showing the new palaeoclimate data (Mg/Ca, MAI and FI) from Shalaih cave and Mg/Ca data from Lake Van. These are compared to developments in urban trajectories in northern and Southern Mesopotamia. Pastel green vertical bar illustrate wet phase in the SHC-03 record and red vertical bar indicates dry phase, coinciding with periods of urbanisation and ruralisation, respectively.

When the palaeoclimate observations are compared to the archaeological cycles of urban development outlined by Ur (2010) in Northern Mesopotamia a broad correlation can be identified (Figure 59). That is, periods of increased moisture availability coincide with phases of expansion of urban settlement in Northern Mesopotamia. Whereas periods of increasing aridity coincide with a time of ruralisation and decentralisation in Northern Mesopotamia. Peak moist conditions are observed at c.5500 Years BP, coinciding exactly with the height of the first phase of indigenous urban development in Northern Mesopotamia, where Tell Brak for instance reaches a size of c.130 ha. A trend of increasing aridity after this coincides with increasing influence from Southern Mesopotamia. While, no sudden ‘event’ is necessarily identified around 5,200 Years BP that coincides with the ‘collapse’ of Uruk expansion into the region, the whole of this time period is characterised by increasing aridity which continues into the early 5<sup>th</sup> millennium BP. The second phase of urban development occurs c.4,600 years BP, coincides with a period of increasing moisture availability, which peaks c.4,200 years BP, before the start of a millennial long drying trend coinciding with a second decline in urban development in the region, albeit still within the context of a relatively wet climate if long-term trends are taken into account. Therefore, the new SHC-03 shows a relatively good correlation between the climate trends and settlement trajectory in Northern Mesopotamia. An additional comment should also be made about the situation in Southern Mesopotamia during this period as explaining the contrasting trajectories of settlement during the middle Holocene has been a key issue. While the SHC-03 record does not provide any information on conditions in Southern Mesopotamia (with the exception of potential variations in river discharge), what is evident is that during dry conditions in Northern Mesopotamia, Southern Mesopotamia continues to see growth, and in fact, a period of hyper-urbanisation coincides nearly exactly with the dry phase between 5,100 – 4,600 years BP.

To test this apparent correlation and potential causal relationship between moisture availability and settlement trajectories in the region during the middle Holocene, I compare the SHC-03 data to other types of archaeological data collated from Northern Mesopotamia.

Firstly, to further explore long-term correlations between demographic/settlement trajectories in the region with the palaeoclimate data I employ two archaeo-demographic reconstructions, discussed in

Chapter 10. The first of these demographic datasets is long-term settlement data (in the form of aggregate settled area) collected from archaeological surveys and excavations from the North Jazira region in Northern Mesopotamia (Lawrence et al., 2012, 2016). Previous attempts have been made using this data to examine human-environmental relationships (Lawrence et al., 2016), although using limited palaeoclimate data. In this former study, it was argued that a moister climate may have assisted population growth between 7,500 years BP and 4,200 years BP, however after 4,000 years BP there is little relationship between moisture availability and settlement trajectories (Lawrence et al., 2016). However, when the new SHC-03 record is compared to these settlement trajectories (Figure 60) a different picture emerges. The comparison exhibits a striking good visual correlation between the two datasets throughout, not only does it show similarities of long-term peaks between 4,500 – 4,000 years BP and 3,500 – 3,000 years BP, it also displays very good agreement in short term fluctuations. The synchronicity between the two records provides further support that settlement patterns in the region could be aligned to moisture availability throughout the middle Holocene, and challenges previous findings. The second archaeo-demographic dataset is relative population estimates based on SPDs of radiocarbon dates from a recently published study (Palmisano et al., 2021). While, there is less similarity between this dataset and the SHC-03 record (Figure 60) as the settlement data, the comparison does show marked increase in population that coincides with increase moisture availability centred around 4,400 years BP, which supports the hypothesis that the development of urban settlement during this period may have been supported by a more favourable (wetter) climate. Interestingly, Palmisano et al., (2021) contended, based on existing palaeoclimate data, that this population peak during the Early Bronze Age coincided with a period of relatively arid conditions and argued for a decoupling between human and environmental trajectories during this time. Consequently, the SHC-03 seems to contradict this finding if the interpretation of the new palaeoclimate record is correct. It should also be highlighted that the absence of synchronicity between the SPD data and the SHC-03 record after 4,000 years BP may in part be related to an underestimation of population by SPDs as archaeological chronologies become increasingly reliant on ceramic dating methods during this period (Palmisano et al., 2021).

While I have identified correlations between climate and settlement/demographic trends, this is still not enough to prove any type of causal relationship between the two. A major aim should also be to try and demonstrate an intermediate mechanism which can link the two sets of data to provide an explanation of mechanism. As explained already, due to the semi-arid nature of the region and its reliance on rainfed agriculture, the link between moisture availability and settlement patterns has normally been explained in terms of agricultural production. An archaeobotanical dataset from Northern Mesopotamia allows us to test this hypothesis. Riehl et al. (2012) studied water stress on crops by employing stable carbon isotope analysis of archaeobotanical remains collected from sites in Northern Mesopotamia, as well as from the northern Levant. Again, previous attempts have already been made to examine the relationship between this data and existing palaeoclimate data. However, unlike the settlement data, a relationship between water stress and palaeoclimate variability had been identified (Riehl et al., 2012). The data produced in this thesis also seems to support this, a comparison between the MAI data and the archaeobotanical data exhibits another good visual correlation, with low water stress occurring during a period of increased moisture availability during the later 5<sup>th</sup> millennium BP, corresponding to a period of increased settled area and higher populations. This therefore provides some support that resource stress due to moisture variability, may have been the cause for the decline of settlements, at least at the end of the 5<sup>th</sup> millennium BP, or alternatively wetter conditions were the cause for settlement development during the middle of the 5<sup>th</sup> millennium BP. Another interesting observation is the quite clear correlation between the archaeobotanical data and SPDs (Figure 60), which would be interesting to explore in the future.

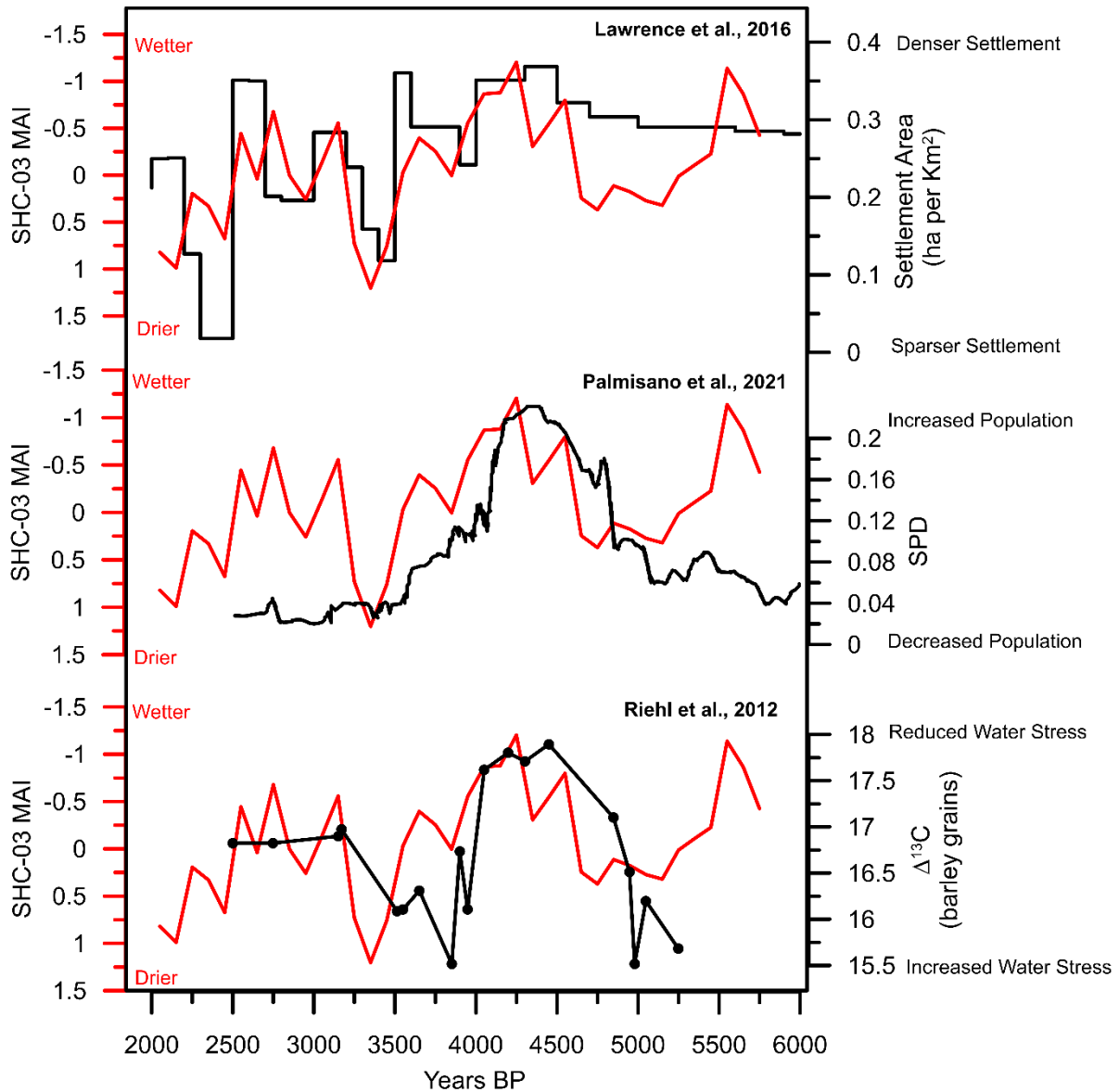


Figure 60: Comparison between the SHC-03 MAI record (red lines) with (top) settlement trajectories in the North Jazira region of Northern Mesopotamia (Lawrence et al., 2016), (middle) SPD population reconstructions from Northern Mesopotamia (Palmisano et al., 2021), and (bottom) isotopic data from archaeobotanical remains from Northern Mesopotamia (Riehl et al., 2012). The strong similarity between settlement trajectories and the climate data throughout the time period supports evidence that settlement patterns in the region might be related to moisture availability. While less synchronous, SPD populations for Northern Mesopotamia show a clear peak in population that is coeval a period of increase moisture availability centred around 4,400 years BP. Finally, the broad similarity between the SHC-03 data and archaeobotanical data supports the suggestion that a causal link between climate and society might be related to agricultural output. The MAI data has been binned into 100-year intervals to match the resolution of the other datasets.

#### 11.4.1.1 Summary

Northern Mesopotamia witnessed some of the earliest global evidence of urbanisation during the middle Holocene, which occurred in two phases (Akkermans and Schwartz, 2003; Ur, 2010; Wilkinson et al., 2014; Lawrence and Wilkinson, 2015). An initial, probably indigenous phase between c.6400 – 5,200 years BP during the Late Chalcolithic and a second, more rapid development beginning c.4,600 years BP during the Early Bronze Age. Several studies have linked climate variability, in the form of moisture availability, to periods of growth as well as periods of ‘collapse’ or decline, particularly related to the 5.2 (Charles et al., 2010) and 4.2 ka event (Weiss et al., 1993; Staubwasser and Weiss, 2006). Until now, however, there have been no high-resolution records from the region to support these claims.

The new SHC-3 record is now the closest high-resolution record that exists to the region and allows us to test existing hypotheses that settlement trajectories in Northern Mesopotamia were correlated to moisture availability. The findings of this project have demonstrated that the general cycles of urbanisation and ruralisation, as outlined by Ur (2010), correlate well with the new SHC-03 record, where wetter conditions are correlated to urban growth and drier conditions to urban decline. Therefore, this project provides some support for previous studies which have suggested a link between climate variability and cultural change in the region. To further investigate this, this project also identified a strong correlation between long-term settlement trajectories in Northern Mesopotamia and the SHC-03 palaeoclimate data between c.5,000 and 2,000 years BP, and some synchronicity with SPD population estimates which support the hypothesis that there is a link between moisture availability and settlement/population patterns in the region. Moreover, to test the hypothesis that a causal link between the climate data and settlement patterns was the result of changes in agricultural output, I compared the SHC-03 data to isotopic data from archaeobotanical remains, which measured water stress. Again, a broad relationship was identified to support this explanation.

While this project provides support to previous studies which have suggested a link between climate variability and settlement trajectories in the region, some caution should be taken. Further work to determine causality should be undertaken. More investigations linking palaeoclimate geochemical data to isotopic data collected from archaeological assemblages, such as that done by Riehl (2012) and

replicated in this project, might help achieve this. The SHC-03 data suggests that drier periods were part of multi-centennial long palaeoclimate cycles and therefore exhibit a gentler, less abrupt nature than others have suggested in the past, who have linked abrupt events to such shifts. Therefore, based on the SHC-03 it is unlikely that a single climate event, was the sole causal factor for urban decline. Moreover, this project, knowingly, has paid little attention towards other non-environmental factors for growth and decline of urban settlements and it is likely that, if a causal link between climate variability and settlement trends is proven, it was as the result of an inter-play of climate and non-climate related factors over a long period. There are also not insignificant chronological uncertainties in the archaeological, and to some extent, the SHC-03 data which exist that should be fixed.

## 12 Conclusions and Future Recommendations

### 12.1 Conclusions

In this project I set out to investigate the nature of Holocene climate change and variability in the EFC to fill a large spatial and temporal gap in palaeoclimate studies which existed in the region. Using the new data produced here, I also wanted to examine human-environmental relationships in the archaeologically important region. To achieve these aims, I analysed a *c.* 3.17m long stalagmite from Shalaih Cave, Iraqi Kurdistan by employing a multi-proxy geochemical approach. The new record (SHC-03) produced from this analysis is the longest spanning (near-Holocene long), high-resolution (near-annual) palaeoclimate record from the EFC, covering a near-continuous period between *c.* 10,560 yr BP – Present day, with only a handful of palaeoclimate records from wider Southwest Asia also able to match (or better) this record. The SHC-03 record offered a new insight into the nature of palaeoclimate change and variability during the Holocene and provided an opportunity to test existing theories about human-environmental relationships during this time.

The key palaeoclimate findings of this project were:

1. A correlation between centennial to millennial  $\delta^{18}\text{O}$  changes of the Eastern Mediterranean Sea and the SHC-03 record suggests that the source effect may have been a dominant control on long-term  $\delta^{18}\text{O}$  values during the Holocene. While the source effect cannot explain all the variation in the SHC-03  $\delta^{18}\text{O}$  record, other effects other than rainfall amount, predominantly changes in seasonality, are likely to have influenced  $\delta^{18}\text{O}$  values. This limits the effectiveness of  $\delta^{18}\text{O}$  as a palaeohydrological proxy for long-term hydrological changes in the EFC, unless supported by other proxies.
2. This study currently suggests that long-term changes in Mg/Ca and Sr/Ca largely respond to changes in the degree of PCP occurring, in the vadose zone above the cave, related to the amount of spring rainfall and the intensity of summer aridity, and for this reason provides a more suitable palaeohydrological proxy than  $\delta^{18}\text{O}$ . High Mg/Ca and Sr/Ca values during the early Holocene indicate that the period was characterised by high seasonality, with longer

### *Conclusions and Future Recommendations*

periods of summer aridity, and consequently drier conditions. Lower Mg/Ca and Sr/Ca values during the middle to later Holocene indicate lower seasonality and thus wetter conditions. A strong similarity between the long-term trends observed in arboreal pollen profiles from EFC lake sediments and the SHC-03 data suggest that the observed delay in the expansion of oak woodland into the EFC during the early to middle Holocene was likely to have been caused by climate aridity rather than other non-climate related processes, providing an important contribution to the ongoing debate for the reasons behind the ‘*early Holocene precipitation paradox*’.

3. The fundamental climatic cause for both previous two findings is related to changes in the timing and position of the north-south oscillations of the Inter-Tropical Convergence Zone (ITCZ). A more northerly positioned ITCZ, and more intense Monsoon, during the early Holocene due to higher northern hemisphere summer solar insolation, resulted in increased (isotopically light) freshwater runoff from North Africa into the Mediterranean resulting in lower sea surface  $\delta^{18}\text{O}$ . Likewise, a more northerly positioned ITCZ caused the displacement of high pressure over the EFC during spring, blocking moist westerlies from penetrating the EFC in spring, leading to drier conditions.
4. By combining multiple proxies to produce a mean anomaly index, this study was also able to semi-empirically identify the existence of shorter, decadal- to centennial-scale climate variability in the EFC. Centennial variability, particularly during the middle to later Holocene, seems to show a quasi-cyclical behaviour, like observations made by other records from Southwest Asia. While the exact causes of short-term hydrological variability were not fully identified in this project, it could be the result of the complex interaction between North Atlantic and Siberian climate regimes.

From an archaeological perspective, this new understanding of climate conditions during the Holocene was used to examine and test existing hypotheses about relationships between humans and environmental change. In this thesis I focused on one important case study. I was able to demonstrate that shorter term centennial scale climate instability identified by the SHC-03 during the middle

Holocene exhibits a close visual correlation to settlements patterns in Northern Mesopotamia, where periods of reduced settlement density seem to occur during periods of lower water availability. Therefore, this study suggests that water availability may have been an important factor in the ability to develop, grow and sustain large urban settlements in Northern Mesopotamia. Whereas, in Southern Mesopotamia, where rainfall was not an important parameter necessary for agricultural production, the region was able to sustain more continuous, less cyclical, and ultimately more intensive urban development during the middle Holocene.

## **12.2 Limitations and Future Recommendations**

This study recognises some limitations to the work carried out here, as well as further questions which have been raised in the course of the project, which would benefit from further exploration.

### **12.2.1 Chronological Limitations**

The study was unable to capture the entire Holocene with the new SHC-03 record as it missed the first *c.*1,000 years of the Holocene and contained a hiatus between 6,540 and 5,780 yr BP. Thus, it was unable to capture the Pleistocene/Holocene transition as well as an important period during the middle Holocene. Consequently, a natural progression of the work conducted in this thesis would be to perform further analysis on more speleothems from the cave, such as stalagmite SHC-04, to fill these temporal gaps and provide a climatic and environmental record for the entire Holocene. Although, it could be that further analysis of other speleothems from the cave might similarly show an absence of growth before *c.*10,560 yr BP, indicating conditions too dry for speleothem formation, providing important and interesting hydrological information in itself.

The accuracy and precision of the chronology of the SHC-03 could be improved, particularly during the early half of the record, where a number of age inversions were present. More samples (E1-E20) for U-Th dating have already been collected which will hopefully improve the chronology of the stalagmite and improve the confidence in the observed timing of shorter-abrupt events present in the record. Similarly, the study was also unable to provide the chronological and resolution requirements necessary to link proxy data from the SHC-03 to instrumental data from the region to help support the interpretation of the proxies and put modern conditions into a more accurate historical context as, for

instance, Flohr et al., (2017) achieved. The SHC-03 speleothem is fast growing and therefore this issue should be easily rectified through further high-resolution proxy analysis combined with new U-Th dates.

### 12.2.2 Proxy Limitations

This project has shown the potential for trace elements from stalagmites in the EFC to address outstanding palaeoenvironmental questions, however there are some uncertainties regarding their interpretation that need to be addressed. Andrews et al., (2020) identified similar trace element profiles in their record from Katakhor Cave in Iran (Andrews et al., 2020), but interpreted the signal in an alternative way not directly related to climatic change. Furthermore, while I have cited dolomitic dust deposition as the potential cause for both short-term and long-term (as a secondary mechanism) Mg/Ca variability, supported by  $^{87}\text{Sr}/^{86}\text{Sr}$  data, the composition of atmospheric dust and the behaviour of dust mobilisation in the EFC is still not fully understood. To address these uncertainties, detailed investigations of the elemental composition of different potential trace element end members (soil profiles above the cave, exogenic sources, the host rock and cave drip waters), a more thorough understanding of dust deposition at the site, and further detailed in-cave monitoring programmes are needed to help verify the findings made in this project.

This is not the first study to suggest source (Kolodny et al., 2005; Develle et al., 2010; e.g. Cheng et al., 2015; Rohling et al., 2015) or seasonal effects (Stevens et al., 2001, 2006; Dean et al., 2018) were significant controls on speleothem or lake sediment long-term  $\delta^{18}\text{O}$  values during the Holocene. Although, it might be one of the first to suggest a combination of these controls may largely explain the long-term  $\delta^{18}\text{O}$  trend observed during the Holocene in the EFC. However there still seems to be a general reluctance to consider these as a major mechanisms for Holocene millennial-scale changes even when considered (e.g., Burstyn et al., 2019; Andrews et al., 2020). Given that  $\delta^{18}\text{O}$  is the predominate proxy used for palaeohydrological changes in the region for both speleothem and lake sediment studies, it is an important issue that needs addressing. To address this problem, more research is needed to examine the influence of long-term changes in seasonality and source  $\delta^{18}\text{O}$  variability on terrestrial  $\delta^{18}\text{O}$  records in Southwest Asia. To test the influence of seasonality, future work should include the

### *Conclusions and Future Recommendations*

examination of seasonally sensitive proxies in archives (e.g. Dean et al., 2018), long-term monitoring studies on the effect of seasonality changes on the  $\delta^{18}\text{O}$  value of karst waters (e.g. Baker et al., 2019) and the use of palaeoclimate models to investigate past changes in the seasonal distribution of rainfall in response to changes in orbital forcings (e.g. Kutzbach et al., 2014). To study the impact of the source  $\delta^{18}\text{O}$  variability, the production of high-resolution marine records from across the Mediterranean which can be used to make comparisons with terrestrial archives will certainly help. Perhaps from a more modern perspective, another more novel way to investigate the influence of the source effect could be done by comparing high resolution palaeoclimate records covering the last century with salinity changes in the Eastern Mediterranean in response to the construction of large Dam projects (e.g. Aswan High Dam in 1964), which should have caused a relatively large change in  $\delta^{18}\text{O}_{\text{EMSS}}$  value over a short period of time, although this latter assumption is itself that really needs studying.

#### 12.2.3 Archaeological Limitations and Future Recommendations

While the predominant analytical focus of this thesis was to improve the chronological coverage of palaeoclimate information from the EFC, more work also needs to be done to refine archaeological chronologies to allow for more reliable comparisons between environmental and archaeological datasets in the EFC. The continued collation of existing survey data and excavation data (e.g. Lawrence et al., 2016), as well as the integration of newer statistical techniques, such as summed probability distributions (SPD) of available calibrated radiocarbon dates (e.g., Lawrence et al., 2021; Palmisano et al., 2021) will continue to improve our understanding and timing of changes in settlement patterns and demographic trends in the region. Of course, one major way to improve the understanding of archaeological chronologies in the EFC is through new excavations and surveys. In some parts of the region, such as Iraqi Kurdistan, field activity has flourished over the last couple of decades (Kopaniak and Macginnis, 2016) and hopefully this continues in a region which was arguably archaeologically neglected for much of the latter half of the 20<sup>th</sup> century. However, in other parts of the EFC, such as north western Iraq and north eastern Syria, the aftermath of the 2003 invasion, the Syrian Civil War, and the devastating impact of Daesh have ceased archaeological fieldwork (Al-Hussainy and Matthews,

### *Conclusions and Future Recommendations*

2008; Matthews et al., 2020b), which unfortunately currently makes it impossible to address archaeological questions through field activity.

### 13 Bibliography

- Adams, R.M., 1981. *Heartland of Cities, Technology and Culture*. The University of Chicago.  
<https://doi.org/10.2307/3104772>
- Adams, R.M., 1965. *Land behind Baghdad: a history of settlement on the Diyala plains*. University of Chicago Press.
- Affolter, S., Fleitmann, D., Leuenberger, M., 2014. New online method for water isotope analysis of speleothem fluid inclusions using laser absorption spectroscopy (WS-CRDS). *Clim. Past* 10, 1291–1304. <https://doi.org/10.5194/cp-10-1291-2014>
- Affolter, S., Häuselmann, A., Fleitmann, D., Lawrence Edwards, R., Cheng, H., Leuenberger, M., 2019. Central Europe temperature constrained by speleothem fluid inclusion water isotopes over the past 14,000 years. *Sci. Adv.* 5, 1–10. <https://doi.org/10.1126/sciadv.aav3809>
- Affolter, S., Häuselmann, A.D., Fleitmann, D., Häuselmann, P., Leuenberger, M., 2015. Triple isotope ( $\delta D$ ,  $\delta^{17}O$ ,  $\delta^{18}O$ ) study on precipitation, drip water and speleothem fluid inclusions for a Western Central European cave (NW Switzerland). *Quat. Sci. Rev.* 127, 73–89. <https://doi.org/10.1016/j.quascirev.2015.08.030>
- Akkermans, P.M.M.G., Schwartz, G.M., 2003. *The archaeology of Syria: from complex hunter-gatherers to early urban societies (c. 16,000-300 BC)*. Cambridge University Press.
- Al-Hussainy, A., Matthews, R., 2008. The Archaeological Heritage of Iraq in Historical Perspective. *Public Archaeol.* 7, 91–100. <https://doi.org/10.1179/175355308x329973>
- Algaze, 2001. Initial Social Complexity in Southwestern Asia: The Mesopotamian Advantage. *Curr. Anthropol.* 42, 199. <https://doi.org/10.2307/3596412>
- Algaze, G., 2018. Entropic cities: The paradox of urbanism in ancient mesopotamia. *Curr. Anthropol.* 59, 23–54. <https://doi.org/10.1086/695983>
- Algaze, G., 2005. The Sumerian Takeoff. *Struct. Dyn.* 1.
- Algaze, G., 1993. *The Uruk world system*. The University of Chicago.

## Bibliography

- Algaze, G., Brenties, B., Knapp, A.B., Kohl, P.L., Wade, R., Schwartz, G.M., Weiss, H., Wenke, R.J., Wright, R.P., Zagarell, A., 1989. The Uruk Expansion: Cross-cultural Exchange in Early Mesopotamian Civilization. *Curr. Anthropol.* 30, 571–608.
- Allcock, S.L., 2017. Long-term socio-environmental dynamics and adaptive cycles in Cappadocia, Turkey during the Holocene. *Quat. Int.* 446, 66–82. <https://doi.org/10.1016/j.quaint.2017.06.065>
- Almogi-Labin, A., Bar-Matthews, M., Shriki, D., Kolosovsky, E., Paterne, M., Schilman, B., Ayalon, A., Aizenshtat, Z., Matthews, A., 2009. Climatic variability during the last ~90ka of the southern and northern Levantine Basin as evident from marine records and speleothems. *Quat. Sci. Rev.* 28, 2882–2896. <https://doi.org/https://doi.org/10.1016/j.quascirev.2009.07.017>
- Altaweel, M., 2003. The roads of Ashur and Nineveh. *Akkadica* 124, 221–228.
- Altaweel, M., Palmisano, A., 2019. Urban and Transport Scaling: Northern Mesopotamia in the Late Chalcolithic and Bronze Age. *J. Archaeol. Method Theory* 26, 943–966. <https://doi.org/10.1007/s10816-018-9400-4>
- Amin Al-Manmi, D.A.M., Ismaeel, S.B., Altaweel, M., 2019. Reconstruction of palaeoclimate in Shalaih Cave, SE of Sangaw, Kurdistan Province of Iraq. *Palaeogeogr. Palaeoclimatol. Palaeoecol.* 524, 262–272. <https://doi.org/10.1016/j.palaeo.2019.03.044>
- Andrews, J.E., Carolin, S.A., Peckover, E., Marca, A.D., Al-Omari, S., Rowe, P.J., 2020. Holocene stable isotope record of insolation and rapid climate change in a stalagmite from the Zagros of Iran. *Quat. Sci. Rev.* 241, 106433. <https://doi.org/10.1016/j.quascirev.2020.106433>
- Arponen, V.P.J., Dörfler, W., Feeser, I., Grimm, S., Grob, D., Hinz, M., Knitter, D., Müller-Scheebel, N., Ott, K., Ribeiro, A., 2019. Environmental determinism and archaeology. Understanding and evaluating determinism in research design. *Archaeol. Dialogues* 26, 1–9. <https://doi.org/10.1017/S1380203819000059>
- Asouti, E., 2017. Human palaeoecology in Southwest Asia during the Early Pre-Pottery Neolithic (c. 9700-8500 cal BC): the plant story, in: Marion Benz, Hans Georg Gebel, T.W. (Ed.), *Neolithic Corporate Identities*. *Oriente Ex*, Berlin, pp. 21–53.

## Bibliography

- Asouti, E., Austin, P., 2005. Reconstructing Woodland Vegetation and its Exploitation by Past Societies, based on the Analysis and Interpretation of Archaeological Wood Charcoal Macro-Remains. *Environ. Archaeol.* 10, 1–18. <https://doi.org/10.1179/env.2005.10.1.1>
- Asouti, E., Kabukcu, C., 2014. Holocene semi-arid oak woodlands in the Irano-Anatolian region of Southwest Asia: Natural or anthropogenic? *Quat. Sci. Rev.* 90, 158–182. <https://doi.org/10.1016/j.quascirev.2014.03.001>
- Asouti, E., Kabukcu, C., White, C.E., Kuijt, I., Finlayson, B., Makarewicz, C., 2015. Early Holocene woodland vegetation and human impacts in the arid zone of the southern Levant. *The Holocene* 25, 1565–1580. <https://doi.org/10.1177/0959683615580199>
- Attiya, A.A., Jones, B.G., 2020. Climatology of Iraqi dust events during 1980–2015. *SN Appl. Sci.* 2, 1–16. <https://doi.org/10.1007/s42452-020-2669-4>
- Avigour, A., Magaritz, M., Issar, A., Dodson, M.H., 1990. Sr isotope study of vein and cave calcites from southern Israel. *Chem. Geol.* 82, 69–81. [https://doi.org/https://doi.org/10.1016/0009-2541\(90\)90075-I](https://doi.org/https://doi.org/10.1016/0009-2541(90)90075-I)
- Ayalon, A., Bar-Matthews, M., Kaufman, A., 1999. Petrography, strontium, barium and uranium concentrations, and strontium and uranium isotope ratios in speleothems as palaeoclimatic proxies: Soreq Cave, Israel, The Holocene.
- Bajo, P., Hellstrom, J., Frisia, S., Drysdale, R., Black, J., Woodhead, J., Borsato, A., Zanchetta, G., Wallace, M.W., Regattieri, E., Haese, R., 2016. “Cryptic” diagenesis and its implications for speleothem geochronologies. *Quat. Sci. Rev.* 148, 17–28. <https://doi.org/10.1016/j.quascirev.2016.06.020>
- Baker, A., Hartmann, A., Duan, W., Hankin, S., Comas-Bru, L., Cuthbert, M.O., Treble, P.C., Banner, J., Genty, D., Baldini, L.M., Bartolomé, M., Moreno, A., Pérez-Mejías, C., Werner, M., 2019. Global analysis reveals climatic controls on the oxygen isotope composition of cave drip water. *Nat. Commun.* 10, 1–7. <https://doi.org/10.1038/s41467-019-11027-w>
- Baker, A., Ito, E., Smart, P.L., McEwan, R.F., 1997. Elevated and variable values of  $^{13}\text{C}$  in speleothems

## Bibliography

- in a British cave system. *Chem. Geol.* 136, 263–270. [https://doi.org/10.1016/S0009-2541\(96\)00129-5](https://doi.org/10.1016/S0009-2541(96)00129-5)
- Baldini, J.U.L., McDermott, F., Baker, A., Baldini, L.M., Matthey, D.P., Railsback, L.B., 2005. Biomass effects on stalagmite growth and isotope ratios: A 20th century analogue from Wiltshire, England. *Earth Planet. Sci. Lett.* 240, 486–494. <https://doi.org/10.1016/j.epsl.2005.09.022>
- Baldini, J.U.L., McDermott, F., Fairchild, I.J., 2006. Spatial variability in cave drip water hydrochemistry: Implications for stalagmite paleoclimate records. *Chem. Geol.* 235, 390–404. <https://doi.org/10.1016/j.chemgeo.2006.08.005>
- Ball, W., Tucker, D., Wilkinson, T.J., 1989. The Tell al-Hawa Project: Archaeological Investigations in the North Jazira 1986-87. *Iraq* 51, 1. <https://doi.org/10.2307/4200295>
- Banner, J.L., Musgrove, M.L., Asmerom, Y., Edwards, R.L., Hoff, J.A., 1996. High-resolution temporal record of holocene ground-water chemistry: Tracing links between climate and hydrology. *Geology* 24, 1049–1053. [https://doi.org/10.1130/0091-7613\(1996\)024<1049:HRTROH>2.3.CO;2](https://doi.org/10.1130/0091-7613(1996)024<1049:HRTROH>2.3.CO;2)
- Bar-Matthews, M., Ayalon, a., Matthews, a., Sass, E., Halicz, L., 1996. Carbon and oxygen isotope study of the active water-carbonate system in a karstic Mediterranean cave.pdf. *Geochim. Cosmochim. Acta* 60, 337–347.
- Bar-Matthews, M., Ayalon, A., 2011. Mid-holocene climate variations revealed by high-resolution speleothem records from soreq cave, israel and their correlation with cultural changes. *Holocene* 21, 163–171. <https://doi.org/10.1177/0959683610384165>
- Bar-Matthews, M., Ayalon, A., Gilmour, M., Matthews, A., Hawkesworth, C.J., 2003. Sea - land oxygen isotopic relationships from planktonic foraminifera and speleothems in the Eastern Mediterranean region and their implication for paleorainfall during interglacial intervals. *Geochim. Cosmochim. Acta* 67, 3181–3199. [https://doi.org/10.1016/S0016-7037\(02\)01031-1](https://doi.org/10.1016/S0016-7037(02)01031-1)
- Bar-Matthews, M., Ayalon, A., Kaufman, A., 1997. Late Quaternary Paleoclimate in the Eastern Mediterranean Region from Stable Isotope Analysis of Spelethems at Soreq Cave, Israel. *Quat.*

## *Bibliography*

- Res. 168, 155–168. <https://doi.org/10.1006/qres.1997.1883>
- Bar-Matthews, M., Ayalon, A., Kaufman, A., Wasserburg, G.J., 1999. The Eastern Mediterranean paleoclimate as a reflection of regional events: Soreq cave, Israel. *Earth Planet. Sci. Lett.* 166, 85–95. [https://doi.org/10.1016/S0012-821X\(98\)00275-1](https://doi.org/10.1016/S0012-821X(98)00275-1)
- Bar-Yosef, O., 2017. Facing climatic hazards: Paleolithic foragers and Neolithic farmers. *Quat. Int.* 428, 64–72. <https://doi.org/10.1016/j.quaint.2015.11.037>
- Barlow, M., Zaitchik, B., Paz, S., Black, E., Evans, J., Hoell, A., 2016. A review of drought in the Middle East and southwest Asia. *J. Clim.* 29, 8547–8574. <https://doi.org/10.1175/JCLI-D-13-00692.1>
- Baruch, U., Bottema, S., 1999. A new pollen diagram from Lake Hula: vegetational, climatic and anthropogenic implications. *Anc. lakes their Cult. Biol. Divers.* 75–86.
- BBC, 2018. Water shortages fuel ongoing protests in Basra, Iraq [WWW Document]. URL <https://www.bbc.co.uk/news/av/world-middle-east-45626170>
- Berger, A., 1988. Milankovitch Theory and climate. *Rev. Geophys.* <https://doi.org/10.1029/RG026i004p00624>
- Berger, A., Loutre, M.F., 1991. Insolation values for the climate of the last 10 million years. *Quat. Sci. Rev.* 10, 297–317. [https://doi.org/10.1016/0277-3791\(91\)90033-Q](https://doi.org/10.1016/0277-3791(91)90033-Q)
- Berger, A.L., 1992. Astronomical theory of Paleoclimates and the last glacial-interglacial cycle. *Quat. Sci. Rev.* 11, 571–581. [https://doi.org/https://doi.org/10.1016/0277-3791\(92\)90014-Y](https://doi.org/https://doi.org/10.1016/0277-3791(92)90014-Y)
- Binford, L., 1968. Post-pleistocene adaptations, in: Binford, R, S., Binford, R, L. (Eds.), *New Perspectives in Archaeology*. Chicago: University of Chicago Press, pp. 313–341.
- Binford, L.R., 2019. *Constructing frames of reference: an analytical method for archaeological theory building using ethnographic and environmental data sets*. University of California Press.
- Black, E., 2012. The influence of the North Atlantic Oscillation and European circulation regimes on the daily to interannual variability of winter precipitation in Israel. *Int. J. Climatol.* 32, 1654–1664.

## Bibliography

<https://doi.org/10.1002/joc.2383>

- Black, E., Brayshaw, D.J., Rambeau, C.M.C.C., 2010. Past, present and future precipitation in the Middle East: Insights from models and observations. *Philos. Trans. R. Soc. A Math. Phys. Eng. Sci.* 368, 5173–5184. <https://doi.org/10.1098/rsta.2010.0199>
- Blisniuk, P.M., Stern, L.A., 2005. Stable isotope paleoaltimetry: A critical review. *Am. J. Sci.* 305, 1033–1074.
- Blockley, S.P.E., Pinhasi, R., 2011. A revised chronology for the adoption of agriculture in the Southern Levant and the role of Lateglacial climatic change. *Quat. Sci. Rev.* 30, 98–108. <https://doi.org/10.1016/j.quascirev.2010.09.021>
- Blyth, A.J., Hartland, A., Baker, A., 2016. Organic proxies in speleothems – New developments, advantages and limitations. *Quat. Sci. Rev.* 149, 1–17. <https://doi.org/10.1016/j.quascirev.2016.07.001>
- Bocquet-Appel, J.P., 2008. Explaining the Neolithic demographic transition. *Neolit. Demogr. Transit. its Consequences* 35–55. [https://doi.org/10.1007/978-1-4020-8539-0\\_3](https://doi.org/10.1007/978-1-4020-8539-0_3)
- Bocquet-Appel, J., 2002. Paleoanthropological Traces of a Neolithic Demographic Transition. *Curr. Anthropol.* 43, 637–650. <https://doi.org/10.1086/342429>
- Boisvenue, C., Running, S.W., 2006. Impacts of climate change on natural forest productivity - Evidence since the middle of the 20th century. *Glob. Chang. Biol.* 12, 862–882. <https://doi.org/10.1111/j.1365-2486.2006.01134.x>
- Bond, G., Kromer, B., Beer, J., Muscheler, R., Evans, M.N., Showers, W., Hoffmann, S., Lotti-Bond, R., Hajdas, I., Bonani, G., 2001. Persistent solar influence on north atlantic climate during the Holocene. *Science* (80-. ). 294, 2130–2136. <https://doi.org/10.1126/science.1065680>
- Bond, G., Showers, W., Cheseby, M., Lotti, R., Almasi, P., DeMenocal, P., Priore, P., Cullen, H., Hajdas, I., Bonani, G., 1997. A pervasive millennial-scale cycle in North Atlantic Holocene and glacial climates. *Science* (80-. ). 278, 1257–1266. <https://doi.org/10.1126/science.278.5341.1257>

## Bibliography

- Borrell, F., Junno, A., Barceló, J.A., 2015. Synchronous environmental and cultural change in the emergence of agricultural economies 10,000 years ago in the levant. *PLoS One* 10. <https://doi.org/10.1371/journal.pone.0134810>
- Bottema, S., 1986. A late quaternary pollen diagram from Lake Urmia (Northwestern Iran). *Rev. Palaeobot. Palynol.* 47, 241–261. [https://doi.org/10.1016/0034-6667\(86\)90039-4](https://doi.org/10.1016/0034-6667(86)90039-4)
- Bowen, G.J., Wassenaar, L.I., Hobson, K.A., 2005. Global application of stable hydrogen and oxygen isotopes to wildlife forensics. *Oecologia* 143, 337–348. <https://doi.org/10.1007/s00442-004-1813-y>
- Brayshaw, D.J., Hoskins, B., Black, E., 2010. Some physical drivers of changes in the winter storm tracks over the North Atlantic and Mediterranean during the Holocene. *Philos. Trans. R. Soc. A Math. Phys. Eng. Sci.* 368, 5185–5223. <https://doi.org/10.1098/rsta.2010.0180>
- Brayshaw, D.J., Rambeau, C.M.C.C., Smith, S.J., 2011a. Changes in mediterranean climate during the holocene: Insights from global and regional climate modelling. *Holocene* 21, 15–31. <https://doi.org/10.1177/0959683610377528>
- Brayshaw, D.J., Rambeau, C.M.C.C., Smith, S.J., 2011b. Changes in mediterranean climate during the holocene: Insights from global and regional climate modelling. *Holocene* 21, 15–31. <https://doi.org/10.1177/0959683610377528>
- Breitenbach, S.F.M., Rehfeld, K., Goswami, B., Baldini, J.U.L., Ridley, H.E., Kennett, D.J., Prufer, K.M., Aquino, V. V., Asmerom, Y., Polyak, V.J., Cheng, H., Kurths, J., Marwan, N., 2012. Constructing proxy records from age models (COPRA). *Clim. Past* 8, 1765–1779. <https://doi.org/10.5194/cp-8-1765-2012>
- Brock, F., Higham, T., Ditchfield, P., Ramsey, C.B., 2010. Current pretreatment methods for ams radiocarbon dating at the oxford radiocarbon accelerator unit (orau). *Radiocarbon* 52, 103–112. <https://doi.org/10.1017/S0033822200045069>
- Bronk Ramsey, C., Higham, T., Leach, P., 2004. Towards High-Precision AMS: Progress and Limitations. *Radiocarbon* 46, 17–24. <https://doi.org/10.1017/S0033822200039308>

## Bibliography

- Brookes, I.A., 1982. Geomorphological evidence for climatic change in Iran during the last 20,000 years, in: J. L. Bintliff and W. van Zeist (Ed.), *Palaeoclimates, Palaeoenvironments and Human Communities in the Eastern Mediterranean Region in Later Prehistory*. Oxford: BAR Int Ser 133, pp. 191– 229.
- Brooks, N., 2012. Beyond collapse: Climate change and causality during the Middle Holocene Climatic Transition, 6400-5000 years before present. *Geogr. Tidsskr.* 112, 93–104. <https://doi.org/10.1080/00167223.2012.741881>
- Brooks, N., 2006. Cultural responses to aridity in the Middle Holocene and increased social complexity. *Quat. Int.* 151, 29–49. <https://doi.org/10.1016/j.quaint.2006.01.013>
- Brotherton, P., Haak, W., Templeton, J., Brandt, G., Soubrier, J., Jane Adler, C., Richards, S.M., Sarkissian, C. Der, Ganslmeier, R., Friederich, S., Dresely, V., Van Oven, M., Kenyon, R., Van Der Hoek, M.B., Korfach, J., Luong, K., Ho, S.Y.W., Quintana-Murci, L., Behar, D.M., Meller, H., Alt, K.W., Cooper, A., Adhikarla, S., Ganesh Prasad, A.K., Pitchappan, R., Varatharajan Santhakumari, A., Balanovska, E., Balanovsky, O., Bertranpetit, J., Comas, D., Martínez-Cruz, B., Melé, M., Clarke, A.C., Matisoo-Smith, E.A., Dulik, M.C., Gaieski, J.B., Owings, A.C., Schurr, T.G., Vilar, M.G., Hobbs, A., Soodyall, H., Javed, A., Parida, L., Platt, D.E., Royyuru, A.K., Jin, L., Li, S., Kaplan, M.E., Merchant, N.C., John Mitchell, R., Renfrew, C., Lacerda, D.R., Santos, F.R., Soria Hernanz, D.F., Spencer Wells, R., Swamikrishnan, P., Tyler-Smith, C., Paulo Vieira, P., Ziegler, J.S., 2013. Neolithic mitochondrial haplogroup H genomes and the genetic origins of Europeans. *Nat. Commun.* 4. <https://doi.org/10.1038/ncomms2656>
- Burstyn, Y., 2013. Multi-decade to Seasonal Climate Change Recorded by Stable Isotope and Trace Element Variability in Modern Cave-waters and Calcite of Soreq Cave, Israel. *Geol. Surv. Isr.* 86. <https://doi.org/GSI/13/2013>
- Burstyn, Y., Martrat, B., Lopez, J.F., Iriarte, E., Jacobson, M.J., Lone, M.A., Deininger, M., 2019. Speleothems from the Middle East: An Example of Water Limited Environments in the SISAL Database. *Quaternary* 2, 16. <https://doi.org/10.3390/quat2020016>

## *Bibliography*

- Butzer, K.W., 1997. Sociopolitical Discontinuity in the Near East C. 2200 B.C.E.: Scenarios from Palestine and Egypt BT - Third Millennium BC Climate Change and Old World Collapse, in: Dalfes, H.N., Kukla, G., Weiss, H. (Eds.), . Springer Berlin Heidelberg, Berlin, Heidelberg, pp. 245–296.
- Capo, R.C., Stewart, B.W., Chadwick, O.A., 1998. Strontium isotopes as tracers of earth surface processes: theory and methods. *Geoderma* 82, 197–225.
- Carleton, W.C., Collard, M., 2020. Recent Major Themes and Research Areas in the Study of Human-Environment Interaction in Prehistory. *Environ. Archaeol.* 25, 114–130. <https://doi.org/10.1080/14614103.2018.1560932>
- Carleton, W.C., Groucutt, H.S., 2020. Sum things are not what they seem: Problems with point-wise interpretations and quantitative analyses of proxies based on aggregated radiocarbon dates. *Holocene*. <https://doi.org/10.1177/0959683620981700>
- Carneiro, R.L., 1972. From autonomous villages to the state, a numerical estimation. *Popul. growth Anthropol. Implic.* 64–77.
- Carolin, S.A., Walker, R.T., Day, C.C., Ersek, V., Sloan, R.A., Dee, M.W., Talebian, M., Henderson, G.M., 2019. Precise timing of abrupt increase in dust activity in the Middle East coincident with 4.2 ka social change. *Proc. Natl. Acad. Sci.* 116, 67–72. <https://doi.org/10.1073/pnas.1808103115>
- Castro, P., Champan, R., Gili, S., Lull, V., Micó, R., Rihuete, C., Risch, R., Sanahuja, M.E., 1998. Aguas Project. Palaeoclimatic reconstruction and the dynamics of human settlement and land-use in the area of the middle Aguas (Almeria), in the south-east of the Iberian Peninsula.
- Cerling, T.E., 1999. Paleorecords of C4 Plants and Ecosystems, in: Sage, R.F., Monson, R.K.B.T.-C.P.B. (Eds.), *Physiological Ecology*. Academic Press, San Diego, pp. 445–469. <https://doi.org/https://doi.org/10.1016/B978-012614440-6/50014-8>
- Chang, S.J., Blake, R.E., Stout, L.M., Kim, S.J., 2010. Oxygen isotope, micro-textural and molecular evidence for the role of microorganisms in formation of hydroxylapatite in limestone caves, South Korea. *Chem. Geol.* 276, 209–224. <https://doi.org/10.1016/j.chemgeo.2010.06.007>

## *Bibliography*

- Charles, M., Pessin, H., Hald, M.M., 2010. Tolerating change at Late Chalcolithic Tell Brak: Responses of an early urban society to an uncertain climate. *Environ. Archaeol.* 15, 183–198. <https://doi.org/10.1179/146141010X12640787648892>
- Chen, Z., Auler, A.S., Bakalowicz, M., Drew, D., Griger, F., Hartmann, J., Jiang, G., Moosdorf, N., Richts, A., Stevanovic, Z., Veni, G., Goldscheider, N., 2017. Le programme de la Carte Mondiale des Aquifères Karstiques: concept, procédure de cartographie et carte de l'Europe. *Hydrogeol. J.* 25, 771–785. <https://doi.org/10.1007/s10040-016-1519-3>
- Cheng, H., Lawrence Edwards, R., Shen, C.C., Polyak, V.J., Asmerom, Y., Woodhead, J., Hellstrom, J., Wang, Y., Kong, X., Spötl, C., Wang, X., Calvin Alexander, E., 2013. Improvements in <sup>230</sup>Th dating, <sup>230</sup>Th and <sup>234</sup>U half-life values, and U-Th isotopic measurements by multi-collector inductively coupled plasma mass spectrometry. *Earth Planet. Sci. Lett.* 371–372, 82–91. <https://doi.org/10.1016/j.epsl.2013.04.006>
- Cheng, H., Sinha, A., Verheyden, S., Nader, F.H., Li, X.L., Zhang, P.Z., Yin, J.J., Yi, L., Peng, Y.B., Rao, Z.G., Ning, Y.F., Edwards, R.L., 2015. The climate variability in northern Levant over the past 20,000 years. *Geophys. Res. Lett.* 42, 8641–8650. <https://doi.org/10.1002/2015GL065397>
- Chmela, H., 2011. *Managing Iraq 's Water Resources : The Path to Stability and Security V.*
- Clark, I., Fritz, P., 1997. *Environmental Isotopes in Hydrogeology*, CRC Press.
- Clarke, J., Brooks, N., Banning, E.B., Bar-Matthews, M., Campbell, S., Clare, L., Cremaschi, M., di Lernia, S., Drake, N., Gallinaro, M., Manning, S., Nicoll, K., Philip, G., Rosen, S., Schoop, U.-D., Tafuri, M.A., Weninger, B., Zerboni, A., 2016. Climatic changes and social transformations in the Near East and North Africa during the 'long' 4th millennium BC: A comparative study of environmental and archaeological evidence. *Quat. Sci. Rev.* 136, 96–121. <https://doi.org/10.1016/J.QUASCIREV.2015.10.003>
- Cohen, M.N., 1975. Archaeological Evidence for Population Pressure in Pre-Agricultural Societies. *Am. Antiq.* 40, 471–475. <https://doi.org/10.2307/279335>
- Collins, M., Knutti, R., Arblaster, J., Dufresne, J.L., Fichetef, T., Friedlingstein, P., Gao, X., Gutowski,

## *Bibliography*

- W.J., Johns, T., Krinner, G., Shongwe, M., 2013. Long-term Climate Change: Projections, Commitments and Irreversibility, in: Qin, D., Plattner, G.K., Tignor, M., Allen, S.K., Boschung, J., Nauels, A. (Eds.), *Climate Change 2013: The Physical Science Basis. Contribution of Working Group I to the Fifth Assessment Report of the Intergovernmental Panel on Climate Change*. Cambridge University Press, Cambridge, United Kingdom and New York.
- Comas-Bru, L., Harrison, S.P., 2019. SISAL: Bringing Added Value to Speleothem Research. *Quaternary* 2, 7. <https://doi.org/10.3390/quat2010007>
- Contreras, D.A., 2016. Correlation is Not Enough – Building Better Arguments in the Archaeology of Human-Environment Interactions, in: Contreras, D.A. (Ed.), *The Archaeology of Human-Environment Interactions*. Routledge, pp. 17–36.
- Contreras, D.A., Meadows, J., 2014. Summed radiocarbon calibrations as a population proxy: A critical evaluation using a realistic simulation approach. *J. Archaeol. Sci.* 52, 591–608. <https://doi.org/10.1016/j.jas.2014.05.030>
- Cook, B.I., Anchukaitis, K.J., Touchan, R., Meko, D.M., Cook, E.R., 2016. Spatiotemporal drought variability in the mediterranean over the last 900 years. *J. Geophys. Res.* 121, 2060–2074. <https://doi.org/10.1002/2015JD023929>
- Cooke, M.J., Stern, L.A., Banner, J.L., Mack, L.E., Stafford Jr., T.W., Toomey III, R.S., 2003. Precise timing and rate of massive late Quaternary soil denudation. *Geology* 31, 853–856. <https://doi.org/10.1130/G19749.1>
- Coombes, P., Barber, K., 2005. Environmental Determinism in Holocene Research: Causality or Coincidence? *Area* 37, 303–311.
- Coplen, T.B., Kendall, C., Hopple, J., 1983. Comparison of stable isotope reference samples. *Nature* 302, 236–238. <https://doi.org/10.1038/302236a0>
- Crémière, A., Lepland, A., Chand, S., Sahy, D., Condon, D.J., Noble, S.R., Martma, T., Thorsnes, T., Sauer, S., Brunstad, H., 2016. Timescales of methane seepage on the Norwegian margin following collapse of the Scandinavian Ice Sheet. *Nat. Commun.* 7, 1–10.

## Bibliography

<https://doi.org/10.1038/ncomms11509>

- Cruz, F.W., Burns, S.J., Jercinovic, M., Karmann, I., Sharp, W.D., Vuille, M., 2007. Evidence of rainfall variations in Southern Brazil from trace element ratios (Mg/Ca and Sr/Ca) in a Late Pleistocene stalagmite. *Geochim. Cosmochim. Acta* 71, 2250–2263. <https://doi.org/10.1016/j.gca.2007.02.005>
- Cruz, F.W., Karmann, I., Viana, O., Burns, S.J., Ferrari, J.A., Vuille, M., Sial, A.N., Moreira, M.Z., 2005. Stable isotope study of cave percolation waters in subtropical Brazil: Implications for paleoclimate inferences from speleothems. *Chem. Geol.* 220, 245–262. <https://doi.org/10.1016/j.chemgeo.2005.04.001>
- Cullen, H.M., De Menocal, P.B., Hemming, S., Brown, F.H., Guilderson, T., Sirocko, F., 2000. Climate change and the collapse of the Akkadian empire: Evidence from the deep sea. *Geology* 28, 379–382. [https://doi.org/10.1130/0091-7613\(2000\)28<379:CCATCO>2.0.CO;2](https://doi.org/10.1130/0091-7613(2000)28<379:CCATCO>2.0.CO;2)
- Cullen, H.M., Kaplan, A., Arkin, P.A., DeMenocal, P.B., 2002. Impact of the North Atlantic Oscillation on Middle Eastern climate and streamflow. *Clim. Change* 55, 315–338. <https://doi.org/10.1023/A:1020518305517>
- Dansgaard, W., 1964. Stable isotopes in precipitation. *Tellus* 16, 436–468. <https://doi.org/10.3402/tellusa.v16i4.8993>
- Davis, K.J., Dove, P.M., De Yoreo, J.J., 2000. The role of Mg<sup>2+</sup> as an impurity in calcite growth. *Science* (80- ). 290, 1134–1137. <https://doi.org/10.1126/science.290.5494.1134>
- Deacon, J., 1974. Patterning in the Radiocarbon Dates for the Wilton / Smithfield Complex in Southern Africa Author ( s ): Janette Deacon Source : The South African Archaeological Bulletin , Jun ., 1974 , Vol . 29 , No . 113 / 114 Published by : South African Archaeologica 29, 3–18.
- Dean, J.R., Jones, M.D., Leng, M.J., Metcalfe, S.E., Sloane, H.J., Eastwood, W.J., Roberts, C.N., 2018. Seasonality of Holocene hydroclimate in the Eastern Mediterranean reconstructed using the oxygen isotope composition of carbonates and diatoms from Lake Nar, central Turkey. *Holocene* 28, 267–276. <https://doi.org/10.1177/0959683617721326>

## Bibliography

- Dean, J.R., Jones, M.D., Leng, M.J., Noble, S.R., Metcalfe, S.E., Sloane, H.J., Sahy, D., Eastwood, W.J., Roberts, C.N., 2015. Eastern Mediterranean hydroclimate over the late glacial and Holocene, reconstructed from the sediments of Nar lake, central Turkey, using stable isotopes and carbonate mineralogy. *Quat. Sci. Rev.* 124, 162–174. <https://doi.org/10.1016/J.QUASCIREV.2015.07.023>
- Delaby, S., 2001. Palaeoseismic investigations in Belgian caves. *Geol. en Mijnbouw/Netherlands J. Geosci.* 80, 323–332. <https://doi.org/10.1017/s0016774600023921>
- DePaolo, D.J., Ingram, B.L., 1985. High-resolution stratigraphy with strontium isotopes. *Science* (80-). 227, 938–941. <https://doi.org/10.1126/science.227.4689.938>
- Develle, A.L., Herreros, J., Vidal, L., Sursock, A., Gasse, F., 2010. Controlling factors on a paleo-lake oxygen isotope record (Yammoûneh, Lebanon) since the Last Glacial Maximum. *Quat. Sci. Rev.* 29, 865–886. <https://doi.org/10.1016/j.quascirev.2009.12.005>
- Diefendorf, A.F., Mueller, K.E., Wing, S.L., Koch, P.L., Freeman, K.H., 2010. Global patterns in leaf  $^{13}\text{C}$  discrimination and implications for studies of past and future climate. *Proc. Natl. Acad. Sci. U. S. A.* 107, 5738–5743. <https://doi.org/10.1073/pnas.0910513107>
- Djamali, M., Akhani, H., Andrieu-Ponel, V., Braconnot, P., Brewer, S., de Beaulieu, J.L., Fleitmann, D., Fleury, J., Gasse, F., Guibal, F., Jackson, S.T., Lézine, A.M., Médail, F., Ponel, P., Roberts, N., Stevens, L., 2010. Indian summer Monsoon variations could have affected the early-Holocene woodland expansion in the Near East. *Holocene* 20, 813–820. <https://doi.org/10.1177/0959683610362813>
- Djamali, M., Brewer, S., Breckle, S.W., Jackson, S.T., 2012. Climatic determinism in phytogeographic regionalization: A test from the Irano-Turanian region, SW and Central Asia. *Flora Morphol. Distrib. Funct. Ecol. Plants* 207, 237–249. <https://doi.org/10.1016/j.flora.2012.01.009>
- Djamali, M., de Beaulieu, J.-L.L., Shah-hosseini, M., Andrieu-ponel, V., Ponel, P., Amini, A., Akhani, H., Leroy, S.A.G.G., Stevens, L., Lahijani, H., Brewer, S., Beaulieu, J. De, Shah-hosseini, M., Andrieu-ponel, V., Ponel, P., Amini, A., Akhani, H., Leroy, S.A.G.G., Stevens, L., Lahijani, H., Brewer, S., 2008. A late Pleistocene long pollen record from Lake Urmia, Nw Iran. *Quat. Res.* 69,

## Bibliography

- 413–420. <https://doi.org/10.1016/j.yqres.2008.03.004>
- Dorale, J.A., Liu, Z., 2009. Limitations of hendi test criteria in judging the paleoclimatic suitability of speleothems and the need for replication. *J. Cave Karst Stud.* 71, 73–80.
- Dreybrodt, W., Scholz, D., 2011. Climatic dependence of stable carbon and oxygen isotope signals recorded in speleothems: From soil water to speleothem calcite. *Geochim. Cosmochim. Acta* 75, 734–752. <https://doi.org/10.1016/j.gca.2010.11.002>
- Drysdale, R., Zanchetta, G., Hellstrom, J., Maas, R., Fallick, A., Pickett, M., Cartwright, I., Piccini, L., 2006. Late Holocene drought responsible for the collapse of Old World civilizations is recorded in an Italian cave flowstone. *Geology* 34, 101–104. <https://doi.org/10.1130/G22103.1>
- Eastwood, W.J., Leng, M.J., Roberts, N., Davis, B., 2007. Holocene climate change in the eastern Mediterranean region: a comparison of stable isotope and pollen data from Lake Gölhisar, southwest Turkey. *J. Quat. Sci.* 22, 327–341. <https://doi.org/10.1002/jqs.1062>
- Eidem, J., Warburton, D., 1996. In the land of Nagar: a survey around Tell Brak. *Iraq* 58, 51–64.
- El-Moslimany, A.P., 1986. Ecology and late-Quaternary history of the Kurdo-Zagrosian oak forest near Lake Zeribar, western Iran. *Vegetatio* 68, 55–63. <https://doi.org/10.1007/BF00031580>
- England, A., Eastwood, W.J., Roberts, C.N., Turner, R., Haldon, J.F., 2008. Historical landscape change in Cappadocia (central Turkey): a palaeoecological investigation of annually laminated sediments from Nar lake. *The Holocene* 18, 1229–1245. <https://doi.org/10.1177/0959683608096598>
- Enzel, Y., Bookman, R., Sharon, D., Gvirtzman, H., Dayan, U., Ziv, B., Stein, M., 2003. Late Holocene climates of the Near East deduced from Dead Sea level variations and modern regional winter rainfall. *Quat. Res.* <https://doi.org/10.1016/j.yqres.2003.07.011>
- Essallami, L., Sicre, M.A., Kallel, N., Labeyrie, L., Siani, G., 2007. Hydrological changes in the Mediterranean Sea over the last 30,000 years. *Geochemistry, Geophys. Geosystems* 8. <https://doi.org/10.1029/2007GC001587>
- Evans, J.P., Smith, R.B., 2006. Water vapor transport and the production of precipitation in the Eastern

## Bibliography

- fertile crescent. *J. Hydrometeorol.* 7, 1295–1307. <https://doi.org/10.1175/JHM550.1>
- Fairchild, I.J., Baker, A., 2012. *Speleothem Science : From Process to Past Environments*. John Wiley & Sons, Incorporated.
- Fairchild, I.J., Borsato, A., Tooth, A.F., Frisia, S., Hawkesworth, C.J., Huang, Y., McDermott, F., Spiro, B., 2000. Controls on trace element (Sr-Mg) compositions of carbonate cave waters: Implications for speleothem climatic records. *Chem. Geol.* 166, 255–269. [https://doi.org/10.1016/S0009-2541\(99\)00216-8](https://doi.org/10.1016/S0009-2541(99)00216-8)
- Fairchild, I.J., Smith, C.L., Baker, A., Fuller, L., Spötl, C., Matthey, D., McDermott, F., 2006. Modification and preservation of environmental signals in speleothems. *Earth-Science Rev.* 75, 105–153. <https://doi.org/10.1016/j.earscirev.2005.08.003>
- Fairchild, I.J., Treble, P.C., 2009. Trace elements in speleothems as recorders of environmental change. *Quat. Sci. Rev.* 28, 449–468. <https://doi.org/10.1016/j.quascirev.2008.11.007>
- Feinman, G., Neitzel, J., 1984. *Too Many Types: An Overview of Sedentary Prestate Societies in the Americas*, *Advances in Archaeological Method and Theory*. Springer.
- Finné, M., Holmgren, K., Sundqvist, H.S., Weiberg, E., Lindblom, M., 2011. Climate in the eastern Mediterranean, and adjacent regions, during the past 6000 years - A review. *J. Archaeol. Sci.* 38, 3153–3173. <https://doi.org/10.1016/j.jas.2011.05.007>
- Fleitmann, D., Burns, S.J., Mangini, A., Mudelsee, M., Kramers, J., Villa, I., Neff, U., Al-Subbary, A.A., Buettner, A., Hippler, D., Matter, A., 2007. Holocene ITCZ and Indian monsoon dynamics recorded in stalagmites from Oman and Yemen (Socotra). *Quat. Sci. Rev.* 26, 170–188. <https://doi.org/10.1016/j.quascirev.2006.04.012>
- Fleitmann, D., Burns, S.J., Mudelsee, M., Neff, U., Kramers, J., Mangini, A., Matter, A., 2003a. Holocene forcing of the Indian monsoon recorded in a stalagmite from Southern Oman. *Science* (80-. ). 300, 1737–1739.
- Fleitmann, D., Burns, S.J., Neff, U., Mangini, A., Matter, A., 2003b. Changing moisture sources over

## Bibliography

- the last 330,000 years in Northern Oman from fluid-inclusion evidence in speleothems. *Quat. Res.* 60, 223–232. [https://doi.org/10.1016/S0033-5894\(03\)00086-3](https://doi.org/10.1016/S0033-5894(03)00086-3)
- Fleitmann, D., Burns, S.J., Neff, U., Mudelsee, M., Mangini, A., Matter, A., 2004. Palaeoclimatic interpretation of high-resolution oxygen isotope profiles derived from annually laminated speleothems from Southern Oman. *Quat. Sci. Rev.* 23, 935–945. <https://doi.org/10.1016/j.quascirev.2003.06.019>
- Fleitmann, D., Cheng, H., Badertscher, S., Edwards, R.L., Mudelsee, M., Göktürk, O.M., Fankhauser, A., Pickering, R., Raible, C.C., Matter, A., Kramers, J., Tüysüz, O., 2009. Timing and climatic impact of Greenland interstadials recorded in stalagmites from northern Turkey. *Geophys. Res. Lett.* 36, 1–5. <https://doi.org/10.1029/2009GL040050>
- Fleitmann, D., Mudelsee, M., Burns, S.J., Bradley, R.S., Kramers, J., Matter, A., 2008. Evidence for a widespread climatic anomaly at around 9.2 ka before present. *Paleoceanography* 23, 1–6. <https://doi.org/10.1029/2007PA001519>
- Flohr, P., Fleitmann, D., Matthews, R., Matthews, W., Black, S., 2016. Evidence of resilience to past climate change in Southwest Asia: Early farming communities and the 9.2 and 8.2 ka events. *Quat. Sci. Rev.* 136, 23–39. <https://doi.org/10.1016/j.quascirev.2015.06.022>
- Flohr, P., Fleitmann, D., Zorita, E., Sadekov, A., Cheng, H., Bosomworth, M., Edwards, L., Matthews, W., Matthews, R., 2017. Late Holocene droughts in the Fertile Crescent recorded in a speleothem from northern Iraq. *Geophys. Res. Lett.* 44, 1528–1536. <https://doi.org/10.1002/2016GL071786>
- Fohlmeister, J., Voarintsoa, N.R.G., Lechleitner, F.A., Boyd, M., Brandstätter, S., Jacobson, M.J., Oster, J.L., 2020. Main controls on the stable carbon isotope composition of speleothems. *Geochim. Cosmochim. Acta* 279, 67–87. <https://doi.org/10.1016/j.gca.2020.03.042>
- Fontugne, M.R., Calvert, S.E., 1992. Late Pleistocene Variability of the Carbon Isotopic Composition of Organic Matter in the Eastern Mediterranean: Monitor of Changes in Carbon Sources and Atmospheric CO<sub>2</sub> Concentrations. *Paleoceanography* 7, 1–20. <https://doi.org/10.1029/91PA02674>

## Bibliography

- Ford, D.C., Williams, P., 2007. *Karst Hydrogeology and Geomorphology*. John Wiley and Sons Ltd.
- Freitag, H., 1977. The Pleniglacial, Late Glacial and Early Postglacial vegetations of Zeribar and their present-day counterparts. A supplement to W. van Zeist & S. Bottema, Palynological investigations in Western Iran. *Palaeohistoria* 19, 87–95.
- Frisia, S., Borsato, A., Fairchild, I.J., McDermott, F., Selmo, E.M., 2002. Aragonite-Calcite Relationships in Speleothems (Grotte De Clamouse, France): Environment, Fabrics, and Carbonate Geochemistry. *J. Sediment. Res.* 72, 687–699. <https://doi.org/10.1306/020702720687>
- Frisia, S., Borsato, A., Preto, N., McDermott, F., 2003. Late Holocene annual growth in three Alpine stalagmites records the influence of solar activity and the North Atlantic Oscillation on winter climate. *Earth Planet. Sci. Lett.* 216, 411–424. [https://doi.org/10.1016/S0012-821X\(03\)00515-6](https://doi.org/10.1016/S0012-821X(03)00515-6)
- Frumkin, A., Ford, D.C., Schwarcz, H.P., 1999. Continental oxygen isotopic record of the last 170,000 years in Jerusalem, *Quaternary Research*. <https://doi.org/10.1006/qres.1998.2031>
- Frumkin, A., Stein, M., 2004. The Sahara-East Mediterranean dust and climate connection revealed by strontium and uranium isotopes in a Jerusalem speleothem. *Earth Planet. Sci. Lett.* 217, 451–464. [https://doi.org/10.1016/S0012-821X\(03\)00589-2](https://doi.org/10.1016/S0012-821X(03)00589-2)
- Fu, Q., Posth, C., Hajdinjak, M., Petr, M., Mallick, S., Fernandes, D., Furtwängler, A., Haak, W., Meyer, M., Mittnik, A., Nickel, B., Peltzer, A., Rohland, N., Slon, V., Talamo, S., Lazaridis, I., Lipson, M., Mathieson, I., Schiffels, S., Skoglund, P., Derevianko, A.P., Drozdov, N., Slavinsky, V., Tsybankov, A., Cremonesi, R.G., Mallegni, F., Gély, B., Vacca, E., Morales, M.R.G., Straus, L.G., Neugebauer-Maresch, C., Teschler-Nicola, M., Constantin, S., Moldovan, O.T., Benazzi, S., Peresani, M., Coppola, D., Lari, M., Ricci, S., Ronchitelli, A., Valentin, F., Thevenet, C., Wehrberger, K., Grigorescu, D., Rougier, H., Crevecoeur, I., Flas, D., Semal, P., Mannino, M.A., Cupillard, C., Bocherens, H., Conard, N.J., Harvati, K., Moiseyev, V., Drucker, D.G., Svoboda, J., Richards, M.P., Caramelli, D., Pinhasi, R., Kelso, J., Patterson, N., Krause, J., Pääbo, S., Reich, D., 2016. The genetic history of Ice Age Europe. *Nature* 534, 200–205. <https://doi.org/10.1038/nature17993>

## Bibliography

- Gambin, B., Andrieu-Ponel, V., Medail, F., Marriner, N., Peyron, O., Montade, V., Gambin, T., Morhange, C., Belkacem, D., Djamali, M., 2016. 7300 years of vegetation history and climate for NW Malta: A Holocene perspective. *Clim. Past* 12, 273–297. <https://doi.org/10.5194/cp-12-273-2016>
- Gat, J.R., Dansgaard, W., 1972. Stable isotope survey of the fresh water occurrences in Israel and the Northern Jordan Rift Valley. *J. Hydrol.* [https://doi.org/10.1016/0022-1694\(72\)90052-2](https://doi.org/10.1016/0022-1694(72)90052-2)
- Genty, D., Blamart, D., Ouahdi, R., Gilmour, M., Baker, A., Jouzel, J., Van-Exter, S., 2003. Precise dating of Dansgaard-Oeschger climate oscillations in western Europe from stalagmite data. *Nature.* <https://doi.org/10.1038/nature01391>
- Ghafur, A. a, 2012. Sedimentology and Reservoir Characteristics of the Oligocene-Early Miocene Carbonates ( Kirkuk Group ) of Southern Kurdistan. PhD Thesis.
- Gillieson, D., 2009. The Cave System and Karst. Caves, Wiley Online Books. <https://doi.org/10.1002/9781444313680.ch1>
- Giorgi, F., 2006. Climate change hot-spots. *Geophys. Res. Lett.* 33, 1–4. <https://doi.org/10.1029/2006GL025734>
- Giorgi, F., Lionello, P., 2008. Climate change projections for the Mediterranean region. *Glob. Planet. Change* 63, 90–104. <https://doi.org/10.1016/j.gloplacha.2007.09.005>
- Gleick, P.H., 2014. Water, Drought, Climate Change, and Conflict in Syria. *Weather. Clim. Soc.* 6, 331–340. <https://doi.org/10.1175/WCAS-D-13-00059.1>
- Goede, A., McCulloch, M., McDermott, F., Hawkesworth, C., 1998. Aeolian contribution to strontium and strontium isotope variations in a tasmanian speleothem. *Chem. Geol.* 149, 37–50. [https://doi.org/10.1016/S0009-2541\(98\)00035-7](https://doi.org/10.1016/S0009-2541(98)00035-7)
- Göktürk, O.M., Fleitmann, D., Badertscher, S., Cheng, H., Edwards, R.L., Leuenberger, M., Fankhauser, A., Tüysüz, O., Kramers, J., 2011. Climate on the southern Black Sea coast during the Holocene: Implications from the Sofular Cave record. *Quat. Sci. Rev.* 30, 2433–2445.

## *Bibliography*

<https://doi.org/10.1016/j.quascirev.2011.05.007>

Grant, K.M., Rohling, E.J., Bar-Matthews, M., Ayalon, A., Medina-Elizalde, M., Ramsey, C.B., Satow, C., Roberts, A.P., 2012. Rapid coupling between ice volume and polar temperature over the past 150,000 years. *Nature* 491, 744+.

Guest, E., Al-Rawi, A., 1966. *Flora of Iraq: Volume One: Introduction to the Flora*. Ministry of Agriculture.

Hajar, L., Khater, C., Cheddadi, R., 2008. Vegetation changes during the late Pleistocene and Holocene in Lebanon: A pollen record from the Bekaa Valley. *Holocene* 18, 1089–1099. <https://doi.org/10.1177/0959683608095580>

Hamamin, D.F., Ali, S.S., 2013. Hydrodynamic study of karstic and intergranular aquifers using isotope geochemistry in Basara basin, Sulaimani, North-Eastern Iraq. *Arab. J. Geosci.* 6, 2933–2940. <https://doi.org/10.1007/s12517-012-0572-z>

Hamidi, M., Kavianpour, M.R., Shao, Y., 2013. Synoptic analysis of dust storms in the Middle East. *Asia-Pacific J. Atmos. Sci.* 49, 279–286. <https://doi.org/10.1007/s13143-013-0027-9>

Hasan, S. Al, 2020. Drought ignites tribal conflicts in Southern Iraq [WWW Document]. *Planet Secur. Initiat.* URL <https://www.planetarysecurityinitiative.org/news/drought-ignites-tribal-conflicts-southern-iraq>

Hassan, F., 1981. *Demographic Archaeology*. Academic Press, New York.

Hellstrom, J., Pickering, R., 2015. Recent advances and future prospects of the U-Th and U-Pb chronometers applicable to archaeology. *J. Archaeol. Sci.* 56, 32–40. <https://doi.org/10.1016/j.jas.2015.02.032>

Hellstrom, J.C., McCulloch, M.T., 2000. Multi-proxy constraints on the climatic significance of trace element records from a New Zealand speleothem. *Earth Planet. Sci. Lett.* 179, 287–297. [https://doi.org/10.1016/S0012-821X\(00\)00115-1](https://doi.org/10.1016/S0012-821X(00)00115-1)

Henderson, G.M., 2006. Caving in to new chronologies. *Science* (80-. ). 313, 620–622.

## Bibliography

<https://doi.org/10.1126/science.1128980>

- Hendy, C.H., 1971. The isotopic geochemistry of speleothems—I. The calculation of the effects of different modes of formation on the isotopic composition of speleothems and their applicability as palaeoclimatic indicators. *Geochim. Cosmochim. Acta* 35, 801–824. [https://doi.org/https://doi.org/10.1016/0016-7037\(71\)90127-X](https://doi.org/https://doi.org/10.1016/0016-7037(71)90127-X)
- Hendy, C.H., Wilson, A.T., 1968. Palaeoclimatic data from speleothems. *Nature* 219, 48–51. <https://doi.org/10.1038/219048a0>
- Hennekam, R., 2015. High-frequency climate variability in the late Quaternary eastern Mediterranean Associations of Nile discharge and basin overturning circulation dynamics.
- Hennekam, R., Donders, T.H., Zwiep, K., de Lange, G.J., 2015. Integral view of Holocene precipitation and vegetation changes in the Nile catchment area as inferred from its delta sediments. *Quat. Sci. Rev.* 130, 189–199. <https://doi.org/10.1016/j.quascirev.2015.05.031>
- Hennekam, R., Jilbert, T., Schnetger, B., De Lange, G.J., 2014. Solar forcing of Nile discharge and sapropel S1 formation in the early to middle Holocene eastern Mediterranean. *Paleoceanography* 29, 343–356. <https://doi.org/10.1002/2013PA002553>
- Heydarizad, M., Raeesi, E., Sorí, R., Gimeno, L., 2019. Developing meteoric water lines for Iran based on air masses and moisture sources. *Water (Switzerland)* 11. <https://doi.org/10.3390/w11112359>
- Hoffmann, D.L., Prytulak, J., Richards, D.A., Elliott, T., Coath, C.D., Smart, P.L., Scholz, D., 2007. Procedures for accurate U and Th isotope measurements by high precision MC-ICPMS. *Int. J. Mass Spectrom.* 264, 97–109. <https://doi.org/10.1016/j.ijms.2007.03.020>
- Hofste, R.W., Reig, P., Schleifer, L., 2019. 17 Countries, Home to One-Quarter of the World's Population, Face Extremely High Water Stress [WWW Document]. *World Resour Inst.* URL <https://www.wri.org/blog/2019/08/17-countries-home-one-quarter-world-population-face-extremely-high-water-stress>
- Hojati, S., Khademi, H., Faz Cano, A., Landi, A., 2012. Characteristics of dust deposited along a

## Bibliography

- transect between central Iran and the Zagros Mountains. *Catena* 88, 27–36.  
<https://doi.org/10.1016/j.catena.2011.09.002>
- Holland, H.D., Kirsipu, T. V., Huebner, J.S., Oxburgh, U.M., 1964. On Some Aspects of the Chemical Evolution of Cave Waters. *J. Geol.* 72, 36–67. <https://doi.org/10.1086/626964>
- Horowitz, A., 1974. Preliminary palynological indications as to the climate of Israel during the last 6000 years. *Paléorient* 2, 407–414. <https://doi.org/10.3406/paleo.1974.4867>
- Hu, Y., Huang, H., Zhou, C., 2018. Widening and weakening of the Hadley circulation under global warming. *Sci. Bull.* 63, 640–644. <https://doi.org/10.1016/j.scib.2018.04.020>
- Hurrell, J.W., Deser, C., 2009. North Atlantic climate variability: The role of the North Atlantic Oscillation. *J. Mar. Syst.* 78, 28–41. <https://doi.org/10.1016/j.jmarsys.2008.11.026>
- IPCC, 2019. Summary for Policymakers, in: Shukla, P.R., Skea, J., Buendia, E.C., Masson-Delmotte, V., Pörtner, H.-O., Roberts, D.C., Zhai, P., Slade, R., Connors, S., Diemen, R. van, Ferrat, M., Haughey, E., Luz, S., Neogi, S., Pathak, M., Petzold, J., Pereira, J.P., Vyas, P., Huntley, E., Kissick, K., Belkacemi, M., Malley, J. (Eds.), *Climate Change and Land: An IPCC Special Report on Climate Change, Desertification, Land Degradation, Sustainable Land Management, Food Security, and Greenhouse Gas Fluxes in Terrestrial Ecosystems*. In Press, pp. 1–15.
- IPCC, 2014. *Climate Change 2014: Impacts, Adaptation, and Vulnerability. Part A: Global and Sectoral Aspects. Contribution of Working Group II to the Fifth Assessment Report of the Intergovernmental Panel on Climate Change*. Cambridge University Press.
- IPCC, 2013. Summary for Policymakers, in: Qin, D., Plattner, G.K., Tignor, M., Allen, S.K., Boschung, J., Nauels, A., Xia, Y., Bex, V., Midgley, P.M. (Eds.), *Climate Change 2013: The Physical Science Basis. Contribution of Working Group I to the Fifth Assessment Report of the Intergovernmental Panel on Climate Change*. Cambridge University Press, Cambridge, United Kingdom and New York.
- Isono, D., Yamamoto, M., Irino, T., Oba, T., Murayama, M., Nakamura, T., Kawahata, H., 2009. The 1500-year climate oscillation in the midlatitude North Pacific during the Holocene. *Geology* 37,

## Bibliography

- 591–594. <https://doi.org/10.1130/G25667A.1>
- Joffé, G., 2016. The Impending Water Crisis in the MENA Region. *Int. Spect.* 51, 55–66. <https://doi.org/10.1080/03932729.2016.1198069>
- Johnson, K.R., Hu, C., Belshaw, N.S., Henderson, G.M., 2006. Seasonal trace-element and stable-isotope variations in a Chinese speleothem: The potential for high-resolution paleomonsoon reconstruction. *Earth Planet. Sci. Lett.* 244, 394–407. <https://doi.org/10.1016/j.epsl.2006.01.064>
- Jones, M.D., 2013. Key Questions Regarding the Paleoenvironment of Iran. *Oxford Handb. Anc. Iran* 1–17. <https://doi.org/10.1093/oxfordhb/9780199733309.013.0037>
- Jones, M.D., Abu-Jaber, N., AlShdaifat, A., Baird, D., Cook, B.I., Cuthbert, M.O., Dean, J.R., Djamali, M., Eastwood, W., Fleitmann, D., Haywood, A., Kwiecien, O., Larsen, J., Maher, L.A., Metcalfe, S.E., Parker, A., Petrie, C.A., Primmer, N., Richter, T., Roberts, N., Roe, J., Tindall, J.C., Ünal-İmer, E., Weeks, L., 2019. 20,000 years of societal vulnerability and adaptation to climate change in southwest Asia. *Wiley Interdiscip. Rev. Water* 6, e1330. <https://doi.org/10.1002/wat2.1330>
- Jones, M.D., Roberts, C.N., Leng, M.J., Türkeş, M., 2006. A high-resolution late Holocene lake isotope record from Turkey and links to North Atlantic and monsoon climate. *Geology* 34, 361–364. <https://doi.org/10.1130/G22407.1>
- Jones, M.D., Roberts, N.C., 2008. Interpreting lake isotope records of Holocene environmental change in the Eastern Mediterranean. *Quat. Int.* 181, 32–38. <https://doi.org/10.1016/j.quaint.2007.01.012>
- Jones, P.D., Harris, I., 2008. Climatic Research Unit (CRU) time-series datasets of variations in climate with variations in other phenomena. *NCAS Br. Atmos. Data Cent.* 15.
- Judkins, G., Smith, M., Keys, E., 2008. Determinism within human-environment research and the rediscovery of environmental causation. *Geogr. J.* 174, 17–29. <https://doi.org/10.1111/j.1475-4959.2008.00265.x>
- Kagan, E.J., Agnon, A., Bar-Matthews, M., Ayalon, A., 2005. Dating large infrequent earthquakes by damaged cave deposits. *Geology* 33, 261–264. <https://doi.org/10.1130/G21193.1>

## Bibliography

- Kaniewski, D., Marriner, N., Cheddadi, R., Guiot, Joel, Van, E., Kaniewski, D., Marriner, N., Cheddadi, R., Guiot, Joel, Campo, E. Van, Kaniewski, D., Marriner, N., Cheddadi, R., Guiot, Joël, Campo, E. Van, 2018. The 4.2 kaBP event in the Levant To cite this version : HAL Id : insu-02269672. *Clim. Past* 14.
- Kaufman, A., Wasserburg, G.J., Porcelli, D., Bar-Matthews, M., Ayalon, A., Halicz, L., 1998. U-Th isotope systematics from the Soreq cave, Israel and climatic correlations. *Earth Planet. Sci. Lett.* 156, 141–155. [https://doi.org/10.1016/s0012-821x\(98\)00002-8](https://doi.org/10.1016/s0012-821x(98)00002-8)
- Kehl, M., 2009. Quaternary climate change in iran - the state of knowledge. *Erdkunde* 63, 1–17. <https://doi.org/10.3112/erdkunde.2009.01.01>
- Kennett, D.J., Kennett, J.P., 2006. Early state formation in southern mesopotamia: Sea levels, shorelines, and climate change. *J. Isl. Coast. Archaeol.* 1, 67–99. <https://doi.org/10.1080/15564890600586283>
- Khadiwi, S., 2010. Tectonic evolution and growth of the Zagros Mountain Belt (Fars, Iran): constraints from magnetostratigraphy, sedimentology and low- temperature thermochronometry. PhD Thesis Pierre Marie Curie Univ. 1–242.
- Khalidi, L., Gratuze, B., Boucetta, S., 2009. Provenance of obsidian excavated from late Chalcolithic levels at the sites of Tell Hamoukar and Tell Brak, Syria. *Archaeometry* 51, 879–893. <https://doi.org/10.1111/j.1475-4754.2009.00459.x>
- Kharajiany, S.O., 2014. The Occurrence Of Early And Middle Miocene Rocks (Euphrates, Dhiban And Jeribe Formations) In Ashdagh Mountain, Sangaw Area. *Iraqi Bull. Geol. Min.* 10, 21–39.
- Kim, S.T., O’Neil, J.R., 1997. Equilibrium and nonequilibrium oxygen isotope effects in synthetic carbonates. *Geochim. Cosmochim. Acta* 61, 3461–3475. [https://doi.org/10.1016/S0016-7037\(97\)00169-5](https://doi.org/10.1016/S0016-7037(97)00169-5)
- Kim, S.T., O’Neil, J.R., Hillaire-Marcel, C., Mucci, A., 2007. Oxygen isotope fractionation between synthetic aragonite and water: Influence of temperature and Mg<sup>2+</sup> concentration. *Geochim. Cosmochim. Acta* 71, 4704–4715. <https://doi.org/10.1016/j.gca.2007.04.019>

## Bibliography

- Kintigh, K.W., Altschul, J.H., Beaudry, M.C., Drennan, R.D., Kinzig, A.P., Kohler, T.A., Limp, W.F., Maschner, H.D.G., Michener, W.K., Pauketat, T.R., Peregrine, P., Sabloff, J.A., Wilkinson, T.J., Wright, H.T., Zeder, M.A., 2014a. Grand Challenges for Archaeology. *Am. Antiq.* 79, 5–24. <https://doi.org/10.7183/0002-7316.79.1.5>
- Kintigh, K.W., Altschul, J.H., Beaudry, M.C., Drennan, R.D., Kinzig, A.P., Kohler, T.A., Limp, W.F., Maschner, H.D.G., Michener, W.K., Pauketat, T.R., Peregrine, P., Sabloff, J.A., Wilkinson, T.J., Wright, H.T., Zeder, M.A., 2014b. Grand challenges for archaeology. *Proc. Natl. Acad. Sci. U. S. A.* 111, 879–880. <https://doi.org/10.1073/pnas.1324000111>
- Kohn, M.J., 2010. Carbon isotope compositions of terrestrial C3 plants as indicators of (paleo)ecology and (paleo)climate. *Proc. Natl. Acad. Sci. U. S. A.* 107, 19691–19695. <https://doi.org/10.1073/pnas.1004933107>
- Kolodny, Y., Stein, M., Machlus, M., 2005. Sea-rain-lake relation in the Last Glacial East Mediterranean revealed by  $\delta^{18}\text{O}$ - $\delta^{13}\text{C}$  in Lake Lisan aragonites. *Geochim. Cosmochim. Acta* 69, 4045–4060. <https://doi.org/10.1016/j.gca.2004.11.022>
- Kopanias, K., Macginnis, J., 2016. The Archaeology of the Kurdistan Region of Iraq and Adjacent Regions Edited by Konstantinos Kopanias and. *Archaeopress Archaeology*.
- Kottek, M., Grieser, J., Beck, C., Rudolf, B., Rubel, F., 2006. World map of the Köppen-Geiger climate classification updated. *Meteorol. Zeitschrift* 15, 259–263. <https://doi.org/10.1127/0941-2948/2006/0130>
- Kouchoukos, N., Wilkinson, T., 2007. Landscape Archaeology in Mesopotamia:, in: Stone, E.C. (Ed.), *Settlement and Society, Essays Dedicated to Robert McCormick Adams*. *Cotsen Institute of Archaeology Press at UCLA*, pp. 1–18. <https://doi.org/10.2307/j.ctvdjrjqp.6>
- Kutiel, H., Benaroch, Y., 2002. North Sea-Caspian pattern (NCP) - An upper level atmospheric teleconnection affecting the Eastern Mediterranean: Identification and definition. *Theor. Appl. Climatol.* 71, 17–28. <https://doi.org/10.1007/s704-002-8205-x>
- Kutiel, H., Maheras, P., Türkeş, M., Paz, S., 2002. North Sea - Caspian Pattern (NCP) - An upper level

## Bibliography

- atmospheric teleconnection affecting the eastern Mediterranean - Implications on the regional climate. *Theor. Appl. Climatol.* 72, 173–192. <https://doi.org/10.1007/s00704-002-0674-8>
- Kutzbach, J.E., Chen, G., Cheng, H., Edwards, R.L., Liu, Z., 2014. Potential role of winter rainfall in explaining increased moisture in the Mediterranean and Middle East during periods of maximum orbitally-forced insolation seasonality. *Clim. Dyn.* 42, 1079–1095. <https://doi.org/10.1007/s00382-013-1692-1>
- Lachniet, M.S., 2009. Climatic and environmental controls on speleothem oxygen-isotope values. *Quat. Sci. Rev.* 28, 412–432. <https://doi.org/10.1016/j.quascirev.2008.10.021>
- Lauesen, L.M., 2013. Natural Environment, in: *Encyclopedia of Corporate Social Responsibility*. Springer Berlin Heidelberg, Berlin, Heidelberg, pp. 1734–1742. [https://doi.org/10.1007/978-3-642-28036-8\\_368](https://doi.org/10.1007/978-3-642-28036-8_368)
- Lawrence, D., Bradbury, J., Dunford, R., 2012. Chronology, Uncertainty and GIS: A Methodology for Characterising and Understanding Landscapes of the Ancient Near East. *eTopoi J. Anc. Stud. Special Vo*, 1007–1014.
- Lawrence, D., Palmisano, A., de Gruchy, M.W., 2021. Collapse and continuity: A multi-proxy reconstruction of settlement organization and population trajectories in the Northern Fertile Crescent during the 4.2kya Rapid Climate Change event. *PLoS One* 16, 1–20. <https://doi.org/10.1371/journal.pone.0244871>
- Lawrence, D., Philip, G., Hunt, H., Snape-Kennedy, L., Wilkinson, T.J., 2016. Long term population, city size and climate trends in the Fertile crescent: A first approximation. *PLoS One* 11, 1–16. <https://doi.org/10.1371/journal.pone.0152563>
- Lawrence, D., Wilkinson, T.J., 2015. Hubs and upstarts: pathways to urbanism in the northern Fertile Crescent. *Antiquity* 89, 328–344. <https://doi.org/10.15184/aqy.2014.44>
- Lawrence Edwards, R., Chen, J.H., Wasserburg, G.J., 1987. <sup>238</sup>U/<sup>234</sup>U/<sup>230</sup>Th/<sup>232</sup>Th systematics and the precise measurement of time over the past 500,000 years. *Earth Planet. Sci. Lett.* 81, 175–192. [https://doi.org/10.1016/0012-821X\(87\)90154-3](https://doi.org/10.1016/0012-821X(87)90154-3)

## Bibliography

- Le Garzic, E., Vergés, J., Sapin, F., Saura, E., Meresse, F., Ringenbach, J.C., 2019. Evolution of the NW Zagros Fold-and-Thrust Belt in Kurdistan Region of Iraq from balanced and restored crustal-scale sections and forward modeling. *J. Struct. Geol.* 124, 51–69. <https://doi.org/10.1016/j.jsg.2019.04.006>
- Lechleitner, F.A., Fohlmeister, J., McIntyre, C., Baldini, L.M., Jamieson, R.A., Hercman, H., Gasiorowski, M., Pawlak, J., Stefaniak, K., Socha, P., Eglinton, T.I., Baldini, J.U.L., 2016. A novel approach for construction of radiocarbon-based chronologies for speleothems. *Quat. Geochronol.* 35, 54–66. <https://doi.org/10.1016/j.quageo.2016.05.006>
- Lemcke, G., Sturm, M., 1997.  $\delta^{18}\text{O}$  and trace element measurements as proxy for the reconstruction of climate changes at Lake Van (Turkey): Preliminary results, in: *Third Millennium BC Climate Change and Old World Collapse*. Springer, pp. 653–678.
- Leng, M.J., Marshall, J.D., 2004. Palaeoclimate interpretation of stable isotope data from lake sediment archives. *Quat. Sci. Rev.* 23, 811–831. <https://doi.org/10.1016/j.quascirev.2003.06.012>
- Lewis, S.L., Maslin, M.A., 2015. Defining the Anthropocene. *Nature* 519, 171–180. <https://doi.org/10.1038/nature14258>
- Lionello, P., Bhend, J., Buzzi, A., Della-Marta, P.M., Krichak, S.O., Jansà, A., Maheras, P., Sanna, A., Trigo, I.F., Trigo, R., 2006. Chapter 6 Cyclones in the Mediterranean region: Climatology and effects on the environment, in: Lionello, P., Malanotte-Rizzoli, P., Boscolo, R.B.T.-D. in E. and E.S. (Eds.), *Mediterranean*. Elsevier, pp. 325–372. [https://doi.org/https://doi.org/10.1016/S1571-9197\(06\)80009-1](https://doi.org/https://doi.org/10.1016/S1571-9197(06)80009-1)
- Litt, T., Ohlwein, C., Neumann, F.H., Hense, A., Stein, M., 2012. Holocene climate variability in the Levant from the Dead Sea pollen record. *Quat. Sci. Rev.* 49, 95–105. <https://doi.org/10.1016/j.quascirev.2012.06.012>
- Liu, Y.H., Henderson, G.M., Hu, C.Y., Mason, A.J., Charnley, N., Johnson, K.R., Xie, S.C., 2013. Links between the East Asian monsoon and North Atlantic climate during the 8,200 year event. *Nat. Geosci.* 6, 117–120. <https://doi.org/10.1038/ngeo1708>

## *Bibliography*

- Liverani, M., 2006. Uruk: the first city. Equinox Publishing Limited.
- López-Moreno, J.I., Vicente-Serrano, S.M., Morán-Tejeda, E., Lorenzo-Lacruz, J., Kenawy, A., Beniston, M., 2011. Effects of the North Atlantic Oscillation (NAO) on combined temperature and precipitation winter modes in the Mediterranean mountains: Observed relationships and projections for the 21st century. *Glob. Planet. Change* 77, 62–76. <https://doi.org/10.1016/j.gloplacha.2011.03.003>
- Ludwig, K.R., 2003. A Geochronological Toolkit for Microsoft Excel. Berkeley Geochronol. Center, Spec. Publ. 4, 71.
- Luterbacher, J., Dietrich, D., Xoplaki, E., Grosjean, M., Wanner, H., 2004. European Seasonal and Annual Temperature Variability, Trends, and Extremes since 1500. *Science* (80-. ). 303, 1499–1503. <https://doi.org/10.1126/science.1093877>
- Luterbacher, J., Xoplaki, E., 2003. 500-year Winter Temperature and Precipitation Variability over the Mediterranean area and its Connection to the Large-scale Atmospheric Circulation. *Mediterr. Clim. - Var. Trends* 133–153. [https://doi.org/10.1007/978-3-642-55657-9\\_7](https://doi.org/10.1007/978-3-642-55657-9_7)
- Lyonnet, B., 1996. Settlement pattern in the Upper Khabur (NE Syria), from the Achaemenids to the Abbasid period: methods and preliminary results from a survey, in: *Continuity and Change in Northern Mesopotamia from the Hellenistic to the Early Islamic Period*. Dietrich Reimer Verlag Berlin, pp. 349–354.
- Maher, L.A., Banning, E.B., Chazan, M., 2011. Oasis or mirage? Assessing the role of abrupt climate change in the prehistory of the southern Levant. *Cambridge Archaeol. J.* 21, 1–29. <https://doi.org/10.1017/S0959774311000011>
- Mallowan, M.E.L., 1947. Excavations at Brak and Chagar Bazar. *Iraq* 9, 1. <https://doi.org/10.2307/4199532>
- Manning, S.W., Höflmayer, F., Moeller, N., Dee, M.W., Ramsey, C.B., Fleitmann, D., Higham, T., Kutschera, W., Wild, E.M., 2014. Dating the Thera (Santorini) eruption: Archaeological and scientific evidence supporting a high chronology. *Antiquity* 88, 1164–1179. 258

## Bibliography

<https://doi.org/10.1017/S0003598X00115388>

- Marsh, A., Fleitmann, D., Al-Manmi, D.A.M., Altaweel, M., Wengrow, D., Carter, R., 2018. Mid- to late-Holocene archaeology, environment and climate in the northeast Kurdistan region of Iraq. *Holocene* 28, 955–967. <https://doi.org/10.1177/0959683617752843>
- Matthews, A., Ayalon, A., Bar-Matthews, M., 2000. D/H ratios of fluid inclusions of Soreq cave (Israel) speleothems as a guide to the Eastern Mediterranean Meteoric Line relationships in the last 120 ky. *Chem. Geol.* 166, 183–191. [https://doi.org/10.1016/S0009-2541\(99\)00192-8](https://doi.org/10.1016/S0009-2541(99)00192-8)
- Matthews, R., 2003. Excavations at Tell Brak. Vol. 4, Exploring an Upper Mesopotamian regional centre, 1994-1996. Cambridge : McDonald Institute for Archaeological Research; London.
- Matthews, R., Matthews, W., Raheem, K.R., Richardson, A., 2020a. The Early Neolithic of the Eastern Fertile Crescent: Excavations at Bestansur and Shimshara, Iraqi Kurdistan. Oxbow Books.
- Matthews, R., Nashli, H.F., 2013. The neolithisation of Iran. Oxbow Books.
- Matthews, R., Rasheed, Q.H., Palmero Fernández, M., Fobbe, S., Nováček, K., Mohammed-Amin, R., Mühl, S., Richardson, A., 2020b. Heritage and cultural healing: Iraq in a post-Daesh era. *Int. J. Herit. Stud.* 26, 120–141. <https://doi.org/10.1080/13527258.2019.1608585>
- Mayewski, P.A., Rohling, E.E., Stager, J.C., Karlén, W., Maasch, K.A., Meeker, L.D., Meyerson, E.A., Gasse, F., van Kreveld, S., Holmgren, K., Lee-Thorp, J., Rosqvist, G., Rack, F., Staubwasser, M., Schneider, R.R., Steig, E.J., 2004. Holocene climate variability. *Quat. Res.* <https://doi.org/10.1016/j.yqres.2004.07.001>
- McDermott, F., 2004. Palaeo-climate reconstruction from stable isotope variations in speleothems: A review. *Quat. Sci. Rev.* 23, 901–918. <https://doi.org/10.1016/j.quascirev.2003.06.021>
- McDermott, F., Atkinson, T.C., Fairchild, I.J., Baldini, L.M., Matthey, D.P., 2011. A first evaluation of the spatial gradients in  $\delta^{18}\text{O}$  recorded by European Holocene speleothems. *Glob. Planet. Change* 79, 275–287. <https://doi.org/10.1016/j.gloplacha.2011.01.005>
- McMahon, A., 2019. Early Urbanism in Northern Mesopotamia, *Journal of Archaeological Research*.

## Bibliography

- Springer US. <https://doi.org/10.1007/s10814-019-09136-7>
- McMahon, A., 2012. The Akkadian Period: Empire, Environment, and Imagination. A Companion to Archaeol. Anc. Near East, Wiley Online Books. <https://doi.org/doi:10.1002/9781444360790.ch34>
- McMahon, A., Oates, J., Al-Quntar, S., Charles, M., Colantoni, C., Hald, M.M., Karsgaard, P., Khalidi, L., Soltysiak, A., Stone, A., Weber, J., 2007. Excavations at Tell Brak 2006–2007. *Iraq* 69, 145–171. <https://doi.org/10.1017/s0021088900001091>
- McMillan, E.A., Fairchild, I.J., Frisia, S., Borsato, A., McDermott, F., 2005. Annual trace element cycles in calcite-aragonite speleothems: Evidence of drought in the western Mediterranean 1200–1100 yr BP. *J. Quat. Sci.* 20, 423–433. <https://doi.org/10.1002/jqs.943>
- Meckler, A.N., Affolter, S., Dublyansky, Y. V., Krüger, Y., Vogel, N., Bernasconi, S.M., Frenz, M., Kipfer, R., Leuenberger, M., Spötl, C., Carolin, S., Cobb, K.M., Moerman, J., Adkins, J.F., Fleitmann, D., 2015. Glacial–interglacial temperature change in the tropical West Pacific: A comparison of stalagmite-based paleo-thermometers. *Quat. Sci. Rev.* 127, 90–116. <https://doi.org/10.1016/j.quascirev.2015.06.015>
- Meijer, D.J.W., 1986. A survey in northeastern Syria. *Nederlands Histor.-Archaeolog. Institution te Istanbul*.
- Menze, B.H., Ur, J.A., 2012. Mapping patterns of long-term settlement in Northern Mesopotamia at a large scale. *Proc. Natl. Acad. Sci. U. S. A.* 109. <https://doi.org/10.1073/pnas.1115472109>
- Mickler, P.J., Stern, L.A., Banner, J.L., 2006. Large kinetic isotope effects in modern speleothems. *GSA Bull.* 118, 65–81. <https://doi.org/10.1130/B25698.1>
- Migowski, C., Stein, M., Prasad, S., Negendank, J.F.W., Agnon, A., 2006. Holocene Climate Variability and Cultural Evolution in the Near East from the Dead Sea Sedimentary Record. *Quat. Res.* 66, 421–431. [https://doi.org/DOI: 10.1016/j.yqres.2006.06.010](https://doi.org/DOI:10.1016/j.yqres.2006.06.010)
- Miller, K.G., Feigenson, M.D., Kent, D. V., Olsson, R.K., 1988. Upper Eocene to Oligocene isotope ( $\delta^{87}\text{Sr}/\delta^{86}\text{Sr}$ ,  $\delta^{18}\text{O}$ ,  $\delta^{13}\text{C}$ ) standard section, Deep Sea Drilling Project Site 522.

## Bibliography

- Paleoceanography 3, 223–233. <https://doi.org/10.1029/PA003i002p00223>
- Mischel, S.A., Scholz, D., Spötl, C., Jochum, K.P., Schröder-Ritzrau, A., Fiedler, S., 2017. Holocene climate variability in Central Germany and a potential link to the polar North Atlantic: A replicated record from three coeval speleothems. *Holocene* 27, 509–525. <https://doi.org/10.1177/0959683616670246>
- Mithen, S., Black, E. (Eds.), 2011. *Water, Life and Civilisation*. Cambridge University Press, Cambridge. <https://doi.org/10.1017/CBO9780511975219>
- Moore, G., 1952. Speleothem — a new cave term. *Natl. Speleol. Soc. Am. News* 10, 2.
- Müller, J., 2015. Eight Million Neolithic Europeans: Social Demography and Social Archaeology On The Scope Of Change – From The Near East To Scandinavia. *Paradig. Found Archaeol. Theory – Present. Past Futur. Essays Honour Evžen Neustupný* 200–214.
- Musgrove, M.L., Banner, J.L., 2004. Controls on the spatial and temporal variability of vadose dripwater geochemistry: Edwards aquifer, central Texas. *Geochim. Cosmochim. Acta* 68, 1007–1020. <https://doi.org/10.1016/j.gca.2003.08.014>
- Mustafa, O., Merkel, B., Weise, S.M., 2015. Assessment of Hydrogeochemistry and Environmental Isotopes in Karst Springs of Makook Anticline, Kurdistan Region, Iraq 48–68. <https://doi.org/10.3390/hydrology2020048>
- Mustafa, O., Tichomirowa, M., Kummer, N.-A.A., Merkel, B., 2016. Assessment of water-rock interaction processes in the Karst Springs of Makook Anticline (Kurdistan Region, Iraq) using Sr-isotopes, rare earth, and trace elements. *Arab. J. Geosci.* 9. <https://doi.org/10.1007/s12517-016-2344-7>
- Nabavi, S.O., Haimberger, L., Samimi, C., 2016. Climatology of dust distribution over West Asia from homogenized remote sensing data. *Aeolian Res.* 21, 93–107. <https://doi.org/10.1016/j.aeolia.2016.04.002>
- Nabih, B., 2018. Basra was once a jewel of a city. Now it's a symbol of what's wrong in Iraq. *Los*

## Bibliography

Angeles Times.

Niklewski, J., Van Zeist, W., 1970. A Late Quaternary Pollen Diagram from Northwestern Syria. *Acta Bot. Neerl.* 19, 737–754. <https://doi.org/10.1111/j.1438-8677.1970.tb00176.x>

NOAA, 2020. State of the Climate: Global Climate Report for Annual 2019 [WWW Document]. NOAA Natl. Centers Environ. Inf. URL <https://www.ncdc.noaa.gov/sotc/global/201913> (accessed 1.1.21).

O'Neil, J.R., Clayton, R.N., Mayeda, T.K., 1969. Oxygen Isotope Fractionation in Divalent Metal Carbonates. *J. Chem. Phys.* 51, 5547–5558. <https://doi.org/10.1063/1.1671982>

Oates, J., McMahon, A., Karsgaard, P., Quntar, S. Al, Ur, J., 2007. Early Mesopotamian urbanism: A new view from the north. *Antiquity* 81, 585–600. <https://doi.org/10.1017/S0003598X00095600>

Olsen, J., Anderson, N.J., Knudsen, M.F., 2012. Variability of the North Atlantic Oscillation over the past 5,200 years. *Nat. Geosci.* 5, 808–812. <https://doi.org/10.1038/ngeo1589>

Ön, Z.B., Akçer-Ön, S., Özeren, M.S., Eriş, K.K., Greaves, A.M., Çağatay, M.N., Bora, Z., On, €., Akçer, S., On, -€, Sinan, M., Ozeren, €, Eri, K.K., Greaves, A.M., Namık, M., Gatay, Ç., Ön, Z.B., Eriş, K.K., Akçer-Ön, S., Greaves, A.M., Çağatay, M.N., Özeren, M.S., 2017. Climate proxies for the last 17.3 ka from Lake Hazar (Eastern Anatolia), extracted by independent component analysis of  $\mu$ -XRF data. *Quat. Int.* 486, 17–28. <https://doi.org/10.1016/j.quaint.2017.08.066>

Oster, J.L., Montañez, I.P., Guilderson, T.P., Sharp, W.D., Banner, J.L., 2010. Modeling speleothem  $\delta^{13}\text{C}$  variability in a central Sierra Nevada cave using  $^{14}\text{C}$  and  $^{87}\text{Sr}/^{86}\text{Sr}$ . *Geochim. Cosmochim. Acta* 74, 5228–5242. <https://doi.org/10.1016/j.gca.2010.06.030>

Owen, R.A., Day, C.C., Hu, C.Y., Liu, Y.H., Pointing, M.D., Blättler, C.L., Henderson, G.M., 2016. Calcium isotopes in caves as a proxy for aridity: Modern calibration and application to the 8.2 kyr event. *Earth Planet. Sci. Lett.* 443, 129–138. <https://doi.org/10.1016/j.epsl.2016.03.027>

Palchan, D., Erel, Y., Stein, M., 2019. Mobilization of fine detritus to the Dead Sea Basin during the late glacial and early Holocene. *Quat. Sci. Rev.* 218, 395–405.

## Bibliography

- <https://doi.org/10.1016/j.quascirev.2019.05.028>
- Palmisano, A., Bevan, A., Shennan, S., 2017. Comparing archaeological proxies for long-term population patterns: An example from central Italy. *J. Archaeol. Sci.* 87, 59–72. <https://doi.org/10.1016/j.jas.2017.10.001>
- Palmisano, A., Lawrence, D., de Gruchy, M.W., Bevan, A., Shennan, S., 2021. Holocene regional population dynamics and climatic trends in the Near East: A first comparison using archaeo-demographic proxies. *Quat. Sci. Rev.* 252, 106739. <https://doi.org/10.1016/j.quascirev.2020.106739>
- Palmisano, A., Woodbridge, J., Roberts, N., Bevan, A., 2019. *For Pre R.* <https://doi.org/10.1177/0959683619826642>
- Pantaléon-Cano, J., Yll, E.I., Pérez-Obiol, R., Roure, J.M., 2003. Palynological evidence for vegetational history in semi-arid areas of the western Mediterranean (Almería, Spain). *Holocene* 13, 109–119. <https://doi.org/10.1191/0959683603hl598rp>
- Pike, A.W.G., Hoffmann, D.L., García-Diez, M., Pettitt, P.B., Alcolea, J., De Balbín, R., González-Sainz, C., De Las Heras, C., Lasheras, J.A., Montes, R., Zilhão, J., 2012. U-series dating of paleolithic art in 11 caves in Spain. *Science* (80-. ). 336, 1409–1413. <https://doi.org/10.1126/science.1219957>
- Proctor, C.J., Baker, A., Barnes, W.L., Gilmour, M.A., 2000. A thousand year speleothem proxy record of North Atlantic climate from Scotland. *Clim. Dyn.* 16, 815–820. <https://doi.org/10.1007/s003820000077>
- Railsback, L.B., Brook, G.A., Jian Chen, Kalin, R., Fleisher, C.J., 1994. Environmental controls on the petrology of a late Holocene speleothem from Botswana with annual layers of aragonite and calcite. *J. Sediment. Res. A Sediment. Petrol. Process.* 64 A, 147–155. <https://doi.org/10.1306/d4267d39-2b26-11d7-8648000102c1865d>
- Ramsey, C.B., 2017. Methods for Summarizing Radiocarbon Datasets. *Radiocarbon* 59, 1809–1833. <https://doi.org/10.1017/RDC.2017.108>

## Bibliography

- Ramsey, C.B., 2009. Bayesian analysis of radiocarbon dates. *Radiocarbon* 51, 337–360.  
<https://doi.org/10.1017/s0033822200033865>
- Rasmussen, S.O., Bigler, M., Blockley, S.P., Blunier, T., Buchardt, S.L., Clausen, H.B., Cvijanovic, I., Dahl-Jensen, D., Johnsen, S.J., Fischer, H., Gkinis, V., Guillevic, M., Hoek, W.Z., Lowe, J.J., Pedro, J.B., Popp, T., Seierstad, I.K., Steffensen, J.P., Svensson, A.M., Vallelonga, P., Vinther, B.M., Walker, M.J.C., Wheatley, J.J., Winstrup, M., 2014. A stratigraphic framework for abrupt climatic changes during the Last Glacial period based on three synchronized Greenland ice-core records: Refining and extending the INTIMATE event stratigraphy. *Quat. Sci. Rev.* 106, 14–28.  
<https://doi.org/10.1016/j.quascirev.2014.09.007>
- Regattieri, E., Zanchetta, G., Drysdale, R.N., Isola, I., Hellstrom, J.C., Dallai, L., 2014. Lateglacial to Holocene trace element record (Ba, Mg, Sr) from Corchia Cave (Apuan Alps, central Italy): Paleoenvironmental implications. *J. Quat. Sci.* 29, 381–392. <https://doi.org/10.1002/jqs.2712>
- Reuter, J., Buening, N., Yoshimura, K., 2018. Evaluating hydrological influences on mid-latitude  $\delta^{18}\text{O}$  in the Middle East. *Clim. Dyn.* 50, 3153–3170. <https://doi.org/10.1007/s00382-017-3798-3>
- Richards, D.A., Dorale, J.A., 2003. Uranium-series Chronology and Environmental Applications of Speleothems. *Rev. Mineral. Geochemistry* 52, 407–460. <https://doi.org/10.2113/0520407>
- Richerson, P., Boyd, R., Bettinger, R., 2001. Was Agriculture Impossible during the Pleistocene but Mandatory during the Holocene? A Climate Change Hypothesis Author (s): Peter J. Richerson, Robert Boyd and Robert L. Bettinger Published by: Cambridge University Press Stable URL: <http://www.js. Am. Antiq. 66, 387–411>.
- Rick, J.W., 1987. Dates as Data: An Examination of the Peruvian Pre-ceramic Radiocarbon Record. *Am. Antiq.* 52, 55. <https://doi.org/10.2307/281060>
- Riehl, S., 2008. Climate and agriculture in the ancient Near East: A synthesis of the archaeobotanical and stable carbon isotope evidence. *Veg. Hist. Archaeobot.* 17, 43–51.  
<https://doi.org/10.1007/s00334-008-0156-8>

## *Bibliography*

- Riehl, S., Pustovoytov, K., Dornauer, A., Sallaberger, W., 2012. Mid-to-late Holocene agricultural system transformations in the northern Fertile Crescent: A review of the archaeobotanical, geoarchaeological, and philological evidence. *Geophys. Monogr. Ser.* 198, 115–136. <https://doi.org/10.1029/2012GM001221>
- Riehl, S., Zeidi, M., Conard, N.J., 2013. Emergence of Agriculture in the Foothills of the Zagros Mountains of Iran. *Science* (80-. ). 341, 65–67. <https://doi.org/10.1126/science.1236743>
- Roberts, M.S., Smart, P.L., Baker, A., 1998. Annual trace element variations in a Holocene speleothem. *Earth Planet. Sci. Lett.* 154, 237–246. [https://doi.org/10.1016/s0012-821x\(97\)00116-7](https://doi.org/10.1016/s0012-821x(97)00116-7)
- Roberts, N., 2014. *The Holocene: An Environmental History*. John Wiley & Sons, Incorporated, Hoboken, UNITED KINGDOM.
- Roberts, N., 2002. Did prehistoric landscape management retard the post-glacial spread of woodla ... *Library (Lond)*. 76, 1002–1010. <https://doi.org/10.1017/S0003598X0009181X>
- Roberts, N., Allcock, S.L., Arnaud, F., Dean, J.R., Eastwood, W.J., Jones, M.D., Leng, M.J., Metcalfe, S.E., Malet, E., Woodbridge, J., Yiğitbaşıoğlu, H., 2016. A tale of two lakes: a multi-proxy comparison of Lateglacial and Holocene environmental change in Cappadocia, Turkey. *J. Quat. Sci.* 31, 348–362. <https://doi.org/10.1002/jqs.2852>
- Roberts, N., Eastwood, W.J., Kuzucuoğlu, C., Fiorentino, G., Caracuta, V., 2011. Climatic, vegetation and cultural change in the eastern mediterranean during the mid-holocene environmental transition. *Holocene* 21, 147–162. <https://doi.org/10.1177/0959683610386819>
- Roberts, N., Moreno, A., Valero-Garcés, B.L., Corella, J.P., Jones, M., Allcock, S., Woodbridge, J., Morellón, M., Luterbacher, J., Xoplaki, E., Türkeş, M., 2012. Palaeolimnological evidence for an east-west climate see-saw in the Mediterranean since AD 900. *Glob. Planet. Change* 84–85, 23–34. <https://doi.org/10.1016/j.gloplacha.2011.11.002>
- Roberts, N., Reed, J.M., Leng, M.J., Kuzucuoğlu, C., Fontugne, M., Bertaux, J., Woldring, H., Bottema, S., Black, S., Hunt, E., Karabiyikoğlu, M., 2001. The tempo of Holocene climatic change in the eastern Mediterranean region: New high-resolution crater-lake sediment data from central Turkey.

## *Bibliography*

- Holocene 11, 721–736. <https://doi.org/10.1191/09596830195744>
- Roberts, N., Stevenson, T., Davis, B., Cheddadi, R., Brewster, S., Rosen, A., 2004. Holocene climate, environment and cultural change in the circum-Mediterranean region BT - Past Climate Variability through Europe and Africa, in: Battarbee, R.W., Gasse, F., Stickley, C.E. (Eds.), . Springer Netherlands, Dordrecht, pp. 343–362. [https://doi.org/10.1007/978-1-4020-2121-3\\_17](https://doi.org/10.1007/978-1-4020-2121-3_17)
- Roberts, N., Woodbridge, J., Bevan, A., Palmisano, A., Shennan, S., Asouti, E., 2017. Human responses and non-responses to climatic variations during the last Glacial-Interglacial transition in the eastern Mediterranean. *Quat. Sci. Rev.* 1–21. <https://doi.org/10.1016/j.quascirev.2017.09.011>
- Roberts, N., Wright, H.E., 1993. Vegetational, lake-level, and climatic history of the Near East and Southwest Asia, in: *Global Climates since the Last Glacial Maximum*. University of Minnesota Press, pp. 194–220.
- Robinson, S.A., Black, S., Sellwood, B.W., Valdes, P.J., 2006. A review of palaeoclimates and palaeoenvironments in the Levant and Eastern Mediterranean from 25,000 to 5000 years BP: setting the environmental background for the evolution of human civilisation. *Quat. Sci. Rev.* 25, 1517–1541. <https://doi.org/10.1016/j.quascirev.2006.02.006>
- Rodwell, M.J., Hoskins, B.J., 2001. Subtropical anticyclones and summer monsoons. *J. Clim.* [https://doi.org/10.1175/1520-0442\(2001\)014<3192:SAASM>2.0.CO;2](https://doi.org/10.1175/1520-0442(2001)014<3192:SAASM>2.0.CO;2)
- Rogerson, M., Dublyansky, Y., Hoffmann, D.L., Luetscher, M., Spötl, C., Töchterle, P., 2018. Enhanced Mediterranean water cycle explains increased humidity during MIS 3 in North Africa. *Clim. Past Discuss.* 1–31. <https://doi.org/10.5194/cp-2018-134>
- Rohling, E.J., De Rijk, S., 1999. Holocene climate optimum and last glacial maximum in the Mediterranean: The marine oxygen isotope record. *Mar. Geol.* 153, 57–75. [https://doi.org/10.1016/S0025-3227\(98\)00020-6](https://doi.org/10.1016/S0025-3227(98)00020-6)
- Rohling, E.J., Grant, K.M., Roberts, A.P., Larrasoaña, J.-C., 2013. Paleoclimate Variability in the Mediterranean and Red Sea Regions during the Last 500,000 Years. *Curr. Anthropol.* 54, S183–S201. <https://doi.org/10.1086/673882>

## *Bibliography*

- Rohling, E.J., Marino, G., Grant, K.M., 2015. Mediterranean climate and oceanography, and the periodic development of anoxic events (sapropels). *Earth-Science Rev.* 143, 62–97. <https://doi.org/10.1016/j.earscirev.2015.01.008>
- Rohling, E.J., Marino, G., Grant, K.M., Mayewski, P.A., Wening, B., 2019. A model for archaeologically relevant Holocene climate impacts in the Aegean-Levantine region (easternmost Mediterranean). *Quat. Sci. Rev.* 208, 38–53. <https://doi.org/10.1016/j.quascirev.2019.02.009>
- Rohling, E.J., Pälike, H., 2005. Centennial-scale climate cooling with a sudden cold event around 8,200 years ago. *Nature*. <https://doi.org/10.1038/nature03421>
- Rosignol-Strick, M., 1995. Sea-land correlation of pollen records in the Eastern Mediterranean for the glacial-interglacial transition: Biostratigraphy versus radiometric time-scale. *Quat. Sci. Rev.* 14, 893–915. [https://doi.org/https://doi.org/10.1016/0277-3791\(95\)00070-4](https://doi.org/https://doi.org/10.1016/0277-3791(95)00070-4)
- Rothman, M.S., 2004. Studying the development of complex society: Mesopotamia in the late fifth and fourth millennia BC. *J. Archaeol. Res.* 12, 75–119. <https://doi.org/10.1023/B:JARE.0000016695.21169.37>
- Rothman, M.S., Peasnell, B., 2002. *Tepe Gawra: The Evolution of a Small Prehistoric Center in Northern Iraq*. University Museum Publications, Philadelphia.
- Rozanski, K., Araguás-Araguás, L., Gonfiantini, R., 1993. Isotopic Patterns in Modern Global Precipitation. *Clim. Chang. Cont. Isot. Rec.*, Geophysical Monograph Series 1–36. <https://doi.org/doi:10.1029/GM078p0001>
- Rutledge, H., Baker, A., Marjo, C.E., Andersen, M.S., Graham, P.W., Cuthbert, M.O., Rau, G.C., Roshan, H., Markowska, M., Mariethoz, G., Jex, C.N., 2014. Dripwater organic matter and trace element geochemistry in a semi-arid karst environment: Implications for speleothem paleoclimatology. *Geochim. Cosmochim. Acta* 135, 217–230. <https://doi.org/10.1016/j.gca.2014.03.036>
- Saaroni, H., Bitan, A., Alpert, P., Ziv, B., 1996. Continental polar outbreaks into the levant and eastern mediterranean. *Int. J. Climatol.* 16, 1175–1191. [https://doi.org/10.1002/\(SICI\)1097-](https://doi.org/10.1002/(SICI)1097-267)

## Bibliography

0088(199610)16:10<1175::AID-JOC79>3.0.CO;2-#

- Saaroni, H., Halfon, N., Ziv, B., Alpert, P., Kutiel, H., 2010. Links between the rainfall regime in Israel and location and intensity of Cyprus lows. *Int. J. Climatol.* 30, 1014–1025. <https://doi.org/10.1002/joc.1912>
- Sadori, L., Narcisi, B., 2001. The Postglacial record of environmental history from Lago di Pergusa, Sicily. *Holocene* 11, 655–670. <https://doi.org/10.1191/09596830195681>
- Salomons, W., Mook, W.G., 1986. Isotope Geochemistry of Carbonates in the Weathering Zone, in: *The Terrestrial Environment*, B. Elsevier, pp. 239–269. <https://doi.org/10.1016/B978-0-444-42225-5.50011-5>
- Schwab, M.J., Neumann, F., Litt, T., Negendank, J.F.W., Stein, M., 2004. Holocene palaeoecology of the Golan Heights (Near East): Investigation of lacustrine sediments from Birkat Ram crater lake. *Quat. Sci. Rev.* 23, 1723–1731. <https://doi.org/10.1016/j.quascirev.2004.05.001>
- Schwarcz, H.P., Blackwell, B.A., 1992. *Archaeological applications*. Clarendon Press, United Kingdom.
- Seither, A., 2016. Isotopic and geomicrobial investigation of darzila karst cave, NE Iraq. *FOG - Freib. Online Geosci.* 45, 1–150.
- Sharifi, A., Pourmand, A., Canuel, E.A., Ferer-Tyler, E., Peterson, L.C., Aichner, B., Feakins, S.J., Daryaee, T., Djamali, M., Beni, A.N., Lahijani, H.A.K., Swart, P.K., 2015. Abrupt climate variability since the last deglaciation based on a high-resolution, multi-proxy peat record from NW Iran: The hand that rocked the Cradle of Civilization? *Quat. Sci. Rev.* 123, 215–230. <https://doi.org/10.1016/j.quascirev.2015.07.006>
- Sharp, Z., 2007. *Principles of Stable Isotope Geochemistry*. Pearson/Prentice Hall.
- Shennan, S., 2000. Population, culture history, and the dynamics of culture change. *Curr. Anthropol.* 41, 811–835. <https://doi.org/10.1086/317403>
- Shennan, S., Downey, S.S., Timpson, A., Edinborough, K., Colledge, S., Kerig, T., Manning, K.,

## *Bibliography*

- Thomas, M.G., 2013. Regional population collapse followed initial agriculture booms in mid-Holocene Europe. *Nat. Commun.* 4, 31–34. <https://doi.org/10.1038/ncomms3486>
- Simpson, I.R., Seager, R., Shaw, T.A., Ting, M., 2015. Mediterranean summer climate and the importance of middle east topography. *J. Clim.* 28, 1977–1996. <https://doi.org/10.1175/JCLI-D-14-00298.1>
- Sinclair, D.J., Banner, J.L., Taylor, F.W., Partin, J., Jenson, J., Mylroie, J., Goddard, E., Quinn, T., Jocsos, J., Miklavič, B., 2012. Magnesium and strontium systematics in tropical speleothems from the Western Pacific. *Chem. Geol.* 294–295, 1–17. <https://doi.org/10.1016/j.chemgeo.2011.10.008>
- Sinha, A., Kathayat, G., Weiss, H., Li, H., Cheng, H., Reuter, J., Schneider, A.W., Berkelhammer, M., Adali, S.F., Stott, L.D., Edwards, R.L., 2019. Role of climate in the rise and fall of the Neo-Assyrian Empire 1, 1–11. <https://doi.org/10.1126/sciadv.aax6656>
- Smith, A.C., Wynn, P.M., Barker, P.A., Leng, M.J., Noble, S.R., Tych, W., 2016. North Atlantic forcing of moisture delivery to Europe throughout the Holocene. *Sci. Rep.* 6, 1–7. <https://doi.org/10.1038/srep24745>
- Snyder, J.A., Wasyluk, K., Fritz, S.C., Wright, J., 2001. Diatom-based conductivity reconstruction and palaeoclimatic interpretation of a 40-ka record from Lake Zeribar, Iran. *Holocene* 11, 737–745. <https://doi.org/10.1191/09596830195753>
- Stanton, T., 2004. Concepts of Determinism and Free Will in Archaeology. *An. Antropol.* 38, 29–83.
- Staubwasser, M., Weiss, H., 2006. Holocene climate and cultural evolution in late prehistoric-early historic West Asia. *Quat. Res.* 66, 372–387. <https://doi.org/10.1016/j.yqres.2006.09.001>
- Stein, G., Wattenmaker, P., Miller, N., 1990. The 1987 Tell Leilan regional survey: preliminary report. *Econ. Settl. Near East Anal. Anc. sites Mater.* 7.
- Stein, G.J., Wattenmaker, P., 2003. Settlement trends and the emergence of social complexity in the Leilan region of the Habur plains (Syria) from the fourth to the third millennium BC. *Orig. north Mesopotamian Civiliz. Ninevite* 5, 361–386.

## Bibliography

- Steiner, M.L., Killebrew, A.E., 2014. *The Oxford Handbook of the Archaeology of the Levant: c. 8000-332 BCE*. Oxford University Press.
- Steinhilber, F., Abreu, J.A., Beer, J., Brunner, I., Christl, M., Fischer, H., Heikkilä, U., Kubik, P.W., Mann, M., McCracken, K.G., Miller, H., Miyahara, H., Oerter, H., Wilhelms, F., 2012. 9,400 Years of cosmic radiation and solar activity from ice cores and tree rings. *Proc. Natl. Acad. Sci. U. S. A.* 109, 5967–5971. <https://doi.org/10.1073/pnas.1118965109>
- Steinhilber, F., Beer, J., Fröhlich, C., 2009. Total solar irradiance during the Holocene. *Geophys. Res. Lett.* 36, 1–5. <https://doi.org/10.1029/2009GL040142>
- Stevanović, Z., Iurkiewicz, A., Maran, A., 2009. New Insights into Karsts and Caves of Northwestern Zagros (Northern Iraq). *Acta Carsologica* 38, 83–96. <https://doi.org/10.1007/978-3-642-12486-0>
- Stevens, L.R., Ito, E., Schwalb, A., Wright, H.E., 2006. Timing of atmospheric precipitation in the Zagros Mountains inferred from a multi-proxy record from Lake Mirabad, Iran. *Quat. Res.* 66, 494–500. <https://doi.org/10.1016/j.yqres.2006.06.008>
- Stevens, L.R., Wright, J., Ito, E., 2001. Proposed changes in seasonality of climate during the Lateglacial and Holocene at Lake Zeribar, Iran. *Holocene* 11, 747–755. <https://doi.org/10.1191/09596830195762>
- Stewart, B.W., Capo, R.C., Chadwick, O.A., 1998. Quantitative strontium isotope models for weathering, pedogenesis and biogeochemical cycling. *Geoderma* 82, 173–195. [https://doi.org/10.1016/S0016-7061\(97\)00101-8](https://doi.org/10.1016/S0016-7061(97)00101-8)
- Stone, E.C., 2007. *Settlement and society: essays dedicated to Robert McCormick Adams*. ISD LLC.
- Stuiver, M., Reimer, P.J., Bard, E., Beck, J.W., Burr, G.S., Hughen, K.A., Kromer, B., McCormac, G., Van Der Plicht, J., Spurk, M., 1998. INTCAL98 Radiocarbon Age Calibration, 24,000–0 cal BP. *Radiocarbon* 40, 1041–1083. <https://doi.org/10.1017/S0033822200019123>
- Tabari, H., Willems, P., 2018. Seasonally varying footprint of climate change on precipitation in the Middle East. *Sci. Rep.* 8, 2–11. <https://doi.org/10.1038/s41598-018-22795-8>

## Bibliography

- Tierney, J.E., Pausata, F.S.R., De Menocal, P.B., 2017. Rainfall regimes of the Green Sahara. *Sci. Adv.* 3, 1–10. <https://doi.org/10.1126/sciadv.1601503>
- Timpson, A., Colledge, S., Crema, E., Edinborough, K., Kerig, T., Manning, K., Thomas, M.G., Shennan, S., 2014. Reconstructing regional population fluctuations in the European Neolithic using radiocarbon dates: A new case-study using an improved method. *J. Archaeol. Sci.* 52, 549–557. <https://doi.org/10.1016/j.jas.2014.08.011>
- Tinner, W., van Leeuwen, J.F.N., Colombaroli, D., Vescovi, E., van der Knaap, W.O., Henne, P.D., Pasta, S., D'Angelo, S., La Mantia, T., 2009. Holocene environmental and climatic changes at Gorgo Basso, a coastal lake in southern Sicily, Italy. *Quat. Sci. Rev.* 28, 1498–1510. <https://doi.org/10.1016/j.quascirev.2009.02.001>
- Treble, P., Shelley, J.M.G., Chappell, J., 2003. Comparison of high resolution sub-annual records of trace elements in a modern (1911-1992) speleothem with instrumental climate data from southwest Australia. *Earth Planet. Sci. Lett.* 216, 141–153. [https://doi.org/10.1016/S0012-821X\(03\)00504-1](https://doi.org/10.1016/S0012-821X(03)00504-1)
- Tremaine, D.M., Froelich, P.N., Wang, Y., 2011. Speleothem calcite formed in situ: Modern calibration of  $\delta^{18}\text{O}$  and  $\delta^{13}\text{C}$  paleoclimate proxies in a continuously-monitored natural cave system. *Geochim. Cosmochim. Acta* 75, 4929–4950. <https://doi.org/10.1016/j.gca.2011.06.005>
- Trouet, V., Esper, J., Graham, N.E., Baker, A., Scourse, J.D., Frank, D.C., 2009. Persistent positive north atlantic oscillation mode dominated the medieval climate anomaly. *Science* (80-. ). 324, 78–80. <https://doi.org/10.1126/science.1166349>
- Tzedakis, P.C., 2007. Seven ambiguities in the Mediterranean palaeoenvironmental narrative. *Quat. Sci. Rev.* 26, 2042–2066. <https://doi.org/10.1016/j.quascirev.2007.03.014>
- Ulbrich, U., Lionello, P., Belušić, D., Jacobeit, J., Knippertz, P., Kuglitsch, F.G., Leckebusch, G.C., Luterbacher, J., Maugeri, M., Maheras, P., Nissen, K.M., Pavan, V., Pinto, J.G., Saaroni, H., Seubert, S., Toreti, A., Xoplaki, E., Ziv, B., 2012. Climate of the mediterranean: Synoptic patterns, temperature, precipitation, winds, and their extremes, in: Lionello, P.B.T.-T.C. of the M.R. (Ed.),

## *Bibliography*

- The Climate of the Mediterranean Region. Elsevier, Oxford, pp. 301–346.  
<https://doi.org/10.1016/B978-0-12-416042-2.00005-7>
- Ur, J., 2017. The archaeological renaissance in the Kurdistan Region of Iraq. *Near East. Archaeol.* 80, 176–187. <https://doi.org/10.5615/neareastarch.80.3.0176>
- Ur, J., 2003. CORONA satellite photography and ancient road networks: A northern Mesopotamian case study. *Antiquity* 77, 102–115. <https://doi.org/10.1017/S0003598X00061391>
- Ur, J., Karsgaard, P., Oates, J., 2011. The Spatial Dimensions of Early Mesopotamian Urbanism: The Tell Brak Suburban Survey, 2003–2006. *Iraq* 73, 1–19.  
<https://doi.org/10.1017/s0021088900000061>
- Ur, J.A., 2010. Cycles of civilization in Northern Mesopotamia, 4400-2000 BC. *J. Archaeol. Res.* 18, 387–431. <https://doi.org/10.1007/s10814-010-9041-y>
- Ur, J.A., 2002. Settlement and Landscape in Northern Mesopotamia: The Tell Hamoukar Survey 2000-2001. *Akkadica* 123, 57–88.
- Ur, J.A., Gibson, M., 2010. Urbanism and cultural landscapes in northeastern Syria: the Tell Hamoukar Survey, 1999-2001. Oriental Institute of the University of Chicago Chicago.
- Ur, J.A., Wilkinson, T.J., 2008. Settlement and economic landscapes of Tell Beydar and its hinterland. na.
- Utida, G., Cruz, F.W., Santos, R. V., Sawakuchi, A.O., Wang, H., Pessenda, L.C.R., Novello, V.F., Vuille, M., Strauss, A.M., Borella, A.C., Stríkis, N.M., Guedes, C.C.F., Dias De Andrade, F.R., Zhang, H., Cheng, H., Edwards, R.L., 2020. Climate changes in Northeastern Brazil from deglacial to Meghalayan periods and related environmental impacts. *Quat. Sci. Rev.* 250. <https://doi.org/10.1016/j.quascirev.2020.106655>
- Van De Noort, R., 2011. Conceptualising climate change archaeology. *Antiquity* 85, 1039–1048. <https://doi.org/10.1017/S0003598X00068472>
- Van Oldenborgh, G.J., Drijfhout, S., Van Ulden, A., Haarsma, R., Sterl, A., Severijns, C., Hazeleger,

## Bibliography

- W., Dijkstra, H., 2009. Western Europe is warming much faster than expected. *Clim. Past* 5, 1–12. <https://doi.org/10.5194/cp-5-1-2009>
- Van Rampelbergh, M., Fleitmann, D., Verheyden, S., Cheng, H., Edwards, L., De Geest, P., De Vleeschouwer, D., Burns, S.J., Matter, A., Claey's, P., Keppens, E., 2013. Mid- to late Holocene Indian Ocean Monsoon variability recorded in four speleothems from Socotra Island, Yemen. *Quat. Sci. Rev.* 65, 129–142. <https://doi.org/10.1016/j.quascirev.2013.01.016>
- van Zeist, W., Baruch, U., Bottema, S., 2009. Holocene Palaeoecology of the Hula Area, Northeastern Israel. *A Timeless Val.* 29–64.
- van Zeist, W., Bottema, S., 1991. Late Quaternary vegetation of the Near East, Beihefte zum Tübinger Atlas des Vorderen Orients: Naturwissenschaften. Reichert.
- van Zeist, W., Bottema, S., 1977. Palynological investigations in Western Iran. *Palaeohistoria* 19, 19–85.
- van Zeist, W., Woldring, H., 1980. Holocene vegetation and climate of Northwestern Syria. *Palaeohistoria* 112–125.
- van Zeist, W., Wright, H.E., 1963. Preliminary Pollen Studies at Lake Zeribar, Zagros Mountains, Southwestern Iran. *Science* (80-. ). 140, 65 LP – 67. <https://doi.org/10.1126/science.140.3562.65>
- Verheyden, S., Nader, F.H., Cheng, H.J., Edwards, L.R., Swennen, R., 2008. Paleoclimate reconstruction in the Levant region from the geochemistry of a Holocene stalagmite from the Jeita cave, Lebanon. *Quat. Res.* 70, 368–381. <https://doi.org/10.1016/j.yqres.2008.05.004>
- Walker, M., Johnsen, S., Rasmussen, S.O., Popp, T., Steffensen, J.P., Gibbard, P., Hoek, W., Lowe, J., Andrews, J., Björck, S., Cwynar, L.C., Hughen, K., Kershaw, P., Kromer, B., Litt, T., Lowe, D.J., Nakagawa, T., Newnham, R., Schwander, J., 2009. Formal definition and dating of the GSSP (Global Stratotype Section and Point) for the base of the Holocene using the Greenland NGRIP ice core, and selected auxiliary records. *J. Quat. Sci.* 24, 3–17. <https://doi.org/10.1002/jqs.1227>
- Wang, Y.J., Cheng, H., Edwards, R.L., An, Z.S., Wu, J.Y., Shen, C.-C., Dorale, J.A., 2001. A High-

## Bibliography

- Resolution Absolute-Dated Late Pleistocene Monsoon Record from Hulu Cave, China. *Science* (80-. ). 294, 2345–2348.
- Wanner, H., Beer, J., Bütikofer, J., Crowley, T.J., Cubasch, U., Flückiger, J., Goosse, H., Grosjean, M., Joos, F., Kaplan, J.O., Küttel, M., Müller, S.A., Prentice, I.C., Solomina, O., Stocker, T.F., Tarasov, P., Wagner, M., Widmann, M., 2008. Mid- to Late Holocene climate change: an overview. *Quat. Sci. Rev.* 27, 1791–1828. <https://doi.org/10.1016/j.quascirev.2008.06.013>
- Wanner, H., Mercolli, L., Grosjean, M., Ritz, S.P., 2015. Holocene climate variability and change; a data-based review. *J. Geol. Soc. London.* 172, 254–263. <https://doi.org/10.1144/jgs2013-101>
- Ward, B.M., Wong, C.I., Novello, V.F., McGee, D., Santos, R. V., Silva, L.C.R., Cruz, F.W., Wang, X., Edwards, R.L., Cheng, H., 2019. Reconstruction of Holocene coupling between the South America Monsoon System and local moisture variability from speleothem  $\delta^{18}\text{O}$  and  $^{87}\text{Sr}/^{86}\text{Sr}$  records. *Quat. Sci. Rev.* 210, 51–63. <https://doi.org/10.1016/j.quascirev.2019.02.019>
- Wassenburg, J.A., Riechelmann, S., Schröder-Ritzrau, A., Riechelmann, D.F.C., Richter, D.K., Immenhauser, A., Terente, M., Constantin, S., Hachenberg, A., Hansen, M., Scholz, D., 2020. Calcite Mg and Sr partition coefficients in cave environments: Implications for interpreting prior calcite precipitation in speleothems. *Geochim. Cosmochim. Acta* 269, 581–596. <https://doi.org/10.1016/j.gca.2019.11.011>
- Wasylikowa, K., 2005a. Palaeoecology of Lake Zeribar, Iran, in the Pleniglacial, Lateglacial and Holocene, reconstructed from plant macrofossils. *The Holocene* 15, 720–735. <https://doi.org/10.1191/0959683605hl846rp>
- Wasylikowa, K., 2005b. Palaeoecology of Lake Zeribar, Iran, in the Pleniglacial, Lateglacial and Holocene, reconstructed from plant macrofossils. *The Holocene* 15, 720–735. <https://doi.org/10.1191/0959683605hl846rp>
- Wasylikowa, K., Witkowski, A., Walanus, A., Hutorowicz, A., Alexandrowicz, S.W., Langer, J.J., 2006. Palaeolimnology of Lake Zeribar, Iran, and its climatic implications. *Quat. Res.* 66, 477–493. <https://doi.org/10.1016/j.yqres.2006.06.006>

## Bibliography

- Weiss, H., Bradley, R.S., 2001. What Drives Societal Collapse? *Science* (80- ). 291, 609 LP – 610.  
<https://doi.org/10.1126/science.1058775>
- Weiss, H., Courty, M.A., Wetterstrom, W., Guichard, F., Senior, L., Meadow, R., Curnow, A., 1993. The genesis and collapse of third millennium north Mesopotamian civilization. *Science* (80- ). 261, 995–1004. <https://doi.org/10.1126/science.261.5124.995>
- Weldeab, S., Lea, D.W., Schneider, R.R., Andersen, N., 2007. 155,000 Years of West African Monsoon and Ocean Thermal Evolution. *Science* (80- ). 316, 1303–1307.  
<https://doi.org/10.1126/science.1140461>
- Weninger, B., Clare, L., Rohling, E.J., Bar-Yosef, O., Böhner, U., Budja, M., Bundschuh, M., Feurdean, A., Gebel, H.G., Jöris, O., Linstädter, J., Mayewski, P., Mühlenbruch, T., Reingruber, A., Rollefson, G., Schyle, D., Thissen, L., Todorova, H., Zielhofer, C., 2009. The Impact of Rapid Climate Change on prehistoric societies during the Holocene in the Eastern Mediterranean. *Doc. Praehist.* 36, 7–59. <https://doi.org/10.4312/dp.36.2>
- Werner, M., Langebroek, P.M., Carlsen, T., Herold, M., Lohmann, G., 2011. Stable water isotopes in the ECHAM5 general circulation model: Toward high-resolution isotope modeling on a global scale. *J. Geophys. Res. Atmos.* 116, 1–14. <https://doi.org/10.1029/2011JD015681>
- Whitmore, T.M., Turner, B.L., Johnson, D.L., Kates, R.W., Gottschang, T.R., 1990. Long-term population change, in: Jordan, M., Meyer, W.B., Kates, R.W., Clark, W.C., Richards, J.F., Turner, B.L., Mathews, J.T. (Eds.), *The Earth as Transformed by Human Action*. CUP Archive, pp. 25–39.
- Wick, L., Lemcke, G., Sturm, M., 2003. Evidence of Lateglacial and Holocene climatic change and human impact in eastern Anatolia: High-resolution pollen, charcoal, isotopic and geochemical records from the laminated sediments of Lake Van, Turkey. *Holocene* 13, 665–675.  
<https://doi.org/10.1191/0959683603hl653rp>
- Wilkinson, A.T.J., Bintliff, J., Curvers, H.H., Halstead, P., Kohl, P.L., Liverani, M., Mccorriston, J., Oates, J., Schwartz, G.M., Thuesen, I., Stales, D., Wilkinson, T.J., 1994. The Structure and

## Bibliography

- Dynamics of in Upper Mesopotamia. *Curr. Anthropol.* 35.
- Wilkinson, A.T.J., Philip, G., Bradbury, J., Dunford, R., Donoghue, D., Lawrence, D., Ricci, A., Smith, S.L., Journal, S., March, N., 2014. Contextualizing Early Urbanization : Settlement Cores , Early States and Agropastoral Strategies in the Fertile Crescent During the Fourth and Third Millennia BC Published by : Springer Stable URL : <https://www.jstor.org/stable/24766148> Contextualizing E. J. World Prehistory 27, 43–108. <https://doi.org/10.1007/s>
- Wilkinson, T.J., 2000. Regional approaches to Mesopotamian archaeology: The contribution of archaeological surveys. *J. Archaeol. Res.* 8, 219–267. <https://doi.org/10.1023/A:1009487620969>
- Wilkinson, T.J., 1993. Linear hollows in the Jazira, Upper Mesopotamia. *Antiquity* 67, 548–562. [https://doi.org/DOI: 10.1017/S0003598X00045750](https://doi.org/DOI:10.1017/S0003598X00045750)
- Wilkinson, T.J., Tucker, D.J., 1995. Settlement development in the North Jazira, Iraq: a study of the archaeological landscape= Tatauwur al-mustawṭan fi'l-ḡazīra al-šimālīya, al-ʿIrāq. Aris & Phillips.
- Willcox, G., 2013. The roots of cultivation in Southwestern Asia. *Science* (80-. ). 341, 39–40. <https://doi.org/10.1126/science.1240496>
- Willcox, G., Buxo, R., Herveux, L., 2009. Late Pleistocene and Early Holocene Climate and the Beginning of Cultivation in Northern Syria. *The Holocene* 19, 151–158.
- Williams, P.W., 2008. The role of the epikarst in karst and cave hydrogeology: A review. *Int. J. Speleol.* 37, 1–10. <https://doi.org/10.5038/1827-806X.37.1.1>
- Wossink, A., 2009. Challenging climate change. Competition and cooperation among pastoralists and agriculturalists in northern Mesopotamia (c. 3000-1600 BC).
- Wright, H.E., 1993. Environmental Determinism in Near Eastern Prehistory. *Curr. Anthropol.* 34, 458–469.
- Wright, H.T., Rupley, E.S.A., Ur, J.A., Oates, J., Ganem, E., 2006. Preliminary Report on the 2002 and 2003 Seasons of the Tell Brak Sustaining Area Survey. *Les Ann. Archéologiques Arab. Syriennes* 49–50, 7–21.

## Bibliography

- Wu, J.Y., Wang, Y.J., Cheng, H., Kong, X.G., Liu, D.B., 2012. Stable isotope and trace element investigation of two contemporaneous annually-laminated stalagmites from northeastern China surrounding the 8.2 ka event. *Clim. Past* 8, 1497–1507. <https://doi.org/10.5194/cp-8-1497-2012>
- Xoplaki, E., González-Rouco, J.F., Luterbacher, J., Wanner, H., 2004. Wet season Mediterranean precipitation variability: Influence of large-scale dynamics and trends. *Clim. Dyn.* <https://doi.org/10.1007/s00382-004-0422-0>
- Yasuda, Y., Kitagawa, H., Nakagawa, T., 2000. The earliest record of major anthropogenic deforestation in the Ghab Valley, northwest Syria: A palynological study. *Quat. Int.* 73–74, 127–136. [https://doi.org/10.1016/S1040-6182\(00\)00069-0](https://doi.org/10.1016/S1040-6182(00)00069-0)
- Zebari, M., Grützner, C., Navabpour, P., Ustaszewski, K., 2019. Relative timing of uplift along the Zagros Mountain Front Flexure (Kurdistan Region of Iraq): Constrained by geomorphic indices and landscape evolution modeling. *Solid Earth* 10, 663–682. <https://doi.org/10.5194/se-10-663-2019>
- Zeder, M.A., 2011. The Origins of Agriculture in the Near East. *Curr. Anthropol.* 52, S221–S235. <https://doi.org/10.1086/659307>
- Zeder, M.A., 2008. Domestication and early agriculture in the Mediterranean Basin: Origins, diffusion, and impact. *Proc. Natl. Acad. Sci.* 105, 11597–11604. <https://doi.org/10.1073/pnas.0801317105>
- Zerboni, A., Nicoll, K., 2019. Enhanced zoogeomorphological processes in North Africa in the human-impacted landscapes of the Anthropocene. *Geomorphology* 331, 22–35. <https://doi.org/10.1016/j.geomorph.2018.10.011>
- Zhou, H., Feng, Y. xing, Zhao, J. xin, Shen, C.C., You, C.F., Lin, Y., 2009. Deglacial variations of Sr and  $^{87}\text{Sr}/^{86}\text{Sr}$  ratio recorded by a stalagmite from Central China and their association with past climate and environment. *Chem. Geol.* 268, 233–247. <https://doi.org/10.1016/j.chemgeo.2009.09.003>
- Zhou, H.Y., Wang, Y., Huang, L.Y., Mai, S.Q., 2011. Speleothem Mg, Sr and Ba records during the MIS 5c-d, and implications for paleoclimate change in NE Sichuan, Central China. *Chinese Sci.*

*Bibliography*

Bull. 56, 3445–3450. <https://doi.org/10.1007/s11434-011-4681-y>

Zohary, M., 1973. Geobotanical foundations of the Middle East. Fishcer.

## 14 Appendix

Appendix

14.1 Appendix A – European and Southwest Asian Speleothem ( $\delta^{18}\text{O}$ ) Records

Country	Site	Calcite (VPDB)	Drip Water (SMOW)	Predicted Calcite (VPDB)	Reference
Iraq	Shalaih Cave	-5.32	-5.49	-5.62	This Study
Ireland	Crag	-3.80	-5.60	-3.84	McDermott et al. (1999) Quaternary Science Reviews 18, 1021-1038. McDermott et al. (2001) Science 294, 1328-1331.
Ireland	Crag	-3.54	-5.60	-3.84	Baldini et al. (2005) Earth and Planetary Science Letters 240, 486–494
Scotland	Uamh an Tartair	-5.20	-7.10	-4.70	Fuller et al. (2008) Hydrol. Earth Syst. Sci., 12, 1065-1074.
Spain	Garma	-3.99	-6.10	-4.68	Baldini, L.M. 2007 Unpubl PhD thesis, University College Dublin
Spain	Garma	-4.48	-5.40	-4.15	Jackson, A. 2009 Unpubl. PhD thesis, University College Dublin
France	Clamouse	-4.95	-6.20	-5.25	McDermott et al. (1999) Quaternary Science Reviews 18, 1021-1038.
France	Clamouse	-5.50	-6.20	-5.25	Frisia et al. pers. comm.
Belgium	Han-sur-Lesse	-5.50	-7.50	-5.58	Verheyden et al. (2006) Geologica Belgica 9, 245-256
Belgium	Han-sur-Lesse	-5.55	-7.50	-5.44	Genty et al. (2006) Quaternary Science Reviews 25, 2118–2142
Germany	B-7	-5.70	-8.37	-6.42	Niggemann et al. (2003) Quaternary Science Reviews 22, 555-568
Italy	Corchia	-4.34	-7.40	-5.06	Zanchetta et al. (2007) Quaternary Science Reviews 26, 279-286
Italy	Ernesto	-7.80	-9.60	-7.10	McDermott et al. (1999) Quaternary Science Reviews 18, 1021-1038.
Italy	Ernesto	-7.40	-9.60	-7.10	Frisia, S. pers. comm.
Austria	Spannagel	-7.49	-11.30	-7.81	Mangini et al. (2005) Earth Planet. Sci. Letts. 235, 741-751
Austria	Spannagel	-7.90	-11.30	-7.81	Vollweiler (2006) Geophys Res Letts 33, 20, 10.1029/2006GL027662
Norway	Rana	-7.33	-10.00	-6.69	Linge et al. (2001) Palaeo3 167, 209-224
Italy	Carburangeli	-6.70	-6.00	-5.98	Frisia et al. (2006) Quaternary Research 66, 388-400.
Italy	Savi	-6.10	-7.28	-5.90	Frisia et al., (2005) Boreas 34, 445-455
Slovenia	Postojna	-6.70	-9.20	-6.96	Horvatincic et al. 2003 Palaeo3, 193,139-157.
Romania	Ursilor Cave	-7.80	-10.30	-8.43	Onac et al., 2002, Journal of Quaternary Science 17, 319–327
Israel	Soreq	-5.17	-5.00	-5.15	Orland et al. (2009) Quaternary Science Reviews 71, 27-35
Israel	Nahal Qunah	-5.30	-5.00	-4.91	Frumkin et al., 1999. The Holocene 9,6 (1999) pp. 677–682

Table 8:  $\delta^{18}\text{O}$  values and references for speleothem records used to calculate to what extent calcite precipitated under conditions of isotopic equilibrium

## 14.2 Appendix B – Record Correlations

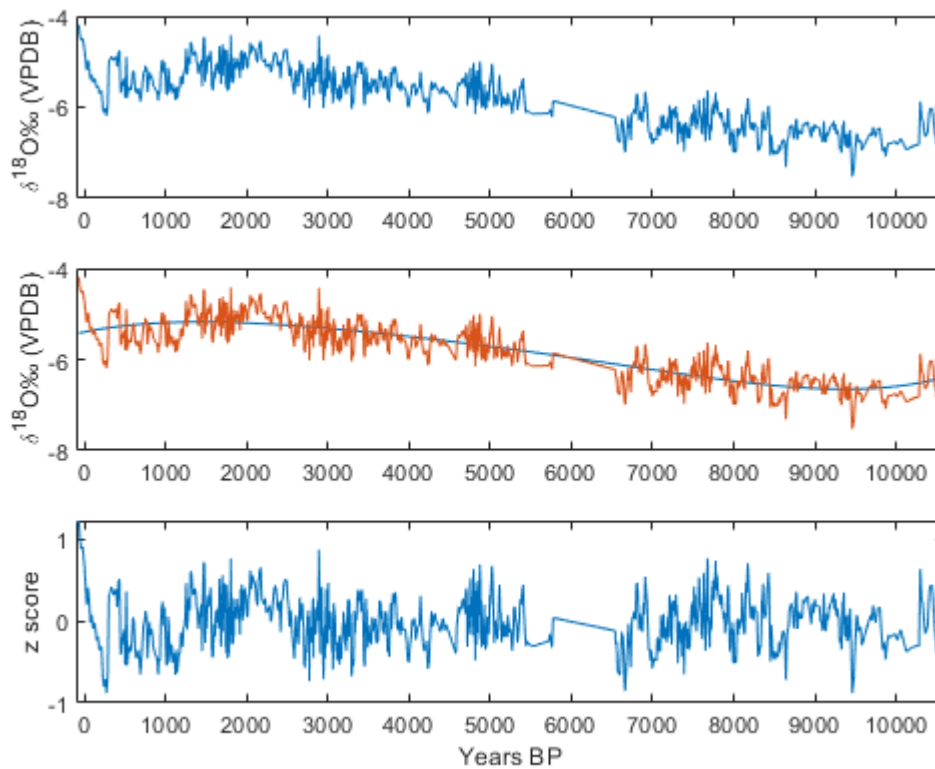
Table 9: Correlation coefficients for key speleothem  $\delta^{18}\text{O}$  records from Southwest Asia and a record from the Eastern Mediterranean Sea (PS009PC), after values were binned into 100-year intervals. All shows significantly strong correlation to one another. Of a particular importance is the strong correlation between SHC-03 and PS009PC, which provides some evidence that  $\delta^{18}\text{O}$  variability in the SHC-03 stalagmite is strongly influenced by the so-called source effect.

		<b>Correlations</b>				
		Shalaih	PS009PC	Qunf	Jeita	Soreq
Shalaih	Pearson Correlation	1	.715**	.791**	.812**	.658**
	Sig. (2-tailed)		.000	.000	.000	.000
	N	99	99	82	93	90
PS009PC	Pearson Correlation	.715**	1	.748**	.612**	.565**
	Sig. (2-tailed)	.000		.000	.000	.000
	N	99	119	90	113	107
Qunf	Pearson Correlation	.791**	.748**	1	.695**	.684**
	Sig. (2-tailed)	.000	.000		.000	.000
	N	82	90	90	88	83
Jeita	Pearson Correlation	.812**	.612**	.695**	1	.628**
	Sig. (2-tailed)	.000	.000	.000		.000
	N	93	113	88	118	101
Soreq	Pearson Correlation	.658**	.565**	.684**	.628**	1
	Sig. (2-tailed)	.000	.000	.000	.000	
	N	90	107	83	101	107

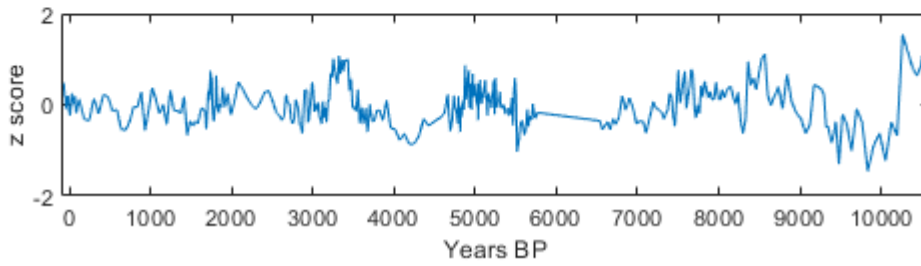
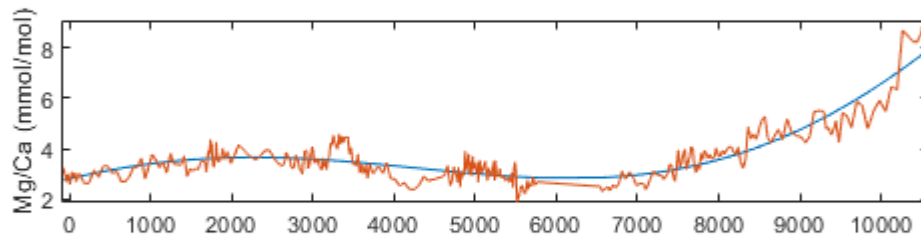
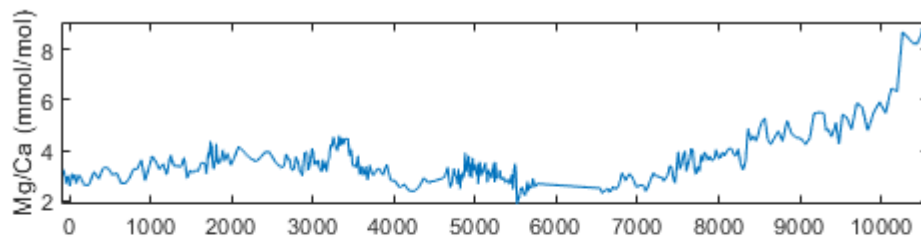
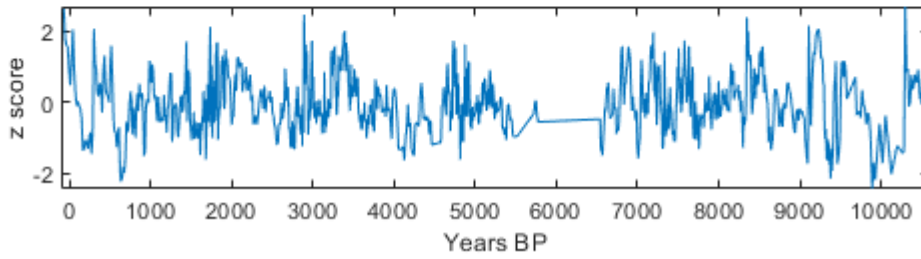
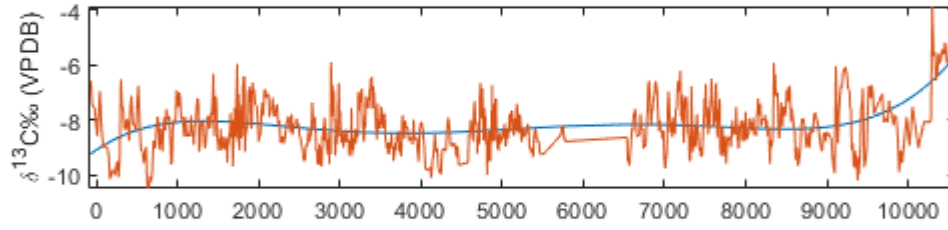
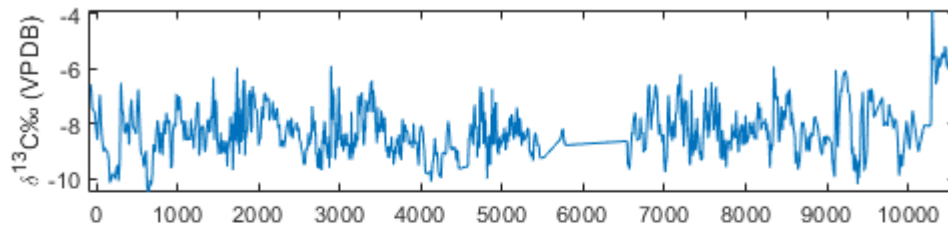
\*\* Correlation is significant at the 0.01 level (2-tailed).

### 14.3 Appendix C - Detrending Normalising and Producing MAI scores

In order avoid autocorrelation due to long-term trends recording orbital-to-millennial-scale information when investigating short term climate variability, data was detrended using Matlab by applying a 5<sup>th</sup> order polynomial spline to the data and subtracting it. This allows the detrended data to reflect centennial-to-decadal-scale variability. When comparing different proxy information, the detrended time series data was normalized by its mean and SD to produce ‘z scores’ using the inbuilt Matlab function *normalise*.



Appendix



Appendix

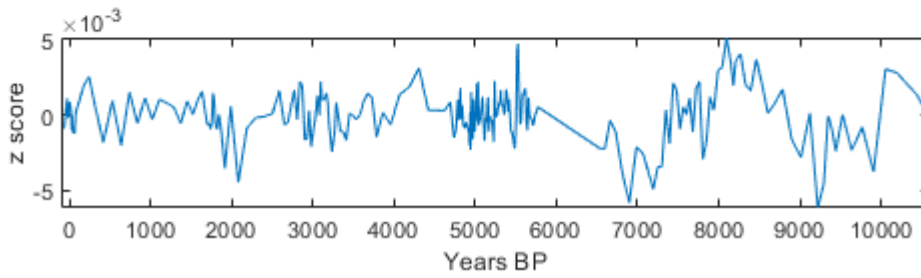
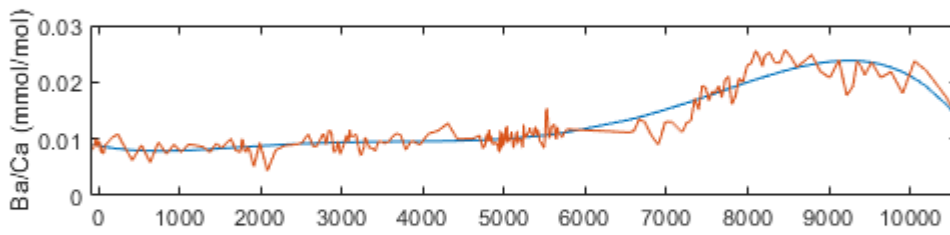
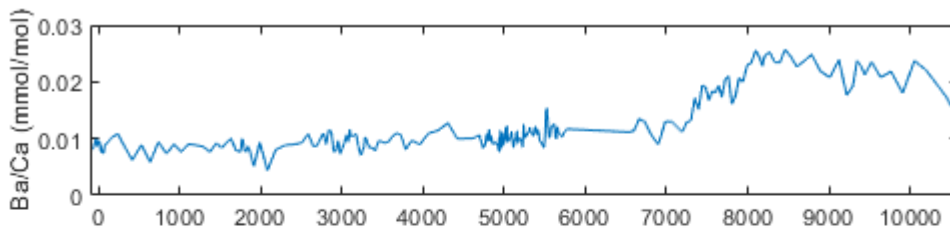
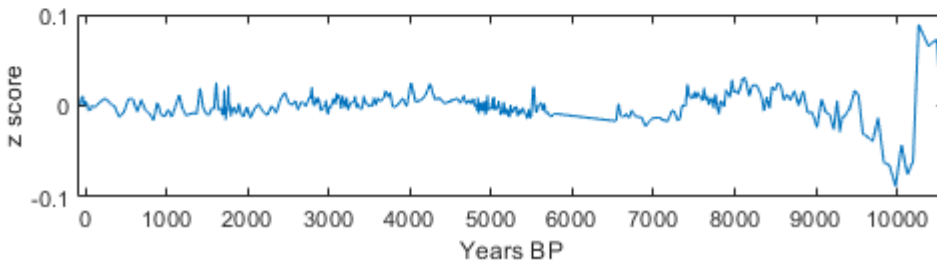
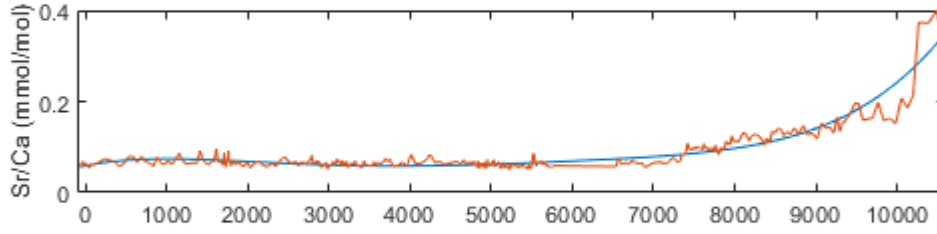
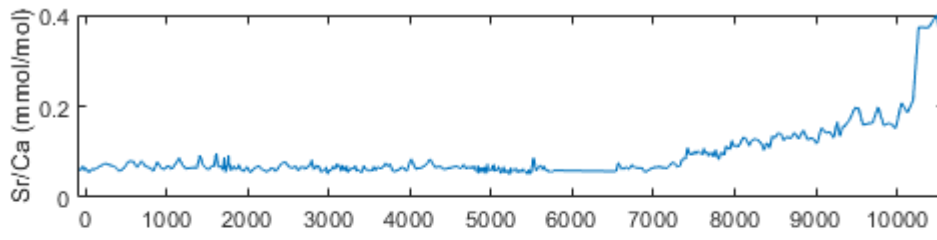


Figure 61: Figures showing the process of detrending and normalising the SHC-03 proxy data in MATLAB. The top plot in all the figures is the original proxy data, the middle plot shows a 5<sup>th</sup> order polynomial spline running through the data which is used to detrend the data by subtracting it. The bottom plot shows the data after it has been detrended and normalised ( $x - \text{mean}/\text{SD}$ ).

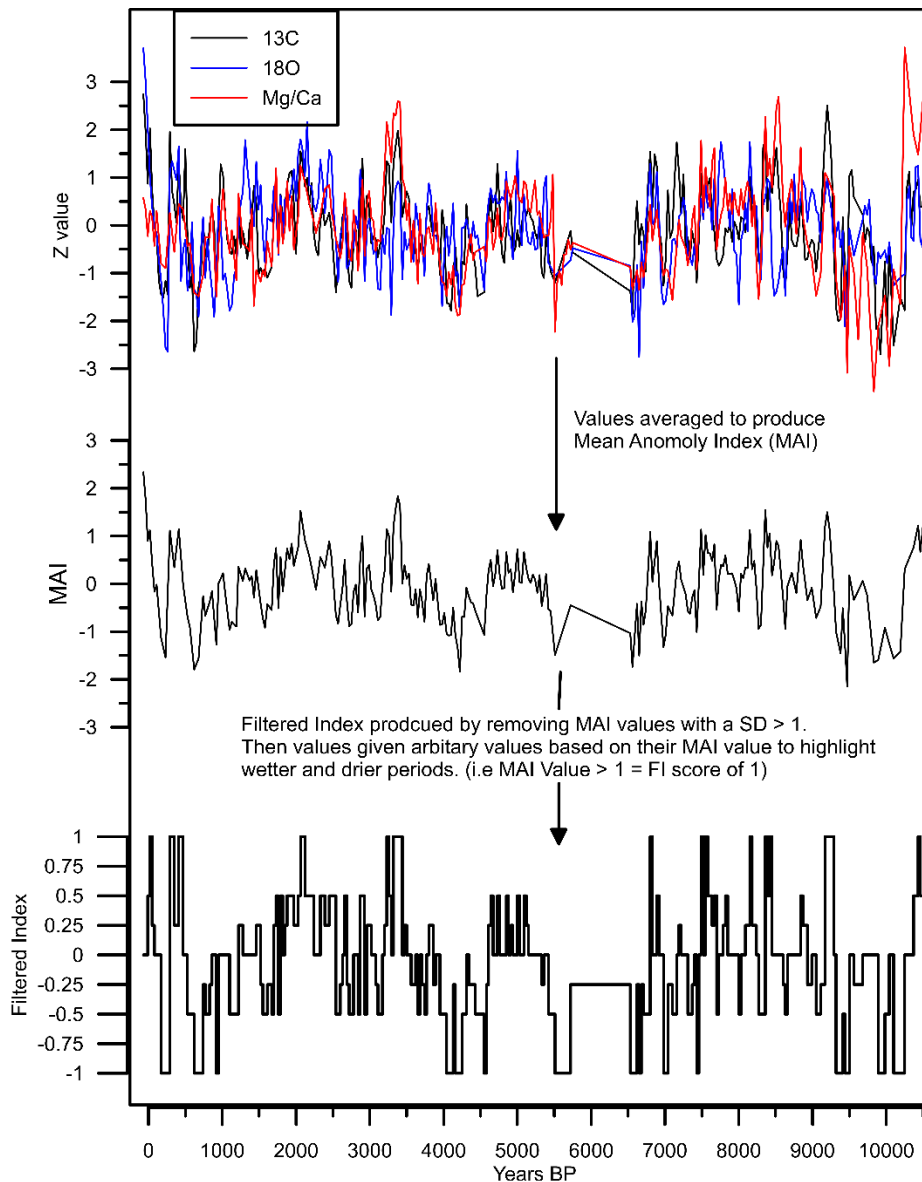


Figure 62: Once the data was detrended the values were then averaged to produce a mean anomaly index. To remove statistical outliers a filtered Index was then produced which removed any MAI with an SD greater than 1, then values were given to mean anomaly index scores that deviated from the mean by 0.25, 0.5 and 1, where positive excursions represent wet intervals and negative excursions represent dry intervals. FI Scores of 1 or -1 represent more extreme events, whereas scores of 0.25 or -0.25 represent still statistically significant, but less extreme events.

## 14.4 Appendix D – Correcting for Interlaboratory Variation

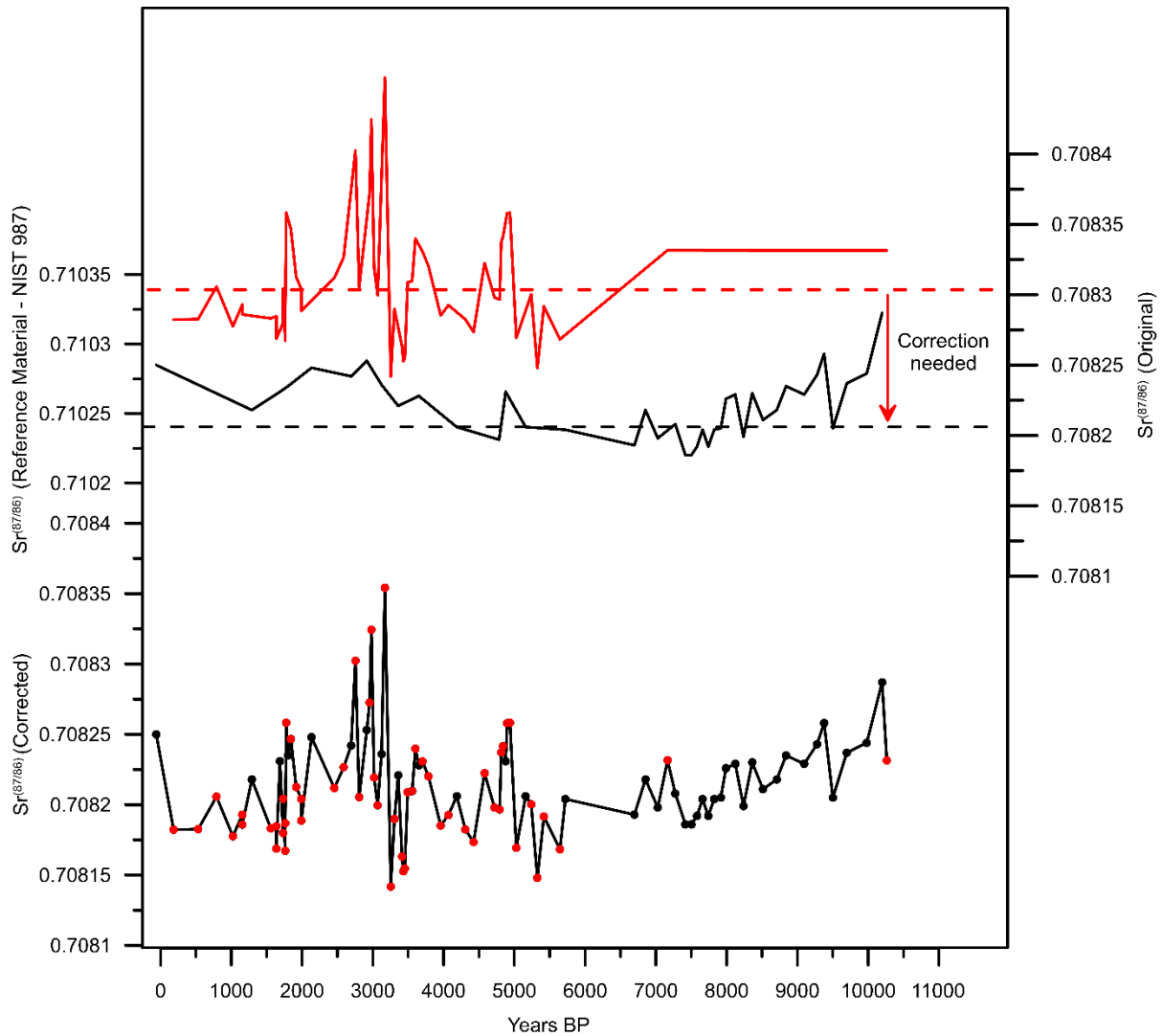


Figure 63: Plot showing the Sr correction needed for the data produced at the two different laboratories (red line = Sweden Lab, black line = UK lab). The was a difference of about 0.0001 between the average values of the reference materials (NIST 987) at the two labs, this value was used to correct the most recent Sr data by subtracting the reference differences from these values. This seems to fully explain the difference between the original data.

#### 14.5 **Appendix E - Organic Carbon Analysis**

Two carbonate samples were collected from the stalagmite to examine the organic content of the speleothem. This was done to determine whether the organic content of the speleothem was sufficient enough for the analysis of organic  $\delta^{13}\text{C}$ , via compound specific isotope analysis, to help in our interpretation of other proxies, particular (carbonate)  $\delta^{13}\text{C}$  (Blyth et al., 2016). Powdered carbonate samples, measuring about 5g in mass, were collected from the SHC-3 stalagmite to conduct a pilot study for the analysis of organic matter within the speleothem. To isolate, the organic carbon from the inorganic carbonate, acid digestion was conducted using 5% HCl. However, the speleothem was found to have no or negligible organic content (M Leng per comms) which would have made further analysis of this of very limited value. Low organic content might be explained by minimal soil coverage above the cave, however, given high levels of bat activity and guano in the cave this was still a surprising result.